Title: Reactivity, Mechanism, and Assembly of the Alternative Nitrogenases

#### **Authors**

Andrew J. Jasniewski, a Chi Chung Lee, a Markus W. Ribbe, \*,a,b Yilin Hu\*,a

#### **Affiliations**

<sup>a</sup>Department of Molecular Biology and Biochemistry, University of California, Irvine, CA 92697-3900; <sup>b</sup>Department of Chemistry, University of California, Irvine, CA 92697-2025

#### **Abstract**

Biological nitrogen fixation is catalyzed by the enzyme nitrogenase, which facilitates the cleavage of the relatively inert triple bond of N<sub>2</sub>. Nitrogenase is most commonly associated with the molybdenum-iron cofactor called FeMoco or the M-cluster, and it has been the subject of extensive structural and spectroscopic characterization over the past 60 years. In the late 1980's and early 1990's, two 'alternative nitrogenase' systems were discovered, isolated, and were found to incorporate V or Fe in place of the Mo. These systems are regulated by separate gene clusters, however, there is a high degree of structural and functional similarity between each nitrogenase. Limited studies with the V- and Fe-nitrogenases initially demonstrated that these enzymes were analogously active as the Mo-nitrogenase, but more recent investigations have found capabilities that are unique to the alternative systems. In this review, we will discuss the reactivity, biosynthetic and mechanistic proposals for the alternative nitrogenases as well as their electronic and structural properties in comparison to the well-characterized Mo-dependent system. Studies over the past 10 years have been particularly fruitful, though, key aspects about V- and Fe-nitrogenases remain unexplored.

#### Index

- 1. Introduction
- 2. Genetic Distribution, Regulation and Evolution of Mo-Independent Nitrogenases
  - 2.1. Assembly of Mo- and V-nitrogenases
- 3. Structure and Properties of Nitrogenase Proteins
  - 3.1. The Characterization of the Reductase Components NifH, VnfH and AnfH
    - 3.1.1. Crystal Structures of NifH and VnfH
    - 3.1.2. Solution and Spectroscopic Properties of Fe Proteins
  - 3.2. The Properties of Mo-nitrogenase
    - 3.2.1. P-cluster from NifDK
    - 3.2.2. M-cluster from NifDK
  - 3.3. The Characterization of V-nitrogenase
    - 3.3.1. Crystal Structures of VnfDGK
    - 3.3.2. P- and V-clusters from VnfDGK
  - 3.4. The Characterization of Fe-only Nitrogenase
- 4. Reactivity of the Alternative Nitrogenases
  - 4.1. Technical Considerations for the Study of Nitrogenase Reactivity
  - 4.2. Standard Nitrogenase Substrate Reduction Activity Towards Dinitrogen, Protons and Acetylene
  - 4.3. Reactions of Nitrogenase with Azide and Cyanide
  - 4.4. Expanded Substrate Reactions for Alternative Nitrogenases
  - 4.5. Activities of the Isolated Nitrogenase Cofactors
  - 4.6. Hybrid Nitrogenase Enzymes and Their Reactivity
  - 4.7. Substrate Reduction by the Reductase Components NifH And VnfH
- 5. Mechanism of Nitrogenase
  - 5.1. N<sub>2</sub> Reduction Mechanism for Mo-nitrogenase
  - 5.2. N<sub>2</sub> Reduction Mechanism for the Alternative Nitrogenases.
  - 5.3. Mechanism of Nitrogenases for the Reduction of Carbon Monoxide
    - 5.3.1. The Binding and Reactivity of CO in Mo-Nitrogenase
    - 5.3.2. The Binding and Reactivity of CO in V-Nitrogenase
- 6. Summary and Perspectives

#### 1. Introduction

Nitrogen fixation occurs in biology through the activity or enzymes known as nitrogenase. The enzyme takes  $N_2$  from the atmosphere or other sources, and at ambient temperature and pressure can cleave the strong triple  $N_2$  bond to generate two equivalents of ammonia, as seen in a simplified reaction 1:

$$\bar{A}_2 + 6\bar{A}^+ + 6\bar{A}^- \to 2\bar{A}\bar{A}_3$$
 (1)

However, as will be discussed in Section 5, the stoichiometry and mechanism of this enzymatic process is more complex. Nitrogenases play a critical role in the global nitrogen cycle and provide bioavailable nitrogen for organisms to form the fundamental building blocks of life – amino acids and nucleobases. In diazotrophic organisms that can express nitrogenase, there are three different variants: Mo-dependent, V-dependent and Fe-only nitrogenases. These three systems are closely related as they are likely products of genetic duplication and evolutionary divergence as opposed to the simple substitution of the transition metal. The Mo-dependent systems have been studied more extensively than the others, however, the focus of this review will be on the mechanism and reactivity of the Mo-independent systems. Inherently there is less characterization reported for the V- and Fe-only nitrogenases due to the relatively recent isolation, so information will be discussed within the context of what is available for the alternative systems and will not constitute an exhaustive description of Mo-nitrogenase.

#### 2. Genetic Distribution, Regulation and Evolution of Mo-Independent Nitrogenases

Within the last decade, genetic sequencing efforts have expanded the genome data bank, and this has allowed for the identification of an array of novel nitrogen fixing organisms. Bioinformatics, in combination with a better understanding of nitrogenase assembly, was used to identify 149 diazotrophs in 2012 after a comprehensive genome search using a minimum gene set *nifHDKENB*;<sup>1</sup> this number increased to 359 organisms from a similar study conducted in 2019.<sup>2</sup> In Archaea, nitrogenase is restricted to the Euryarchaeota phylum whereas in Bacteria, nitrogenase can be found in 13 different phyla; primarily in Proteobacteria, Firmicutes, Cyanobacteria and Bacteroidetes.<sup>1-3</sup> The sources of these organisms were shown to be far more diverse than previously understood. Beyond the conventional soil dwellers in agricultural sites,<sup>1,3</sup>

nitrogen fixing organisms have been found in a variety of environments ranging from marine, coastal and freshwater sediments,<sup>4</sup> to waste and sewage stacks,<sup>5</sup> the termite midgut<sup>6</sup> and in human pathogens.<sup>3</sup> The number of organisms identified with putative alternative nitrogenases also increased proportionately with the number of available genomes,<sup>7,8</sup> indicating a more widespread taxonomic distribution of alternative nitrogenases than considered previously. One study by Morel and co-workers estimated that alternative nitrogenases constitute 14–21% of the total nitrogenase activity, and are major participants of diazotrophic activity in almost a quarter of environments where biological nitrogen fixation is detected.<sup>3</sup>

The increasing prevalence of alternative nitrogenases identified in genomic databases highlights a potential for ecological importance and a role in the global nitrogen cycle, which raises the question of how alternative nitrogenase expression may be regulated. Most organisms that fix N<sub>2</sub> only encode for Mo-nitrogenase (nif), but organisms that encode the alternative nitrogenases (vnf and/or anf) also encode for Mo-nitrogenase. 1,9-12 Several prokaryotes, namely Azotobacter vinelandii, Methanosarcina acetivorans, and Rhodopseudomonas palustris, have the genes for all three nitrogenases, <sup>13</sup> however, some diazotrophs only encode Mo- and Fe-only nitrogenases (*Rhodobacter* species), <sup>14</sup> while others only encode Mo- and V-nitrogenases (Anabaena species). 15 In A. vinelandii, the putative regulatory pathway involves the master regulator genes nifA, vnfA and anfA, which are responsible for the expression of Mo-, V- and Fenitrogenase encoding genes, respectively. 16 In the presence of Mo, the gene product NifA turns on the expression of the *nif*-encoding genes while *vnfA* and *anfA* are both transcriptionally repressed. In the presence of V and absence of Mo, VnfA is expressed and it transcriptionally suppresses the *nif*- and *anf*- encoding nitrogenase genes. Lastly, in the absence of both Mo and V, the anfA gene is activated to turn on the synthesis of Fe-nitrogenase. <sup>17</sup> There is certain degree of overlap between these nitrogenase systems given that neither the vnf nor the anf gene clusters contain the entire set of necessary biosynthetic genes. For one example, in A. vinelandii the biosynthesis of all nitrogenases require the action of NifU, NifS and NifB. 18 Interestingly, transcriptome analysis also revealed that many of the genes required for V-nitrogenase assembly are also turned on when the organism was expressing Fe-nitrogenase. <sup>18</sup> The NifA-mediated regulation framework seems to be employed by other diazotrophic proteobacteria, albeit with some modifications. For instance, in *Rhodobacter capsulatus*, NifA is believed to be necessary for the synthesis of Fe-only nitrogenase, although this is facilitated through a NifA-dependent

factor known as RpoN.<sup>19</sup> Alternatively, there are instances where the *nifA* gene does not appear have any encoded homologs, with many examples found in diazotrophic cyanobacteria. In one example, in *Anabaena variabilis*, nitrogenase expression is controlled by an interplay of a number of environmental factors, and ultimately through regulation of the *nifB* promoter.<sup>20</sup> More recent evidence has revealed a more complex picture of alternative nitrogenase usage. Sequencing results taken from lichen and termite hindgut samples indicated a small or inconsistent correlation between alternative nitrogenase expression with trace metal availability.<sup>6,21,22</sup> Even in the well-established system of *A. vinelandii*, it is known that "hybrid" nitrogenases, such as the V-dependent protein containing the Mo-dependent cofactor, can be produced under specific growth conditions (see Section 4.6).<sup>23</sup> Thus, there are still many questions that remain concerning the gene regulation of alternative nitrogenase, and addressing them will become increasingly important for the future.

Due to improvements in sequencing techniques and the widespread availability of genetic information, the potential evolution of nitrogenase has been reassessed. Based on the availability of fixed nitrogen, Fe, and Mo in the ancient oceans, an initial proposal posited that the alternative nitrogenases predated Mo-nitrogenase. 10,24 However, recent phylogenetic studies point to the existence of a proto-nitrogenase species that was a common ancestor of all three known nitrogenases, and it was suggested to contain a precursor cofactor that lacked Mo.<sup>2,12,25</sup> Peters, Boyd and co-workers have argued that the structural genes of the modern Mo-nitrogenase, namely *nifHDK*, were the first to evolve from the proto-nitrogenase genes, potentially through gene duplication of *nifD* and differentiation events. <sup>17,25</sup> Subsequently, it was proposed that the nifDK genes might have been duplicated in order to give rise to cofactor biosynthetic genes nifEN, thereby allowing for the development of a fully functional Mo-nitrogenase.<sup>2</sup> Based on a concatenated phylogenetic lineage of the *nifHDK* genes, it was further suggested that the structural genes of V-nitrogenase, i.e. vnfHDGK, were derived from nifHDK while structural genes of Fe-only-nitrogenase, anfHDGK, were subsequently evolved from the vnf genes.<sup>25</sup> This notion is consistent with the fact that the assembly of the V- and Fe-only nitrogenase cofactors rely on *nif*-encoded genes, particularly *nifUS* and *nifB* as well as *nifEN* for organisms other than A. vinelandii and R. palustris which instead encode for vnfEN. 11,26 This proto-nitrogenase proposal was also compared with studies of ancient sedimentary rock from marine and fluvial sources that investigated the nitrogen isotope ratios of the encapsulated biomass from that time

period.<sup>27,28</sup> Nitrogenases are known to produce fixed nitrogen that disfavors the heavier <sup>15</sup>N isotope relative to the natural isotopic abundance of  $N_2$ . This can represented by the nitrogen fractionation where ( $\delta^{15}N = [(^{15}N/^{14}N)\text{sample}/(^{15}N/^{14}N)\text{standard}] - 1$ ), and Mo-nitrogenase can show  $\delta^{15}N$  values between -1% to -4% whereas the alternative nitrogenases favor <sup>14</sup>N products more strongly with  $\delta^{15}N$  values between -6% and -8%.<sup>27-29</sup> The sediments tested were between 3.2 and 2.75 billion years old, and in that time frame, the observed fractionation was  $\delta^{15}N \sim 0\%$ , which is more consistent with Mo-nitrogenase than the Mo-independent variants.<sup>28</sup> Compared to the phylogenetic analysis, the isotope experiments support the notion that Mo-nitrogenase predates the alternative systems. However, the isotope fractionation of a proto-nitrogenase cannot be accurately known, but it has been suggested that such a nitrogenase ancestor would be promiscuous, inefficient, and likely unable to discriminate against the heavy nitrogen isotope.<sup>17</sup> Additionally, there is no clear time point of when such a proto-nitrogenase would have started to incorporate Mo. A detailed picture for the evolution of nitrogenase proteins has begun to emerge, but it will be interesting to see how this changes as further investigation unveils new nitrogen fixing species and probes the biochemistry the nitrogenase proteins from these sources.

# 2.1. Assembly of Mo- and V-Nitrogenases

Extensive characterization efforts in the past two decades have provided valuable insight into the biochemistry and assembly of the catalytic component of Mo-nitrogenase, called the MoFe protein or NifDK. NifDK is a heterotetrameric protein that contains two cofactors – the [Fe<sub>8</sub>S<sub>7</sub>] P-cluster and the [MoFe<sub>7</sub>S<sub>9</sub>C-(*R*)-homocitrate] M-cluster (also called FeMoco). For *A. vinelandii*, it is understood that the synthesis of the P- and M-clusters of NifDK require a minimum set of proteins that include NifU, NifS, NifB, NifEN, NifV and NifZ, in addition to the structural gene products NifH and NifDK.<sup>30</sup> The functions of these *nif* gene products have been studied in great detail and are briefly summarized in Table 1. Overall, the P-cluster of the MoFe protein was determined to be synthesized *in situ*, *i.e.* on the NifDK polypeptide scaffold, and the M-cluster was synthesized *ex situ*, *i.e.* outside of the NifDK protein.<sup>30-32</sup> In the former case, a biosynthetic precursor of the P-cluster, denoted as the P\*-cluster, was identified as a pair of [Fe<sub>4</sub>S<sub>4</sub>]-like clusters. The conversion of this P\*-cluster to the fully matured P-cluster was described as the fusion of the two [Fe<sub>4</sub>S<sub>4</sub>] clusters, with the loss of a sulfur atom. The process also involves the action of NifZ and NifH in an ATP- and electron-dependent manner (Figure

1).<sup>33</sup> The catalytic component of V-nitrogenase, called VFe protein or VnfDGK, has a similar composition as the Mo-dependent system, with a P-cluster and a V-containing analog of the M-cluster called the V-cluster. Interestingly, a significant degree of similarity was observed between the P\*-cluster in the pre-matured MoFe protein and the matured P-cluster in V-nitrogenase based upon electron paramagnetic resonance (EPR) and X-ray absorption spectroscopic (XAS) analyses (see Section 3).<sup>34</sup> The synthesis of the M-cluster involves a series of transformative steps, starting from a pair of [Fe<sub>4</sub>S<sub>4</sub>] clusters (denoted as the K-cluster). The K-cluster is then converted into a [Fe<sub>8</sub>S<sub>9</sub>C] core (denoted as the L-cluster), and finally Mo and *R*-homocitrate are incorporated to yield the matured M-cluster (Figure 1).<sup>30-33,35-37</sup> It has been suggested that the M- and V-clusters share the same biosynthetic pathway until the formation of the L-cluster, and after this point the pathways diverge as either Mo or V is inserted along with the organic ligand *R*-homocitrate.<sup>31,32</sup>

Table 1. Description of Relevant Gene Products from the nif, vnf and anf Operonsa

gene	gene product label	known function		
nifH <sup>b</sup>	NifH, dinitrogenase reductase, component 2, reductase component, γ subunit, Fe protein	Mediation of ATP-dependent electron transfer during catalytic turnover, facilitates formation of P-cluster on NifDK, facilitates conversion of L- to M-cluster on NifEN <i>via</i> insertion of Mo and <i>R</i> -homocitrate  Facilitates chemical transformation of N <sub>2</sub> to NH <sub>3</sub> at the active cofactor site		
nifD,K <sup>b</sup>	NifDK, dinitrogenase, component 1, catalytic component, MoFe protein			
nifL	-	serves as a negative transcription regulator of <i>nif</i> genes		
nifA	-	serves as a positive transcription regulator of <i>nif</i> genes		
nifF	NifF, flavodoxin	involved in the transfer of electrons to nitrogenase during catalysis and/or assembly		
nifS	NifS, cysteine desulfurase	transfers sulfur to NifU for the assembly of small FeS clusters		
nifU	NifU	serves as a scaffold for the assembly of small FeS clusters, which can then be used for M- and P-cluster assembly		
$nifB^b$	NifB	mediates the radical SAM-dependent insertion of carbon concomitant with the formation of a Mo/homocitrate-free precursor of the M-cluster		
nifE,N <sup>b</sup>	NifEN	serves as a scaffold for the maturation of the M-cluster; a structural/functional homolog of NifDK		
nifV	NifV, homocitrate synthase	synthesizes <i>R</i> -homocitrate for M-cluster assembly		

nifZ	NifZ	serves as a key factor in the stepwise maturation of P-clusters		
nıjz		in NifDK, possibly through a chaperone-like function		
nifM	NifM, peptidyl-proyl <i>cis-trans</i> isomerase	involved in the maturation of Fe protein		
nifX	NifX	proposed intermediate carrier in M-cluster assembly		
nifY	NifY	proposed intermediate carrier in M-cluster assembly		
nafY	NafY	proposed intermediate carrier in M-cluster assembly		
nifW	NifW	putative role in protecting nitrogenase from oxygen damage		
nifO	NifO	function unknown, although it resembles thioredoxin		
nifT	NifT	Unknown function		
vnfH	VnfH, dinitrogenase reductase, component 2, reductase component, γ subunit, Fe protein	Mediation of ATP-dependent electron transfer during catalytic turnover, likely participates in biosynthesis of VnfDGK cofactors by analogy to <i>nif</i> system but this has not been shown		
vnfD,G,K	VnfDGK, dinitrogenase, component 1, catalytic component, VFe protein	Facilitates chemical transformation of N <sub>2</sub> to NH <sub>3</sub> and CO/CO <sub>2</sub> into hydrocarbons at the active cofactor site		
vnfE,N	VnfEN	Putative involvement in V-cluster biosynthesis by analogy to NifEN		
vnfA	-	serves as a positive transcription regulator of <i>vnf</i> genes, also correlated to expression of <i>anf</i> genes		
vnfX	VnfX	Unknown function		
vnfY	VnfY	Unknown function		
vnfO	VnfO	Unknown function		
vnfU	VnfU	Unknown function		
anfH	AnfH, dinitrogenase reductase, component 2, reductase component, γ subunit, Fe protein	Mediation of ATP-dependent electron transfer during catalytic turnover, may participate in biosynthesis of AnfDGK cofactors but has not been shown		
anfD,G,K	AnfDGK, dinitrogenase, component 1, catalytic component FeFe protein	Facilitates chemical transformation of N <sub>2</sub> to NH <sub>3</sub> at the active cofactor site		
anfA	-	serves as a positive transcription regulator of anf genes		
anfO	AnfO	Unknown function		
anfR	AnfR	Unknown function		
anfU	AnfU	Unknown function		

<sup>&</sup>lt;sup>a</sup> Adapted from ref 32 with additions from ref 17. <sup>b</sup> The essential gene set for Mo-nitrogenase maturation and activity is *nifHDKENB*.

While the topic of Mo-nitrogenase assembly has been covered in a number of reviews, there is currently little understanding of the assembly process for the alternative nitrogenases aside from indirect association to what is known about the Mo-dependent system. In light of this, a brief synopsis will be outlined in this portion of the review with a focus on the biosynthesis of the M-, V- and Fe-clusters. The intention is to emphasize the potential commonalities shared by the biosynthetic pathways of these analogous nitrogenase cofactors.

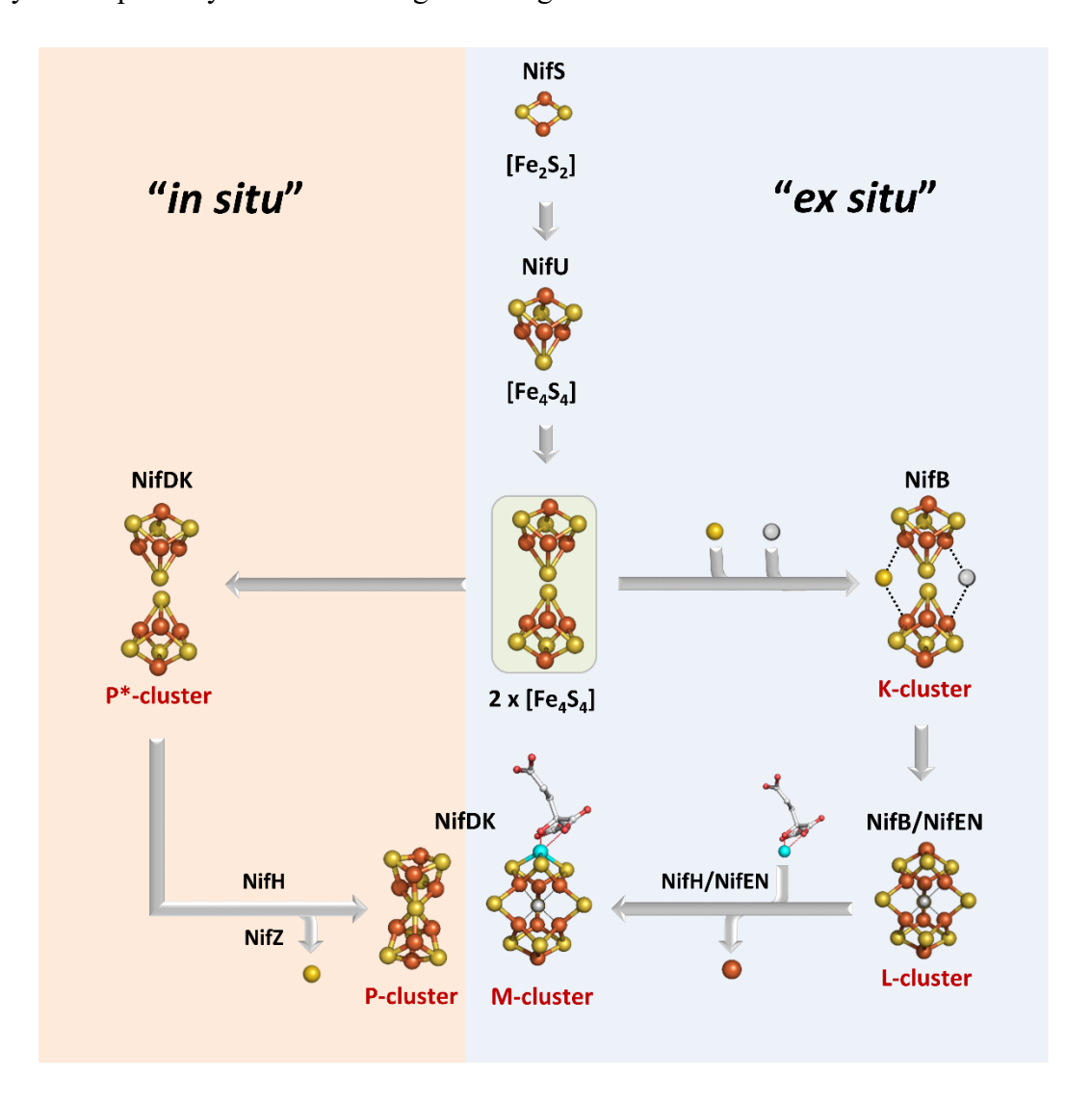


**Figure 1**. Flow diagram for the assembly of nitrogenase cofactors. The orange "in situ" pathway represents the assembly of the P-cluster on NifDK, whereas the blue "ex situ" block shows the assembly of the M-cluster. Assembly proteins are labeled in black; cluster species are labeled in red. Atoms are represented as ball-and-stick models and colored as follows: Fe, orange; S, yellow; C, grey; O, red; Mo, teal. Adapted with permission from ref 32. Copyright 2014 American Chemical Society.

The biosynthesis of the M-cluster starts with the assembly of [Fe<sub>4</sub>S<sub>4</sub>] units, composed of mobilized iron and sulfur (Figure 1).<sup>38,39</sup> In A. vinelandii the NifU and NifS gene products accomplish this task, 18 however, not all diazotrophs encode nifUS but alternative systems can be used. In the genome of *Paenibacillus* sp. WLY78, there is no encoded *nifUS*, but several genes exist that can facilitate the same function, including a complete suf (sufCBSUD) operon, and partial suf (sufABC) and isc (iscR and fdx) systems. <sup>17,40</sup> Additionally, it has been demonstrated that plasmids carrying the iscSUA and hscABfdx genes that encode for [Fe<sub>4</sub>S<sub>4</sub>] cluster assembly proteins can be used to heterologously express structural nitrogenase proteins from methanogenic organisms in Escherichia coli. 41 These FeS biosynthetic building blocks are then loaded onto NifB, the radical S-adenosyl-L-methionine (SAM)-dependent enzyme that serves as the site where the precursor 8Fe core (L-cluster) is generated. On NifB, two types of FeS clusters were found as predicted by sequence analysis.<sup>42</sup> The first is a [Fe<sub>4</sub>S<sub>4</sub>] cluster that is bound to a radical SAM-motif, referred to as the SAM cluster, 43 and the second type is actually a pair of [Fe<sub>4</sub>S<sub>4</sub>]-like clusters, known as the K-cluster, <sup>43</sup> that serves as building blocks for the L-cluster (Figure 1). When the NifB protein is reduced using dithionite (S<sub>2</sub>O<sub>4</sub><sup>2</sup>-), these two sets of metal clusters give rise to a composite EPR signal with g-values at 2.02, 1.95, and 1.90.43 Upon addition of SAM, this signal is greatly diminished, and is accompanied by the appearance of a signal at g = 1.94 associated with the L-cluster. 44,45 This observation pointed to a mechanism where the two [Fe<sub>4</sub>S<sub>4</sub>] components of the K-cluster fused into the 8Fe L-cluster through the action of radical SAM cleavage. Indeed, radiolabel tracing has provided strong evidence for this proposal, as a <sup>14</sup>C-labeled L-cluster can be generated through the addition of [methyl-<sup>14</sup>C] SAM to NifB. 46,47 The carbon labeling along with the detection of the reaction product S-adenosyl-Lhomocysteine (SAH), was strongly indicative of a S<sub>N</sub>2-type methyl transfer reaction. This is a common reactivity among SAM enzymes, <sup>48</sup> and implied that the SAM cluster transferred carbon to the substrate K-cluster, which gave rise to the central carbide of L-cluster. The reaction of SAM with NifB (Figure 2) also yielded 5'-deoxyadensine (5'dA), indicating involvement of a 5'-deoxyadensyl radical (5'dA'). Deuterium labeling demonstrated that the radical species was involved in the hydrogen abstraction of the methyl group that was transferred to the K-cluster. 46 Furthermore, methanethiol (CH<sub>3</sub>SH) was also detected upon acid quenching of the reaction, demonstrating that the SAM-derived methyl group is transferred to an acid-labile sulfur atom instead of an iron atom associated with the K-cluster. 49 More recently, the site-directed

mutagenesis of NifB has led to the identification of the so-called K2 cluster, one 4Fe half of K-cluster that is coordinated by Cys<sup>264</sup>, Cys<sup>274</sup> and Cys<sup>277</sup>, as being the site of methyl transfer.<sup>50</sup> The other half of K-cluster, designated as the K1 cluster, is coordinated by Cys<sup>30</sup>, Cys<sup>63</sup> and Cys<sup>129</sup>, and was studied using advanced pulse EPR techniques and a NifB variant carrying only the K1 cluster.<sup>50</sup> It was demonstrated that a histidine ligand from the protein might be coordinating to the K1 module and this coordination was lost upon the conversion of K- to L cluster.<sup>50</sup> Further analysis of NifB is currently hindered by a lack of a reported crystal structure.

Taken together, a mechanistic model emerges where the conversion of the K-cluster begins with the S<sub>N</sub>2-methyl transfer reaction from the first molecule of SAM to the K2 cluster, followed by hydrogen atom abstraction of the K2-bound methyl group by 5'dA' to generate a substrate bound methylene radical (Figure 2). This would then trigger a core rearrangement, possibly facilitated by the His ligand on K1, and the two K-cluster modules would fuse to form an [Fe<sub>8</sub>S<sub>8</sub>C] core. Biochemical and spectroscopic characterization of this core, designated the L\*cluster, suggested that it might have very similar topology compared to the L-cluster, with the so-called "9th-sulfur" atom missing. 51 XAS analysis detected a slightly more open conformation of L\*-cluster compared to L-cluster, and collectively, this was interpreted to mean that the missing 9<sup>th</sup> sulfur atom on L\*-cluster was from one of the three 'belt'  $\mu_2$ -sulfide positions.<sup>52</sup> Surprisingly, the source of the 9<sup>th</sup>-sulfur atom is not derived from SAM or NifS as previously understood, <sup>53,54</sup> but rather from sulfite (SO<sub>3</sub><sup>2-</sup>) in solution. <sup>51 35</sup>S tracing experiments conclusively showed the sulfur incorporation into L-cluster from sulfite by incubating <sup>35</sup>SO<sub>3</sub><sup>2-</sup> with NifB and SAM.<sup>51</sup> Sulfite is one of the three central hubs of prokaryotic sulfur metabolism,<sup>55</sup> the other two being sulfate (SO<sub>4</sub><sup>2</sup>-) and sulfide (S<sup>2</sup>-), and this intriguing finding offers a potential link between nitrogenase cofactor biosynthesis and cellular sulfur metabolism. Another interesting connection can also be drawn to the potential involvement of a bridging  $\mu_2$  sulfur atom in catalysis. As observed in Mo- and V-nitrogenase, the S2B atom that bridges between Fe2 and Fe6 in M- and V-clusters was displaced by incoming inhibitor or substrate-like ligand (See Sections 3 and 5). The mechanism of this process remains unclear, but it could bear similarities with the sulfur incorporation process observed for the L\*-cluster.

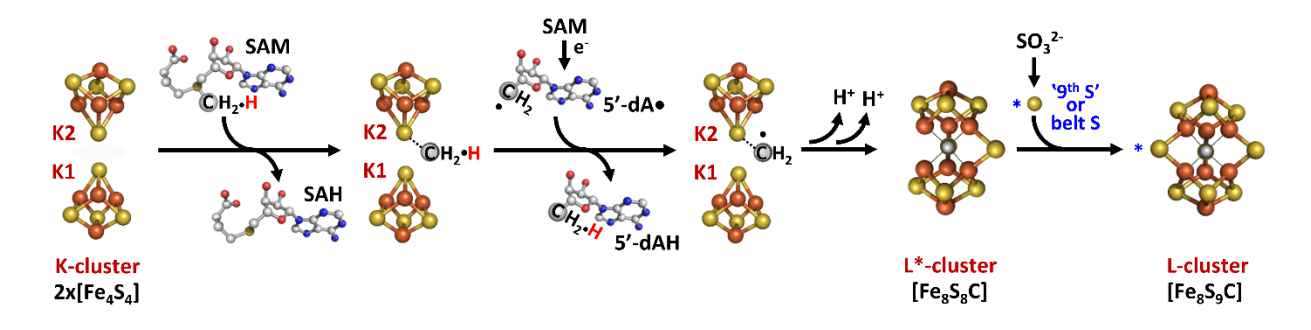


**Figure 2**. Proposed model for L-cluster assembly on NifB. Cluster species are represented as ball-and-stick models with N atoms as colored in blue and the other atoms colored as described in Figure 1. Adapted with permission from ref 51. Copyright 2018 Springer Nature.

In Mo-nitrogenase, the L-cluster is transferred from NifB to NifEN after its formation. NifE and NifN are paralogs of NifD and NifK, and as mentioned above, NifEN is a scaffold necessary for nitrogenase assembly. On NifEN, maturation of the L- to M-cluster occurs through the participation of NifH, which mobilizes both molybdate (MoO<sub>4</sub><sup>2</sup>-) and R-homocitrate, subsequently interacting with NifEN in order to insert these components into the L-cluster. 56,57 This process *in vitro* requires the hydrolysis of ATP and a high concentration of dithionite as reductant.<sup>57</sup> The role of NifH as Mo/homocitrate insertase was suggested by Mo K-edge XAS analysis, which pointed to a change in the oxidation state and the coordination environment of the NifH-bound Mo.<sup>58</sup> EPR analysis also revealed perturbations to the [Fe<sub>4</sub>S<sub>4</sub>] cluster of NifH as Mo/homocitrate were loaded onto the protein.<sup>58</sup> Additionally, Mo/homocitrate-loaded NifH could be separately purified and then reused as a reagent for the conversion of L- to M-cluster. After Mo and homocitrate insertion, NifEN undergoes a conformational rearrangement in which the newly matured M-cluster becomes less solvent exposed.<sup>59</sup> In vitro experiments demonstrated that the M-cluster containing NifEN can then form a direct protein-protein complex together with apo-NifDK (i.e. M-cluster deficient yet P-cluster intact NifDK). 60 In this complex, the Mcluster is directly transferred and inserted into the NifDK protein through a positively charged funnel of amino acid residues that also allows for the facile reconstitution of apo-NifDK with isolated M-cluster (or V-cluster, see Section 4).<sup>61</sup> The ferrying of the M-cluster between NifEN and NifDK is made possible because NifEN lacks a number of key residues that either provide a covalent ligand for the cluster or sterically enclose the M-cluster within a positively charged insertion channel, analogous to that found in NifDK. 33,36,62

In the V-nitrogenase system from A. vinelandii, cofactor assembly diverges from the Modependent pathway as the NifB-bound L-cluster is likely transferred onto VnfEN instead of NifEN (Figure 3). Based on the high sequence homology between NifEN and VnfEN due to a gene duplication event, as well as the homology between NifH and VnfH, a similar mechanism of L-cluster maturation could be proposed in the alternative nitrogenase systems to make V- and Fe-cluster on VnfEN. This is substantiated by the fact that the residues ligating to the L- and Mclusters on NifEN are all conserved in VnfEN.<sup>31</sup> Moreover, the expression of nifV, coded for homocitrate synthetase, has been observed when A. vinelandii cultures were grown under V- and Fe-nitrogenase expressing conditions, lending further support for this proposal. <sup>18,38</sup> In addition, it has been shown that attempts to insert V and R-homocitrate into the L-cluster using NifEN and NifH have led to a cluster species with low V occupancy and limited ability to reconstitute and activate apo-NifDK.<sup>63</sup> This observation emphasizes the optimization of NifEN/NifH and VnfEN/VnfH for the insertion of Mo and V atoms, respectively. In contrast, the combination of VnfEN/AnfH appears to be responsible for the *in vivo* biosynthesis of Fe cluster. In A. vinelandii deletion of the vnfEN gene was previously shown to eliminate the synthesis of functional V- and Fe-nitrogenases, <sup>64</sup> and transcriptome analysis also demonstrated that the *vnfEN* gene is highly overexpressed (as much as 50-fold from baseline) under nitrogen fixing conditions in the absence of Mo-nitrogenase. 18 By analogy to the Mo-nitrogenase system, V- or Fe-cluster could be delivered directly from VnfEN to its target via protein-protein interactions (Figure 3). If this hypothesis holds true, it would also imply that VnfEN might be able to dock to both VnfDGK and AnfDGK to deliver the V- and Fe-clusters respectively. This is conceivable, considering the homology between NifEN and VnfEN, but also between NifDK, VnfDKG and AnfDKG.<sup>38</sup> Significantly, a number of residues that have been suggested to be important for the M-cluster insertion in NifD are either observed or substituted to similar residues in VnfD as well as in AnfD.<sup>38</sup> This provides a rudimentary framework for future investigations of the alternative nitrogenase assembly.

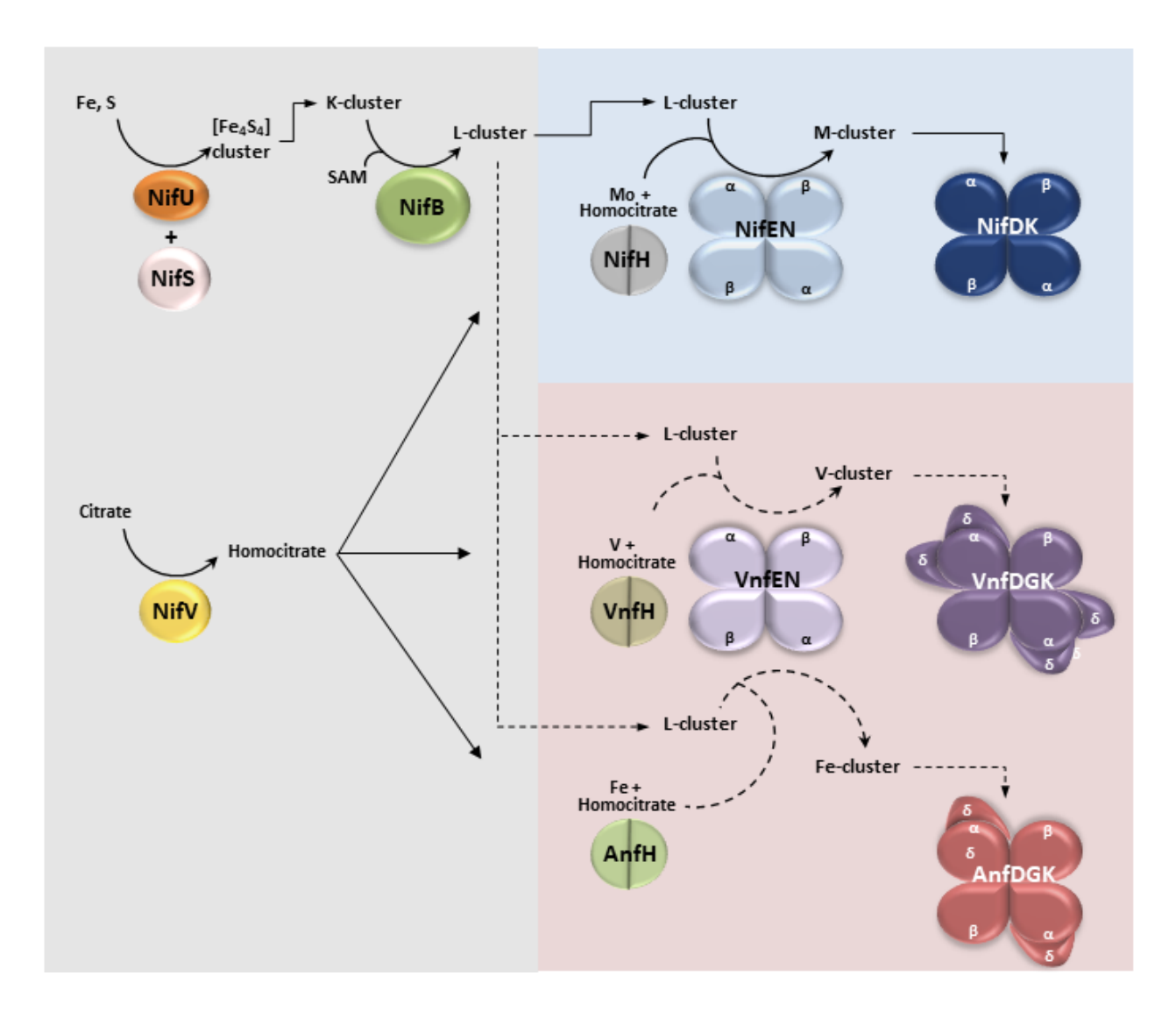


**Figure 3**. Proposed pathways for M-, V- and Fe-cluster biosynthesis. Area shaded in gray represents the common portion of the pathway, including the proteins NifU, NifS, NifV and NifB. Area shaded in blue represents the M-cluster specific maturation pathway, and the red shaded area depicts the V- and Fe-cluster specific maturation pathways. Experimentally verified steps are indicated by solid arrows whereas putative assignments are indicated by dotted arrows. See the main text for detailed descriptions.

## 3. Structure and Properties of Nitrogenase Proteins

A key to understanding nitrogenase has come from the structural and spectroscopic analysis of the two protein components and the transition metal cofactors housed therein.<sup>65,66</sup> In 1992, Rees and co-workers solved the crystal structures of both the catalytic (NifDK)<sup>67,68</sup> and reductase (NifH) components<sup>69</sup> of the Mo-dependent nitrogenase from *A. vinelandii*. These structures, along with the structure of the NifH:NifDK complex<sup>70,71</sup> provided necessary three-

dimensional depictions of the enzyme in various states. This allowed for the contextualization of much of the spectroscopic and biochemical analysis that had been accumulated to that point. While the extent of this characterization for the Mo-dependent system is vast, relatively little is available for the Mo-independent nitrogenases in comparison. Initial structural information came in 1987 and 1988 from XAS analysis of the VFe proteins from *A. vinelandii* and *Azotobacter chroococcum* using the unique V atom as a spectroscopic probe, <sup>72,73</sup> but a crystal structure would not be solved until 2017 when Sippel and Einsle reported the structure of the *Av* VFe protein. <sup>74</sup> The following year, the structure of the Fe protein from the V-dependent system, VnfH, was also reported by Einsle and co-workers. <sup>75</sup> Crystal structures from the Fe-only nitrogenase have not yet been reported, though in 2002, Fe K-edge XAS and <sup>57</sup>Fe Mössbauer spectroscopy were used to analyze the cofactors of the FeFe protein from *R. capsulatus*, and this study suggested there is structural homology to the Mo- and V-nitrogenases. <sup>76</sup>

In general, the proteins from the different nitrogenase systems are broadly similar and share common structural features. For the reductase proteins, each contain a [Fe<sub>4</sub>S<sub>4</sub>]-cluster and nucleotide binding sites that facilitate the obligate electron transfer coupled to ATP hydrolysis during catalysis.<sup>77</sup> On the other hand, the catalytic proteins contain two different cluster species; one is the [MFe<sub>7</sub>S<sub>9</sub>C-(*R*)-homocitrate] (M = Mo, V, Fe) cluster called the Mo-, V-, or Fe-cluster for the respective nitrogenase system and is the active site of substrate reduction, whereas the other cluster is the [Fe<sub>8</sub>S<sub>7</sub>] P-cluster, responsible for the transfer of electrons between the reductase and the active site.<sup>65,66</sup> Each of these clusters also have spectroscopic properties that have been used to generate structural models prior to the availability of crystallographic evidence. Additionally, the V- and Fe-only nitrogenases also contain an additional cofactorless protein subunit that Mo-nitrogenase lacks. This section will cover the structural similarities and differences between the nitrogenase systems, and as the focus of this review is on the alternative nitrogenases, details will be briefly summarized for the Mo-dependent variant.

# 3.1. The Characterization of the Reductase Components – NifH, VnfH and AnfH

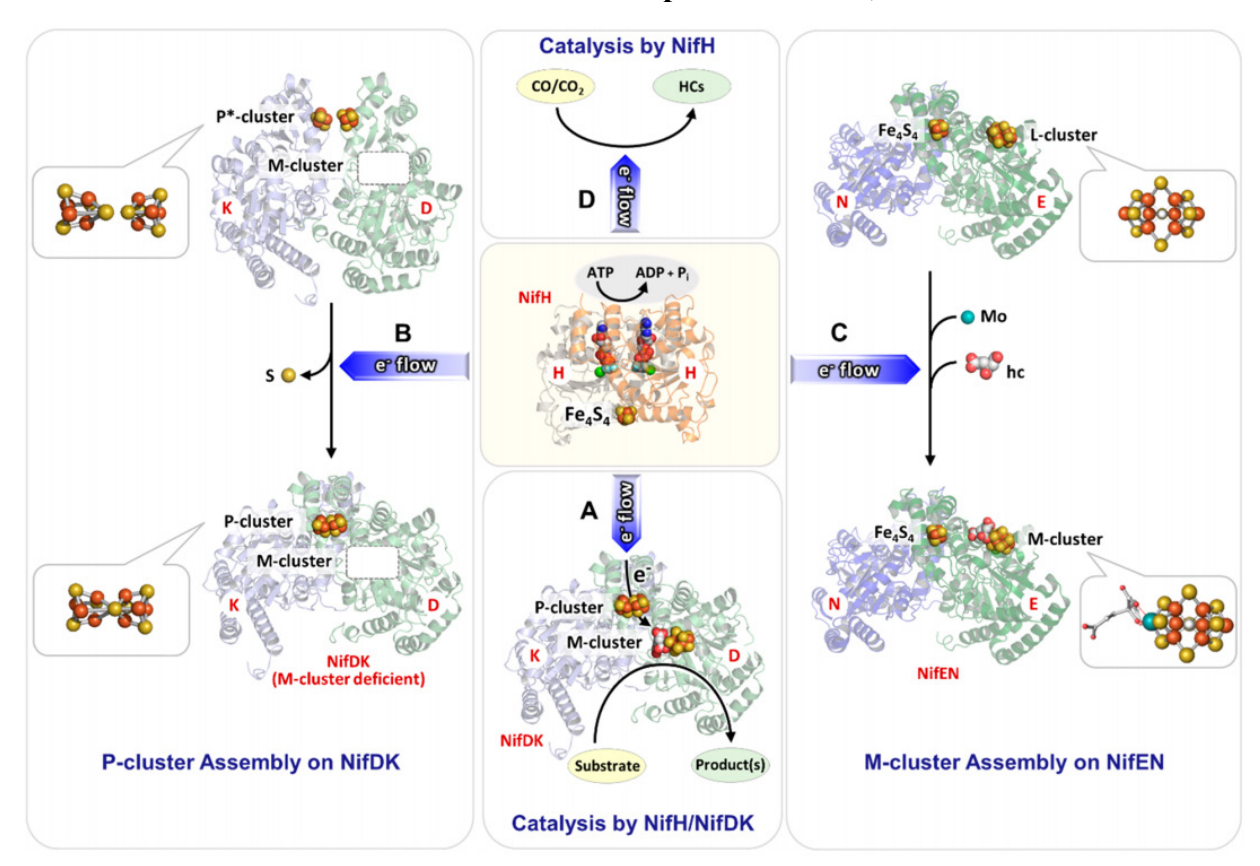


**Figure 4**. An overview of the functions of the Fe protein, as exemplified by NifH. Atoms are represented by ball-and-stick models with coloration as described in Figure 2. Reproduced with permission from ref 78. Copyright 2019 American Chemical Society.

The reductase proteins of nitrogenase, also referred to as the Fe protein, component 2, or by the gene product (NifH, VnfH, AnfH for Mo-, V-, and Fe-only nitrogenases, respectively), are critical for both substrate turnover and for the biosynthesis of the clusters (Figure 4).<sup>77</sup> The best characterized protein, *Av* NifH, has been recognized for three primary functions: (1) Mo and homocitrate insertase for the maturation of the precursor L-cluster to the M-cluster;<sup>58</sup> (2) reductase that carries out P-cluster synthesis on the catalytic NifDK protein;<sup>34,79-82</sup> (3) obligate electron transfer partner to NifDK for substrate turnover with concomitant hydrolysis of two ATP molecules per electron.<sup>83</sup> Additionally, NifH and VnfH were also found to be capable of the interconversion of CO<sub>2</sub> to CO, a reactivity that will be discussed in Section 4.7. While the Fe proteins all have been shown to behave as reductases for catalysis as in function 3, functions 1 and 2 for VnfH and AnfH have yet to be demonstrated experimentally. However, there is a high

degree of structural similarity between the Fe proteins despite differences in sequence. Although, VnfH is more similar to NifH than is AnfH (91% and 61% homology, respectively),<sup>35</sup> so there is an underlying assumption that each protein will function analogously. This allows for the cautious application of insights gained from one system (Mo-dependent) to the others.

## 3.1.1 Crystal Structures of NifH and VnfH

The Mo-nitrogenase reductase component, NifH, is encoded by the *nifH* gene and forms a homodimer (γ<sub>2</sub>) approximately 60 kDa in size (Figure 5A).<sup>69</sup> The protein contains a [Fe<sub>4</sub>S<sub>4</sub>] cluster positioned on a 2-fold rotation axis at the subunit interface, bound by the Cys97 and Cys132 residues from each subunit. The reductase from V-nitrogenase, VnfH, is similarly sized (~60 kDa) and analogously structured, with Cys98 and Cys133 from each monomer providing a binding site for the [Fe<sub>4</sub>S<sub>4</sub>] cluster (Figure 5B). NifH and VnfH also bind nucleotides, one molecule to each subunit, in a Walker's motif A protein fold, 84 found between residues 9 and 16 (or residues 11 to 17 in VnfH). <sup>69,75</sup> In the 1992 structure of NifH, an ADP molecule was modeled in with partial occupancy in this position, though subsequent reports yielded a structure with MgADP bound to Av NifH, 85 as well as a structure with MgATP bound to a Av NifH variant that is unable to hydrolyze ATP.86 In contrast, the crystal structure of VnfH has only been reported with MgADP bound, and this overlays well with the analogous MgADP-bound NifH structure.<sup>75</sup> The structures of the nucleotide-bound or free NifH proteins are rather similar, and only show minor conformational changes between the nucleotide-bound and unbound states.<sup>77</sup> This finding initially conflicted with earlier biochemical and spectroscopic studies that implied there should be changes to the protein and/or [Fe<sub>4</sub>S<sub>4</sub>] cluster upon addition of nucleotide. The EPR spectra of Av NifH (and Av VnfH) become broadened in the presence of nucleotide, 66,87 indicating a connection between the [Fe<sub>4</sub>S<sub>4</sub>] cluster and the coordination of the nucleotide ~20 Å away from the cluster. Chelation agents such has bathophenathrolinedisulfonate or 2,2'-bipyridine are limited or unable to extract Fe from the [Fe<sub>4</sub>S<sub>4</sub>] cluster of NifH, but in the presence of MgATP the Fe is rapidly removed. 88-90 This indicated that in the presence of nucleotide, the cluster becomes more solvent exposed. Additionally, structural perturbations were measured for NifH using small angle X-ray scattering (SAXS) which showed an observable change to the protein conformation in the presence of MgATP compared to the MgADP-bound or nucleotide-free species. 91 Collectively, these observations are consistent with a more dynamic structure of NifH

(and by analogy, VnfH and AnfH) that can selectively expose the [Fe<sub>4</sub>S<sub>4</sub>] cluster to solvent in the presence of nucleotide.

In 1997<sup>70</sup> and later in 2005<sup>71</sup> structures of the NifH:NifDK complex were reported that helped clarify the discrepancy between the solution state and solid state characterizations of NifH. The two nitrogenase components form a 2:1 complex, with one NifH unit binding to each αβ heterodimer of NifDK. Additionally, this complex had been crystallized with nucleotide-free, MgADP-bound and non-hydrolysable MgATP analog-bound (MgADP•AlF4 and MgAMPPCP) NifH proteins. If the Fe protein portions of the crystal structures are compared and overlaid (Figure 5C), the overall structures of the polypeptide are rather similar, but there is a ~3 Å displacement of the cluster between the nucleotide-bound and nucleotide-free states of the protein, with the MgATP analog-bound variant being the most exposed. <sup>71,77</sup> This observation is in agreement with the solution studies, and likely reflects the structural changes that may be operative in the solution state. Unfortunately, structures of the VnfH:VnfDGK complex or of any Fe-only nitrogenase proteins are not yet available, but these species would likely be structurally similar to the partners in the Mo-dependent system.

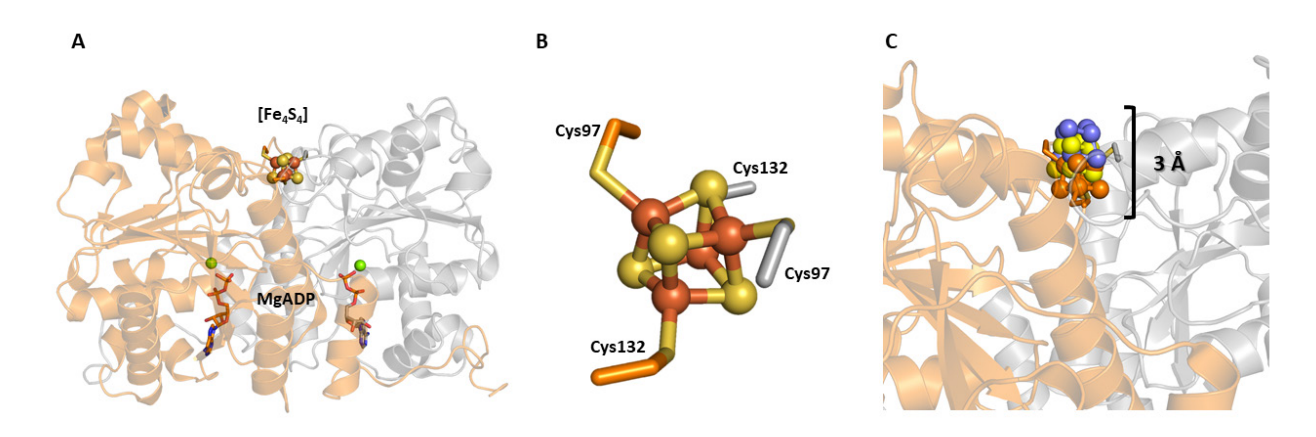


**Figure 5**. Crystal structure of NifH and the effect of nucleotide binding on [Fe<sub>4</sub>S<sub>4</sub>] position. A: Crystal structure of the MgADP-bound Av NifH (PDB ID 1FP6) with each subunit of the homodimer ( $\gamma_2$ ) colored differently (orange and grey). B: [Fe<sub>4</sub>S<sub>4</sub>] cluster of NifH. C: Overlay of [Fe<sub>4</sub>S<sub>4</sub>] clusters of the nucleotide bound (ATP analog in blue, ADP in yellow) and nucleotide free forms of NifH.

# 3.1.2 Solution and Spectroscopic Properties of Fe Proteins

The  $[Fe_4S_4]$  cluster of the Fe protein can support three oxidations states,  $[Fe_4S_4]^0$ ,  $[Fe_4S_4]^{1+}$ , and  $[Fe_4S_4]^{2+}$ , which is relatively uncommon for FeS proteins, as they generally

support the two redox states required for one electron transfers.  $^{77,92}$  During catalytic turnover, the Fe protein is proposed to cycle between the reduced  $[Fe_4S_4]^{1+}$  and oxidized  $[Fe_4S_4]^{2+}$  states, and the reduction of the Fe protein is driven *in vivo* by a physiological reductant such as flavodoxin or ferredoxin.  $^{93-97}$  During *in vitro* studies, the ubiquitous chemical reductant dithionite  $(S_2O_4^{2-})$  stabilizes the  $[Fe_4S_4]^{1+}$  state, whereas redox active dyes such as viologens or indigodisulfonate (IDS) can be used to oxidize the protein to the  $[Fe_4S_4]^{2+}$  state.  $^{66}$  The  $[Fe_4S_4]^0$  state is the so called all-ferrous "super-reduced" state first reported in Av NifH by Watt and Reddy,  $^{98}$  but the nature and relevance of this species is still controversial, and this will be discussed below.

The redox properties of the Fe proteins have been studied through potentiometric titrations, as opposed to other electrochemical methods. The midpoint potential  $(E_m)$  for the [Fe<sub>4</sub>S<sub>4</sub>]<sup>2+/1+</sup> redox couple in Av NifH was found to be approximately –300 mV versus the standard hydrogen electrode (SHE) at pH 8 in an Ar atmosphere. 99,100 The potentials for NifH and VnfH from A. vinelandii were also determined in a CO<sub>2</sub> atmosphere and found to be -301 mV and -346 mV versus SHE, respectively. 87 When nucleotides are bound to the Fe proteins, the midpoint potentials decrease by ≥100 mV, consistent with the biochemical characterization described in Section 3.1.1. In an atmosphere of argon, potential values of  $E_{\rm m} = -430~{\rm mV}$  and -440 mV versus SHE were found for the MgATP- and MgADP-bound species of Av NifH, respectively. 99,100 The midpoint potential for the [Fe<sub>4</sub>S<sub>4</sub>]<sup>2+/1+</sup> couple for both NifH and VnfH from A. chroococcum with MgADP bound had also been determined, with values of -450 mV and –463 mV versus the normal hydrogen electrode (NHE). <sup>101</sup> This showed that the potentials for both Av and Ac NifH are similar to each other. Interestingly, the  $E_{\rm m}$  values shift by approximately +30 mV for MgADP-bound Av NifH and Av VnfH (compared to Ac VnfH) in an atmosphere of CO<sub>2</sub> (-405 mV and -430 mV versus SHE, respectively).<sup>87</sup> This observation could be consistent with CO<sub>2</sub> interacting with the [Fe<sub>4</sub>S<sub>4</sub>] clusters of the Fe proteins, as these have been shown to facilitate the reversible conversion of CO<sub>2</sub> into CO (See Section 4.7).

EPR and Mössbauer spectroscopies have also been invaluable techniques for the study of the Fe proteins, as each cluster oxidation state has associated signals that can be used to understand the electronic properties of the protein. In all cases, the fully oxidized  $[Fe_4S_4]^{2+}$  state of the Fe protein is EPR silent, and so with Av NifH, Mössbauer spectroscopy was employed to determine that the species was diamagnetic with an S = 0 ground spin state. The  $[Fe_4S_4]^{1+}$ 

state, the resting state of the cluster in the presence of dithionite, was also studied using parallel EPR and Mössbauer experiments. Av NifH was reported with a mixture of two spin states (Figure 6) in roughly equal proportions, one S = 1/2 species and one S = 3/2 species (Table 2). The S = 1/2 species had a rhombic signal with g-values of 2.05, 1.94, and 1.88, referred to as the "g = 1.94 signal," and the signal was consistent with spectra obtained from other [Fe<sub>4</sub>S<sub>4</sub>]<sup>1+</sup> species. <sup>102,103</sup> On the other hand, the S = 3/2 species had an axial signal with g = 5.8, 5.15, and this spin state is unique to the nitrogenase Fe proteins. <sup>102,103</sup> The ratio of the mixture could be modulated through additives such as glycerol (Figure 6), which pushed the mixture to primarily S = 1/2, or urea, which shifts the spectra to the opposite composition. <sup>102</sup> Similar EPR signals have also been reported for VnfH from A. vinelandii and from the methanogenic archaeon M. acetivorans, as well as Av AnfH (Table 2). <sup>35,87,104</sup> Nucleotide binding to the Fe proteins broaden the line shapes of both sets of signals, but this does not strongly change the spin state mixture of the protein-bound cluster. <sup>87,103-105</sup>

The controversial "super-reduced" state, at the time of discovery, represented the first [Fe<sub>4</sub>S<sub>4</sub>]-containing species with all of the Fe centers having the 2+ oxidation state; 98 VnfH from A. vinelandii and from M. acetivorans were subsequently shown to support the  $[Fe_4S_4]^0$  state as well. 87,104 The physiological relevance of the super-reduced Fe protein is not clear, but Watt has proposed the 2-electron [Fe<sub>4</sub>S<sub>4</sub>]<sup>2+/0</sup> couple to be operative in nitrogenase. This would allow for concomitant hydrolysis of only two molecules of ATP (compared to four ATP molecules), and NifH could then function more efficiently than as a 1-electron agent. 106 However, the experiments discussed below by Burgess, Farmer and co-workers are not in agreement with this proposal.<sup>107</sup> The generation of these species has been reported using several reductants; methyl viologen and flavodoxin hydroquinone yield a brown colored protein, whereas Ti(III)citrate, Cr(II)EDTA (EDTA = ethylenediaminetetraacetic acid) or a Eu(II)-reductant yield Fe protein that has a red-pink color in contrast to the typical brown hues associated with other FeS proteins.  $^{87,98,104,106,108,109}$  The  $[Fe_4S_4]^{1+/0}$  redox couple has been assessed for Av NifH, though, there are discrepancies in the reported midpoint potentials depending on the method of measurement. In the initial 1994 report by Watt, reduced methyl viologen was used as a titrant and an E<sub>m</sub> value of -460 mV versus NHE was determined. 98 Subsequently in 2006, Watt reported that the all-ferrous Fe protein could also be generated using the flavodoxin hydroquinone from A. vinelandii ( $E_m = -515$  mV versus NHE), resulting in the same species that is generated from methyl viologen. <sup>106</sup> In contrast, Burgess, Farmer and co-workers in 2002 used the more reducing Cr(II)EDTA (-1 V versus NHE at pH 8) as the redox titrant, and determined the  $E_{\rm m}$  for the all-ferrous redox couple to be  $-790~{\rm mV}$  versus NHE. <sup>107</sup> Additionally, they reported that the use of reduced methyl viologen or the hydroquinone form of flavodoxin II resulted in no observable reduction of the [Fe<sub>4</sub>S<sub>4</sub>]<sup>1+</sup> state to all-ferrous NifH.<sup>107</sup> The superreduced state of Av NifH has also been analyzed in detail using a variety of spectroscopic and computational methodologies. 98,106,108,110-112 The [Fe<sub>4</sub>S<sub>4</sub>]<sup>0</sup> species reported by Watt and coworkers was found to have an EPR silent S = 0 ground state, measured using the Evans method but not Mössbauer spectroscopy. 98,106 The super-reduced Av NifH generated using Ti(III) citrate is the best characterized, with an observed g = 16.4 signal in the parallel mode EPR spectrum,  $^{108,112}$  consistent with an S=4 ground state established from Mössbauer spectroscopy and density functional theory (DFT) calculations. 108,110-112 The Av and Ma VnfH proteins treated with Eu(II) reductants also show a similar EPR signal, but lack Mössbauer characterization. 87,104 However, the Cr(II)EDTA reduced Av NifH protein has only been studied using electrochemical methods and UV-visible absorption spectroscopy, but has similar absorption features as the Ti(III)citrate-reduced Fe protein. 107

This set of seemingly contradictory results involving the  $[\text{Fe}_4\text{S}_4]^0$  state of the Fe protein does not lend itself to clear interpretation. The best characterized example is the Ti(III)citrate-reduced Av NifH protein, but this species lacks a measured midpoint potential. Electrochemical measurements were carried out for the Cr(II)EDTA-reduced Fe protein, and this species has similar UV-vis absorption features as the Ti(III)citrate-reduced protein (red-pink color) but lacks EPR or Mössbauer spectroscopic characterizations. <sup>107</sup> Additionally, the Av and Ma VnfH proteins treated with Eu(II) also share a red-pink color as well as similar EPR signals as the Ti(III)citrate-reduced species, but lack a measured midpoint potential or study by Mössbauer spectroscopy. <sup>87,104</sup> In a sense, the proteins produced under these conditions could all reflect the same species, but without analogous characterization for every condition, it is difficult to determine with certainty. This set of  $[\text{Fe}_4\text{S}_4]^0$  Fe proteins also differs from the diamagnetic methyl viologen/flavodoxin hydroquinone-reduced protein that has a brown color and an  $E_m$  value that is 330 mV more positive than the Cr(II)-reduced species. <sup>106,107</sup> One interpretation is that the all-ferrous Fe protein can exist in two different spin states, one that is capable of functioning under physiological conditions (S = 0) and one that cannot (S = 4) because of the

potentials required to generate the species. The possibility of a spin state mixture is not unprecedented; it has been well established that the  $[Fe_4S_4]^{1+}$  state of NifH is a mixture of S=1/2 and S=3/2 states, the composition of which is highly dependent on the solvent and chemical additives. However, Watt and co-workers claim to generate the S=0 state while Burgess, Farmer and co-workers stated that reduction of the Fe protein with Watt's reported reductants was not possible. It is also unclear how such a spin state change would drastically affect the measured redox potentials. Another interpretation is that one of the forms of the  $[Fe_4S_4]^0$  state is an artifact, produced from adventitious binding of reductant molecules or other components of the solution. Further still, it is possible that neither form of the all-ferrous state of the Fe protein is relevant for the physiological function of nitrogenase. There is simply not enough information to clearly validate these interpretations, so additional characterization of the  $[Fe_4S_4]^0$  state of the Fe proteins remains necessary.

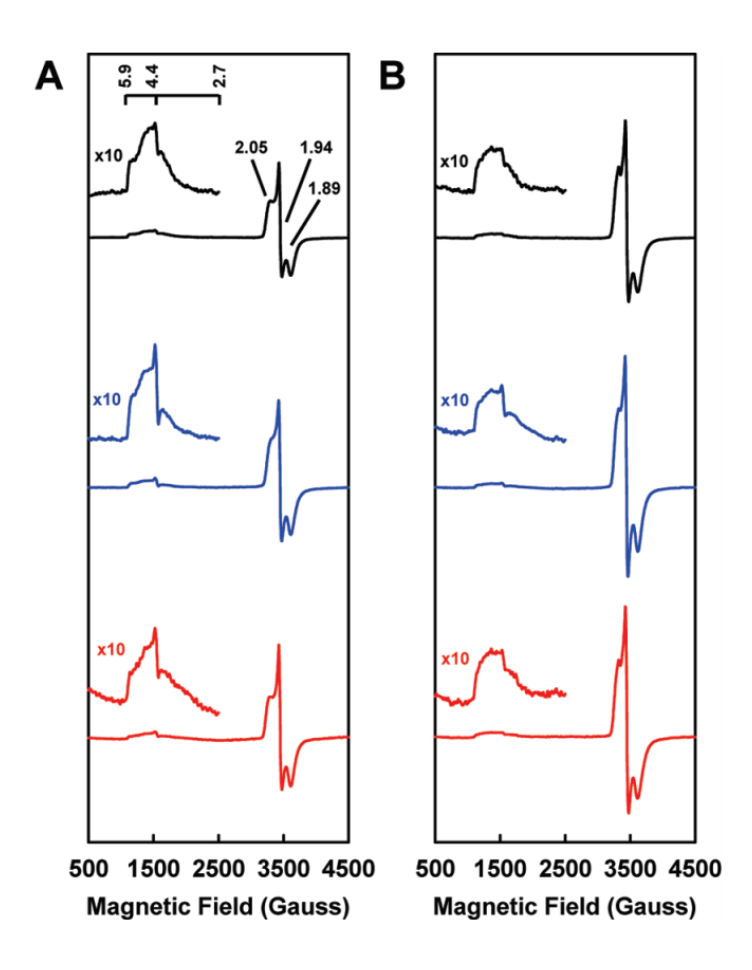


**Figure 6.** EPR spectra of Fe proteins in the dithionite-reduced form (NifH = black, VnfH = blue, AnfH = red) in the absence (A) or presence (B) of 50% glycerol. Reproduced with permission from ref 35. Copyright 2011 American Chemical Society.

Table 2. EPR features of the Fe protein components from A. vinelandii<sup>a</sup>

Protein	Oxidation state	Nucleotide	Spin State (S)	g-values	refs
	$[Fe_4S_4]^{2+}$	-	0	-	102
	$[Fe_4S_4]^{1+}$		1/2	2.05, 1.94, 1.88	102
NifH	[[6484]	-	3/2	5.8, 5.15	
	$[Fe_4S_4]^{1+}$	ADP	1/2	2.02, 1.92	105
			3/2	4.8	
	$[Fe_4S_4]^{1+}$	ATP	1/2	2.02, 1.92	103,105
			3/2	4.8	,
	$[Fe_4S_4]^0$	-	0	-	98,106
	$[Fe_4S_4]^0$	-	4	16.4	108,112
VnfH <sup>b</sup>	$[Fe_4S_4]^{2+}$	-	0	-	87
	$[Fe_4S_4]^{1+}$	-	1/2	2.05, 1.94, 1.89	35,87
			3/2	5.9, 4.4	,
	$[Fe_4S_4]^{1+}$	ADP	1/2	2.02, 1.92	104
			3/2	Unresolved	
	$[Fe_4S_4]^{1+}$	ATP	1/2	2.02, 1.92	104
			3/2	unresolved	
	$[Fe_4S_4]^0$	-	4 <sup>c</sup>	16.4	87
AnfH	[Fe <sub>4</sub> S <sub>4</sub> ] <sup>1+</sup>	-	1/2	2.05, 1.94, 1.89	35
			3/2	5.9, 4.4	

<sup>&</sup>lt;sup>a</sup> X-band EPR spectra collected at temperatures between 2 and 12 K. <sup>b</sup> The *Ma* VnfH data from ref <sup>104</sup> is similar to the *Av* VnfH data shown. <sup>c</sup> This spin state assignment has not been made from Mössbauer or other analysis, but by analogy to the NifH system.

As discussed previously, the crystal structures of the free NifH proteins in various states had very similar physical metrics despite changes in the biochemical behavior that suggested otherwise (See Section 3.1.1). The structure of *Av* NifH with the [Fe<sub>4</sub>S<sub>4</sub>]<sup>0</sup> state has also been reported, 113 but similar to the other structures, the bonding metrics of the cluster do not vary from the more oxidized species discussed above. This difference could be due to experimental limitations, such as oxidation reactions that occur during the crystallization process or radiation damage to the protein during data collection, but could also could reflect accurate bond metrics. One method to further assess the solution state structural properties of the Fe protein [Fe<sub>4</sub>S<sub>4</sub>] clusters is the use of X-ray absorption spectroscopy. 35,114 The Fe K-edge XAS analysis was reported for all three Fe proteins from *A. vinelandii* in the dithionite-reduced [Fe<sub>4</sub>S<sub>4</sub>]<sup>1+</sup> state. The extended X-ray absorption fine structure (EXAFS) region of the data can be used to obtain absorber-scatterer distances from the Fe atoms in the protein, and gain information about the

structural configuration. Largely, the structural metrics from EXAFS were fit similarly for NifH, VnfH and AnfH, with 4 Fe–S distances at ~2.30 Å, 1 short Fe---Fe distance at ~2.50 Å and 2 longer Fe---Fe scatterers at ~2.70 Å. 35 Additionally, NifH benefitted from the inclusion of a third Fe---Fe distance at 2.62 Å, distinguishing it from the other two proteins. These structural metrics differ slightly from the distances reported for the NifH and VnfH crystal structures (PDB codes 1G5P and 6Q93, respectively). 75,113 In both crystal structures, the Fe-S distances range from 2.3 to 2.4 Å which is in agreement with the EXAFS derived data, but the Fe---Fe distances for the NifH structure range between 2.6 and 2.7 Å, whereas the VnfH structure has distances that range between 2.7 and 2.8 Å. There is not an Fe---Fe length in either crystal structure consistent with the short ~2.50-Å pathway from the XAS model, but the longer 2.70-Å distance agrees with the crystallographically determined metrics. Overall, the combined X-ray absorption and X-ray diffraction data suggests that the clusters in both the crystal and in solution have similar structures and continues to support that the [Fe<sub>4</sub>S<sub>4</sub>] cluster remains in similar configuration in all three of the Fe proteins. It is also important to note that the MgADP molecule bound to VnfH in the crystal structure could be the source of the perturbation relative to the NifH structure, but additional data would be needed to explore this facet further.

## 3.2. The Properties of Mo-Nitrogenase

The Mo-nitrogenase from *A. vinelandii* is the best characterized nitrogenase system, though the catalytic proteins have also been isolated from *A. chroococcum*, *Klebsiella pneumoniae*, *Clostridium pasteurianum*, and *R. capsulatus*. <sup>66,115</sup> The *nifD* ( $\alpha$  subunit) and *nifK* ( $\beta$  subunit) genes encode for a heterotetrameric  $\alpha_2\beta_2$  protein, NifDK, that is ~220 kDa in size. <sup>65</sup> NifDK contains two different complex metalloclusters in each  $\alpha\beta$ -dimer that are essential for electron transfer and substrate turnover, designated as the P- and M-clusters (Figure 7). <sup>67,116,117</sup> The P-cluster is a [Fe<sub>8</sub>S<sub>7</sub>] cofactor that facilitates electron transfer from NifH to the M-cluster during catalysis, and the cluster is positioned at the  $\alpha/\beta$  interface of NifDK ~10 Å below the surface of the protein. <sup>67,118</sup> In the resting state, the P-cluster appears as two [Fe<sub>4</sub>S<sub>3</sub>] cubane cluster units that share a common vertex, a  $\mu$ <sub>6</sub>-sulfide, and is additionally ligated by two Cys residues ( $\alpha$ -Cys88,  $\beta$ -Cys95), each in a bridging mode. A total of six cysteine residues, three from each subunit, ( $\alpha$ -Cys62,  $\alpha$ -Cys88,  $\alpha$ -Cys154,  $\beta$ -Cys70,  $\beta$ -Cys95, and  $\beta$ -Cys153) coordinate

to the P-cluster. The M-cluster (also known as FeMoco) is a [MoFe<sub>7</sub>S<sub>9</sub>C-(R)-homocitrate] cofactor that is responsible for substrate reduction. This cluster is buried below the surface of the protein in each of the  $\alpha$  subunits of NifDK and is located ~19 Å from the P-cluster (Figure 7). The M-cluster appears as an asymmetric combination of two partial cubane units, [Fe<sub>4</sub>S<sub>3</sub>] and [MoFe<sub>3</sub>S<sub>3</sub>], with a  $\mu$ <sub>6</sub>-insterstitial carbide as a shared vertex, and is additionally bridged by three "belt"  $\mu$ <sub>2</sub>-sulfide ligands (Figure 8C). <sup>67,116,117,119</sup> The Mo atom is further coordinated to (R)-homocitrate by the 2-hydroxy and 2-carboxy groups of the organic acid. NifDK binds to the M-cluster though two amino acid residues;  $\alpha$ -Cys275 at the Fe-capped end and  $\alpha$ -His442 at the Mocapped end. <sup>32</sup> As mentioned in Section 3.1.1, NifDK can also form a 2:1 NifH:NifDK complex that places the [Fe<sub>4</sub>S<sub>4</sub>] cluster of the Fe protein between ~18 and 24 Å away from the P-cluster depending on if a nucleotide is bound (Figure 7). <sup>71</sup>

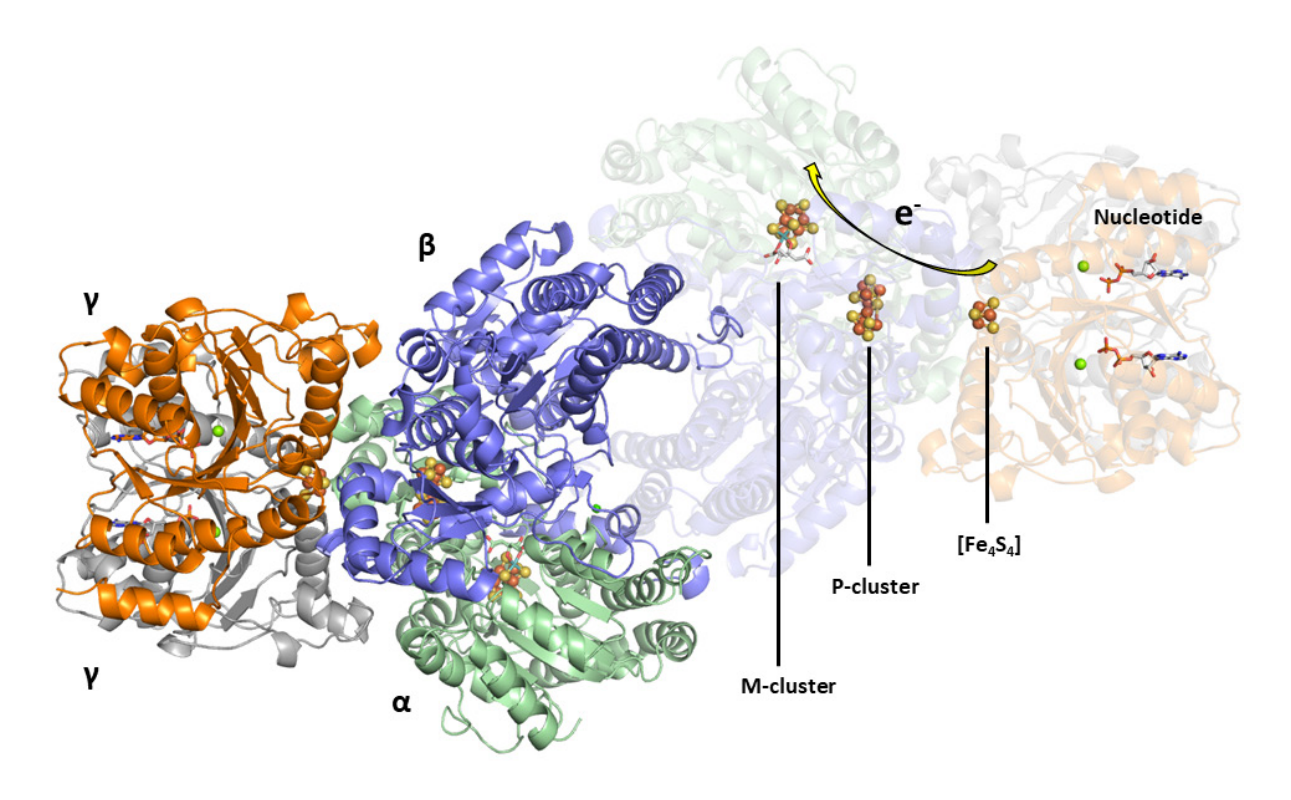


**Figure 7**. The crystal structure of the NifH:NifDK complex with [Fe<sub>4</sub>S<sub>4</sub>], P- and M-clusters shown (PDB ID 1N2C). The arrow shows the proposed flow of electrons through the enzyme. The coloring of the protein: NifD (green), NifK (blue), NifH (orange and grey). The clusters are represented as ball-and-stick models with the same coloration as described in Figure 2.

#### 3.2.1. P-cluster from NifDK

There are three recognized reversible states of the P-cluster in Mo-nitrogenase; the reduced P<sup>N</sup> state, the one-electron-oxidized P<sup>1+</sup> state and the two-electron-oxidized P<sup>OX</sup> state. The cluster can be further oxidized but it is not clear if there is physiological relevance due to observed degradation of the cluster.<sup>66</sup> The resting state of the P-cluster is the P<sup>N</sup> state, and this is obtained under dithionite reducing conditions. Mössbauer and EPR analysis indicates that all 8 of the Fe atoms in the  $P^N$  state are ferrous, and result in a diamagnetic S=0 spin state. <sup>120,121</sup> The structure of this P-cluster species is described in the section above as a fusion of two cubanes incorporating the  $\mu_6$ -sulfide, a feature that is unique to the P<sup>N</sup>-cluster and not observed in any other biological system. The one-electron-oxidized P1+ state has been studied by EPR and magnetic circular dichroism (MCD) spectroscopies, and this analysis assigns the cluster as a mixture of S = 1/2 and S = 5/2 species, with g-values of 2.06, 1.95, 1.81 for the S = 1/2 system and two sets of g-values (A,B) for the 5/2 system,  $g_A = 6.7$ , 5.3 and  $g_B = 7.3$ . The structure of P<sup>1+</sup> has not been definitively observed through X-ray diffraction methods, but Lawson and coworkers reported a structure of NifDK from K. pneumoniae with evidence that a P-cluster species consistent with the P<sup>1+</sup> may have a conformation somewhere between the P<sup>N</sup> and P<sup>OX</sup> states. 123 However, MCD analysis of the Av NifDK protein is consistent with an electronic description of the P1+ state as two connected [Fe<sub>4</sub>S<sub>4</sub>]1+ clusters.122 The oxidation of PN to POX was shown to have a midpoint potential of -307 mV versus NHE for the two electron event, 120,124 which is a more positive potential than for nucleotide-bound NifH (-430 mV versus SHE). 100 Subsequent analysis by EPR and Mössbauer spectroscopies assign an S = 3 or 4 spin state to  $P^{OX}$ , with a sharp signal observed at g = 11.9. <sup>120,125</sup> It was also observed that P<sup>OX</sup> has a structure that undergoes drastic rearrangement compared to the P<sup>N</sup> state (Figure 8, A and B). 126 Two of the Fe atoms from one cubanoid half of the P-cluster break the Fe–S bonds from the central  $\mu_6$ -sulfide and each form a new bond; one Fe center binds to the O atom of α-Ser188 and the other to the backbone N atom of α-Cys88. Despite the rearrangement, the observed changes are reversible, though there is no clear consensus about which P-cluster states are operative during substrate turnover.66

While it may be unclear which redox states of the P-cluster are functional during substrate reduction, one proposal has been put forth by Seefeldt, Hoffman and co-workers called

the 'deficit-spending electron transfer' model. <sup>83,127</sup> If the normal flow of electrons during catalysis starts with the Fe protein, then transfers to the M-cluster through the P-cluster, the deficit-spending model begins with the P<sup>N</sup> cluster slowly transferring one electron to the M<sup>N</sup> state of the M-cluster (the deficit), and then the P-cluster in the P<sup>1+</sup> state is quickly re-reduced by the Fe protein, regenerating P<sup>N</sup> (repaying the deficit). <sup>83</sup> The logic is that the P<sup>N</sup> cluster is composed of all ferrous iron centers, <sup>120,121</sup> and generating Fe centers in the 1+ oxidation state is not favored in biological FeS clusters, therefore, the P-cluster must first transfer an electron before it can receive an electron. <sup>83</sup> This was supported by experiments showing that the P-cluster was redox active during substrate reduction, <sup>128</sup> and that electron transfer from the Fe protein to the MoFe protein is conformationally gated, thus, when NifH and NifDK form a complex, gated electron transfer is somehow allowed to occur. <sup>127,129</sup> The deficit-spending electron transfer model is certainly intriguing, however, analogous experiments have not been reported for either the V- or Fe-only nitrogenases, so it is unclear if the model holds for the alternative systems. Further investigation will be necessary to better understand this process across all nitrogenase proteins.

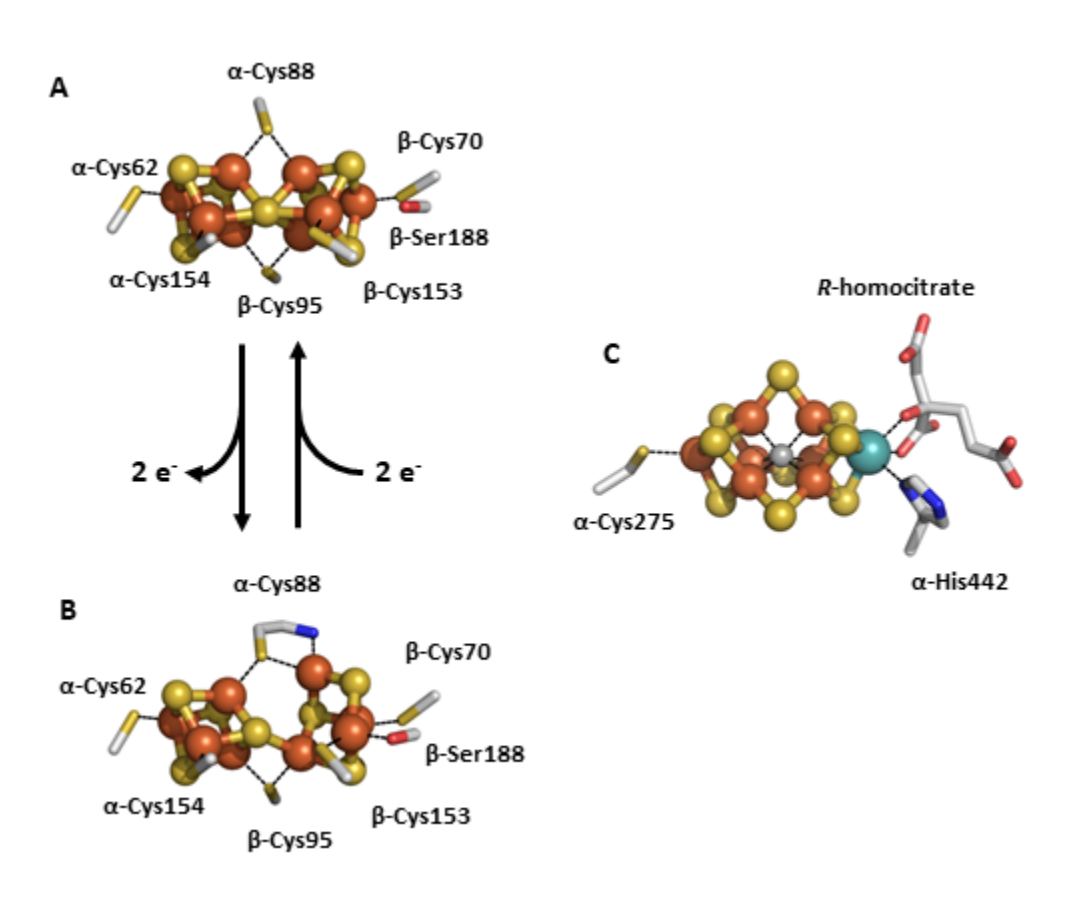


**Figure 8**. The P- and M-clusters of NifDK. The P-clusters can undergo a conversion from the all-ferrous  $P^N$  state (A) *via* 2-electron oxidation to the  $P^{OX}$  state (B). This opens the cluster and causes the cleavage of two Fe–S bonds from the central  $\mu_6$ -sulfide and Fe centers bind to the backbone of α-Cys88 and β-Ser188. The M-cluster is bound in NifD to α-Cys275 and α-His442. The atoms represented as ball-and-stick models, and are colored as follows: Fe, orange; S, yellow; C, grey; O, red; N, blue (PDB IDs: 1MIN and 3MIN).

#### 3.2.2. M-cluster from NifDK

The M-cluster is an interesting metallocofactor in biology for many reasons other than the capability to facilitate N<sub>2</sub> reduction. The cluster is asymmetric, with one Fe-capped end and one Mo-capped end, employing a chiral *R*-homocitrate ligand to bind to the heterometal, and unlike the P-cluster, the M-cluster is only coordinated to the protein through two amino acid residues despite the high nuclearity (Figure 8C).<sup>68,117</sup> In the initial stages, the resolution of the protein crystal structures was not sufficient to see all of the atoms of the M-cluster, so it was unclear if there was a central atom or what the identity of that atom was.<sup>68,118</sup> Subsequent improvements of the resolution allowed for the identification of an interstitial atom,<sup>117</sup> and a 1.0 Å resolution crystal structure in combination with X-ray emission spectroscopy (XES) identified the atom as a carbon.<sup>116,119</sup> Ribbe, Hu and co-workers were able to definitively confirm that the central atom of the M-cluster was a carbon derived from SAM.<sup>46</sup> Another notable feature is that the cofactor is synthesized on proteins other than NifDK, and is only transferred to the *apo*-protein in the final step of the assembly (see Section 2.1).<sup>32</sup> The M-cluster can also be selectively extracted from NifDK in a destructive process discussed in Section 4.5, but the isolated cofactor has never been crystallized independently from the protein.

The catalytic cofactor of NifDK has a characteristic rhombic EPR signature, with intense signals at g = 4.3, 3.7 and 2.0 that are associated with an S = 3/2 spin system. This state (M<sup>N</sup>) is the most commonly observed, as it is stabilized in the presence of dithionite, though the metallocluster can be readily oxidized by one electron to an S = 0 diamagnetic state (M<sup>OX</sup>). The EPR spectrum of the isolated M-cluster still maintains the S = 3/2 spin state, but with broader, shifted resonances (g = 4.6, 3.3, 2.0) indicative of a different ligand environment. The redox behavior of Mo-nitrogenase is challenging to study because of the multiple redox states that both the P- and M-clusters can support, however, the signature EPR signal for the M-cluster can be monitored during potentiometric titrations with chemical redox mediators to obtain a midpoint potential. O'Donnell and Smith were able to determine the  $E_m$  for the M<sup>N</sup> to M<sup>OX</sup>

redox couple in Av and Ac NifDK, with values of -42 mV versus NHE for both proteins. <sup>132</sup> The equivalent midpoint potential reported for Rc NifDK was also found in the same range ( $E_m \sim -50$  mV versus SHE). <sup>133</sup> The  $E_m$  for the one-electron reduced M-cluster,  $M^R$ , has also been measured to be -465 mV versus NHE, but this could only be obtained in the presence of NifH. <sup>134-136</sup> Interestingly, the isolated M-cluster has a much more negative potential than when bound to the protein, with reported values for the  $M^{OX}/M^N$  couple between -320 and -270 mV versus SHE. For a more specific example, the isolated M-cluster in the solvent N-methylformamide (NMF) was found to have potentials for the  $M^{OX}/M^N$  and  $M^N/M^R$  redox events at -320 mV and -1.00 V versus NHE, respectively. <sup>137-139</sup> The dramatic change observed in the reduction potentials for the M-cluster bound to and free from the nitrogenase protein demonstrates that the protein environment plays a significant role in tuning the properties of the M-cluster.

In a recent study by Minteer and co-workers, the electrochemical properties of the MoFe protein were also studied by immobilizing the protein on a pyrene-modified hydrogel film that allows the protein to be attached to an electrode directly as opposed to requiring redox mediators in solution. 140 Square wave voltammetry was employed and the MoFe protein was found to have two redox features, one at  $-230 \text{ mV} (E_{1/2}^A)$  and the other at  $-590 \text{ mV} (E_{1/2}^B)$  versus NHE. Protein variants with single-point mutations at the P-cluster and M-cluster sites, as well as apo-NifDK, were used to correlate the redox features to a metallocofactor. This resulted in  $E_{1/2}^A$  and  $E_{1/2}^B$ being assigned to the P<sup>N</sup>/P<sup>1+</sup> and M<sup>N</sup>/M<sup>R</sup> couples of the P- and M-clusters, respectively. Additionally, the V- and Fe-only nitrogenase proteins were also studied, and assignment by analogy resulted in the P-cluster in both alternative systems being the same as in Monitrogenase, but the V- and Fe-clusters were respectively assigned to potentials of -380 mV and -400 mV versus NHE. <sup>140</sup> The  $E_{1/2}^{A}$  potential for the MoFe protein initially appears similar to the  $E_m = -307$  mV value reported by Hagen and co-workers, <sup>120</sup> but what is important to note is that  $E_{1/2}^{A}$  is assigned to a one-electron event,  $P^{N}/P^{1+}$ , whereas the previous midpoint potential from Hagen was assigned to a two-electron event PN/POX. It is also interesting that the P-cluster potential would remain invariant across all three nitrogenases, considering that the P-cluster of V-nitrogenase does not appear to have identical properties as the P-cluster of Mo-nitrogenase (discussed in Section 3.3.2). Additionally,  $E_{1/2}^B = -590$  mV for the M-cluster is ~200 mV more negative than the analogous redox couple for either the V- or Fe-clusters. These differences are not clearly discussed in the report by Minteer, 140 though, the alternative nitrogenases are not

particularly stable (see Sections 3.3 and 3.4 for details), so immobilization of the proteins in a film for the electrochemical experiments may substantially affect the observed properties. There was also no characterization of the nitrogenase proteins reported to assess the properties of the cofactor before or after immobilization, so it may also be possible that the P-, M-, V- and Feclusters were adversely affected by this process. Additional experiments will be necessary to rectify the observed differences between solution state and immobilized nitrogenase variants.

# 3.3. The Characterization of V-Nitrogenase

While the Mo-dependent nitrogenase is preferentially expressed in most organisms, the alternative nitrogenases provide important backup systems for when molybdenum is not readily available. As will be discussed in Section 4, the effectiveness of the alternative systems with respect to dinitrogen fixation ranks Mo > V > Fe-only, with a bias in V- and Fe-only nitrogenases towards proton reduction to  $H_2$ . To date, the V-nitrogenase protein (VnfDGK, or VFe protein) has only been isolated from only two organisms, *A. chroococcum* and *A. vinelandii*, <sup>141,142</sup> but *vnf* genes have been observed in a wide range of other species. This section will describe the characterization of these V-nitrogenases, including the recently reported crystal structures of Av V-nitrogenase and the relevant comparisons to Mo-nitrogenase.

The catalytic component of V-nitrogenase, VnfDGK or VFe protein, is encoded by the vnfDGK genes, and the VnfD ( $\alpha$ , ~53.8 kDa) and VnfK ( $\beta$ , ~53 kDa) gene products have a ~30% conserved sequence identity as compared to the NifD and NifK proteins. V-nitrogenase additionally has a VnfG subunit ( $\delta$ , ~13.3 kDa) that Mo-nitrogenase lacks. The exact function of the additional subunit is still unknown, V-144,145 but it has been proposed to be involved in the transfer of the V-cluster to the *apo*-enzyme based on sequence similarity to identified cofactor chaperones from *A. vinelandii* and *K. pneumoniae*. VnfDGK forms a  $\alpha_2\beta_2$  hetrotetrameric core analogous to NifDK, but the amount of the VnfG subunit is variable depending on the conditions of protein purification (Figure 9). Preparations of the *Ac* VFe protein were consistent with an  $\alpha_2\beta_2\delta_2$  formulation with an  $M_r = 239600$  Da. VFe protein were consistent with an  $\alpha_1\beta_2\delta_2$  formulation with an  $\alpha_2\beta_2\delta_2$  formulation with an  $\alpha_1\beta_2(\delta)$  variants with a variable amounts of VnfG, but the  $M_r \sim 240$  kDa based on a heterohexameric  $\alpha_1\beta_2\delta_2$  formulation. VnfB and  $\alpha_2\beta_2\delta_2$  formulation.

Ribbe, Hu and Lee later reported a histidine-affinity-tagged version of the Av VFe protein that was consistent with a heterooctameric  $\alpha_2\beta_2\delta_4$  formulation (Figure 9) having  $M_r \sim 270$  kDa, demonstrating the variability and sensitivity of the VnfDGK protein compared to NifDK. Then in 2017, the crystal structure of VnfDGK was reported by Sippel and Einsle showing an  $\alpha_2\beta_2\delta_2$  formulation, which supports that  $\alpha_2\beta_2\delta_4$  and/or  $\alpha_2\beta_2\delta_2$  could be active in solution.

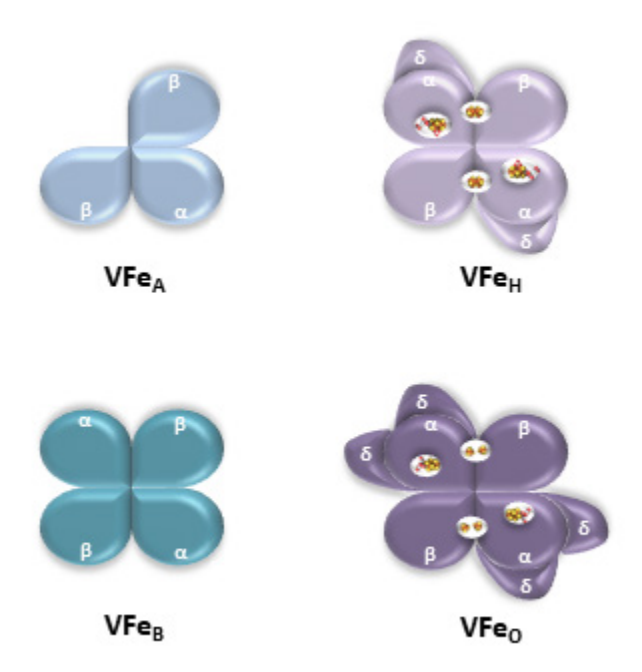


**Figure 9**. Summary of different conformations of the VFe protein that have been reported. VFe<sub>A</sub> =  $\alpha\beta_2(\delta)$ , VFe<sub>B</sub> =  $\alpha_2\beta_2(\delta)$ , the hexameric VFe protein (VFe<sub>H</sub>) =  $\alpha_2\beta_2\delta_2$ , the octameric VFe protein (VFe<sub>O</sub>) =  $\alpha_2\beta_2\delta_4$ . Information known of the metal cofactors were incorporated into VFe<sub>H</sub> and VFe<sub>O</sub>. See the main text for details.

# 3.3.1 Crystal Structures of VnfDGK

VnfDGK has a structure that is very similar to that for NifDK but with some key differences (Figure 10). The VnfD and VnfK subunits form the pair of VnfDK dimers consistent with the same overall  $\alpha_2\beta_2$  core as NifDK, but VnfG is a globular 113-amino acid protein with a fold composed of 4  $\alpha$ -helices that bind exclusively to the VnfD subunit. This raises a possible concern that the 2 VnfG subunits (or 4 subunits in solution) might interfere with the binding of VnfH to the catalytic component. While the VnfH:VnfDGK structure has not yet been reported, overlaying the structures of NifH:NifDK complexes with various nucleotide-

bound states on the VnfDGK crystal structure showed that the VnfG protein is sufficiently removed such that there would not be interference, however, it is unclear where additional VnfG units may bind.<sup>74</sup>

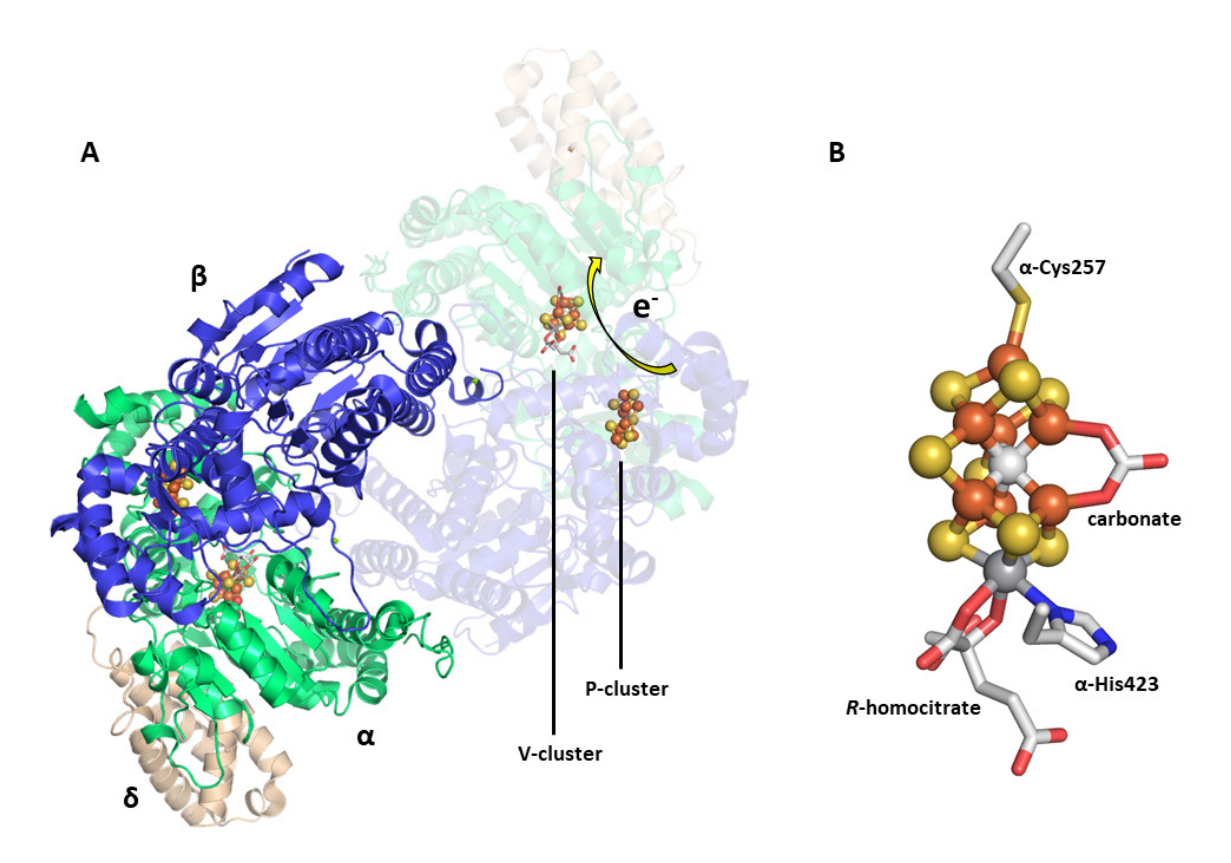


**Figure 10**. The crystal structure of *Av* VnfDGK (A) and the carbonate-containing V-cluster (B). The protein is colored as follows: VnfD (green), VnfG (tan), VnfK (blue). The atoms of the V-cluster are shown as a ball-and-stick model, with the carbonate, *R*-homocitrate and protein residues shown as sticks. Atomic coloring: Fe, orange; S, yellow; V, dark grey; C, light grey; N, blue; O, red (PDB ID 5N6Y).

Like NifDK, VnfDGK houses two types of metalloclusters necessary for electron transfer and substrate turnover, similarly designated as the P-cluster and V-cluster (Figure 10A). Crystallographically, the VnfDGK structure reveals that the P-cluster appears primarily as the  $P^N$  cluster does in NifDK, with the [Fe<sub>8</sub>S<sub>7</sub>] cofactor positioned between the VnfD and VnfK subunits *via* six cysteine residues ( $\alpha$ -Cys49,  $\alpha$ -Cys75,  $\alpha$ -Cys138,  $\beta$ -Cys31,  $\beta$ -Cys56, and  $\beta$ -Cys115) with a central  $\mu_6$ -sulfide atom.<sup>74</sup> However, additional electron density consistent with one of the Fe atoms (Fe6) moving closer to  $\beta$ -Ser153 was observed. This is somewhat analogous to the changes observed for the  $P^{OX}$  state of NifDK where the equivalent Fe6 and Fe5 break from the central sulfide atom and bind to a serine ( $\alpha$ -Ser188) and the backbone of a cysteine residue

(α-Cys88). 126 In the VnfDGK structure only one of these changes occurs, and based on this, the authors assign the partially occupied state of the P-cluster to the one-electron-oxidized P<sup>1+</sup> state.<sup>74</sup> However, EPR or other magnetic measurements were not reported for the V-nitrogenase protein used, to corroborate this assignment. The V-cluster reported in the structure is formulated as a [VFe<sub>7</sub>S<sub>8</sub>C(CO<sub>3</sub><sup>2</sup>-)(R-homocitrate)] cluster that is buried in the  $\alpha$  subunit near the P-cluster, and is anchored to the protein by two residues,  $\alpha$ -Cys257 and  $\alpha$ -His423, on the Fe- and V-capped ends, respectively (Figure 10B). While the overall structure of the V-cluster core is similar to that of M-cluster from NifDK, there are several observations that should be noted. While the V atom occupies the same place as the Mo center, including coordination by His and R-homocitrate ligands, the average V–Fe distance of 2.77 Å to the closest three Fe centers in the V-cluster is slightly longer than the analogous 2.69-Å Mo–Fe distance in the M-cluster. 74,116 This causes the V-cluster to appear slightly elongated relative to the M-cluster. The largest difference between the M- and V-clusters is the replacement of one of the  $\mu_2$ -sulfide ligands (S3A) by a CO<sub>3</sub><sup>2</sup>moiety in the V-cluster. 74 Substituting other molecules such as nitrate (NO<sub>3</sub><sup>-</sup>) or acetate (CH<sub>3</sub>COO<sup>-</sup>) during refinement did not result in adequate agreement with the electron density, but an independent confirmation of the carbonate ligand has not been reported. There is currently no definitive function for, or source of the carbonate ligand identified in the crystal structure.

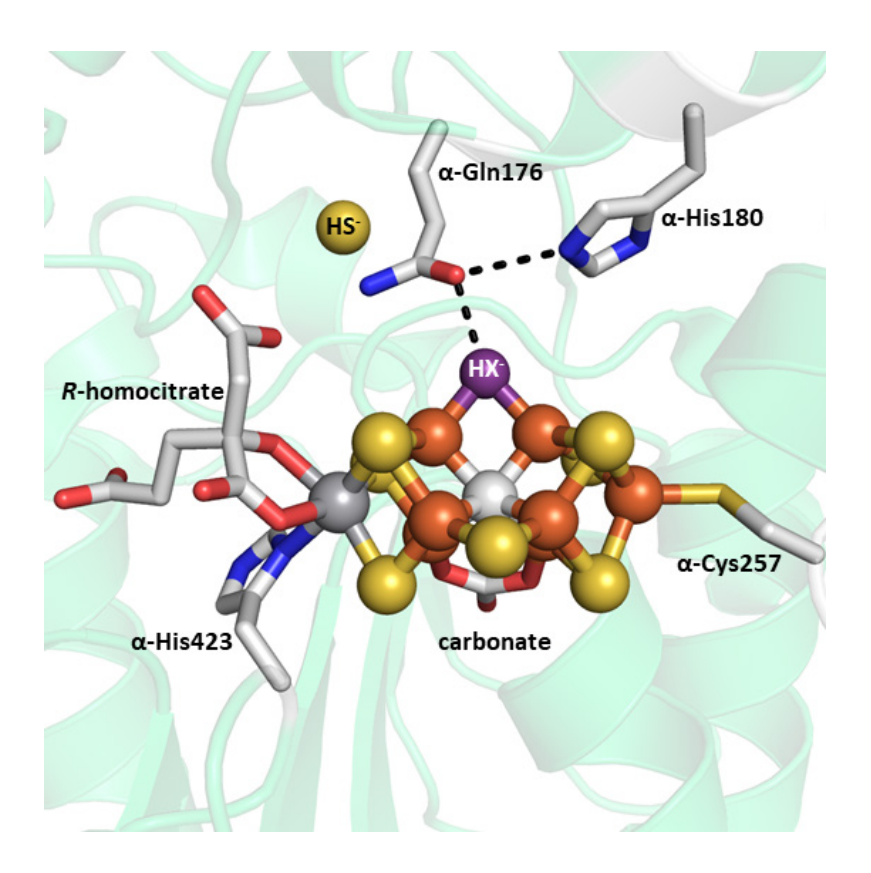


**Figure 11**. Crystal structure of a putative reaction intermediate bound to Av VnfDGK (PDB ID 6FEA). The cluster atoms are shown as ball-and-stick models, the exogenous HS<sup>-</sup> molecule is shown as a sphere, and the remaining atoms are shown as stick models. HX<sup>-</sup> ligand (purple) is shown with hydrogen bonding interaction (black dashed line) to  $\alpha$ -Gln176, which is itself interacting with  $\alpha$ -His180. The coloring is as described in Figure 10.

In 2018, Einsle and co-workers reported a second crystal structure of VnfDGK with a reaction intermediate purportedly bound to the V-cluster, achieved through the limited use of dithionite as reductant. The structure of the protein fold as well as the P- and V-clusters were largely unchanged from the previous structure, except for the loss of another  $\mu_2$ -sulfide ligand (S2B) and its replacement by a light atom (X) with Fe–X distances of 2.01 Å (Figure 11). Electron density was observed ~7 Å away from the S2B position on the V-cluster, near the  $\alpha$ -Gln176 residue, that was best fit with a hydrosulfide ion (HS $^-$ , Figure 11). This location was then proposed to be the 'holding pocket' for the displaced S2B sulfur atom. The same  $\alpha$ -Gln176 residue also becomes reoriented relative to the previous structure, such that the side chain amide O atom is 2.55 Å from the X atom and 2.84 Å from the nearby  $\alpha$ -His180 residue, implying the formation of hydrogen bonding interactions (Figure 11). The equivalent residues in Monitrogenase ( $\alpha$ -Gln191,  $\alpha$ -His195 in *A. vinelandii*) have been shown to play important roles in substrate reduction, The equivalent investigations have not been carried out using V-

nitrogenase. Based on this information, the X atom was tentatively assigned to a nitrene (HN<sup>-</sup>) species, and a hydroxide (HO<sup>-</sup>) was ruled out based on the assumption that water binding to the V-cluster after the release of S2B would make water a competitive inhibitor of N<sub>2</sub> reduction. <sup>150</sup> Additionally, the authors note that the Fe–XH bond distances of  $\sim 2.0$  Å were in line with Fe<sub>2</sub>–( $\mu$ -NH) diiron model complexes. However, the synthetic complex cited has metrics that are incongruent with those from the VnfDGK structure. Peters and co-workers reported an Fe(II)- $(\mu-NH)(\mu-H)$ -Fe(II) complex supported by phosphine ligands that features Fe–NH bond distances of 1.826 and 1.790 Å, an Fe---Fe separation of 2.659 Å, with an Fe-N-Fe angle of 94.7°. 155 The equivalent measurements from VnfDGK are 2.0 Å for Fe-X, 2.6 Å for Fe---Fe and 82° for the Fe-X-Fe angle. 150 While hydrogen bonding can cause perturbations to bond lengths, a ~0.2 Å elongation is not reasonable and would be inconsistent with assignment to a nitrene species based on the synthetic model cited. Additionally, quantum mechanics / molecular mechanics (QM/MM) calculations carried out by Bjornsson and co-workers favor the X ligand as a hydroxide species (HO<sup>-</sup>), citing better agreement between the bonding metrics and hydrogen bonding interactions. 156 It is clear that further investigation of the identity of the light atom will be necessary to address the situation.

## 3.3.2. P- and V-clusters from VnfDGK

Prior to the report of the V-nitrogenase crystal structure, the identity and composition of the metallocofactors in the protein was derived from a combination of EPR, Mössbauer, MCD and XAS spectroscopic analyses. The study of the clusters on the protein is made challenging due to several overlapping paramagnetic signals in addition to the VnfDGK composition issues described earlier. Initial reports of the EPR spectra of dithionite reduced forms of the Ac and Av VFe proteins had an intense S = 1/2 signal in the high field region with g = 2.04, 1.93, and a series of resonances in the low field region between g = 3.0–6.0 (Table 3, Figure 12 A and B). <sup>141,142</sup> In the spectrum of the Ac VFe protein, the specific g-values found were 5.60, 4.35, 3.77. These were assigned to a mixture of S = 3/2 species affiliated with the V-cluster based on analogy to the M-cluster, but with an order of magnitude lower intensity than in the MoFe protein. <sup>141</sup> The S = 1/2 species observed for VnfDGK was believed to be an irrelevant contamination. This assignment was, in part, supported by the EPR spectrum of V-cluster extracted from the Ac VFe protein, where g = 4.5, 3.6 resonances were observed, albeit in a very

noisy spectrum.<sup>157</sup> In addition, the  $P^{OX}$  state for the Ac VFe protein was observed with a g=12 signal in parallel mode EPR and was assigned to an S=4 system, while the intensity of the S=1/2 signal was not found to be correlated to the specific activity of the protein.<sup>158</sup>

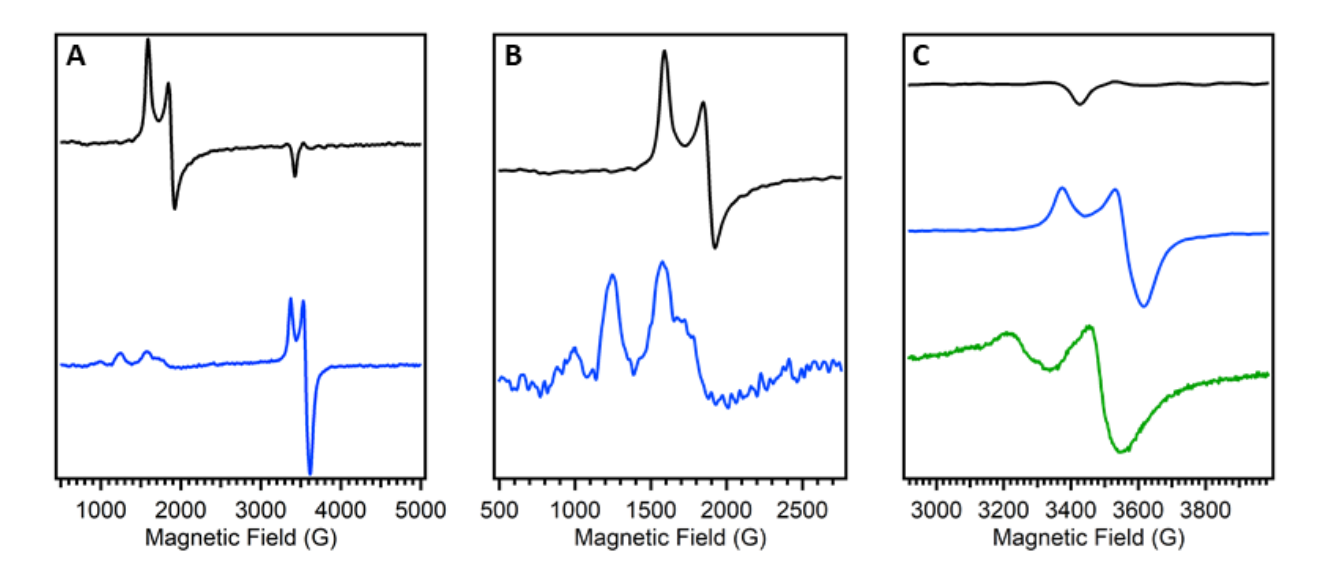


**Figure 12**. Representative EPR spectra of Av NifDK (black) and Av VnfDGK (blue). A: Spectrum of the full range of data. B: Spectrum of the low field region, Av VnfDGK data has been scaled for visibility. C: Spectrum of the high field region, additionally the apo-VFe protein ( $Av \Delta nifB$  VnfDGK, green) is included. Data for the MoFe and VFe proteins was reported in ref 149 and data for apo-VFe protein was reported in ref 34. Note that the spectra shown in the figure were not recorded under identical conditions.

The properties of Av VnfDGK have more extensively been explored and these results are summarized in Table 3. <sup>148,159-161</sup> The EPR spectrum of the Av VFe protein at low field showed signals at g = 5.80, 5.40 that demonstrated temperature-dependent behavior, and they were assigned to the ground state and an excited state of the same S = 3/2 system, respectively. <sup>160</sup> The S = 3/2 signal was spin quantified to one spin per V atom, consistent with assignment to V-cluster, and the S = 1/2 signal was determined to be a minor component with 0.2 spins per V atom per protein. There was also an additional signal around g = 4.3 that was thought to be from adventitious Fe(III) bound to the protein. MCD analysis established that one of the cluster species in the dithionite reduced state of VnfDGK was an S = 3/2 system that becomes diamagnetic when it undergoes one-electron oxidation. <sup>159</sup> The other cluster was diamagnetic in the dithionite reduced state, then becomes a paramagnetic S = 5/2 system upon oxidation. Further, Mössbauer spectroscopy was employed to provide oxidation state information about the clusters. <sup>161</sup> In the as-isolated form, the VFe protein contained 5-10% of clusters in an oxidized

state, so additional samples were prepared with limiting reductase (1:10 molar ratio of VnfH:VnfDGK) which served to reduce the oxidized species to simplify the analysis. The VnfH-reduced VFe protein (VFe<sup>R</sup>) was consistent with 52% of the Fe centers being assigned to P-clusters in the all-ferrous  $P^N$  state, analogous to MoFe protein, and 48% of the Fe was associated with the V-cluster, with a small amount of adventitiously bound Fe covering the difference. It was then suggested that both the S = 3/2 and 1/2 EPR signals should be associated with the V-cluster, as the  $P^N$  clusters would be EPR silent. Together, these results were interpreted to mean that (1) the P-clusters were in the diamagnetic  $P^N$  state when reduced by VnfH, (2) the dithionite-reduced VFe protein contained some amount of an oxidized P-cluster, and further oxidation of the VFe protein clearly produced a paramagnetic S = 5/2 system, (3) the V-cluster was associated with the S = 3/2 and 1/2 signals in the resting dithionite reduced state ( $V^N$ ), but the spin quantification of these spin systems by EPR did not agree.  $V^N$ 0

After the discovery that Av VnfDGK could be isolated in two forms,  $\alpha\beta_2$  (VFe<sub>A</sub>) and  $\alpha_2\beta_2$ (VFe<sub>B</sub>), the spectroscopic data was reanalyzed and further explored because previous samples of VnfDGK were recognized as mixtures of the two forms (Table 3). 148,162,163 The VFe<sub>B</sub> variant is more active, with VFe<sub>A</sub> having ~75% of the activity of the former, so VFe<sub>B</sub> will be the primary focus. In the as-isolated dithionite reduced form (VFe<sub>B</sub><sup>N</sup>), the EPR spectrum shows g-values of 6.67, 5.68, 5.45 as well as a broad resonance at 4.3 at low field, and the g = 2.04, 1.93 S = 1/2signal at high field. The V-cluster was assigned to the g = 5.68, 5.45 signals as part of an S =3/2 system, in line with previous observations, but the identity of the remaining g-values was unclear. 160 The protein could be reduced further using substoichiometric VnfH (VFe<sub>B</sub><sup>R</sup>), and this showed loss of the g = 6.67 resonance and the broad signal at g = 4.3, while the S = 3/2 signals shift to g = 5.71, 5.42 (Table 3, Figure 13A). <sup>162</sup> Subtraction of these spectra (VFe<sub>B</sub><sup>N</sup>-VFe<sub>B</sub><sup>R</sup>), revealed the same g = 6.67, 4.3 signals from the spectrum of VFe<sub>B</sub><sup>N</sup> as well as a new derivative signal at g = 5.3. Tittsworth and Hales previously reported similar signals (g = 6.67, 5.3) for the Av MoFe protein that were assigned to the one-electron-oxidized  $S = 5/2 \text{ P}^{1+}$  state of the Pcluster, so those observed in VFe<sub>B</sub> were designated analogously (Table 3). 162,164 Oxidation of VFe<sub>B</sub><sup>R</sup> by 1.5 equivalents of thionine caused g = 6.67, 4.3 signals to reappear (Figure 13B), and an additional 1.5 eq. increased the intensities of both signals similarly (Figure 13C), so the broad g = 4.3 was also assigned to the  $P^{1+}$  state, but it was unclear which spin system was the origin of the signal.  $^{162}$  Oxidation by a total of 6 eq. (VFe<sub>B</sub><sup>OX</sup>) produced a new broad signal at g = 11.5 in

perpendicular mode EPR, and at g = 12.8 in parallel mode. This compares reasonably well to the two-electron oxidized  $P^{OX}$  state of the P-cluster in the MoFe protein (sharp signal at g = 11.8 in parallel mode), and so was assigned to an S = 3  $P^{OX}$  species (Table 3). Further oxidation of  $VFe_B^{OX}$  eliminates all signals other than the sharp g = 4.34 feature (Figure 13D), which increases, and was assigned to adventitious high-spin Fe(III), likely from degradation of the P-and V-clusters. 162

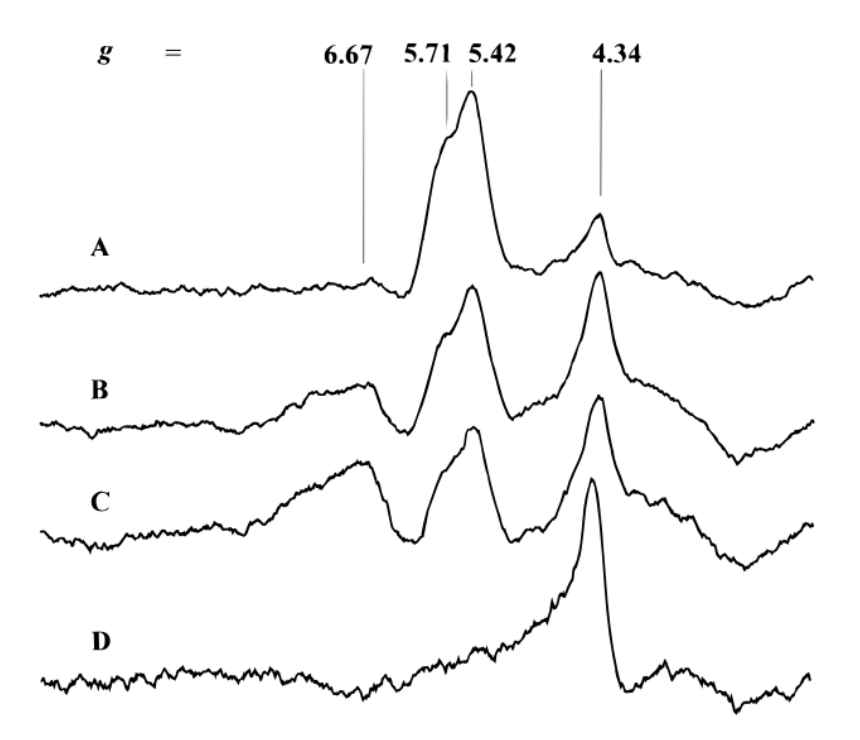


**Figure 13**. EPR spectra of the low field region of the thionine-titrated *Av* VFe<sub>B</sub> protein. A: VnfH-reduced VFe<sub>B</sub><sup>R</sup>; B: VFe<sub>B</sub><sup>R</sup> oxidized by 1.5 equivalents of thionine; C: VFe<sub>B</sub><sup>R</sup> oxidized by 3 equivalents; D: VFe<sub>B</sub><sup>R</sup> oxidized by 6 equivalents (VFe<sub>B</sub><sup>OX</sup>). Reproduced with permission from ref 162. Copyright 1996 American Chemical Society.

The remaining high field signals in the EPR spectra, however, were more complicated to analyze. The authors reported that upon reduction of VFe<sub>B</sub><sup>N</sup> to VFe<sub>B</sub><sup>R</sup>, the S = 1/2 signal would disappear, but only on occasion. The signal could be recovered with 1 eq of oxidant if it had disappeared (VFe<sub>B</sub><sup>R</sup>  $\rightarrow$  VFe<sub>B</sub><sup>N</sup>), but if it remained, it would disappear with the addition of 1 eq of oxidant. This bizarre behavior suggested that the signal was only a minor component of the system, but the identity was unclear. Hales and co-workers also reported a hybrid VFe protein generated by adding isolated M-cluster to cell extracts of an *A. vinelandii* strain expressing an *apo*-VFe protein that lacked the V-cluster (Figure 14). The resultant protein that was purified

contained the M-cluster instead of the V-cluster (M-VFe). EPR spectroscopy showed that the prominent S = 3/2 signal for the M-cluster on NifDK (g = 4.32, 3.68, 2.01, Figure 14A) was shifted and drastically broadened in the dithionite reduced M-VFe sample (g = 4.65, 3.49, Figure 14B). Additionally, the S = 1/2 region yielded the same g = 2.04, 1.93 signal for both the VFe protein and M-VFe (Figure 14 B and C). This suggested that the S = 1/2 system was not a property of the V-cluster, but was instead inherent to the VFe protein, lending assignment to a P-cluster signal. However, this was still inconsistent with the Mössbauer analysis that showed the P-cluster was primarily composed of S = 0 P<sup>N</sup> clusters. <sup>161</sup>

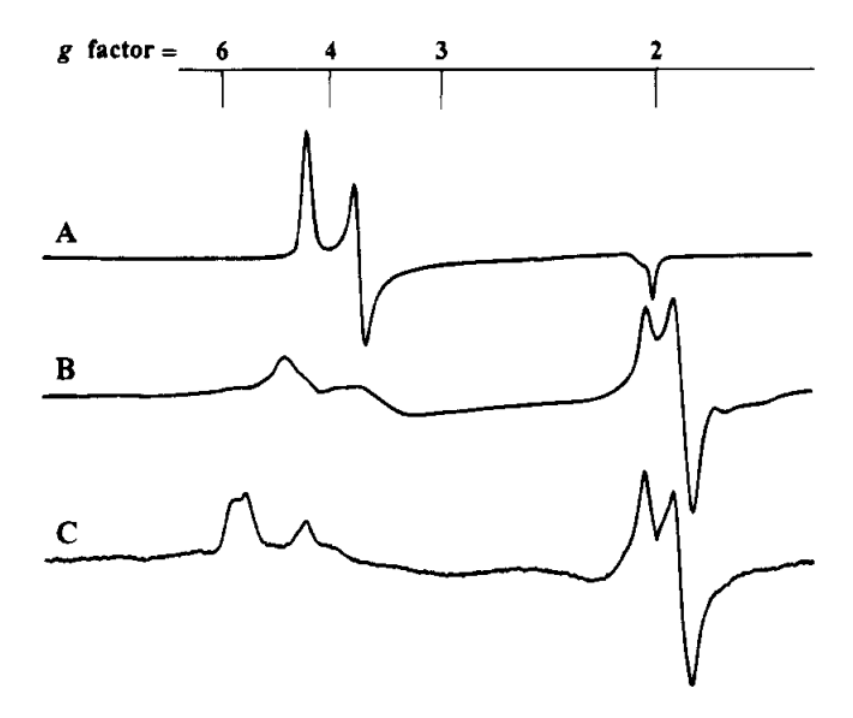


**Figure 14**. EPR spectra of the *Av* MoFe protein (A), *Av* M-VFe protein (B), and *Av* VFe protein (C) in the dithionite reduced state. Reproduced with permission from ref 163. Copyright 1994 American Chemical Society.

Ribbe, Hu and Lee also reported EPR studies of Av VnfDGK, but used a protein purified with a His-affinity tag and a heterooctameric composition of  $\alpha_2\beta_2\delta_4$  (VFe<sub>O</sub>) in contrast to VFe<sub>B</sub> (Figure 9). This VFe<sub>O</sub> protein is highly active (see Section 4) and as such, provided a good opportunity to study the spectroscopic properties of V-nitrogenase. The dithionite reduced form, VFe<sub>O</sub><sup>N</sup>, shows an EPR spectrum with resonances at g = 6.68, 5.50, 4.32, 3.77, 2.03, 1.92, which are similar to those seen for the Ac VFe protein and Av VFe<sub>B</sub><sup>N</sup> (Table 3). 141,160,162</sup> The g = 6.68 signal was assigned to an S = 5/2 species, likely associated with the P<sup>1+</sup> state of the P-cluster,

analogous to the assignment for Av VFe<sub>B</sub>.  $^{162}$  VFe<sub>O</sub> could also be oxidized (VFe<sub>O</sub><sup>OX</sup>), and this species showed a very minor signal at  $g \sim 12$  that was previously assigned to the P<sup>OX</sup> state of the P-cluster in VFe<sub>B</sub><sup>OX</sup>.  $^{162}$  The g-values at 5.50, 4.32, 3.77 were attributed to S = 3/2 signals, and when Av VFe<sub>O</sub> was put under substrate turnover conditions with C<sub>2</sub>H<sub>2</sub>, N<sub>2</sub> or Ar atmospheres, the S = 3/2 signals diminished, supporting that those signals were associated with the V-cluster.  $^{149}$  However, there was an additional observation that the g = 5.50 resonance had a different temperature dependence than the g = 4.32, 3.77 signals. This was interpreted to mean that each set of signals corresponded to different S = 3/2 species, similar to VFe<sub>B</sub> where the g = 5.68 signal was assigned to the S = 3/2 V-cluster and the broad signal at  $g \sim 4.3$  was likely associated with a P<sup>1+</sup>-cluster but without a clear spin assignment.  $^{162}$ 

The S = 1/2 signal was also found to behave differently for VFe<sub>O</sub> than in previous reports. <sup>149</sup> The intensity of the S = 1/2 EPR features appeared to increase with increasing specific activity, similar to the S = 3/2 signal, and in stark contrast to Ac VnfDGK. <sup>141,158</sup> Additionally, when VFe<sub>0</sub> was under catalytic turnover conditions, the g = 2.03, 1.92 signal was attenuated. These observations suggested that the S = 1/2 signal is related to the activity of the protein and not just an adventitious species, and further, was attributed to the P-cluster (Table 3). 149 This is in agreement with S = 1/2 signals observed for the M-VFe protein by Hales and co-workers. <sup>163</sup> Additionally, an isolated *apo*-VnfDGK protein (Δ*nifB* background, lacking V-cluster but with Pclusters present) was also studied by Ribbe and co-workers using EPR and X-ray absorption spectroscopies.<sup>34</sup> The protein was purified as a trimeric αβ<sub>2</sub> species ~160 kDa in size, similar to the V-cluster replete VFe<sub>A</sub>. <sup>148</sup> The EPR spectrum of the *apo*-VFe protein shows a similar S = 1/2feature to the holo-VFe proteins, with g-values at 2.08, 1.89 (Figure 12C, green trace), which supports the association of the signal with the P-cluster.<sup>34</sup> Additionally, it was found that unlike the P-clusters on the MoFe protein, the *apo*-VFe protein was unable to be oxidized to the P<sup>OX</sup> state, which suggested that the P-cluster on VnfDGK may not look like the 'normal' P-clusters of NifDK. Further, the XAS data showed a feature in the Fourier transform at  $R + \Delta \sim 2.4 \text{ Å}$ composed of primarily Fe---Fe contributions associated with a [Fe<sub>4</sub>S<sub>4</sub>]-like species, and this feature is completely absent in the analogous apo-MoFe protein with typical P-clusters (Figure 15, red versus black trace). 34,81 To further complicate matters, Sippel and Einsle report the EPR of the Av VFe protein used to obtain a crystal structure that showed the same S = 1/2 signal, but the P-clusters in the structure are modeled similarly to those in MoFe. 150 It seems that it may be

possible for the P-clusters on the VFe protein to take on conformations similar to those found in MoFe protein under certain conditions. However, the solution state characterization is not entirely consistent with a well-behaved P-cluster and suggests that an alternative conformation may be operative in V-nitrogenase. Additional work will be necessary to further elucidate the structure of the P-cluster.

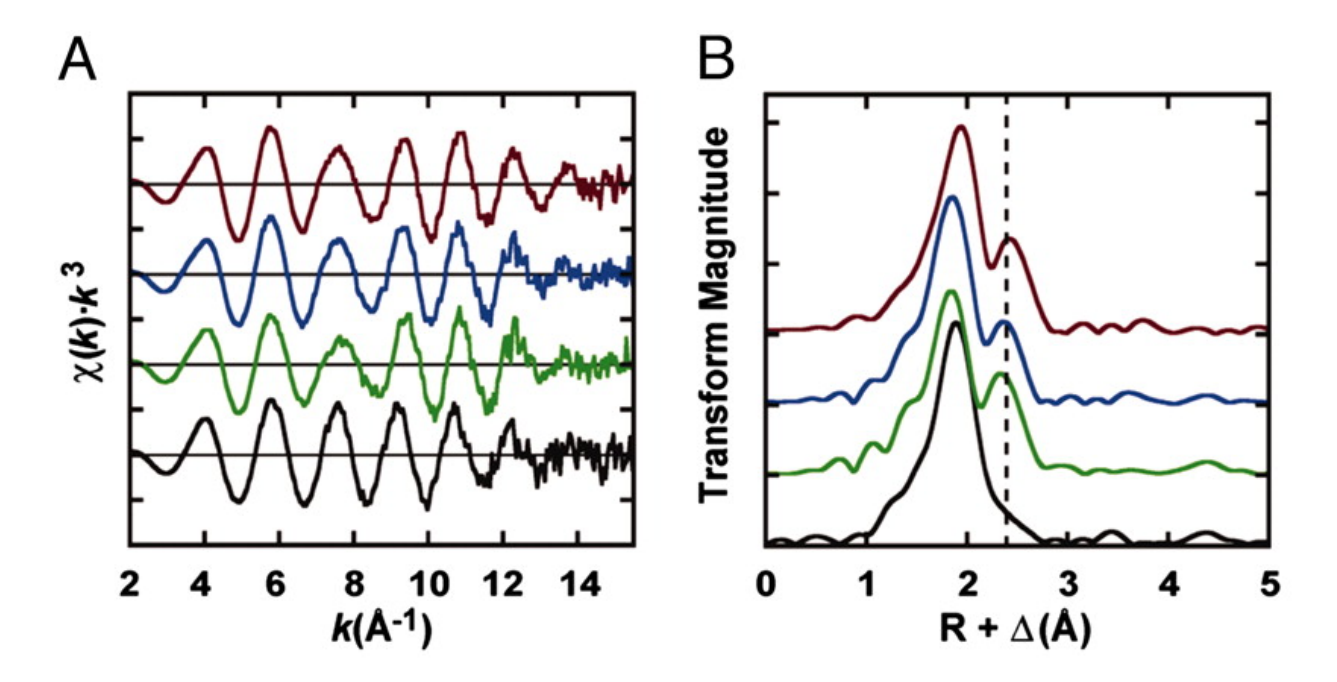


**Figure 15**. Fe K-edge  $k^3$ -weighted EXAFS (A) and Fourier transforms of the data (B) for a series of *apo*-nitrogenase proteins lacking the catalytic cofactor (M- or V-cluster) but containing a P-cluster variant.  $\Delta nifB$  NifDK with normal P-cluster (black),  $\Delta nifH$  NifDK in the presence (blue) or absence (green) of NifH with P-cluster variants, and  $\Delta nifB$  VnfDGK (red) with P-cluster. Adapted with permission from ref 34. Copyright 2005 National Academy of Sciences.

The structures of the metallocofactors of the V-nitrogenases from *A. chroococcum*<sup>73,157,165,166</sup> and *A. vinelandii* <sup>72,167-170</sup> had primarily been explored using X-ray absorption spectroscopy before the recent appearance of crystal structures. Smith and co-workers first reported the V K-edge XAS data of V-nitrogenase from *A. chroococcum* in 1987, and a parallel study with better resolution of the *Av* VFe protein followed in 1988 by Cramer and co-workers (Figure 16). <sup>72,73</sup> Both proteins were fit similarly with an octahedral environment around the V-center from the cluster, with V–S of 2.32 and 2.34 Å, V–O of 2.14 and 2.13 Å, and V---Fe distances of 2.74 and 2.76 Å, for the *Ac* and *Av* VFe proteins, respectively. This compared well to the analogous Mo K-edge experiments for the Mo-nitrogenase of *C. pasteurianum* and *K. pneumoniae*, though the Mo---Fe distance was slightly shorter at 2.69 Å. <sup>72</sup> The V K-edge XAS

of the VnfH-reduced (VFe<sup>R</sup>) and thionine-oxidized forms of Ac VFe protein were also investigated. 165 The X-ray absorption near edge structure (XANES) for the VFe<sup>R</sup>, dithionite reduced VFe<sup>N</sup>, and thionine-oxidized (VFe<sup>OX</sup>) forms were largely similar, with identical K-edge energies (5466 eV) and similar pre-edge intensities, though the data for VFe<sup>R</sup> was of poor quality and prevented additional analysis. The oxidation state of the V atom was estimated to be between V(II) and V(IV). 73,165 The EXAFS of the oxidized form was essentially identical to the dithionite reduced form, with 3 V-S distances at 2.34 Å, 3 V-O at 2.13 Å and 3 V---Fe at 2.74 Å, indicating that with respect to the V center, there is no large-scale rearrangement of the cluster upon oxidation. The Fe K-edge XAS data for Av VFe<sup>N</sup> and Av VFe<sup>OX</sup> were also reported and compared to a series of FeS model complexes to assist with structural determination. <sup>167</sup> These experiments were further complicated because the Fe from both the P- and V-clusters contribute to the average signal observed in the XAS experiment. The EXAFS fits of VFe<sup>N</sup> and VFe<sup>OX</sup> were very similar, with distances for Fe-S at ~2.30 Å, and for Fe---Fe scatterers at 2.67 and 3.76 Å. The Av MoFe protein was also analyzed in parallel, and the distances fit for both MoFe and VFe proteins were in agreement, supporting that the M- and V-clusters have similar structure. 167 Interestingly, Fe---Mo scatterers were necessary to obtain the best fit of the Mo-nitrogenase EXAFS data, but an analogous Fe---V was not required. This is likely because V and Fe have similar scattering characteristics, and so any V-specific interactions are averaged with Fe signals. Additionally, XES experiments in combination with DFT calculations were carried out on the VFe protein from A. vinelandii to establish the existence of a central carbon atom, similar to what was observed in the MoFe protein. 119,169,315 These studies identified that there was indeed a carbide present in the V-cluster similar to the M-cluster, though analogous biochemical confirmation though the use of isotopically labeled carbon has not yet been reported.

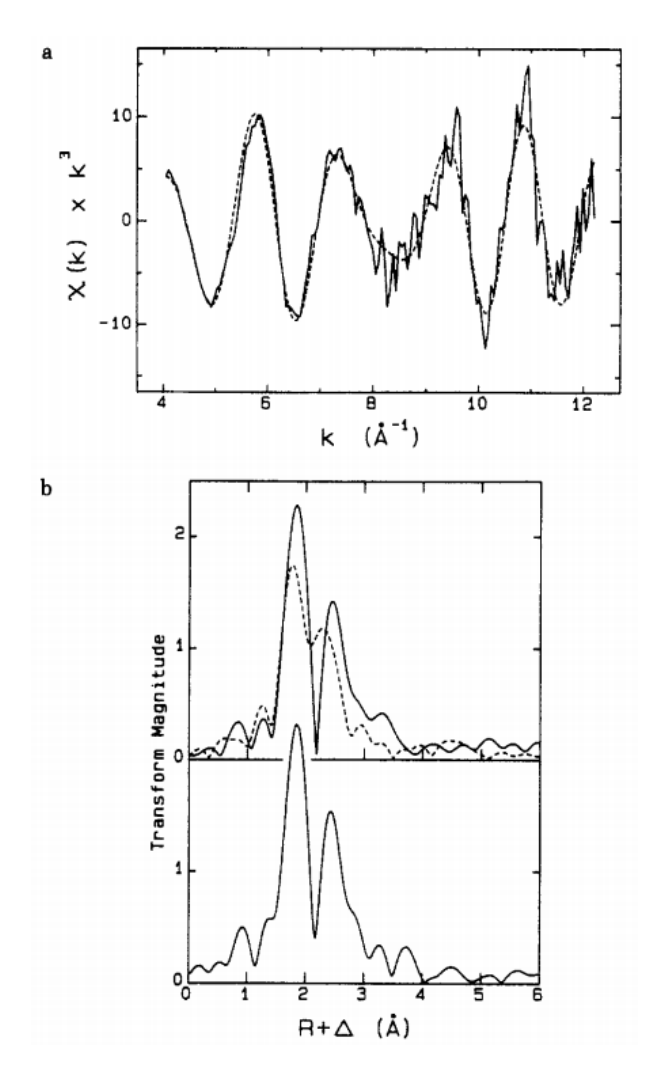


**Figure 16**. The V K-edge EXAFS data from Av VnfDGK. a: the best fit (dotted) of the  $k^3$ -weighted EXAFS data (solid) for Av VnfDGK. b: Fourier transforms of the EXAFS data for Av VnfDGK compared to Kp NifDK (top, black vs dashed, respectively) and to the model complex [Me<sub>4</sub>N][VFe<sub>3</sub>S<sub>4</sub>Cl<sub>3</sub>(DMF)<sub>3</sub>]•2DMF (bottom, solid). Reproduced with permission from ref 72. Copyright 1988 American Chemical Society.

The extracted V-cluster has also been studied from V-nitrogenase from both A. chroococcum and A. vinelandii. Smith and co-workers first demonstrated the extraction of V-cluster from the Ac VFe protein in 1988, and were able to use the cluster to reconstitute apo-MoFe protein. However, the reconstitution of the protein with the V-cluster only conferred a partial restoration of activity to the protein, leaving the resulting V-MoFe protein unable to reduce  $N_2$ . As mentioned previously, the V-cluster extracted from the Ac VFe protein also showed weak EPR signals at g = 4.5, 3.6, 2.0, and while these resonances are similar to those found for the isolated M-cluster (g = 4.6, 3.3, 2.0), the spectrum of the isolated V-cluster

was rather noisy. 130 Then in 2010, Ribbe and coworkers also reported the extracted V-cluster, but the cluster came from A. vinelandii. 168 The isolated Av V-cluster was capable of restoring activity to apo-MoFe protein, including the ability to fix nitrogen. Characterization by EPR spectroscopy showed g-values for the extracted V-cluster at 5.55, 3.25, 2.00, though the g = 3.25 resonance is very broad, which differs from the extracted Ac V-cluster signals (Table 3, Figure 17A). 157,168 The g = 5.55 signal from the isolated Av V-cluster compares well to the S = 3/2 g = 5.5-5.7resonance from the spectrum of the VFe protein, assigned to the V-cluster (Figure 17A, black versus blue trace). In addition, the isolated Av V-cluster showed a much less intense signal at g =2.00, which is not likely to substantially contribute to the S = 1/2 signal in the protein. The EPR spectrum of the V-MoFe protein showed resonances at g = 5.50, 4.32, 3.72 that are broader than the analogous region for the wild-type VFe protein, and also displayed much weaker g-values at 2.01, 1.93 (Figure 17B, black versus red trace). This supports the notion that the protein environment plays a large role in tuning the properties of the nitrogenase cofactors. Both the isolated V-clusters from A. chroococcum and A. vinelandii have also been characterized by Fe Kedge XAS. 166,168 The EXAFS analysis for each cluster is similar, showing a best fit consisting of ~3 Fe–S scatterers at 2.23 Å, ~2.5 Fe---Fe distances at 2.63 Å, 1 Fe---Fe/V scatterer at 2.90 Å and a longer Fe---Fe scatterer at 3.69 Å. Additionally, the isolated Av V-cluster was fit with Fe-O and Fe---C scatterers from bound solvent molecules. 168 These fits are quite comparable to the Fe K-edge data obtained for the Av V-nitrogenase holo-protein, consistent with a similar structure, 167 though the data does not give an indication of the presence or absence of the carbonate (CO<sub>3</sub><sup>2-</sup>) ligand that is observed in the crystal structure.<sup>74</sup>

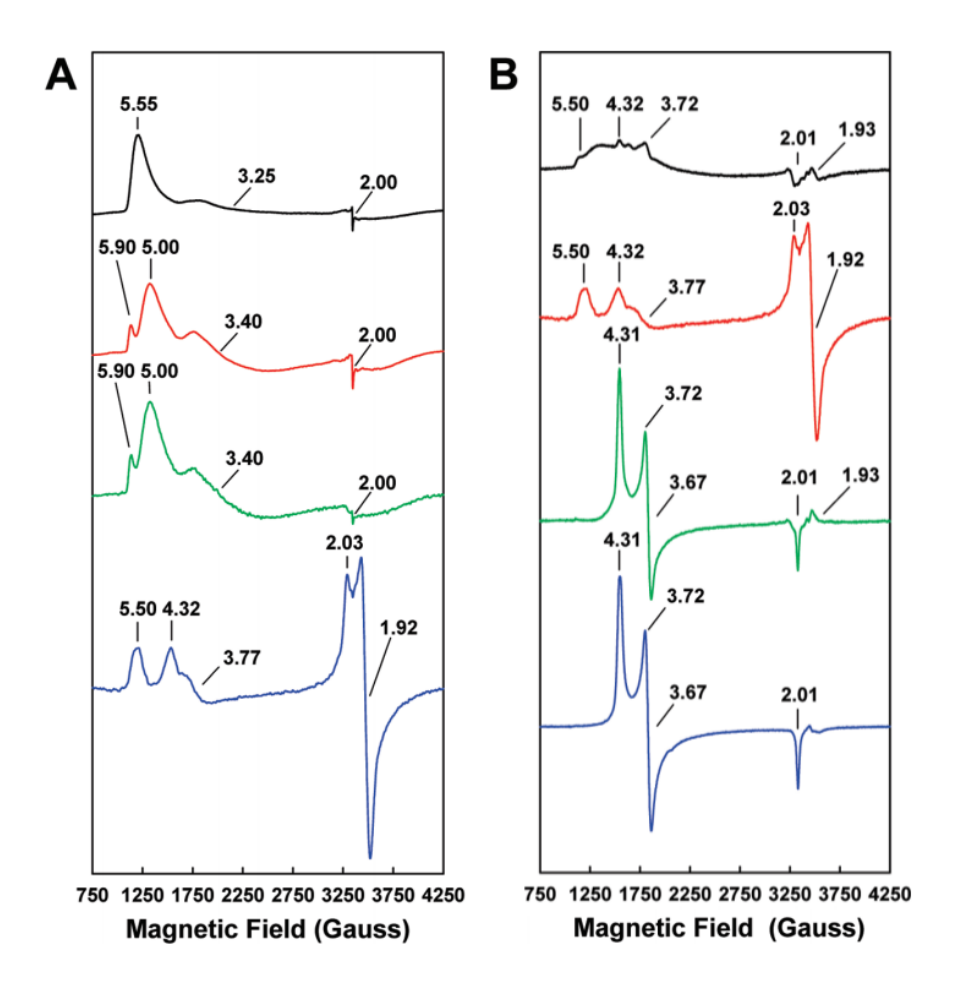


**Figure 17**. EPR spectra of the isolated *Av* V-cluster (A) and *apo*-MoFe protein from *A. vinelandii*, reconstituted with V- or M-cluster (B). A: EPR spectra of V-cluster in NMF (black), in NMF plus 10 mM thiophenol (red), in NMF plus 1,4-benzenedithiol (green) or in the wild-type VFe protein (blue). B: EPR spectra of V-cluster reconstituted *apo*-MoFe protein (V-MoFe, black), wild-type VFe protein (red), M-cluster reconstituted *apo*-MoFe protein (green) and wild-type MoFe protein (blue). Adapted with permission from ref 168. Copyright 2010 American Chemical Society.

More recently, DeBeer, Kovacs and co-workers<sup>170</sup> used a combination of DFT calculations, high-energy resolution fluorescence detected (HERFD) XAS, as well as non-resonant XES techniques to further probe the electronic properties of the isolated *Av* V-cluster. The calculations suggested that the oxidation state of the V atom in the V-cluster was V(III), which is similar to the assignment made of Mo(III) in the M-cluster using a similar methodology. <sup>170-172</sup> Interestingly, the subsequent X-ray analysis also suggested that the Fe atoms of the V-cluster were in a more reduced state compared to the M-cluster counterparts. <sup>170</sup> This observation seems to correlate with the measured midpoint potentials of –414 mV and –270 mV versus SHE for the isolated V- and M-clusters, respectively, <sup>139</sup> with the more negative potential

relating to a seemingly more reduced V-cluster. Further, the iron-heterometal bonding interactions were found to be weaker for the V-cluster compared to the M-cluster, which would align with the elongated V---Fe distances observed by XAS of the protein, cofactor and crystallographically characterized V-cluster relative to the Mo-dependent counterpart. 170

Table 3. Selected EPR signals and g-values associated with the metallocofactors of the alternative nitrogenases

Species	Redox State <sup>a</sup>	Spin State (S)	g-values	ref	
	$M^R$	0	-	103	
	$M^N$	3/2	4.3, 3.7, 2.0		
	$M^{OX}$	0	-	120,124	
Av MoFe	$P^{N}$	0	-	120,121	
	P <sup>1+</sup>	1/2	2.06, 1.95, 1.81	120,122	
	-	5/2	A = 6.7, 5.3; B = 7.3		
	$\mathbf{P}^{\mathrm{OX}}$	3 or 4	11.9	120,125	
Av V-MoFe	V-cluster	3/2	5.50, 4.32, 3.72, 2.01	168	
AV V-MOFE		1/2	1.93		
Av M-cluster	$M^{N}$	3/2	4.6, 3.3, 2.0	130	
	$V^N$	3/2	5.60, 4.35, 3.77	141	
4 a V/E a	$P^{N}$	0	-	158	
Ac VFe	$P^{OX}$	3 or 4	12	158	
	?	1/2	2.04, 1.93	141	
Av VFe	$V^N$	3/2	5.80, 5.40	160	
AVVIE	?	1/2	2.04, 1.93		
	$V^{N}$	3/2	5.71, 5.42		
Av VFe <sub>B</sub> <sup>R</sup>	$P^{N}$	0	-		
AVVIEB	?	1/2	2.04, 1.93		
	Fe(III)	5/2	4.34 (sharp)		
	$V^N$	3/2	5.68, 5.45	162	
Av VFe <sub>B</sub> <sup>N</sup>	$P^{1+}$	5/2	6.67, 5.3, 4.3 (broad)		
AV VreB	?	1/2	2.04, 1.93		
	Fe(III)	5/2	4.34 (sharp)		
Av VFe <sub>B</sub> OX	P <sup>OX</sup>	3	$11.5 \; (\perp)^b, \; 12.8 \; (\parallel)^c$		
Av VFe <sub>O</sub> <sup>N</sup>	$V^N$	3/2	5.50, 4.32, 3.77		
	$\mathbf{P}^{1+}$	5/2	6.68	149	
	P-cluster	1/2	2.03, 1.92		
Av VFe <sub>O</sub> OX	$\mathbf{P}^{\mathrm{OX}}$	3 or 4	3 or 4 ~12 (weak)		
	$M^N$	3/2	4.65, 3.49	163	
Av M-VFe	M-VFe P-cluster?		2.04, 1.93		

Ac V-cluster	$V^N$	3/2	4.5, 3.6, 2.0	157
Av V-cluster	$V^{N}$	3/2	5.55, 3.25, 2.00	168
	Fe <sup>R</sup>	1/2	1.96, 1.92, 1.77	
<i>Rc</i> FeFe	$Fe^{N}$	0	-	
	$Fe^{OX}$	1/2	2.27, 2.06	133
	$P^{N}$	0	-	
	$P^{3+}$	1/2	2.00, 1.98, 1.96	
Av L-cluster <sup>d</sup>	$L^{N}$	1/2	1.97, 1.83	45

 $<sup>^</sup>a$  Relates to the assigned redox state of the cluster, N = dithionite reduced form of the cluster, OX = an oxidized cluster, ? = not been assigned, Fe(III) = adventitious high-spin iron, P-cluster = has not been assigned to a specific state of the cluster.  $^b$  observed in perpendicular mode EPR.  $^c$  observed in parallel mode EPR.  $^d$  The [Fe<sub>8</sub>S<sub>9</sub>C] cluster that serves as the precursor to the M-cluster, and likely the V- and Fe-clusters as well.

### 3.4. The Characterization of Fe-only Nitrogenase

The Fe-only nitrogenase catalytic protein (AnfDGK or FeFe protein) is encoded by the anfDGK genes, and has been expressed in bacterial strains that delete or inactivate the genes for Mo- and V-nitrogenases, or the cells are grown in the presence of tungstate (WO<sub>4</sub><sup>2-</sup>) to repress the expression of Mo-nitrogenase (when the organism lacks genes for VnfDGK). <sup>173-177</sup> The AnfDGK protein has been isolated from A. vinelandii, R. capsulatus, Rhodospirillum rubrum, and R. palustris, but the determination of the subunit composition was fraught with issues similar to those observed for V-nitrogenase. <sup>178,179</sup> There were initially two compositions reported for Av AnfDGK, an  $\alpha_2\beta_2$  variant analogous to the Mo-nitrogenase, and an  $\alpha\beta_2$  species similar to that observed for the Av VFe<sub>A</sub> protein. 66,148 Subsequent studies resulted in a composition for FeFe protein from A. vinelandii and R. capsulatus consistent with a heterohexameric  $\alpha_2\beta_2\delta_2$ formulation and a size of  $M_r = \sim 250$  kDa (AnfD  $\sim 59$  kDa, AnfK  $\sim 51$  kDa, AnfG  $\sim 14$ kDa). 115,180 To date, there is no reported crystal structure of AnfDGK, though, one might anticipate that the protein would retain a structure analogous to those of the Mo- and Vdependent systems based on the similarity between the three systems. AnfDGK has similar subunit size and composition to V- and Mo-nitrogenases (noting that Mo-nitrogenase lacks a NifG subunit), and when the V- and Mo-nitrogenase crystal structures are overlaid, there is modest overlap, with a root-mean-squared deviation of 1.97 Å for all atoms.<sup>74</sup> However, these

factors alone are not sufficient to predict structure, so additional comparison will need to wait for the crystallography of AnfDGK.

Fe-nitrogenase has limited characterization compared to the other nitrogenase species discussed, however, spectroscopic analysis of the catalytic protein from R. capsulatus by EPR, XAS and Mössbauer spectroscopies provided insight into the structure and properties of the cofactors. <sup>76,115,133</sup> In the presence of dithionite, the EPR spectrum of the Rc FeFe protein (FeFe<sup>N</sup>) is featureless, indicating that both the Fe- and P-clusters have a diamagnetic S = 0 spin state. 115 This deviates from the observations in the MoFe protein where the dithionite-reduced state (M<sup>N</sup>) of the protein has a characteristic S = 3/2 signal (g = 4.29, 3.67, 2.01 for Rc MoFe protein) assigned to the M-cluster (Table 3). The Mössbauer spectrum of the <sup>57</sup>Fe-enriched FeFe protein demonstrated that the Fe-cluster in the resting state (Fe<sup>N</sup>) was consistent with 8 total Fe centers, 4 Fe(II) and 4 Fe(III), while the P-cluster was composed of 8 ferrous centers, consistent with the P<sup>N</sup> assignment from Mo-nitrogenase. <sup>76</sup> However, there are some caveats associated with the Mössbauer analysis. The P- and Fe-clusters were not separately labeled with <sup>57</sup>Fe like has been done for the MoFe protein, <sup>181,182</sup> so the contributions from both clusters appeared in the spectra of AnfDGK. The Mössbauer analysis of the VFe protein also suffers from this uniform <sup>57</sup>Fe labeling, and similar methodology is employed for its analysis. 161 As such, for the V- and Feonly nitrogenases an assumption was made that the P-clusters of the alternative systems were spectroscopically analogous to those in NifDK. This was based on the similarity of the fit parameters for the Mössbauer features associated with the P-cluster in NifDK, but also as a means to reduce the number of free variables required for least-squares fitting of the data. <sup>76,161</sup> The remaining V/Fe-cluster contributions were fit, and isomer shifts as well as quadrupole splittings were extracted that compare well to those of the M-cluster. <sup>161,181</sup> For AnfDGK, the oxidation state assignment for the Fe sites of the Fe-cluster was then based on the observed diamagnetism in the Fe<sup>N</sup> state, which could be achieved with equal amounts of ferrous and ferric Fe sites. <sup>76</sup> More recently, X-ray spectroscopy, DFT calculations, and crystallographic methods have been used to reassess the oxidation states of the Fe sites in the M-cluster due to the controversial assignment of the Mo center to be in the 3+ rather than the previously assumed 4+ state. 171,183-187 While these efforts have raised questions about the previous Mössbauer analysis, there have been no studies published in parallel for the alternative systems, so it is unclear how the oxidation state assignments would differ, if at all.

The FeFe protein can also be subjected to turnover conditions, and with a component ratio of 1:10 AnfH:AnfDGK a new rhombic S=1/2 signal appeared in the EPR spectrum with resonances at g=1.96, 1.92, 1.77, which were assigned to the one-electron-reduced form of the Fe-cluster (Fe<sup>R</sup>).<sup>133</sup> Under the same conditions, the MoFe protein yielded a featureless EPR spectrum, further differentiating the Fe-only nitrogenase. Attempts to oxidize the Fe- and P-clusters were also carried out using potentiometric titrations to correlate the EPR signals to the redox behavior. Two S=1/2 species were observed (Figure 18, spectrum 3 and 4), one species had a narrow signal with g=2.00, 1.98, 1.96 and an  $E_{\rm m}=-80$  mV versus SHE, and the other signal was broad with g=2.27, 2.06 and an  $E_{\rm m}\sim+80$  mV versus SHE (Table 3).<sup>133</sup> The narrow signal compared well to the three-electron-oxidized P<sup>3+</sup> species observed for the Av MoFe protein, so was assigned analogously for the Rc FeFe protein.<sup>120</sup> The broad signal was tentatively assigned to the one-electron-oxidized state of the Fe-cluster (FeFe<sup>OX</sup>).<sup>133</sup> Surprisingly, there was no evidence of the P<sup>1+</sup> or P<sup>OX</sup> states of the P-cluster, as both produce EPR active signals in Monitrogenase (see Section 3.2.1).

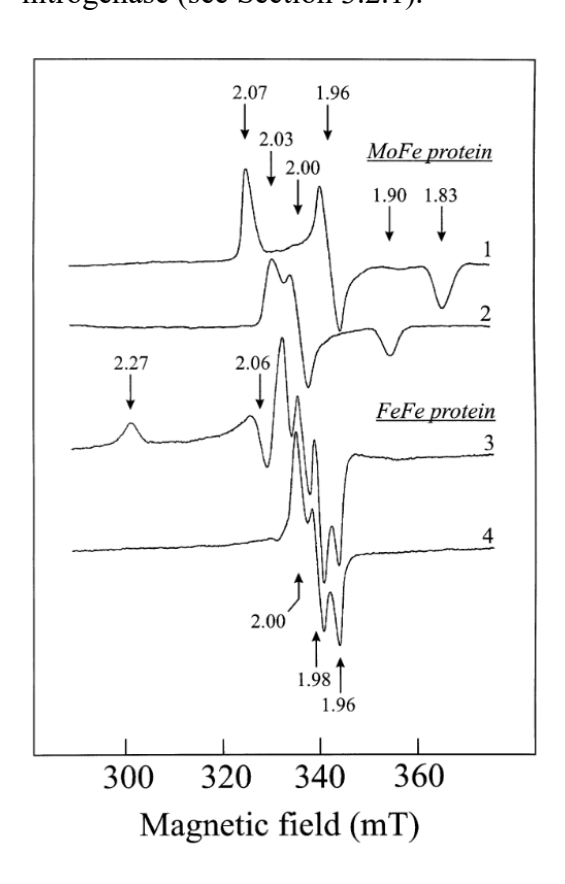


**Figure 18**. The EPR spectra of the Rc MoFe protein (1, 2) and the Rc FeFe protein (3, 4). The Rc MoFe protein oxidized with 2 mM (spectrum 1) and 4 mM (spectrum 2)  $K_3$ [Fe(CN)<sub>6</sub>]. The Rc

FeFe protein oxidized with 2.5 mM K<sub>3</sub>[Fe(CN)<sub>6</sub>] and measured at 16 K (spectrum 3) or 10 K (spectrum 4). Reproduced with permission from ref 133. Copyright 2002 John Wiley and Sons.

The structural information available about AnfDGK and its metallocofactors is limited to the Fe K-edge XAS analysis that provided characterization of the metal clusters housed in the protein. 76 The Rc FeFe protein was analyzed, but XAS provides average information, so the absorber-scatterer pairs that were fit reflect contributions from both the P- and Fe-clusters in the protein. Other methods of analysis have been used for the MoFe protein that involve obtaining XAS data on the *holo*-protein (P- and M-clusters) and the *apo*-protein (P-cluster only) then performing a weighted subtraction to characterize the M-cluster contributions alone, 44 but this type of study has not yet been extended to the FeFe protein. Despite the logistically challenging circumstances, the EXAFS analysis of Rc AnfDGK provided data that appeared similar to analogously collected Rc NifDK, both in the position and general intensity of the Fourier transform features and  $k^3$ -weighted data. Importantly, an Fe---Fe separation of 3.68 Å was a necessary component for the best fit of the data, and this feature is diagnostic in the M-cluster of trigonal prismatic Fe sites, assigned to Fe---Fe distances between the 6 core Fe centers of the cluster (Figure 19). The 3.68-Å distance paired with the other fitting parameters allowed for the proposal that the Fe-cluster is structurally analogous to the M-cluster. This also agrees with the XAS characterization of the precursor L-cluster, as this species should be effectively the same as the Fe-cluster, absent the *R*-homocitrate ligand. 45,56,59

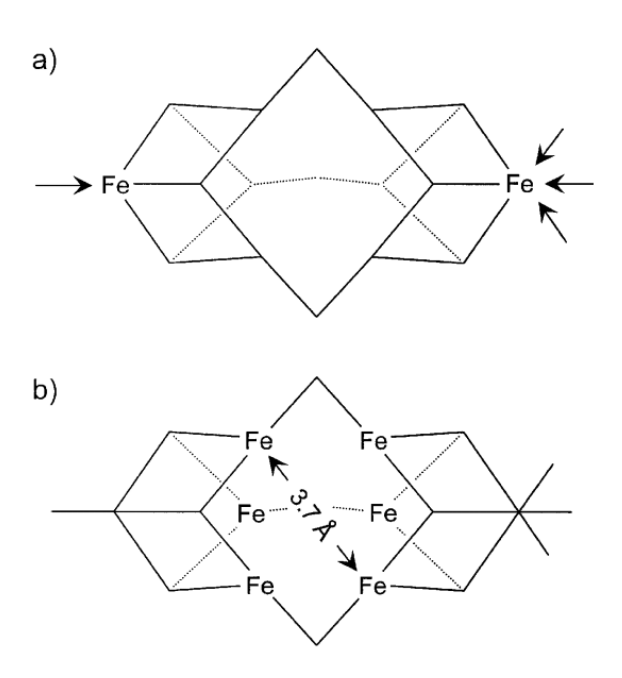


**Figure 19**. Structural elements of the Fe-cluster from the *Rc* FeFe protein based on spectroscopic analysis, the terminal Fe-capped ends of the cluster (a) and the trigonal prismatic Fe-atom arrangement of the cofactor from EXAFS analysis (b). Reproduced with permission from ref 76. Copyright 2001 Springer Nature.

## 4. Reactivity of the Alternative Nitrogenases

The reactivity of nitrogenase is intriguing, as it is the only biological system capable of completely cleaving the strong triple bond of  $N_2$  to generate ammonia under ambient temperature and pressure. It is a multi-electron, multi-proton transfer process that requires nucleotide-dependent electron transduction from the reductase component (Fe protein) to the catalytic component (MFe protein; M = Mo, V or Fe), where the P- and M/V/Fe-clusters facilitate transfer to the substrate.  $^{66,83,101,188,189}$  Proton translocation and substrate hydrogenation are also key aspects of nitrogenase that have been explored through biochemical,  $^{190-192}$  crystallographic,  $^{193}$  and theoretical studies.  $^{194-196}$  However, the data is primarily from Mo-nitrogenase and has yet to be replicated to the same degree, if at all, in the V- or Fe-only nitrogenases. Thus, relevant detail will be described as it relates to the alternative systems but will not constitute an exhaustive review of the MoFe protein.

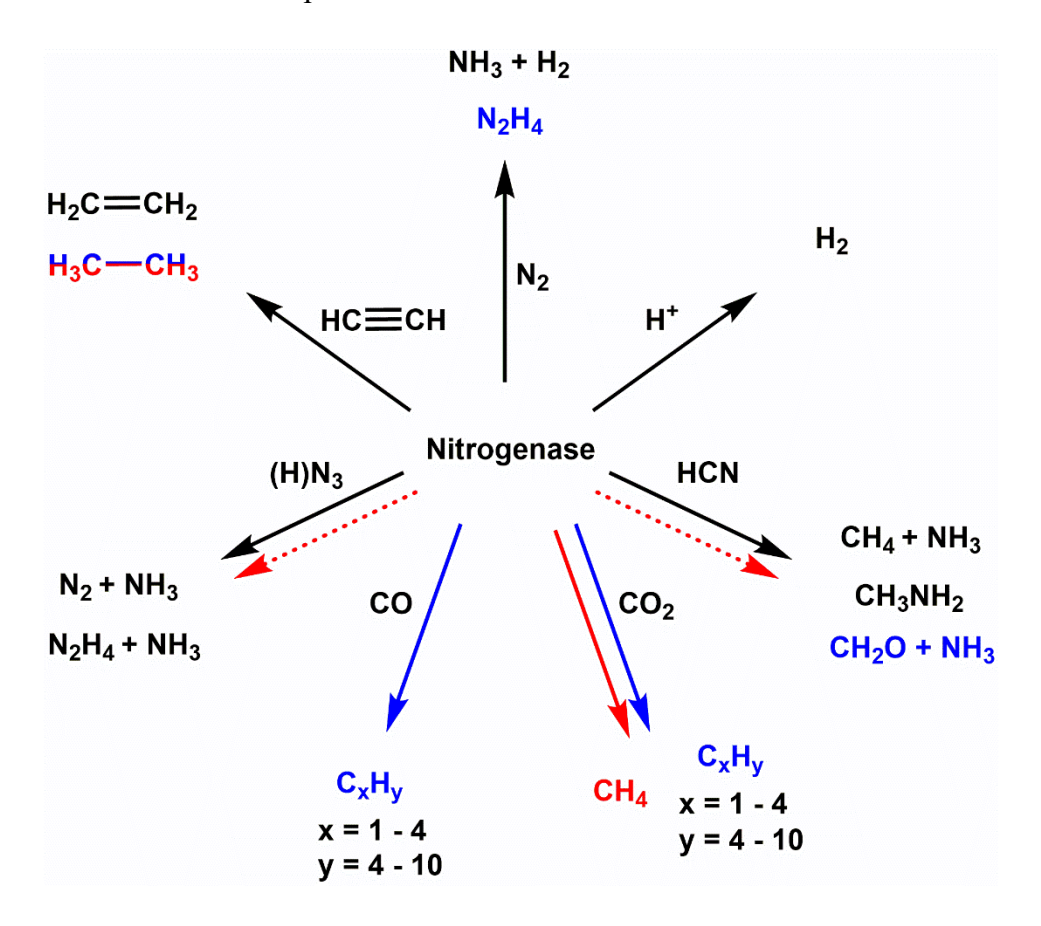


**Figure 20**. Overall summary of the reactions catalyzed by the alternative nitrogenases. Black lines and products represent the capabilities of all nitrogenases, blue and red lines and products represent the capabilities of V/Fe-nitrogenases, respectively. The dotted red lines reflect that Fenitrogenase may be able to carry out the reaction, but it has not been shown experimentally.

 $N_2$  is reduced using 8 H<sup>+</sup> and 8 e<sup>-</sup> equivalents in Mo-nitrogenase, even though N=N bond scission requires 6 H<sup>+</sup>/e<sup>-</sup> equivalents (reaction 1). This is because one equivalent of H<sub>2</sub> is generated as part of the mechanism for N<sub>2</sub>, a phenomenon that is described in more detail in Section 5. In the absence of N<sub>2</sub> or any other substrate, nitrogenase continues to generate H<sub>2</sub> from protons (reaction 2) concurrent with ATP hydrolysis, demonstrating hydrogenase activity.<sup>66,197</sup>

$$2\bar{A}^+ + 2\bar{A}^- \to \bar{A}_2 \tag{2}$$

Over time, other gaseous substrates with triple bonds, such as acetylene ( $C_2H_2$ ) and carbon monoxide (CO) have been investigated as  $C_2$  analogs with differing behavior. Subsequent study expanded the substrate scope to include nitrile compounds such as hydrogen cyanide (HCN), nitrogen-containing species such as azide ( $C_2$ ), nitrite ( $C_2$ ) and nitric oxide ( $C_2$ ), unsaturated cyclic compounds (cyclopropene, diazirine) and alkyne species with terminal triple bonds such as propyne ( $C_2$ ) and propargyl alcohol ( $C_2$ ). These substrates are reactive to varying degrees, some of which mildly or strongly inhibit the enzyme. Most of these compounds have no real physiological relevance but are useful for understanding the reductive capability of nitrogenase. An overall summary of the substrate reactivity with respect to the alternative nitrogenases is shown in Figure 20.

The following section will cover the reactivity of the alternative nitrogenases, including the individual catalytic and reductase components, and how they compare to the well-characterized Mo-dependent system. The reactions of V- and Fe-only nitrogenases have been explored with the 'standard' scope of nitrogenase substrates, N<sub>2</sub>, H<sup>+</sup> and C<sub>2</sub>H<sub>2</sub>, the 'alternative' substrates azide and cyanide, as well as the 'newly-discovered' substrates carbon monoxide and carbon dioxide. The reductase proteins NifH and VnfH are also independently reactive, and have been recently shown to facilitate the reversible conversion of CO to CO<sub>2</sub> in addition to their electron transfer capabilities.

### 4.1. Technical Considerations for the Study of Nitrogenase Reactivity

An important concept for the study of nitrogenase and the associated reactivity is called the electron flux or electron flow, which is the availability of electrons during a reaction. The reduction of protons to H<sub>2</sub> in the absence of any other substrate provides a direct measure of the electron flux in nitrogenase, and as there is no other substrate known to increase H<sub>2</sub> production, the proton reduction activity reflects a maximum turnover rate for the system. 198 Along with this, Watt and Burns showed that the total electron flux through nitrogenase is not sensitive to the substrate,<sup>201</sup> so the total electron equivalents found in substrate reduction products should be equivalent to H<sub>2</sub> production in the absence of substrate, in general, for a well behaved system. For example, V-nitrogenase can reduce acetylene to ethylene (2-electron product) and ethane (4electron product) but will also generate H<sub>2</sub> (2-electron product) in the acetylene atmosphere. The rate of electron consumption with respect to C<sub>2</sub>H<sub>4</sub>, C<sub>2</sub>H<sub>6</sub> and H<sub>2</sub> formed from this reaction should roughly equal H<sub>2</sub> production in an Ar atmosphere, and for this reason, the concept has also been referred to as the electron balance. There are examples of inhibitors, like cyanide (CN<sup>-</sup>), that reduce the total electron flow through the system (i.e. CN binding decreases all substrate reduction including of H<sup>+</sup> under Ar, but CO binding arrests substrate reduction, but H<sup>+</sup> under Ar is unchanged) though this is not as common. The electron flux can also be controlled through the amount of reductase component that is used during catalytic turnover. The nucleotide-loaded Fe protein needs to dock with the MFe component to form a complex before an electron can be transferred and ATP can be hydrolyzed, so increasing the molar ratio of Fe protein to MFe protein can allow for an increased rate of electron consumption, and thus a higher electron flux. The component ratio can affect the activity of the enzyme, but each species of nitrogenase and each substrate may require different ratios to fine tune the system. Typical 'high-flux' ratios are 20:1 or 30:1, but Fe protein can be at saturating concentrations at ~8:1 under certain conditions, <sup>202</sup> and 'low-flux' would constitute ratios at ~1:1 or smaller.

Another important aspect to the reactivity is the quality of the proteins that are used in assays. Acquisition of the individual nitrogenase component proteins is nontrivial, and the method of purification can potentially affect the activity. Both the MFe and Fe proteins contain FeS clusters, each of which is sensitive to O<sub>2</sub>, so all of the purification is necessarily done under anaerobic conditions.<sup>202</sup> Nitrogenase proteins do not overexpress particularly well in the organism, and so hundreds of grams of cells are required to yield protein on a scale of a few hundred milligrams, and up to a gram. Initial reactivity studies often began with cell extracts, the

soluble fraction of the cell lysate, which contain the target nitrogenase proteins with many other proteins from the cell for this reason. Whole cell assays, with acetylene as a substrate, have also been used as a diagnostic tool for identifying nitrogen fixation capability in bacteria, as obtaining isolated protein is time intensive and the direct measure of NH<sub>4</sub><sup>+</sup> is challenging.<sup>203,204</sup> Purification can take several days in some cases, but longer when affinity tags are not used. The alternative nitrogenase proteins are also rather sensitive, and can produce material with variable subunit composition, complicating characterization.<sup>148,175,178</sup>

# 4.2 Standard Nitrogenase Substrate Reduction Activity Towards Dinitrogen, Protons and Acetylene.

Nitrogenase reactivity has been extensively studied, but the proteins utilized do not always originate from the same organisms. The Mo-nitrogenase from A. vinelandii (Av) is one of the best characterized, but the MoFe protein from K. pneumoniae (Kp), C. pasteurianum (Cp), A. chroococcum (Ac), and R. capsulatus (Rc) have also been reported. However, alternative nitrogenase proteins have been isolated and studied from a smaller selection of organisms. V-nitrogenase has only been isolated from A.  $vinelandii^{142}$  and A. chroococcum,  $^{141}$  while the Feonly variant has been isolated from A. vinelandii,  $^{175,176}$  R. capsulatus,  $^{115}$  R. rubrum (Rr),  $^{173}$  and R. palustris (Rp).  $^{177}$  Generally, each subset of nitrogenase proteins reacts in similar ways to proteins from other organisms, though the same experiments or same analysis is not always available. Table 4 reflects a selection of reported specific activities for the reaction of various nitrogenase proteins with the physiological substrates  $N_2$  and  $H^+$ , as well as  $C_2H_2$ .

For Mo-nitrogenase, the proteins from *A. vinelandii* and *A. chroococcum* are similarly active, however, making a comparison of activity can be difficult because the molar ratio of Fe:MoFe proteins is not consistent for each set of experiments, even for the same protein. For instance, specific activities (units of nmol product  $\times$  min<sup>-1</sup>  $\times$  (mg MFe protein)<sup>-1</sup>) for NH<sub>3</sub> formation in *Ac* and *Av* MoFe proteins are 436 and 520, respectively, but the *Ac* experiments report a component ratio of 4:1, whereas the *Av* experiments state that Fe protein is present in saturating concentrations, with a likely ratio of  $\sim$ 10:1.  $^{142,205}$  At first glance, it appears that the *Av* MoFe protein is  $\sim$ 20% more active than the *Ac* MoFe protein, though with a higher electron flux they might be comparable. Proton and acetylene reduction for both species was reported with

saturating amounts of Fe protein, and the *Ac* MoFe protein appears ~30% less active during proton turnover (1541 compared to 2200), but is comparable to the *Av* MoFe for the reaction with acetylene (~2000). 175,206,207 Taking electron balance into account, in the *Ac* MoFe protein series, the N<sub>2</sub> reduction products roughly equal H<sub>2</sub> production under Ar (~3000 nmol electrons per minute) whereas C<sub>2</sub>H<sub>4</sub> formation accounts for 4200 nmol of electrons per minute, and does not include H<sub>2</sub> formed (was not reported, Table 4). This difference could reflect variable reaction conditions between the N<sub>2</sub>, H<sup>+</sup> and C<sub>2</sub>H<sub>2</sub> experiments, or could be the result of either changing protein ratios or batch-to-batch variation of the proteins used. To further illustrate this point, Einsle and co-workers reported ammonia and ethylene formation from reaction with the *Av* MoFe protein, and the specific activities were 78 and 1003, respectively. 150,208 These values reflect a smaller percentage (15% and 50%) of the previously reported activities for the *Av* MoFe protein, but the H<sub>2</sub> production is not reported under any conditions, so it is not possible to accurately assess the electron balance. The smaller values are not likely the result of low electron flux, as the component ratio is 60:1. The *Rc* MoFe protein appears to be genuinely less active than either *Ac* or *Av* MoFe proteins, even with a 40:1 molar ratio of reductase. 115

The activities for various reports of V- and Fe-only nitrogenase are also summarized in Table 4. In general, there is a decrease in activity by the alternative systems across the standard scope of substrates compared to Mo-nitrogenase from the same organism. The Ac VFe protein is ~60% as active for N<sub>2</sub> reduction as the Ac MoFe protein, and Av VnfDGK is ~75% as active as the respective Mo-system. 142,149,205 The FeFe protein from A. vinelandii shows an even lower N<sub>2</sub> reduction activity, 35% compared to MoFe protein, but the Rc FeFe protein maintains 80% of the specific activity of Rc NifDK (190 versus 235). However, the activities for Av and Rc AnfDGK are similar (180 and 190, respectively). 115,176,180 Compared to MoFe protein, the alternative nitrogenases direct a larger fraction of electron equivalents towards H<sub>2</sub> formation during N<sub>2</sub> turnover (Table 4) with FeFe protein> VFe protein> MoFe protein, and this has been interpreted to mean there is a general inefficiency of VnfDGK and AnfDGK to facilitate the reduction of N<sub>2</sub>. The differential production of H<sub>2</sub> during turnover is still an active area of investigation and has important mechanistic considerations that will be discussed further in Section 5. Proton reduction is also decreased in the alternative systems compared to the Mo-dependent nitrogenase, except in the case the Rc FeFe protein, which has an H<sub>2</sub> formation rate two times that of the Rc MoFe protein (Table 4).<sup>115</sup>

Similar to NifDK, the VFe proteins from A. chroococcum and A. vinelandii are comparably active towards the standard substrates, but the electron flux conditions should be taken into account for the best comparisons. The Ac VFe protein fortunately has been reported with varying degrees of completeness using different ratios of Fe protein to VFe protein, and the general trend observed is an increase in activity with an increase of the ratio from ~4:1 to 20:1 (Table 4). Av VnfDGK has been shown to generate products with component ratios of 4:1 to 60:1, but the closest comparison is at 20:1 for Ac and 30:1 for Av. 141,149 VnfDGK from A. chroococcum is ~25% less active for N<sub>2</sub> turnover than A. vinelandii (specific activity of 350 compared to 458), but Ac VFe protein produces 15% more hydrogen during N<sub>2</sub> turnover than Av VFe protein (928 versus 792). This suggests that the Av VFe protein is slightly more efficient at nitrogen fixation than the Ac VFe protein. The reduction of protons is also found with a 20% higher rate for the A. vinelandii protein (1730) compared to A. chroococcum (1348), supporting that the Av VFe protein is more active in general. Interestingly, Dilworth and Eady found that Ac VnfDGK was able to additionally turnover N<sub>2</sub> and release hydrazine (N<sub>2</sub>H<sub>4</sub>) as a product with a specific activity of 1.25 nmol product × min<sup>-1</sup> × (mg VFe protein)<sup>-1</sup> at 40 °C using 3:1 ratio of reductase.<sup>207</sup> Hydrazine was also found not to serve as a substrate for the VFe protein, which is in contrast to the Mo-systems that will turnover hydrazine but do not produce it, except when the protein is acid or base quenched. 209-211 This activity has not been reported for the V-nitrogenase from A. vinelandii.

The comparison of Fe-only nitrogenase proteins also echoes similar reactivity trends towards the physiological substrates as the V-nitrogenase. The activity of the Av FeFe protein has been reported several times,  $^{175,176,180}$  but the highest activity comes from Seefeldt and coworkers using a protein component ratio of 30:1. $^{180}$  The FeFe protein produces even more H<sub>2</sub> during N<sub>2</sub> turnover than the VFe protein, diverting ~50% of the electron flux towards H<sub>2</sub> and decreasing efficiency of the reaction, whereas the Av VFe and MoFe proteins employ 37% and ~20% of electrons towards proton reduction, respectively. AnfDGK from R. capsulatus favors H<sub>2</sub> formation to an even higher degree, using 70% of the total electron flow under an N<sub>2</sub> atmosphere, and consequently has a much higher specific activity for proton reduction in an Ar atmosphere than Av AnfDGK (2600 versus 1085). The Fe-only nitrogenases from R. palustris and R. rubrum are capable of 40% and 2% of the activity observed for N<sub>2</sub> reduction by Av and Rc FeFe proteins, respectively, and are not particularly active towards proton reduction (Table 4),

implying further optimization of conditions may be necessary. Though, the Rr FeFe protein was reported with a Fe protein to FeFe protein ratio of 1:1, reflecting low flux conditions, and a component ratio was not provided for the Rp FeFe protein at all.

Generally, the alternative nitrogenases are not particularly efficient at converting  $N_2$  to  $NH_3$  and are biased toward  $H_2$  formation as compared to the Mo-dependent system, but the non-physiological substrate acetylene reacts differently with the alternative systems. Acetylene is a good substrate for Mo-nitrogenase with apparent  $K_m$  values reported between 0.3–2 kPa, and Mo-nitrogenase exclusively produces ethylene ( $C_2H_4$ ) with a specific activity upwards of 2000 nmol product × min<sup>-1</sup> × (mg MoFe protein)<sup>-1</sup> following the general reaction 3.  $^{142,206,212,213}$ 

$$\bar{A}_2\bar{A}_2 + 2\bar{A}^+ + 2\bar{A}^- \to \bar{A}_2\bar{A}_4$$
 (3)

A small amount of  $H_2$  is produced during acetylene turnover, but the substrate strongly inhibits proton reduction such that >90% of electron flux is funneled towards ethylene formation. <sup>66,214</sup> Further, as the concentration of acetylene is increased,  $H_2$  production can be completely stopped, whereas  $H_2$  is always produced during  $N_2$  turnover. <sup>215,216</sup>

Compared to the MoFe protein, acetylene is generally considered a poor substrate for the alternative nitrogenases. The VFe and FeFe proteins have a slightly lower affinity for the substrate, with apparent  $K_{\rm m}$  values of 6 kPa for Av and Ac VFe proteins  $^{179,217}$  and 14 kPa $^{180}$  and 12.5 kPa $^{115}$  for Av and Rc FeFe proteins, respectively. In contrast, the VFe and FeFe proteins achieve ~30% and ~20% of the specific activity for the formation of  $C_2H_4$  relative to the Modependent system (Table 4). Despite the lower activity, formation of  $C_2H_4$  by VnfDGK (and extension AnfDGK) is proposed to follow a similar pathway as NifDK.  $^{217}$  Eady and co-workers found the transformation catalyzed by the Ac VFe protein to be highly stereospecific, producing  $[cis^{-2}H_2]C_2H_4$  when  $^2H_2O$  is used in the buffer, in line with observations of the Mo-dependent system.  $^{217}$  Unlike for MoFe protein, the alternative nitrogenases are less affected by the  $C_2H_2$ -induced inhibition of proton reduction, as only ~35% and ~15% of the electron flow is diverted to  $C_2H_4$  formation by VFe and FeFe proteins, respectively, while the majority is converted into  $H_2$ .  $^{115,217}$  Ethane can also be generated from acetylene, likely following reaction 4, but it is only observed in the alternative nitrogenases and equates to  $\leq 5\%$  of electron flux for ethylene formation.  $^{178,179}$ 

$$\bar{A}_2\bar{A}_2 + 4\bar{A}^+ + 4\bar{A}^- \to \bar{A}_2\bar{A}_6$$
 (4)

The exclusivity of ethane as a product has led to its use in the identification of nitrogen fixation activity by alternative nitrogenases in whole cell assays.  $^{13,14,218,219}$  It is not exactly clear how the reduction occurs, but free  $C_2H_4$  is not a reaction intermediate. This implies there might be different mechanisms for the formation of  $C_2H_4$  and  $C_2H_6$ , because pure  $C_2H_4$  is not reduced to  $C_2H_6$ . The reaction also has different pH profiles for the VFe and FeFe proteins. *Ac* VnfDGK is able to maintain consistent ethane production across a pH range of 6.5 to 7.5, then the specific activity decreases above pH 7.5; <sup>217</sup> this is in contrast to the *Rc* FeFe protein where product formation maximizes at ~pH 6.6 and steadily decreases at increased pH values. <sup>115</sup>

It is not understood why there is a difference in reactivity between the Mo-dependent and Mo-independent nitrogenases. One possible contributing factor for the V-nitrogenase protein is that it may be more sensitive than the Mo-dependent counterpart. Blanchard and Hales reported that during purification of the *A. vinelandii* VFe protein, two forms of the enzyme were isolated, one with an  $\alpha_2\beta_2(\delta)$  structure, and another slightly less active form with an  $\alpha\beta_2(\delta)$  composition where the amount of the  $\delta$  subunit was variable. There were no isolated alternative forms of the *A. chroococcum* VFe protein reported, however, there were mentions of multiple unresolvable forms of V-nitrogenase with lower activities during the 6-day purification, but these less active fractions were discarded. The use of a histidine-affinity-tag on the *A. vinelandii* VFe protein substantially reduced the time and column runs required to obtain purified protein, and while there may be several factors involved, the His-tagged VFe protein currently produces the highest specific activities for substrate reduction for the system (Table 4). 149

Within the literature, there are several indications that expression and purification of the VFe protein could play roles in the observed reactivity. The *A. vinelandii* VFe protein expressed and purified by Einsle and co-workers is interesting, as it came from a wild-type organism, unlike the gene deletion variants expressed by others.<sup>208</sup> The resulting protein was selectively expressed through repeated growths under strictly Mo-free conditions in the presence of Na<sub>3</sub>VO<sub>4</sub> as a vanadium source. VnfDGK was purified without reported alternate conformations, in contrast to the previous studies of non-tagged VnfDGK from *A. chroococcum* and *A. vinelandii*.<sup>141,148</sup> Specific activities of 454 and 4.93 nmol product × min<sup>-1</sup> × (mg VFe)<sup>-1</sup> for the generation of C<sub>2</sub>H<sub>4</sub> and C<sub>2</sub>H<sub>6</sub>, respectively, were indicative of alternative nitrogenase activity

(Table 4). However, neither  $N_2$  or  $H^+$  reduction activities, nor metal analyses are reported. Subsequently, this protein variant was used to generate the first crystal structure of V-nitrogenase, as well as to trap a putative  $N_2$  reduction intermediate *in crystallo*, though, the specific activity for  $N_2$  reduction was reported with a value of 19, reflecting ~5% of the activity of untagged or tagged *A. vinelandii* VFe protein. Seefeldt and co-workers showed  $N_2$  reduction activity of ~400 with the VFe protein obtained using the same strain and purification protocols reported by Einsle, but acetylene and proton reduction activities are not presented in the study. Additionally, Minteer and co-workers also use the same methodology to obtain and study the VFe protein, and report specific activities of 11 and 0.26 for the formation of  $C_2H_4$  and  $C_2H_6$  from acetylene, reflecting ~3% of the activity seen by Einsle. So far, the field has not yet reached a general consensus with the standardized activity of Av VFe protein for  $C_2H_2$  reduction.

For AnfDGK, it was initially unclear if the first reported protein from A. vinelandii had inherently low activity, <sup>175</sup> or if minor Mo incorporation into the FeFe protein was responsible for the reactivity, <sup>176</sup> implying that the Fe-only cofactor was not active. Like for the VFe protein, the FeFe proteins have also been reported to be generally unstable during purification, which may also have contributed to the attenuated activity. 115,175 However, Müller and co-workers were able to purify AnfDGK from R. capsulatus using a faster protocol, demonstrating specific activities that were much higher than the contemporary A. vinelandii and R. rubrum variants, and additionally showed that Mo was not being incorporated into the FeFe protein. 115,173,178 More recently, Seefeldt and co-workers<sup>180</sup> reported the purification of A. vinelandii FeFe protein from a  $\Delta nifDK$ ,  $\Delta vnfK$  deletion strain analogous to previous reports, <sup>175,176</sup> but the activities were higher, similar to what was observed for Rc FeFe. 115,178 The most active Av and Rc proteins show similar specific activities for N<sub>2</sub> and C<sub>2</sub>H<sub>2</sub> reduction (181 vs 190 and 306 vs 260, respectively) though the R. capsulatus FeFe protein produces between 2 to 4 times more H<sub>2</sub> than the A. vinelandii FeFe protein (Table 4). Metal analysis of the A. vinelandii protein variant showed that Mo and V levels were at or below the detection limit, supporting that the Fe-only cofactor is indeed active. 180 A FeFe protein from R. palustris has also been reported by Harwood and coworkers, and is the first Fe-only nitrogenase to implement a histidine-affinity-tag on the protein to assist with purification. <sup>177</sup> The *R. palustris* FeFe protein appears to be mildly active in general; NH<sub>3</sub> production is found with a specific activity of  $\sim 80$  nmol product  $\times$  min<sup>-1</sup>  $\times$  (mg FeFe)<sup>-1</sup>,

reflecting 40% of the activity as compared to the Av or Rc proteins. A complete substrate study has not yet been shown, so it is unclear the reasons for the difference in activity.

Table 4. Specific Activities for Standard Nitrogenase Substrate Assays $^a$ 

		Products										
Sp.	Protein	NH3 <sup>gg</sup>	$H_2^{gg}$	$C_2H_4^b$	C2H6 <sup>b</sup>	$H_2^b$	$\mathrm{H}_2^c$	N <sub>2</sub> H <sub>4</sub> <sup>gg</sup>	Protein	Ref		
		$(N_2)$	$(N_2)$	$(C_2H_2)$	(C <sub>2</sub> H <sub>2</sub> )	$(C_2H_2)$	(Ar)	$(N_2)$	Ratio <sup>d</sup>			
	NifDK											
Ac	$MoFe^{e}$	436±32	296±4.9	~2100 <sup>f</sup>	-	-	1541 <sup>f</sup>	-	4:1	205-207		
Av	$MoFe^g$	520	-	2000	-	303	2200	-	$\sim 10:1^{f}$	142,175		
Av	MoFe	$78^{h}$	-	1003±93	-	-	-	-	60:1	150,208		
Av	M-MoFe <sup>i,j</sup>	715±82	218±13	1393±101	< 0.3	-	1481±110	-	30:1	168,222		
Av	V-MoFe <sup>i,j</sup>	166±17	174±10	366±27	6±1	-	363±39	-	30:1	168,222		
Rc	$MoFe^k$	235	210	1200	-	$170^{l}$	1300	-	40:1	115		
					VnfDGK							
Ac	$VFe^m$	$259\pm 8^{h}$	$375\pm18^{h}$	-	-	-	1516	$1.25^{n}$	3:1	205,207		
		$(177^n)$										
Ac	$VFe^m$	265	-	426	8.5	-	1094	-	10:1	217		
Ac	$VFe^m$	350	928	608	15	998	1348	-	20:1	141		
Av	$VFe^{o}$	330	-	220	-	-	1400	-	$\sim 10:1^{f}$	142		
Av	$VFe^p$	$\sim 400^{dd}$	-	ı	-	-	-	-	20:1	220		
Av	$VFe^p$	-	-	454±21	4.93±0.64	-	-	-	60:1	208		
Av	$VFe^p$	19	-	"similar	-	-	-	-	4:1	150		
				range to ref 208"								
Av	$VFe^p$	_	_	11.0±1	0.258±0.05	_	_	-	60:1	221		
Av	VFe <sup>i,q</sup>	458	792	560	17	_	1730	-	30:1	149		
Av	M-VFe <sup>i,r</sup>	20±3 <sup>ee</sup>	52±3 <sup>ee</sup>	39±1 <sup>ee</sup>	3.6±0.1 <sup>ee</sup>	61±3 <sup>ee</sup>	104±7.8 <sup>ee</sup>	-	30:1	23		
Av	M-VFe <sup>i,s</sup>	15±1	188±23	66±4	_	-	183±11	-	30:1	34		
AnfDGK												
Av	$FeFe^t$	181±5	599±57	306±3	_	484±3	1085±41	-	30:1	180		
Av	$FeFe^u$	110	220	58	26	226	350	-	20:1	176		
Av	FeFe <sup>v</sup> (3 <sup>Slow</sup> )	38	213	28	-	202	253	-	10:1	175		
Av	FeFe <sup>v</sup>	30	145	18	-	124	203	-	10:1	175		

	(3 <sup>Fast</sup> )									
Rc	$FeFe^{w}$	190	1300	260	ND	$1800^{l}$	2600	-	40:1	115,178
				$(345^{x})$						
Rr	FeFe <sup>y</sup>	$3.6^{z}$	67	6.5	0.22	63	71	-	1:1	173
Rp	FeFe <sup>i,aa</sup>	$\sim \! \! 80^{bb}$	-	-	-	-	$\sim 480^{bb}$	-	-	177
W-incorporation										
Rc	W-MoFe <sup>cc</sup>	$\mathrm{ND}^{hh}$	-	1	-	-	102	-	2:1	223
Av	W-MoFe <sup>ff</sup>	145	165	550	-	70	610	-	~10:1 <sup>f</sup>	224

<sup>a</sup> Examples are selected for comparison of relevant Mo-dependent and Mo-independent systems. The protein labels with a dash indicate the metallocluster before the dash, and the polypeptide used after the dash (e.g. W-MoFe is the tungsten cluster inside of the MoFe protein). Specific activities are reported with units of nmol product  $\times \min^{-1} \times (\text{mg protein})^{-1}$ . Temperature of assays reported at 30 °C. Gas in parenthesis reflects the substrate conditions used for the assay. b assays reported in 10% C<sub>2</sub>H<sub>2</sub>, 90% Ar atmosphere. c assays reported in 100% Ar atmosphere. d ratio of the reductase Fe protein to catalytic nitrogenase protein. e purified from a WO<sub>4</sub><sup>2</sup>tolerant strain MCD50. f reported under saturating conditions of Fe protein. g purified from WT strain UW. h reduction assay uses 4:1 ratio of Fe protein: MFe protein. i histidine affinity tag. j apo-MoFe protein purified from  $\Delta nifB$  deletion strain DJ1143. The appropriate isolated cofactor, M- or V-cluster are then used to reconstitute the protein. k purified from the WT strain B10S. assay reported in 5% C<sub>2</sub>H<sub>2</sub> atmosphere. <sup>m</sup> purified from ΔnifHDK deletion, WO<sub>4</sub><sup>2-</sup> tolerant strain MCD1155. <sup>n</sup> assay reported at 40 °C. <sup>o</sup> purified from ΔnifHDK deletion strain modified from WT UW. purified from WT Lipman 1903 strain, after growing cells multiple times in liquid culture and agar plates with Na<sub>3</sub>VO<sub>4</sub> media in lieu of Na<sub>2</sub>MoO<sub>4</sub>-containing media as described in ref 208. <sup>q</sup> purified from  $\Delta nifHDK$  deletion,  $WO_4^{2-}$  tolerant strain YM68A. r protein purified from  $\Delta nifHDK$  deletion,  $WO_4^{2-}$  tolerant strain YM68A. Cells grown after depletion of V salt from the fermenter, with subsequent inclusion of excess Mo salts. s apo-VnfDK protein was purified from  $\triangle nifHDKB$  deletion,  $WO_4^{2-}$  tolerant strain YM7A. The protein was then reconstituted with M-cluster, was found to have a  $\alpha\beta_2$ composition.  $^t$  purified from  $\Delta nifDK$ ,  $\Delta vnfK$  deletion,  $WO_4^{2-}$  tolerant strain DJ1255.  $^u$  purified from  $\Delta nifHDK$ ,  $\Delta vnfDGK$  deletion, Motolerant strain RP306. <sup>ν</sup> purified from ΔnifHDK deletion, WO<sub>4</sub><sup>2-</sup> tolerant strain CA11. <sup>w</sup> purified from ΔnifHDK deletion strain modified from WT B10S. x assay reported in 100% C<sub>2</sub>H<sub>2</sub> atmosphere. purified from WT strain UR206 in the presence of NaWO<sub>4</sub>. z assay reported in 46% <sup>15</sup>N<sub>2</sub>, 54% Ar atmosphere. <sup>aa</sup> purified from ΔnifH, ΔνnfH deletion strain CGA7554. <sup>bb</sup> converted from nmol product  $\times$  nmol protein to nmol product  $\times$  min<sup>-1</sup>  $\times$  (mg protein)<sup>-1</sup>. cc purified from an anfA mutant of the WT strain B10S that inactivates Fe-only nitrogenase, cells grown with Na<sub>2</sub>WO<sub>4</sub>.  $^{dd}$  converted from nmol product  $\times$  s<sup>-1</sup>  $\times$  (nmol protein)<sup>-1</sup> at 1 atm N<sub>2</sub> to nmol product  $\times$  min<sup>-1</sup>  $\times$  (mg protein)<sup>-1</sup>. ee activities reported with units of nmol product  $\times$  min<sup>-1</sup>  $\times$  (nmol cofactor)<sup>-1</sup>, where nmol cofactor is determined by metal analysis of the protein. f purified from WO<sub>4</sub><sup>2</sup>- tolerant strain UW-LM2, after a series of growths under Mo-free conditions to deplete Mo-stores in the cell. gg assay reported in 100%  $N_2$  atmosphere. gg and detected.

### 4.3 Reactions of Nitrogenase with Azide and Cyanide

The so-called 'standard' nitrogenase substrates beyond dinitrogen are C<sub>2</sub>H<sub>2</sub> and H<sup>+</sup>, and these have been successfully employed in biochemical assays due to their predictable gaseous reaction products that allow for facile detection. The acetylene to ethylene and proton to hydrogen reductions are 2e<sup>-</sup> and 2H<sup>+</sup> processes that have a clear product; ethylene can also be further reduced by 2e<sup>-</sup>/2H<sup>+</sup> to ethane by the alternative nitrogenases, as described earlier. Other non-gaseous substrates have also been explored for their reactivity with nitrogenase. The triatomic azide (N<sub>3</sub><sup>-</sup>) is a logical extension of N<sub>2</sub> as a substrate, being a multiply bonded nitrogen-containing species, and the same can be said for cyanide (CN<sup>-</sup>), as an isoelectronic alternative to dinitrogen. However, these substrates have more complex reduction pathways than the standard counterparts, and they can generate products that stay in solution which can be challenging to detect.

Azide was first shown to be a substrate for Mo-nitrogenase in 1967 by Schöllhorn and Burris, reporting the two-electron reduction using cell extracts from nitrogenase-expressing A. *vinelandii* and C. *pasteurianum* strains, that produced equal amounts of  $N_2$  and  $NH_3$  as shown in reaction  $5.^{225}$ 

$$\bar{A}_3^- + 3\bar{A}^+ + 2\bar{A}^- \to \bar{A}_2 + \bar{A}\bar{A}_3$$
 (5)

Subsequently, Dilworth and Thorneley, then later Burgess and co-workers, reinvestigated this reaction using purified protein components from *A. vinelandii* and *K. pneumoniae*, finding that ammonia was not generated with equal stoichiometry to dinitrogen, but in excess.<sup>226,227</sup> This was interpreted to mean that there was more than one reaction pathway for azide reduction. To further rationalize the observation, extensive product analysis revealed that hydrazine, previously established as a substrate of Mo-nitrogenase,<sup>209</sup> was also a product of the reaction. This led to the proposal that nitrogenase could facilitate two additional azide reduction reactions (reaction 6, 7).

$$\bar{A}\bar{A}_3 + 6\bar{A}^+ + 6\bar{A}^- \to \bar{A}_2\bar{A}_4 + \bar{A}\bar{A}_3$$
 (6)

$$\bar{A}_{3}^{-} + 9\bar{A}^{+} + 8\bar{A}^{-} \rightarrow 3\bar{A}\bar{A}_{3}$$
 (7)

While reactions 5–7 were consistent with the experimental observations, it was also possible that excess ammonia could be produced either by the additional reduction of hydrazine

into ammonia, or through the reduction of the  $N_2$  produced from the 2-electron reaction of azide shown in reaction 5. To test for hydrazine, Dilworth and Thorneley used isotopically labeled  $^{15}N_2H_4$  in azide reduction assays, and found that none of the resulting ammonia detected contained the labeled nitrogen, demonstrating that under those conditions hydrazine was not being further reduced.  $^{226}$  Burgess and co-workers were able to assess if the generated  $N_2$  could be reduced through native nitrogenase reaction by conducting the experiment using an atmosphere of  $^2H_2$  ( $D_2$ ).  $^{227}$  When  $D_2$  was added to the azide reduction assay, the amount of  $N_2$  produced increased, and a corresponding amount of  $N_3$  decreased, while  $N_2H_4$  was unaffected. The inhibition of  $N_3$  production by  $D_2$  was consistent with the well-known inhibition of  $N_2$  reduction by  $H_2(D_2)$ ,  $^{228}$  and supported that  $N_2$  was the source of the excess ammonia. This  $H_2$  inhibition behavior will be discussed with more detail in Section 5.

A further complication arose with the analysis due to the speciation of the azide in solution.  $N_3^-$  is a weak base (pK<sub>a</sub> = 4.6)<sup>229</sup> and nitrogenase is active between pH 7 and 8, so both azide and the conjugate hydrazoic acid (HN<sub>3</sub>) can exist in the reaction; however, the major component would be  $N_3^-$ . As a result, the pH-dependence of the reactions 5 and 6 were also explored, and it was found that  $N_3^-$  was the substrate for reaction 5 while HN<sub>3</sub> was the substrate for reaction 6.<sup>226,227</sup> Additionally, Mo-nitrogenase was found to have a much higher affinity for HN<sub>3</sub> ( $K_m = 12 \mu M$ ) than N<sub>3</sub><sup>-</sup> ( $K_m = \sim 1$ -3 mM), so even with the low concentration of HN<sub>3</sub> in solution, it could still serve as a substrate. It was also unclear if and how reaction 7 was participating during the assay.

V-nitrogenase from *A. vinelandii* was also investigated for a reaction with azide, and compared to Mo-nitrogenase from the same organism by Newton and co-workers. <sup>230</sup> In general, the V-dependent enzyme generated the same set of products, including excess NH<sub>3</sub> but was less active than the Mo-dependent counterpart, producing N<sub>2</sub> and N<sub>2</sub>H<sub>4</sub> at 8% and 33% of the rates for the MoFe protein, respectively (Table 5). It was also found that the VFe protein has a slightly higher affinity for HN<sub>3</sub> ( $K_m = \sim 4 \mu M$ ) than what was reported for the MoFe protein. <sup>227</sup> Interestingly, when the electron pairs required to generate the product are taken into account (e.g., N<sub>2</sub>H<sub>4</sub> is produced from a 6-electron reduction, or 3 electron pairs), the rates of formation by the VFe protein for N<sub>2</sub> and N<sub>2</sub>H<sub>4</sub> are roughly equivalent, whereas N<sub>2</sub> is formed at a rate 4 times higher than N<sub>2</sub>H<sub>4</sub> for the MoFe protein. <sup>230</sup> This was interpreted to mean that the VFe protein has

no preference for the 2-electron (reaction 5) or the 6-electron (reaction 6) processes, while the MoFe protein preferentially carries out the 2-electron reduction. The source of the excess ammonia formation was also probed by carrying out the reaction in the absence or presence of an H₂ atmosphere. The specific activities for NH₃ and N₂H₄ formation of ~110 and 26 nmol product × min<sup>-1</sup> × (mg protein)<sup>-1</sup>, respectively, were determined under both sets of conditions, implying that N<sub>2</sub> generated from azide was not the source of excess ammonia in the V-dependent system, and it was proposed that reaction 7 was instead responsible.<sup>230</sup> However, several things should be noted from the study. One point is that an analogous experiment to assess VnfDGK-catalyzed hydrazine reduction was not reported, nor if hydrazine could be generated from N<sub>2</sub> formed through reaction 5. This is a salient point, as it has been shown that N<sub>2</sub>H<sub>4</sub> is produced from N<sub>2</sub>, but not reduced by the VFe protein from A. chroococcum. 207 Another point is that the Vdependent reductase, VnfH, was not used for the reported assays and instead NifH was employed, which could potentially contribute to the differences in observed results for the VFe protein. Further, Newton reports that they observe no change in azide reduction products in the presence or absence of H<sub>2</sub> in the wild-type and variant Av Mo-nitrogenase systems, in contrast to the study by Burgess using the same enzyme. 151,227,230 It is clear that additional investigation is required to clarify and better understand azide reduction by nitrogenase.

Cyanide reduction by nitrogenase is equally complex, as the substrate is capable of forming several carbon-containing products in addition to ammonia. Hardy and Knight first showed that HCN could be reduced using Mo-nitrogenase containing cell extracts from *A. vinelandii* and *C. pasteurianum*.<sup>231</sup> They observed methane (CH<sub>4</sub>), ammonia, and a small amount of another base that they proposed was methylamine (CH<sub>3</sub>NH<sub>2</sub>) by the following reactions:

$$\bar{A}\bar{A}\bar{A} + 6\bar{A}^+ + 6\bar{A}^- \to \bar{A}\bar{A}_4 + \bar{A}\bar{A}_3$$
 (8)

$$\bar{\mathbf{A}}\bar{\mathbf{A}}\bar{\mathbf{A}} + 4\bar{\mathbf{A}}^{+} + 4\bar{\mathbf{A}}^{-} \rightarrow \bar{\mathbf{A}}\bar{\mathbf{A}}_{3}\bar{\mathbf{A}}\bar{\mathbf{A}}_{2} \tag{9}$$

Further, Hardy and Knight put forward the idea that cyanide was reduced in 2-electron steps in analogy to N<sub>2</sub> fixation, starting from HCN to methyleneimine (CH<sub>2</sub>=NH) in the first step shown by reaction 10,

$$\bar{A}\bar{A}\bar{A} + 2\bar{A}^+ + 2\bar{A}^- \rightarrow \bar{A}\bar{A}_2\bar{A}\bar{A}$$
 (10)

then subsequently to methylamine in the next 2-electron reduction, finally ending with the cleavage of the C–N bond to form methane and ammonia after a total addition of 6 electrons. However, methyleneimine was not detected in their experiments, and the methylamine product was proposed but the extra base could not be clearly identified.<sup>231</sup> Kelly and co-workers were also able to show that cyanide reduction occurred using cell-free extracts from *A. chroococcum*, and formed a very small amount (< 0.1% of methane formed) of the C<sub>2</sub> products ethylene and ethane.<sup>232</sup>

The use of cell extracts complicates analysis because of the plethora of additional proteins present in solution, so Burgess and co-workers used purified Mo-nitrogenase components from A. vinelandii to probe cyanide reduction. 233 Similar to azide, cyanide is present as either the free base CN or the conjugate acid HCN in solution; a pK<sub>a</sub> of 9.11 indicates that the major species under the reaction conditions is HCN.<sup>234</sup> The pH-dependent reduction studies revealed that in the base form, CN is a strong reversible inhibitor of electron flow through nitrogenase, but was not the substrate for the reaction. HCN was the substrate ( $K_m = 4.5 \text{ mM}$ ), and could be reduced by 6 electrons as in reaction 8, or by 4 electrons as in reaction 9, and unsurprisingly produces H<sub>2</sub> in parallel. The specific activities for the formation of CH<sub>4</sub>, NH<sub>3</sub>, CH<sub>3</sub>NH<sub>2</sub> and H<sub>2</sub> were found to be 190, 250, 70 and 500 nmol product × min<sup>-1</sup> × (mg protein)<sup>-1</sup>, respectively (Table 5). However, NH<sub>3</sub> was generated in excess relative to the amount of CH<sub>4</sub> produced, which raised the possibility that either an unobserved 2-electron reduced CH<sub>2</sub>=NH or the 4-electron reduced CH<sub>3</sub>NH<sub>2</sub> could be responsible. Methylamine was tested as a substrate for Mo-nitrogenase, and CH<sub>4</sub> was not detected, indicating that the product could not be further reduced by the enzyme and was likely not a source of the NH<sub>3</sub>.<sup>233</sup> This left a putative 2-electron reduced product as the source of excess ammonia, as methyleneimine would be susceptible to hydrolysis, forming formaldehyde (CH<sub>2</sub>O) and NH<sub>3</sub> (reaction 11), though CH<sub>2</sub>O was not detected. It was also possible that C-C bond formation from coupling HCN molecules could generate ammonia, but ethylene and ethane were only observed after doubling the protein concentration and still only yielded 0.036% and 0.02% of the CH<sub>4</sub> formed, invalidating them as a potential source of ammonia.

$$\bar{A}\bar{A}_2\bar{A}\bar{A} + \bar{A}_2\bar{A} \rightarrow \bar{A}\bar{A}_2\bar{A} + \bar{A}\bar{A}_3$$
 (11)

Newton and co-workers also investigated cyanide reduction by V-nitrogenase from A. vinelandii, with a specific goal to determine if formaldehyde could be produced and detected.<sup>230</sup> There were no pH-dependence experiments done analogously to the Burgess studies with the MoFe protein, <sup>233</sup> so the assumption was made that HCN was the substrate for the reaction. Subsequently, CN<sup>-</sup> was assigned as the inhibitor species in solution. Overall, the VFe protein was less active than the MoFe protein, but was determined to have a similar affinity for the substrate as the MoFe protein ( $K_{\rm m} = 1.9$  mM), and experience less inhibition from CN<sup>-</sup> than for Monitrogenase (Table 5).<sup>230</sup> The product distribution was similar for the VFe and MoFe proteins, though the VFe protein produces a higher amount of CH<sub>3</sub>NH<sub>2</sub> relative to CH<sub>4</sub> than the MoFe protein, with CH<sub>3</sub>NH<sub>2</sub>:CH<sub>4</sub> ratios of 0.66:1 and 0.39:1, respectively. The V-dependent system also generated excess NH<sub>3</sub>, so to assess if reactions 10 and 11 were operative, extensive effort went into the detection and identification of CH<sub>2</sub>O or a further reduced CH<sub>3</sub>OH as products. There were many problems that arose while conducting the analysis, but Newton and co-workers reported the detection and quantification of formaldehyde as a product of HCN reduction, but no methanol was observed, suggesting that the 2-electron reduced product, CH<sub>2</sub>=NH, is generated. However, the small amount of CH<sub>2</sub>O detected does not correspond to the excess ammonia observed, so further investigation is necessary to clarify the source of the additional NH<sub>3</sub>.<sup>230</sup>

Table 5. Specific Activities for the Reduction of Cyanide and Azide by Nitrogenase<sup>a</sup>

		Product						
Protein	Substrate	H <sub>2</sub>	N <sub>2</sub>	CH <sub>3</sub> NH <sub>2</sub>	N <sub>2</sub> H <sub>4</sub>	CH <sub>4</sub>	NH <sub>3</sub>	ref
		$(1)^{h}$	(1)	(2)	(3)	(3)	(3)	
Av MoFe	$KN_3$	1300	630	-	53	-	$290^{b}$	152
Av VFe	KN <sub>3</sub>	470	51	-	18	-	54 <sup>b</sup>	230
Av MoFe	$HCN^{c,f}$	270	-	29	-	50	50	151
Av MoFe	$HCN^{d,f}$	500 <sup>e</sup>	-	$70^{e}$	-	190 <sup>e</sup>	$250^{e}$	233
Av VFe	$HCN^{c,f}$	560	-	20	-	20	20	230
Av VFe	$HCN^{c,g}$	260	-	27	-	17	22	230

<sup>&</sup>lt;sup>a</sup> The reactions are all reported at 30 °C in an Ar atmosphere with a 20:1 molar ratio of the reductase component to the catalytic component. Units are reported as nmol product × min<sup>-1</sup> × (mg protein)<sup>-1</sup>, converted from nmol of electron pairs × min<sup>-1</sup> × (mg protein)<sup>-1</sup> from ref 230. <sup>b</sup> there are several potential routes that can generate NH<sub>3</sub> from N<sub>3</sub><sup>-</sup>, the activities were converted based on a 6-electron reduction. <sup>c</sup> substrate added as NaCN dissolved in HEPES buffer pH 7.4 with added HCl. <sup>d</sup> substrate added as NaCN dissolved in Tes-KOH buffer, adjusted to pH 7.3 with HCl. <sup>e</sup> reactions reported at pH 7.3 using 8:1 molar ratio of reductase component to catalytic component. <sup>f</sup> 5 mM NaCN used. <sup>g</sup> 50 mM NaCN used. <sup>h</sup> the number in parenthesis refers to the number of electron pairs required to generate the product.

### 4.4 Expanded Substrate Reactions for Alternative Nitrogenases

Carbon monoxide is a small gaseous molecule that is isoelectronic to dinitrogen, and therefore was of interest in the study of nitrogenase as a substrate analog.<sup>66</sup> The strong triple bond of CO can be completely cleaved and converted into methane and water in a 6-electron reduction that is analogous to the basic reduction of  $N_2$  (reaction 1).

$$\bar{A}\bar{A} + 6\bar{A}^+ + 6\bar{A}^- \to \bar{A}\bar{A}_4 + \bar{A}_2\bar{A}$$
 (12)

Carbon monoxide can also be used in coupling reactions to produce longer chain, complex hydrocarbons in a process known as Fischer-Tropsch synthesis, often employing  $H_2$  as a source of both protons and electrons.<sup>235</sup> In a fundamental sense, coupling of two CO molecules requires 8 protons and electrons to form  $C_2H_4$  as a product, shown in the following reaction:

$$2\bar{A}\bar{A} + 8\bar{A}^{+} + 8\bar{A}^{-} \rightarrow \bar{A}_{2}\bar{A}_{4} + 2\bar{A}_{2}\bar{A}$$
 (13)

With respect to nitrogenase, CO has been established as an inhibitor of substrate reactions with the exception of H<sup>+</sup> reduction, and the Mo-dependent system has been extensively explored.<sup>66</sup> However, recent discoveries over the past decade have revealed that CO can also behave as a substrate for the V-dependent nitrogenase, showing Fischer-Tropsch-like chemistry. These studies, as well as reactions with carbon dioxide, will be described in the following section.

Like in Mo-nitrogenase, the V-nitrogenases from Av and Ac as well as the Rc Fe-only nitrogenase, in the presence of CO, show complete inhibition of N<sub>2</sub> reduction with increasing partial pressures of CO, but C<sub>2</sub>H<sub>2</sub> reduction is affected for the alternative systems less than the Mo-dependent system. This apparent insensitivity to CO for the reaction has been interpreted to suggest that in some nitrogenases there are multiple acetylene and CO binding sites, each with different affinities for CO, but this is not supported for all of the alternative systems. Aside from the difference in acetylene reduction, it has been broadly considered that MoFe protein and the alternative nitrogenases react with CO in a similar manner, though careful analysis reveals differences between the systems that are quite intriguing. It was observed that for acetylene reduction by Av VnfDGK in the presence of CO, low electron flux (1:5, VnfH:VnfDGK) led to an increase in ethylene formation relative to higher flux (8:1) conditions, and further, ethane formation was enhanced at low pressures of CO. This seems to be a unique feature of the Av Vinelandii system, as the VFe protein from Av Chroococcum

demonstrates more typical inhibition of acetylene reduction in the presence of CO. $^{217}$  Rc AnfDGK has also been shown to feature analogous inhibition of substrate reduction as the MoFe and VFe proteins, particularly at lower partial pressures of CO. $^{115}$  However, acetylene reduction by AnfDGK in the presence of high concentrations of CO produces an amount of ethane that exceeds ethylene production by ~80%, whereas in V-nitrogenase the two products formed are inhibited with similar behavior. $^{174}$  As mentioned, hydrogen production by the MoFe and Ac VFe proteins is unsurprisingly stable in a CO environment, $^{217}$  however, for Av V-nitrogenase it was reported that increasing the atmosphere from 0 to 100% CO (while balancing the pressure with Ar), resulted in a decrease in the specific activity for proton reduction of ~75%. $^{149}$  It is uncertain why the Av protein has this inhibition pattern, but it has been proposed that there may be two separate mechanisms for  $H_2$  evolution, one of which is more sensitive to CO binding. $^{149}$ 

It was also discovered that Av V-nitrogenase is capable of reducing CO to longer chain hydrocarbon products, forming C-C bonds (Table 6). 237,238 For comparison, Av Mo-nitrogenase is minimally able to convert CO to hydrocarbons with specific activities for C<sub>2</sub>H<sub>4</sub> and C<sub>2</sub>H<sub>6</sub> of 0.025 and 0.013, compared to 32 and 1 for the VFe protein. These CO-based activities are much lower than the standard N<sub>2</sub>, C<sub>2</sub>H<sub>2</sub>, and H<sup>+</sup> substrates, as a high degree of electron equivalents are diverted to  $H_2$  formation (specific activities of 1700 and 540 nmol  $H_2 \times (mg \text{ protein})^{-1} \times min^{-1}$  for the MoFe and VFe proteins, respectively).<sup>238</sup> The product distribution changes when <sup>2</sup>H<sub>2</sub>O and deuterated Tris buffer are used to carry out these reactions. <sup>237,238</sup> Greater yields of product are observed in the presence of deuterated solvent and C<sub>4</sub> products are generated by NifDK, whereas similar products are observed for VnfDGK in proteo- and deutero-solvents (Table 6).<sup>237</sup> These differences also show inverse kinetic isotope effects (KIE) for product formation from CO by the MoFe and VFe proteins, with average KIEs of ~0.1 and ~0.5, respectively. The KIE can be affected by many contributing factors, particularly from modified dynamics of the protein, so more work would be necessary to ascertain the meaning of these effects. Another observation was that the presence of H<sub>2</sub> inhibits the formation of C<sub>2</sub>H<sub>4</sub> from CO by ~10% at lower concentrations of H<sub>2</sub> (~10% H<sub>2</sub>, 90% CO) and upwards of 25% at higher concentrations (67% H<sub>2</sub>, 33% CO).<sup>238</sup> H<sub>2</sub> is only known to inhibit N<sub>2</sub> reduction for nitrogenases, <sup>66,217</sup> so inhibition of CO reduction by H<sub>2</sub> may indicate that there are similar mechanistic features between the CO and N<sub>2</sub> reduction reactions.

CO has not only been shown to be a substrate during *in vitro* assays with purified enzyme, but *A. vinelandii* cells expressing VnfDGK (strain YM68A) are also competent for CO reduction.<sup>239</sup> When the cell cultures have depleted the ammonium from the initial growth media, a CO atmosphere is added and the headspace of the reaction vessel is monitored over 8 hours. Ethylene, ethane and propane are observed with maximum hydrocarbon formation occurring in a 15% CO, 85% Ar atmosphere (specific activity ~6 nmol product × (mg protein)<sup>-1</sup> × min<sup>-1</sup>; mg protein is based on average yield from cells), which reflects ~20% of the activity of isolated VnfDGK in a 100% CO atmosphere for the same products.<sup>237,238</sup> Above 15% CO, the hydrocarbon yield drops; in a 37.5% CO atmosphere the specific activity for hydrocarbon formation is ~2.5.<sup>239</sup> This *in vivo* activity is suggestive of vestigial metabolic ability of nitrogenase and may not simply be an adventitious feature.

Carbon dioxide is another carbon-containing small molecule in a more oxidized state than CO and can serve as a potential substrate for nitrogenase. CO<sub>2</sub> has been shown by Seefeldt and co-workers to be reduced to CO and H<sub>2</sub>O (reaction 14) by the wild-type Av MoFe protein, and to CH<sub>4</sub> and H<sub>2</sub>O (reaction 15) by a modified Av MoFe protein variant.<sup>240,241</sup>

$$\bar{A}\bar{A}_2 + 2\bar{A}^+ + 2\bar{A}^- \to \bar{A}\bar{A} + \bar{A}_2\bar{A}$$
 (14)

$$\bar{A}\bar{A}_2 + 8\bar{A}^+ + 8\bar{A}^- \to \bar{A}\bar{A}_4 + 2\bar{A}_2\bar{A}$$
 (15)

These reactions proceed with specific activities of 0.8 and ~5 nmol product × (mg protein)<sup>-1</sup> × min<sup>-1</sup>, respectively, though no CO<sub>2</sub> reduction to CH<sub>4</sub> was observed for the wild-type enzyme. This is markedly slower than reaction with the standard nitrogenase substrates, or with CO (Table 6). CO<sub>2</sub> reduction was then revisited by Ribbe and co-workers using *Av* V-nitrogenase in addition to the Mo-dependent enzyme.<sup>242</sup> Reaction of CO<sub>2</sub> with the MoFe protein was able to produce CO, CH<sub>4</sub> and C<sub>2</sub>H<sub>4</sub> with specific activities of 3.3, 0.27 and 0.14 (units of ×10<sup>-3</sup>), where the VFe protein generated CO comparable with MoFe protein, but no other observed products. However, both enzymes saw an order of magnitude increase of CO formation in D<sub>2</sub>O, and the VFe protein also produced CD<sub>4</sub>, C<sub>2</sub>D<sub>4</sub> and C<sub>2</sub>D<sub>6</sub> with higher rates than observed for Monitrogenase in H<sub>2</sub>O (Table 6). This means that CO production from CO<sub>2</sub> has an inverse KIE for both nitrogenases, with similar activities, indicating that this reaction is carried out with a similar mechanism. However, the fact that use of H<sub>2</sub>O/D<sub>2</sub>O results in different profiles for C–C bond formation indicates that the MoFe and VFe proteins may undergo chain extension through

different routes.<sup>242</sup> The isolated Fe-only nitrogenase from *R. palustris* was also shown to react with  $CO_2$  to produce  $CH_4$  with a specific activity of  $\sim 10 \times 10^{-3}$  nmol product  $\times$  (mg protein)<sup>-1</sup>  $\times$  min<sup>-1</sup>, which is a higher activity than measured for the MoFe or VFe proteins, though longer chain hydrocarbon products or CO were not reported.<sup>177</sup>

CO<sub>2</sub> reduction by alternative nitrogenases has been observed to have metabolic relevance in the native organism.  $^{177}$  Harwood and co-workers reported that a strain of the phototrophic R. palustris expressing V-nitrogenase produced a small, but detectible amount of methane from CO<sub>2</sub>, whereas a strain expressing the Fe-only nitrogenase produced roughly an order of magnitude more methane than V-nitrogenase, and methane formation was found to increase commensurate with light intensity. Isotopically labeled NaH<sup>13</sup>CO<sub>3</sub> was incubated with the Feonly nitrogenase strain as a source of CO<sub>2</sub> and <sup>13</sup>CH<sub>4</sub> formation was measured, confirming a CO<sub>2</sub>-based chemical transformation. Additionally, the Fe-only nitrogenase expressing organisms R. rubrum, R. capsulatus and A. vinelandii were also tested for in vivo CO<sub>2</sub> reduction activity. 177 When the cells were grown under nitrogen-fixing conditions (no supplemented source of reduced nitrogen species), R. palustris, R. rubrum, and R. capsulatus produced 400–500 nmol CH<sub>4</sub> × (mg total protein)<sup>-1</sup> in the absence of supplemented Mo, but with a Mo source present, the Fenitrogenase proteins were repressed and the activity was absent. This indicated that the Fe-only nitrogenase was the reactive species. Similar behavior was observed with wild-type A. *vinelandii*, but CH<sub>4</sub> production reflected only ~1% of the activity for the other organisms. <sup>177</sup> This difference could indicate that the Av FeFe protein is not efficient at CO<sub>2</sub> reduction, or it could be that the VFe protein is being preferentially expressed in the absence of Mo, despite the fact that VO<sub>4</sub><sup>3-</sup> is not added to the growth media.

The reduction of  $CO_2$  is a challenging 8 electron process (reaction 15), not dissimilar from  $N_2$  reduction, and in nitrogenase, electron delivery is intimately linked to the reductase Fe protein. Efforts from several groups have been made to understand how the Fe protein and associated electron delivery can change  $CO_2$  reduction. Ribbe and co-workers studied  $CO_2$  reduction using a Eu-based chemical reductant  $Eu^{II}DTPA$  (DTPA = diethylenetriamine pentaacetic acid) in an ATP-independent reaction without Fe protein. VnfDGK from A. vinelandii was studied under these conditions, and  $C_1$  to  $C_4$  products were observed, with the primary products being CO and  $CH_4$  (4.3 and  $0.92 \times 10^{-3}$  nmol product  $\times$  (mg protein) $^{-1} \times min^{-1}$ ,

respectively). This reflects an improvement in the activity for the VFe protein, as products from CO<sub>2</sub> were not observed in proteo-buffers in the presence of the reductase protein, <sup>242</sup> but the VFe protein is still more active towards CO reduction. <sup>237,238</sup> The CO<sub>2</sub> reduction has also been carried out analogously in isotope labeled buffers, and KIEs have been reported for product formation. In comparison, for CO reduction under ATP-dependent conditions, all products had inverse KIE values, <sup>237</sup> but in the ATP-independent system for the reduction of CO<sub>2</sub>, VnfDGK has an inverse KIE for all but methane, which has a more classical KIE value of ~4.8. <sup>243</sup> This may indicate there could be a change in mechanism for methane formation from CO<sub>2</sub> compared to CO reduction, as the latter has an inverse KIE of ~0.9. The Fe protein may also play a role in the generation of methane (or lack thereof, see Section 4.7). However, the introduction of the chemical reductant could have additional effects on the protein or the reaction, so detailed mechanistic experiments would be necessary to further interpret this phenomenon.

The electrocatalytic reduction of CO<sub>2</sub> has been explored by Minteer and co-workers using the V-dependent nitrogenase from A. vinelandii in combination with derivatives of cobaltocene as electron meditators.<sup>221</sup> The VFe protein was added to an electrolyte solution containing NaHCO<sub>3</sub> as the CO<sub>2</sub> source, and when potential was applied, CH<sub>4</sub>, C<sub>2</sub>H<sub>4</sub> and C<sub>3</sub>H<sub>6</sub> products were measured in roughly equal amounts (Table 6). Interestingly, CO is not observed in the analysis, in contrast to the ATP-dependent and ATP-independent systems reported by Ribbe where CO formation constitutes ≥75% of observed products. <sup>242,243</sup> However, the rate of typical acetylene reduction reported by Minteer is rather low (Table 4), and may indicate that the VFe protein used was less active and therefore not reflective of the full product distribution.<sup>221</sup> Seefeldt and coworkers also report the electrocatalytic, as well as ATP-driven, reduction of CO<sub>2</sub> by the MoFe and FeFe proteins from A. vinelandii. 244 It was shown that both proteins were able to generate formate (HCO<sub>2</sub><sup>-</sup>), a 2-electron reduced product, using Fe protein or an electrode, though in the FeFe protein, a higher percentage of electron equivalents (31% vs 9% for the MoFe protein) go towards CO<sub>2</sub> reduction instead of H<sub>2</sub> production. If CO<sub>2</sub> is primarily converted to formate, this set of results may be consistent with the *in vivo* observation of low CH<sub>4</sub> production by Harwood for A. vinelandii, 177 but further studies would be necessary to confirm this finding.

Table 6. Reported Specific Activities for CO and CO<sub>2</sub> Reduction by Nitrogenase<sup>a</sup>

		Products									
Sp.	Protein	H <sub>2</sub>	CH <sub>4</sub>	C <sub>2</sub> H <sub>4</sub>	C <sub>2</sub> H <sub>6</sub>	СзН6	СзН8	C <sub>4</sub> H <sub>8</sub>	C4H10	Protein	ref
		$(CO)^q$	(CO)	(CO)	(CO)	(CO)	(CO)	(CO)	(CO)	Ratio <sup>h</sup>	
Av	$MoFe^{b,c}$	~1700000	-	25	13	2.9	5.9	-	-	10.1	237,238
	More			[730]	[110]	[55]	[63]	[6.8]	[7.4]	10:1	
1	$VFe^{d,c}$	~540000 <sup>f</sup>	510	32000	1000	43	560	2.1	3.3	10:1	237,238
Av	v re <sup>a,,</sup>		[1200]	[35000]	[1500]	[220]	[590]	[6.4]	[9.8]		
4	M M - E - e. C	-	-	26	13	3.0	4.5	-	-	20.1	222
Av	M-MoFe <sup>e,c</sup>		[100]	[410]	[71]	[43]	[31]	[6.6]	[7.0]	30:1	
4	V-MoFe <sup>e,c</sup>	-	-	33	8.8	3.4	3.1	-	-	20.1	222
Av	v-More"		[81]	[370]	[93]	[49]	[21]	[6.5]	[10]	30:1	
Av	M-VFe <sup>g,c</sup>	$42200^{p}$	-	$650^{p}$	21 <sup>p</sup>	$1.7^{p}$	$7.3^{p}$	-	$0.75^{p}$	30:1	23
					Prod	ucts					
Sp.	Protein	CO	CH <sub>4</sub>	C <sub>2</sub> H <sub>4</sub>	C <sub>2</sub> H <sub>6</sub>	C <sub>3</sub> H <sub>6</sub>	C <sub>3</sub> H <sub>8</sub>	C <sub>4</sub> H <sub>8</sub>	C4H10	Protein	ref
-		$(CO_2)^i$	(CO <sub>2</sub> )	(CO <sub>2</sub> )	(CO <sub>2</sub> )	(CO <sub>2</sub> )	(CO <sub>2</sub> )	(CO <sub>2</sub> )	(CO <sub>2</sub> )	Ratioh	
4	MoFe <sup>b,c</sup>	3.3	0.27	0.14	-	-	-	-	-	6.1	242
Av		[14]								6:1	
Av	$VFe^{d,c}$	4.3	-	-	-	-	-	-	-	6.1	242
		[13]	[8.7]	[1.5]	[0.083]					6:1	
1	VFe <sup>d,c</sup>	4.3	0.92	0.15	0.15	0.078	0.054	0.021	0.021	j	243
Av	vre '	[5.5]	[0.19]	[0.34]	[0.22]	[0.21]	[0.099]	[0.070]	[0.045]		
Av	$VFe^k$	-	~35 <sup>l</sup>	$25\pm5^{l}$	-	42±7 <sup>l</sup>	-	-	-	m	221
Rp	FeFe <sup>n,c</sup>	-	~10°	-	-	-	-	-	-	-	177

<sup>&</sup>lt;sup>a</sup> Activities in [brackets] were run in <sup>2</sup>H<sub>2</sub>O and deuterated buffer and correspond to the deuterated product. Values reported in units of 10<sup>-3</sup> nmol product × min<sup>-1</sup> × (mg protein)<sup>-1</sup> except where indicated otherwise. Temperature of assays reported at 30 °C. <sup>b</sup> purified from strain YM13A with His-affinity-tagged MoFe. <sup>c</sup> Histidine affinity tag. <sup>d</sup> purified from ΔnifHDK deletion, WO<sub>4</sub><sup>2-</sup> tolerant strain YM68A. <sup>e</sup> apo-NifDK protein purified from ΔnifB deletion strain DJ1143. The appropriate cofactor, M- or V-cluster are then used to reconstitute the protein. <sup>f</sup> ratio of reductase to nitrogenase used is 30:1. <sup>g</sup> protein purified from ΔnifHDK deletion, WO<sub>4</sub><sup>2-</sup> tolerant strain YM68A. Cells grown after depletion of V salt from the fermenter, with subsequent inclusion of excess Mo salts. <sup>h</sup> ratio of the reductase Fe protein to catalytic nitrogenase protein. <sup>i</sup> NaHCO<sub>3</sub> is the CO<sub>2</sub> source in an Ar atmosphere. <sup>j</sup> no reductase protein used,

chemical reductant only – Eu<sup>II</sup>DTPA (DTPA = diethylenetriamine pentaacetic acid).  $^k$  purified from WT Lipman 1903 strain, after growing cells multiple times in liquid culture and agar plates with Na<sub>3</sub>VO<sub>4</sub> media in lieu of Na<sub>2</sub>MoO<sub>4</sub>-containing media as described in ref 208.  $^l$  reported values with units of  $10^{-3}$  nmol product × (nmol protein) $^{-1}$ .  $^m$  reaction driven electrocatalytically.  $^n$  purified from  $\Delta nifH$ ,  $\Delta vnfH$  deletion strain CGA7554.  $^o$  assay reported 0.45 atm of CO<sub>2</sub> (no counter gas specified – likely Ar).  $^p$  activities reported with units of nmol product × min $^{-1}$  × (nmol cofactor) $^{-1}$ , where nmol cofactor is determined by metal analysis of the protein.  $^q$  100% atmosphere of CO.

## 4.5 Activities of the Isolated Nitrogenase Cofactors

The alterative nitrogenase proteins have been studied and their enzymatic properties have been compared to the well-characterized Mo-dependent system. However, while each nitrogenase has conserved structural features and reactivity, it can often be challenging to untangle the effects of the protein from the cofactor when analyzing the Mo-, V- and Fe-only nitrogenases. To this end, the catalytic nitrogenase clusters can be extracted from the protein in order to explore their properties, as first demonstrated for Mo-nitrogenase by Shah and Brill in 1977.<sup>245</sup> Over the years, several methodologies have been utilized to acquire cofactor, <sup>131,246</sup> but the general outline involves the purification of large quantities (gram scale) of nitrogenase enzyme and carefully denaturing the protein using acids and organic solvent under strictly anaerobic conditions. The denatured protein can then be neutralized, pelleted by centrifugation and subsequently washed with organic solvent to prepare for cluster extraction. NMF (Nmethylformamide), DMF (dimethylformamide) and MeCN (acetonitrile) in the presence of base have all been used to extract the target cofactor, though basified NMF has the highest success. Initial study of the isolated cofactor was done to obtain spectroscopic parameters associated with the M- and then later V-cluster directly, but also as a method to obtain active nitrogenase from the apo-enzyme. 66,131

The M- and V-clusters from *A. vinelandii*, but not the Fe-cluster, have been isolated and had their catalytic abilities studied, but the precursor L-cluster lacking the *R*-homocitrate ligand has been investigated as a Fe-cluster analog.  $^{247-251}$  The substrate reduction activity of the M- and V-clusters with small molecules was first reported in 2012 by Ribbe and co-workers, using Tris-HCl buffer at pH 8 with Eu<sup>II</sup>DTPA as the reductant, in the presence of both CO and NaCN.  $^{247}$  The cofactors were shown to be stable in the aqueous media, as both the M- and V-clusters are able to reactivate the *apo-*( $\Delta nifB$ )-MoFe protein with similar proton reduction activities over the course of an hour, indicating that the cofactors are not decomposing. CO reduction generated a distribution of C<sub>1</sub>–C<sub>4</sub> products with comparable activity for both the M- and V-clusters, verified through using isotopically labeled  $^{13}$ CO (Table 7).  $^{247,249}$  However, the total turnover number (TON; nmol product × (nmol cofactor)  $^{-1}$  × n, where n is the number of C for each product (C $_n$ H $_m$ )) for product formation is  $\sim$ 0.3 indicating a substoichiometric reaction. The reduction of CN $^-$  was slightly more successful, producing up to C $_6$  hydrocarbons that were identified from

 $^{13}$ CN $^{-}$  with the primary carbon product being  $C_2H_4$  (~60% of hydrocarbon products formed). The total TON for carbon products from cyanide was reported as 17 for M-cluster and 16 for Vcluster, however, ammonia production had a slightly higher TON than total hydrocarbon formation, for both clusters.<sup>249</sup> Later, the L-cluster was reported along with the M- and Vclusters using the same buffer system as well as reductant, and the L-cluster was found to be as stable, and react with CO and CN<sup>-</sup> similarly to the M- and V-clusters (Table 7).<sup>249</sup> Reduction of CO yielded a total TON of 0.3, whereas the reaction with CN<sup>-</sup> reflected carbon-based TON of 20. There is a tendency for the L-cluster to form more methane from both CO and CN<sup>-</sup> than the other two clusters, and one suggested rationale for this difference was that the M- and V-clusters both had the organic acid ligand bound to the heterometal site, whereas L-cluster lacks the native ligand and therefore has an additional open reaction site.<sup>249</sup> This was additionally supported through the use of Anderson-Schulz-Flory plots that are often used to describe product distributions in Fischer-Tropsch synthesis. For the M- and V-clusters these plots demonstrated that for the reduction of CO and CN<sup>-</sup>, the generation of methane deviates from the predicted behavior, whereas for the L-cluster the behavior does not. This indicated that the M- and Vclusters are somehow capable of facilitating the coupling of CH<sub>x</sub> groups to produce longer chain hydrocarbons which disfavors the release of methane.<sup>249</sup>

The isolated cofactor chemistry was further explored by changing the solvent to dry DMF, introducing 2,6-lutidinium triflate and triethyl amine as a buffering system, and using the stronger samarium (II) iodide (SmI<sub>2</sub>) reductant to replace Eu<sup>II</sup>DTPA ( $E^{0}$ , Sm = -1.55 V versus SCE in tetrahydrofuran compared to  $E^{0}$ , Eu = -1.14 V at pH 8). The carbon-based TON for CO reduction by all three cofactors is increased by an order of magnitude with SmI<sub>2</sub>, having values of 3, 2.7, 4.5 from CO for the M-, V- and L-clusters, respectively. Cyanide reduction was mildly increased by use of the more reducing SmI<sub>2</sub> (Table 7). Compared to the Eu-reductant experiments, all of the clusters tended to strongly favor formation of C<sub>1</sub> (CH<sub>4</sub>) and C<sub>2</sub> (C<sub>2</sub>H<sub>4</sub>, C<sub>2</sub>H<sub>6</sub>) products instead of chain elongation, though C<sub>4</sub> products (C<sub>4</sub>H<sub>8</sub>, C<sub>4</sub>H<sub>10</sub>) are observed from gas chromatography – mass spectrometry (GC-MS) analysis and confirmed by <sup>13</sup>C labeling. This tendency to form methane from CO differs from the protein-based activity of the MoFe protein, where C<sub>2</sub> and C<sub>3</sub> (C<sub>3</sub>H<sub>6</sub>, C<sub>3</sub>H<sub>8</sub>) products are observed, but not methane. <sup>237,238</sup> Additionally, the stronger reductant system was able to facilitate reduction of CO<sub>2</sub>, which produces C<sub>1</sub>, C<sub>2</sub> and C<sub>3</sub> products with total TONs ~50% less than those for CO reduction, and

favors formation of CO and CH<sub>4</sub> (Table 7).<sup>248</sup> By far the most abundant product formed in these isolated cofactor reactions is H<sub>2</sub>, with TON from reaction with CO and CO<sub>2</sub> of ~5 for all three cofactors, but in the presence of CN<sup>-</sup> proton reduction is slightly higher at ~14 for M- and Feclusters and ~11 for the V-cluster. Although, there is nonzero H<sub>2</sub> formation from the SmI<sub>2</sub> directly, this reduction also happens to be the 'standby' reaction facilitated by the respective enzymes when other substrates are absent. 66 Subsequent refinement of conditions, in addition to using triethylammonium tetrafluoroborate (Et<sub>3</sub>NH(BF<sub>4</sub>)) instead of 2,6-luitdinium triflate as the proton source for the organic buffer system, and SmI<sub>2</sub> reductant allowed for further increased TON of substrate reduction for the M- and L-clusters. 250,251 For the M-cluster, the carbon-based TON for CO, CN<sup>-</sup> and CO<sub>2</sub> reduction increased to 230, 910 and 68, respectively, with longer chain hydrocarbons being observed up to C<sub>5</sub> (C<sub>5</sub>H<sub>10</sub>, C<sub>5</sub>H<sub>12</sub>).<sup>251</sup> CO<sub>2</sub> reduction with the optimized conditions yielded up to C<sub>4</sub> hydrocarbons (up from C<sub>3</sub>), with a compensating decrease in the percentage of C<sub>1</sub> (CO, CH<sub>4</sub>) formation (97% vs 63% C<sub>1</sub>). The same reactions facilitated by the Lcluster reflect 70%, 80% and 40% of the total TON compared to M-cluster for CO, CN-, and CO<sub>2</sub>, respectively, though a similar shift from C<sub>1</sub> to longer chain hydrocarbon products is observed (Table 7).<sup>250</sup> The chemistry of the V-cluster with these improved conditions was also explored for CO and CO<sub>2</sub>, with TON of 300 and 55, respectively. The TON for CO is higher than for the M or L-clusters, though the values for CO<sub>2</sub> reduction fall in between the other clusters (Table 7). Collectively, these experiments with isolated cofactor demonstrate that all three of the clusters studied react in broadly similar ways, but there are indeed some differences that seem to derive from the choice of heterometal as well as the organic ligand that binds to the cluster.

The isolated M-cluster has also been shown to reduce and couple formaldehyde and acetaldehyde to longer chain hydrocarbons using a Eu(II) reductant in buffered aqueous solution. These reactions cannot be analogously studied with the protein systems as aldehydes tend to denature or otherwise disrupt the protein structure. Compared to CO reduction, formaldehyde has a much higher total TON of 67 as compared to 1.5 for CO with the same product scope. Primarily, formaldehyde produces methane with C2 carbon products being the next most abundant, but minor amounts of C3 and C4 products are observed. Acetaldehyde on the other hand features a total turnover of 112 for substrate reduction, and is primarily reduced to ethane, followed by butylene, ethylene and butane. Additionally, it was observed that both

aldehyde substrates can be coupled with  $C_1$  compounds CO and  $CN^-$  to produce up to  $C_4$  carbon products, confirmed by isotope labeling studies. For the reaction of formaldehyde with CO, the total TON was 42, with methane as the primary product, though coupling to  $CN^-$  is slightly more successful with TON of 64, and methane, ethylene and ethane are produced in roughly equal amounts. Acetaldehyde appears to be less reactive towards coupling with CO or  $CN^-$  (TON of 84 for either), as ~70% of the total product is ethane, similar to the aldehyde alone, though  $C_3$  products are observed, demonstrating that coupling does occur.

 ${\bf Table~7.~Activity~Values~for~the~Reactions~of~Isolated~Nitrogenase~Cofactors~with~Small~Molecule~Substrates}^a$ 

				Products											
Cluster	Red.	Sol.	Sub.	CH <sub>4</sub>	C <sub>2</sub> H <sub>4</sub>	C <sub>2</sub> H <sub>6</sub>	C <sub>3</sub> H <sub>6</sub>	C <sub>3</sub> H <sub>8</sub>	C <sub>4</sub> H <sub>8</sub>	C <sub>4</sub> H <sub>10</sub>	C <sub>5</sub> H <sub>10</sub>	C <sub>5</sub> H <sub>12</sub>	NH <sub>3</sub> /CO	Sum <sup>j</sup>	Ref
M	Eu(II)	H <sub>2</sub> O	$CO^b$	0.081	0.050	0.021	0.018	0.0060	0.0074	0.0026	-	-	-	0.19	247,249
	. ,			0.081	0.10	0.042	0.054	0.018	0.030	0.010	-	-	-	0.34	
M	Eu(II)	H <sub>2</sub> O	$CN^c$	0.38	5.5	0.087	1.3	0.057	0.25	0.030	0.10	0.017	18/-	7.7	247,249
	, ,			0.38	11	0.17	3.8	0.17	0.98	0.12	0.50	0.086	18/-	17 <sup>h</sup>	
M	$SmI_2$	$DMF^d$	CO	1.3	0.15	0.37	0.061	0.10	0.010	0.027	-	-	_	2	248
				1.3	0.30	0.73	0.18	0.31	0.040	0.11	-	-	-	3.0	
M	$SmI_2$	$DMF^d$	CN <sup>e</sup>	7.2	1.6	1.4	0.18	0.23	0.041	0.052	-	-	-	11	248
				7.2	3.2	2.7	0.55	0.68	0.16	0.21	-	-	-	15	
M	$SmI_2$	$DMF^d$	$CO_2^f$	0.81	0.013	0.020	0.00070	0.0010	-	-	-	-	-/0.55	1.4	248
				0.81	0.026	0.040	0.0021	0.0030	-	-	-	•	-/0.55	1.4	
M	$SmI_2$	$DMF^g$	CO	150	3.0	23	1.6	4.7	0.30	0.80	0.08	0.13	-	180	251
				150	6.0	46	4.8	14	1.2	3.2	0.40	0.65	-	230	
M	$SmI_2$	$DMF^g$	CNe	580	42	56	22	13	5.3	2.5	0.56	0.43	-	720	251
				580	84	110	66	39	21	10	2.8	2.2	-	910	
M	$SmI_2$	$DMF^g$	$CO_2^f$	43	1.5	7.6	0.70	1.3	0.09	0.17	-	-	-	54	251
				43	3.0	15	2.1	3.9	0.36	0.68	-	•	-	68	
V	Eu(II)	$H_2O$	CO	0.055	0.046	0.015	0.013	0.0053	0.0048	0.0014	-	-	-	0.14	247,249
				0.055	0.092	0.030	0.039	0.016	0.019	0.0056	-	-	-	0.26	
V	Eu(II)	$H_2O$	$CN^c$	0.76	4.8	0.13	1.1	0.042	0.31	0.029	0.12	0.011	17/-	7.4	247,249
				0.76	9.6	0.25	3.3	0.13	1.2	0.11	0.62	0.056	17/-	16 <sup>h</sup>	
V	$SmI_2$	$DMF^d$	CO	1.2	0.17	0.29	0.048	0.084	0.0091	0.025	-	-	-	1.8	248
				1.2	0.33	0.58	0.14	0.25	0.036	0.10	-	-	-	2.7	
V	$SmI_2$	$DMF^d$	$CN^e$	6.2	1.4	1.1	0.14	0.20	0.051	0.067	-	-	-	9.2	248
				6.2	2.9	2.3	0.43	0.59	0.20	0.27	-	-	-	13	
V	$SmI_2$	$DMF^d$	$CO_2^f$	1.2	0.017	0.029	0.0012	0.0013	-	-	-	-	-/0.58	1.8	248
				1.2	0.034	0.058	0.0036	0.0039	-	-	-	-	-/0.58	1.8	
V	$SmI_2$	$DMF^g$	CO	250	2.3	20	0.83	2.8	0.14	0.36	0.046	0.014	-	270	i
				250	4.6	39	2.5	8.3	0.57	1.4	0.23	0.069	-	300	

V	$SmI_2$	$DMF^g$	$CO_2^f$	44	0.57	3.6	0.34	0.39	0.20	0.028	-	-	-	49	i
				44	1.1	7.2	1.0	1.2	0.81	0.11	-	-	-	55	
L	Eu(II)	H <sub>2</sub> O	CO	0.12	0.035	0.012	0.014	0.0058	0.0052	0.0020	-	-	-	0.19	249
				0.12	0.070	0.024	0.042	0.017	0.021	0.0080	-	-	•	0.30	
L	Eu(II)	$H_2O$	$CN^c$	3.401	3.753	0.78	1.068	0.202	0.32	0.089	0.159	0.044	23/-	9.9	249
				3.401	7.5	1.6	3.2	0.61	1.3	0.36	0.80	0.22	23/-	$20^h$	
L	$SmI_2$	$DMF^d$	CO	2.4	0.12	0.50	0.066	0.15	0.017	0.024	-	-	-	3.3	248
				2.4	0.25	1.0	0.20	0.45	0.068	0.096	-	-	-	4.5	
L	$SmI_2$	$DMF^d$	$CN^e$	8.3	0.88	1.2	0.068	0.15	0.0070	0.013	-	-	-	11	248
				8.3	1.8	2.4	0.20	0.45	0.028	0.052	-	-	•	13	
L	$SmI_2$	$DMF^d$	$CO_2^f$	1.5	0.021	0.040	0.0017	0.0023	-	-	-	-	-/0.66	2.3	248
				1.52	0.042	0.080	0.0051	0.0069	-	-	-	-	-/0.66	2.3	
L	$SmI_2$	$DMF^g$	CO	110	2.2	19	1.4	4.2	0.22	0.59	0.030	0.090	-	140	250
				110	4.4	38	4.2	13	0.88	2.4	0.15	0.45	-	180	
L	$SmI_2$	$DMF^g$	$CN^e$	390	27	33	16	8.1	3.7	1.7	0.63	0.33	-	480	250
				390	54	66	48	24	15	6.8	3.2	1.7	•	610	
L	$SmI_2$	$\mathrm{DMF}^g$	$CO_2^f$	21	0.40	2.8	0.20	0.50	0.040	0.11	-	-	-	25	250
				21	0.80	5.6	0.60	1.5	0.16	0.44	-	-	-	30	

<sup>&</sup>lt;sup>a</sup> Activity numbers are reported in plain text for yield in units of nmol product × (nmol cofactor)<sup>-1</sup>, and corresponding turnover numbers are reported in bold with units of nmol product × (nmol cofactor)<sup>-1</sup> × n, where n is the number of C for each product (C<sub>n</sub>H<sub>m</sub>) to reflect total C-substrate consumption. <sup>b</sup> 100% CO atmosphere. <sup>c</sup> from NaCN. <sup>d</sup> DMF was buffered with 2,6-lutidinium triflate and triethylamine. <sup>e</sup> from tetrabutylammonium cyanide [Bu<sub>4</sub>N(CN)]. <sup>f</sup> 100% CO<sub>2</sub> atmosphere. <sup>g</sup> DMF was buffered with triethylammonium tetrafluoroborate Et<sub>3</sub>NH(BF<sub>4</sub>) and triethylamine. <sup>h</sup> C<sub>6</sub> products (C<sub>6</sub>H<sub>12</sub>, C<sub>6</sub>H<sub>14</sub>) observed for M-, V-, L-clusters. Yield (nmol product × (nmol cofactor)<sup>-1</sup> [TON (nmol product × (nmol cofactor)<sup>-1</sup> × n, where n is the number of C for each product)]. C<sub>6</sub>H<sub>12</sub>: M-cluster 0.051 [0.30], V-cluster 0.065 [0.39], L-cluster 0.067 [0.40]; C<sub>6</sub>H<sub>14</sub>: M-cluster 0.0051 [0.030], V-cluster 0.0042 [0.025], L-cluster 0.031 [0.19]. <sup>i</sup> unpublished results. <sup>j</sup> Sum of yield and turnover values for C-based products.

## 4.6 Hybrid Nitrogenase Enzymes and their Reactivity

The activity of the alternative nitrogenases compared to Mo-nitrogenase raises questions about the origins of the differentiation in reactivity – is it derived from the heterometal of the cofactor or more to deal with the specific protein environment? As described above, the individual proteins and the isolated cofactors have been studied in an effort to understand their inherent properties. 66,131 Primarily, isolated cofactors were used for the reactivation of aponitrogenase that lacks the catalytic cofactor, a protein expressed in a cell line with a deletion of the *nifB* gene.<sup>32</sup> Reactivation was often accomplished first through lysis of the cells expressing  $\Delta nifB$  nitrogenase, followed by an initial centrifugation of the lysate to remove cell debris. The resulting 'cell extract' then contained the target protein along with many others, and the mixture could be incubated with isolated cofactor to form holo-nitrogenase. Subsequent purification and substrate reduction assays would then be done to demonstrate activity. 131 This reactivation could also be achieved through the initial isolation of the apo-enzyme, followed by a 'clean' incubation of only the protein and the isolated cofactor. In principle, there isn't a restriction on which isolated cofactor can be incorporated into a given apo-nitrogenase. M-cluster could be incubated with the *apo-VFe* protein to produce a hybrid enzyme (M-VFe), or vice versa (V-MoFe). In this way, the native protein, isolated cofactor, and hybrid protein can all be analyzed to better understand the reactivity of nitrogenase. This strategy has been employed by several groups to further explore the properties that are inherent to both the protein framework (MoFe or VFe proteins) and the cofactor (M- or V-cluster). 157,163,168,222 Additionally, a cell strain expressing a particular nitrogenase could be grown in the presence of an alternative heterometal in order to generate a hybrid in vivo that can be purified from the cell directly. The in vivo method has been used in the VFe system to incorporate M-cluster, and with the MoFe protein to incorporate tungsten into the catalytic cofactor. <sup>23,223,224</sup> A collection of various hybrid nitrogenase enzymes has been summarized in Table 8.

Table 8. Hybrid Enzymes and the Reported Reactivity<sup>a</sup>

			Products Observed				
Protein (cell background)	Hybrid <sup>b</sup>	Method <sup>c</sup>	NH <sub>3</sub>	C <sub>2</sub> H <sub>4</sub>	C <sub>2</sub> H <sub>6</sub>	$H_2$	ref
$Kp$ NifDK $(\Delta nifB)$	V-MoFe	Apo-NifDK cell extract or isolated protein incubated with V-cluster	ND	+	+	+	157
$Av$ NifDK $(\Delta nifB)$	V-MoFe	Apo-NifDK cell extract incubated with V-cluster	NR	+	+	NR	157
Av VnfDGK (ΔnifHDKB)	M-VFe	Apo-VnfDGK cell extract incubated with M-cluster	+	+	+	+	163
Av NifDK (ΔnifB)	V-MoFe	Isolated <i>apo</i> -NifDK incubated with V-cluster	+	+	+	+	168,222
Av VnfDGK (ΔnifHDKB)	M-VFe	Isolated <i>apo</i> -VnfDGK incubated with M-cluster	+	+	NR	+	34
Av VnfDGK (ΔnifHDK)	M-VFe	Cells grown with excess Na <sub>2</sub> MoO <sub>4</sub> (-Na <sub>3</sub> VO <sub>4</sub> )	+	+	+	+	23
Av NifDK (W-resistant)	W/Mo-MoFe	Cells grown with Na <sub>2</sub> WO <sub>4</sub> (-Na <sub>2</sub> MoO <sub>4</sub> )	+	+	NR	+	224
Rc NifDK (FeFe-suppressed)	W-MoFe	Cells grown with Na <sub>2</sub> WO <sub>4</sub> (-Na <sub>2</sub> MoO <sub>4</sub> )	ND	+	NR	+	223

<sup>a</sup> ND = not detected. NR = not reported. Plus (+) sign indicates that the activity is observed/reported. <sup>b</sup> the nomenclature of the hybrid protein is listed as 'cluster-protein' where cluster can be the M, V or W-clusters and the protein is NifDK (also called MoFe protein) or VnfDGK (also called VFe protein). Thus, V-MoFe refers to the hybrid protein that has the Mo nitrogenase polypeptide (NifDK) with the V nitrogenase cofactor (V-cluster). <sup>c</sup> the description for the method used to obtain the hybrid protein

After the isolation of V-nitrogenase from *A. chroococcum* and *A. vinelandii*, there was a great deal of interest in studying the V-containing analog of the M-cluster. <sup>141,142</sup> One strategy carried out by Smith and co-workers involved the extraction of the V-cluster from the *Ac* VFe protein, followed by incubation of the cofactor with extracts of cells expressing the  $\Delta nifB$  MoFe protein from *K. pneumoniae* and *A. vinelandii*. <sup>157</sup> When the incubated extracts for both systems were assayed for C<sub>2</sub>H<sub>2</sub> reduction, both demonstrated the formation of C<sub>2</sub>H<sub>4</sub> and C<sub>2</sub>H<sub>6</sub>, showing that V-cluster had been incorporated. The  $\Delta nifB$  *Kp* MoFe protein was also isolated, then

incubated with V-cluster and the resultant protein showed minor but detectible activity with specific activity values of 2 (nmol product × min<sup>-1</sup> × (mg protein)<sup>-1</sup>) for H<sup>+</sup> reduction in an Ar atmosphere, as well as 1.1 and 0.09 for the formation of C<sub>2</sub>H<sub>4</sub> and C<sub>2</sub>H<sub>6</sub>, respectively.<sup>157</sup> Additionally, H<sub>2</sub> production was only mildly hindered in a 10% acetylene atmosphere. This pattern of reactivity for V-MoFe is indicative of the wild-type VFe protein, but not wild-type MoFe protein, suggesting that the V-cluster is able to confer the activity. However, the *Kp* V-MoFe protein was reported to not be competent for N<sub>2</sub> reduction to NH<sub>3</sub>, and the other substrate activities reflect only a small percentage of the wild-type VFe protein, indicating that there might be problems with either the protein or the cofactor.

Hales and co-workers were also able to generate a hybrid nitrogenase, but reversed the components from the Smith study, using an A. vinelandii  $\Delta nifB$  VFe strain and isolated M-cluster to produce M-VFe. 163 Cell extracts containing the cofactor-deficient VFe protein were incubated with isolated M-cluster from the Av MoFe protein, and the resultant M-VFe protein was isolated and characterized. In general, the hybrid reacts towards N<sub>2</sub> with similar electron allocation as NifDK, with 70% of electrons going towards NH<sub>3</sub> production and the remaining 30% going to H<sub>2</sub> evolution. In comparison, wild-type VnfDGK has a 50:50 split between N<sub>2</sub> and H<sup>+</sup> reduction in a nitrogen atmosphere, and the Kp V-MoFe hybrid was not reported to react with N<sub>2</sub> at all. <sup>157,163</sup> The ability of the M-VFe protein to produce H<sub>2</sub> in an argon atmosphere is hindered, demonstrating ~40% of the activity of the wild-type Av VFe protein (Table 4), suggesting that there may be issues with proton delivery to the M-cluster site in V-nitrogenase. Additionally, C<sub>2</sub>H<sub>2</sub> reduction by Av M-VFe has a product distribution more closely resembling the wild-type VFe protein with 35%, 10% and 55% of electrons going towards C<sub>2</sub>H<sub>4</sub>, C<sub>2</sub>H<sub>6</sub> and H<sub>2</sub> formation, respectively, whereas 95% of electrons goes toward C<sub>2</sub>H<sub>4</sub> for the MoFe protein without observation of ethane. 163 This seems to imply that the VFe protein is also able to confer the ability to produce ethane from acetylene, even with the M-cluster present.

The formation of hybrid enzymes was also explored by Ribbe, Hu and co-workers using histidine-tagged  $\Delta nifB$  apo-MoFe/VFe proteins from A. vinelandii, reconstituted with isolated cofactor as well as protein expressed in the presence of an alternative metal. <sup>23,34,168,222</sup> The isolated  $\Delta nifB$  apo-MoFe protein was incubated with both the M- and V- clusters to compare the reactivity towards the standard nitrogenase assays (N<sub>2</sub>, C<sub>2</sub>H<sub>2</sub> and H<sup>+</sup> reduction). <sup>168</sup> The protein

reconstituted with M-cluster (M-MoFe) was able to recover most, but not all, of the enzymatic activity as compared to the wild-type MoFe protein (Table 4). This observation demonstrates that reconstituted nitrogenase is slightly less active than the wild-type enzyme, in accordance with previous reports. 157,163 However, the affinity-tagged Av V-MoFe protein displays a greatly increased activity compared to Kp V-MoFe, including the reduction of N<sub>2</sub> to NH<sub>3</sub>, and the formation of ethane from acetylene. 168 The activity of Av V-MoFe reflects ~25% of the formation observed for Av M-MoFe for comparably reported products. This shows that purification using affinity tags helps to increase the reactivity of the protein, and further finds that the V-cluster can impart the acetylene reduction phenotype to the hybrid protein but is less active than the M-cluster containing variant. An affinity-tagged  $\Delta nifB$  apo-VFe protein was analogously isolated and reconstituted with M-cluster (M-VFe).<sup>34</sup> The hybrid was shown to have substrate reducing capability that reflected < 20% of the activity of the M-MoFe control, though, it was unclear if the V-nitrogenase acetylene reduction phenotype was observed as ethane formation was not reported. The decreased activity in this instance was attributed to the unstable  $\Delta nifB \ apo$ -VFe protein with an  $\alpha\beta_2$  composition, notably without the  $\delta$  subunit.<sup>34</sup> It was later reported that M-VFe could also be generated in vivo by expressing the protein in the presence of excess Na<sub>2</sub>MoO<sub>4</sub>.<sup>23</sup> The resultant *in vivo* hybrid had an  $\alpha_2\beta_2(\delta)$  composition, had the Vnitrogenase phenotype, producing ethylene and ethane from acetylene, and H<sub>2</sub> formation was only mildly attenuated by acetylene. However, metal analysis indicates that only one M-cluster is incorporated per protein, likely leaving the second cofactor site empty, in agreement with the generally decreased activity relative to the native VFe protein.

The CO reduction capabilities for the heterologous V-MoFe and M-VFe hybrids were also investigated and compared to the wild-type enzymes. <sup>23,222</sup> Both hybrid nitrogenases were capable of facilitating C–C bond formation from the reduction of CO; V-MoFe formed C<sub>2</sub> and C<sub>3</sub> products in proteo-solvent whereas M-VFe generated C<sub>2</sub>–C<sub>4</sub> products under similar conditions (Table 6). The V-MoFe hybrid was found to yield an increased amount of hydrocarbon products in deutero-solvent, including C<sub>4</sub> products, with inverse KIEs similar to the native MoFe system. <sup>222</sup> Of particular note is that CD<sub>4</sub> is observed with V-MoFe (and wild-type VFe protein) but not with the wild-type MoFe protein. This strongly suggested that while the presence of the V-cluster can subtly tune the reactivity of the enzyme, the polypeptide plays a larger role in determining product formation. In support of this notion, the *in vivo* M-VFe hybrid converted

CO to  $C_2H_4$  and  $C_2H_6$  with higher specific activities (650 and  $21 \times 10^{-3}$  nmol product  $\times$  min<sup>-1</sup>  $\times$  (nmol cofactor)<sup>-1</sup> for  $C_2H_4$  and  $C_2H_6$ , respectively) relative to V-MoFe (33 and  $8.8 \times 10^{-3}$  nmol product  $\times$  min<sup>-1</sup>  $\times$  (mg protein)<sup>-1</sup>) and wild-type MoFe protein (25 and  $13 \times 10^{-3}$  nmol product  $\times$  min<sup>-1</sup>  $\times$  (mg protein)<sup>-1</sup>), in line with  $C_2$  hydrocarbons being primary products of the native VFe protein.<sup>23</sup>

Attempts have also been made to generate hybrid enzymes through the incorporation of the non-native tungsten as a heterometal for the catalytic nitrogenase cofactor. 223,224 Hales and Case grew a MoFe protein-expressing W-resistant A. vinelandii strain in the presence of WO<sub>4</sub><sup>2</sup>-, transferring the culture multiple times in an attempt to deplete the Mo stores of the organism as much as possible. 224 The resulting MoFe protein was purified, and incorporation of one equivalent of both Mo and W into each heterotetramer was observed, consistent with one Mcluster and one W-cluster per protein. The hybrid W/Mo-MoFe protein was active towards substrate reduction but reached only ~30% of the activity of the native MoFe protein, so it was unclear if the W-cluster was active and if the reduction of activity simply reflected the lower Mcluster incorporation. Subsequently, Müller and co-workers developed a strain of R. capsulatus that inactivated the regulatory gene anfA responsible for the expression of the FeFe protein under Mo-depleted conditions.<sup>223</sup> This strain was grown in Mo-free conditions, in the presence of WO<sub>4</sub><sup>2</sup>, the MoFe protein that was expressed was consistent with the incorporation of one Wcluster per  $\alpha_2\beta_2$  heterotetramer, without the detection of substantial Mo. The Rc W-MoFe protein was then assayed with the standard substrate scope and was not particularly active towards C<sub>2</sub>H<sub>2</sub> or H<sup>+</sup>, with specific activities of 1 and 102 nmol product  $\times$  min<sup>-1</sup>  $\times$  (mg protein)<sup>-1</sup>, respectively (Table 4). Additionally, the hybrid was not active towards N<sub>2</sub> reduction indicating that the Wcluster is generally inert for nitrogenase activity.

### 4.7 Substrate Reduction by the Reductase Components NifH and VnfH

As described in Section 3.1, nitrogenase is a two-component system comprised of the catalytic protein that contains the M-, V- or Fe-cluster, as well as the [Fe<sub>4</sub>S<sub>4</sub>]-containing reductase protein. In the Mo-dependent system, the reductase, NifH, has been shown to have three primary physiological functions; the protein is involved with insertion of Mo and homocitrate to convert the L-cluster to the M-cluster on NifEN, the biosynthesis P-cluster on

NifDK, and the ATP-dependent electron transfer during nitrogenase catalysis. These functions have largely been unexplored for the reductase proteins from the alternative nitrogenase systems, VnfH and AnfH for the V- and Fe-only nitrogenases, respectively. Though it has been shown that Av NifH is capable of reducing VO<sub>4</sub><sup>3-</sup> to VO<sup>2+</sup>, to VO<sup>2+</sup>, the lack of a reported VnfEN, and various  $\Delta nifZ$  and  $\Delta vnfH$  VnfDGK/AnfDGK variants prevents the extensive characterization of biosynthetic reactivity. However, a seemingly adventitious reactivity of NifH and VnfH was discovered recently. It was found by Hu and co-workers that the Fe proteins could facilitate the conversion of CO<sub>2</sub> to CO. S7,254 This section will detail the observed activity of these reactions.

CO<sub>2</sub> reduction by NifH and VnfH was studied in parallel by modifying the redox agent and the presence of a nucleotide. 87 Using nucleotide-free conditions and sodium dithionite as the reductant, the two reductases generated CO with specific activities of 0.10 and 0.13 (10<sup>-3</sup> nmol product × min<sup>-1</sup> × (nmol protein)<sup>-1</sup>) for NifH and VnfH, respectively, and these values moderately increased in the presence of ATP (Table 9). For comparison, MoFe and VFe proteins can facilitate CO<sub>2</sub> reduction to CO an order of magnitude faster than the reductase components alone (Table 6).<sup>242</sup> The difference in reactivity for the Fe proteins in the presence or absence of nucleotide was attributed to the ~100 mV decrease in redox potential that is observed for the Fe proteins in the presence of nucleotide.<sup>87</sup> To further investigate this phenomenon, dithionite was exchanged for the more reducing Eu<sup>II</sup>DTPA, and this resulted in specific activities for CO formation of  $\sim 3 \times 10^{-3}$  nmol product  $\times$  min<sup>-1</sup>  $\times$  (nmol protein)<sup>-1</sup>, which is similar to the rate for the catalytic nitrogenase proteins. Repeated additions of Eu<sup>II</sup> reductant to the system continued to drive CO formation with near-linear increases of product. Unsurprisingly, in the presence of the oxidant indigo disulfonate (IDS), neither Fe protein could facilitate appreciable CO production, however, it was found that CO could be oxidized back to CO2 with much faster rates compared to CO<sub>2</sub> reduction (Table 9).<sup>87</sup> This established the nitrogenase Fe protein as a mimic of the enzyme CO dehydrogenase, which is the only other known system that can facilitate the reversible interconversion of CO<sub>2</sub> and CO, albeit with much higher rates.

Additionally, the *in vivo* reduction of CO<sub>2</sub> was reported in *A. vinelandii* strains that express either the NifH or VnfH components without the paired catalytic component (NifDK and VnfDGK, respectively).<sup>87</sup> In the presence of supplemented ammonia, which represses expression of Fe protein, effectively no CO was observed. However, when the ammonia was depleted, CO

could be measured and was maximally produced in a 40% CO<sub>2</sub>, 60% Ar atmosphere with higher specific activities ( $\sim 170 \times 10^{-3}$  nmol product  $\times$  min<sup>-1</sup>  $\times$  (nmol protein)<sup>-1</sup>) than observed in the *in vitro* assays (Table 9). These results indicate that there may be a native electron donor in *A. vinelandii* that permits the high degree of CO<sub>2</sub> reduction carried out by the Fe proteins. It is unclear what physiological relevance this activity has, but the CO<sub>2</sub> activity paired with the recent discovery that a homolog of NifH can generate longer chain hydrocarbons, further highlights the versatility of the Fe protein and warrants additional investigation.<sup>78,254</sup>

Table 9. Substrate Reduction Activity Facilitated by NifH and VnfH<sup>a</sup>

			Product			
Protein	Redox Agent	Nucleotide	$CO_p$	$\mathrm{CO}_2{}^c$		
	DT	-	0.10	-		
	DT	+	0.15	-		
Av NifH	IDS	-	0.0056	200		
	Eu <sup>II</sup> DTPA	-	$3.2/7.7^d$	-		
	Eu <sup>II</sup> DTPA	+	$7.6^{d}$	-		
	DT	-	0.13	-		
	DT	+	0.17	-		
Av VnfH	IDS	-	0.0083	190		
	Eu <sup>II</sup> DTPA	-	$3.2/7.8^d$	-		
	Eu <sup>II</sup> DTPA	+	$7.6^{d}$	-		

<sup>&</sup>lt;sup>a</sup> The data is reported from ref 87, all proteins are from *A. vinelandii*. Units reported as  $10^{-3}$  nmol product × min<sup>-1</sup> × (nmol protein)<sup>-1</sup>. All reactions reported at 30 °C. DT = sodium dithionite. IDS = indigo disulfonate. <sup>b</sup> assay reported in 100% CO<sub>2</sub> atmosphere. <sup>c</sup> assay reported in 99.9% CO atmosphere. <sup>d</sup> CO production after multiple additions of Eu<sup>II</sup> reductant; values reported with units of nmol CO × (nmol protein)<sup>-1</sup>.

# 5. Mechanism of Nitrogenase

The multi-electron reduction of dinitrogen has been the focus of long-term multi-pronged research that utilizes biochemical, kinetic, spectroscopic, and structural biology approaches. 66,143,197 This process is challenging because the individual components of nitrogenase have been studied, providing spectroscopic detail and physical properties. However, the study of substrate reduction requires both the catalytic and reductase components to function together, complicating the analysis. As described in Section 3, there are several metallocofactors housed between the two components of nitrogenase, a [Fe<sub>4</sub>S<sub>4</sub>] cluster on NifH and both the P-

and M-clusters on the catalytic NifDK protein.<sup>32</sup> Each of these clusters can contribute in spectroscopic studies, so it can be difficult to isolate the components from a single source. The crystallography of nitrogenase proteins has shed light on structural aspects of nitrogenase catalysis and has assisted the spectroscopic assignments, but the X-ray diffraction structures represent a snapshot of the solid-state protein and do not necessarily reflect the solution-state dynamics in the reaction mixture. To study the reactions of nitrogenase under physiological conditions requires a combination of rapid freeze-quench and stopped-flow methods to identify reaction intermediates and analyze the multi-step pathway. 197 The bulk of the published kinetic and mechanistic work on substrate reduction has focused on N2 reduction through the characterization of the Mo-dependent nitrogenases from A. vinelandii<sup>66,197</sup> and K. pneumoniae<sup>255</sup> <sup>258</sup> among others. Although, the kinetic and detailed spectroscopic studies have not all been conducted with one specific nitrogenase system. The mechanisms for the alternative Vdependent and Fe-only nitrogenases from A. vinelandii, A. chroococcum, and R. capsulatus have been studied alongside the Mo-dependent system, 143,178 however, it wasn't until recently that reports indicated that the alternative nitrogenases from A. vinelandii operate with similar mechanisms to the Mo-dependent system.<sup>220,259</sup> The N<sub>2</sub> reduction mechanism for Mo-dependent nitrogenase has been extensively detailed by Hoffman and co-workers in 2014, 197 but this does not address the recent developments for the alternative nitrogenase systems. Below we provide a general summary of the mechanism proposed for N<sub>2</sub> reduction, as well as other substrates with comparisons for the Mo-, V-, and Fe-only nitrogenases.

#### 5.1. N<sub>2</sub> Reduction Mechanism for Mo-nitrogenase

The most well described kinetic framework for  $N_2$  reduction by Mo-nitrogenase, including a mechanistic outline, involved the work of many research groups and resulted in the Lowe-Thorneley (LT) model (Figure 21). <sup>188,255-258</sup> This model was later updated by Hoffman and co-workers, <sup>197</sup> and subsequent additions have been made in recent years. <sup>220,259,260</sup> This model described the kinetics of the chemical transformations that occur on NifH and NifDK from K. *pneumoniae* during nitrogenase catalysis, and the delivery of proton and electron equivalents to the catalytic component is tracked with an  $E_n$  notation, where n is the number of electrons and protons accumulated on one  $\alpha\beta$ -dimer of NifDK. <sup>188,197</sup> This formalism does not distinguish the

location of the electrons or protons, whether it be associated with the P-cluster or the M-cluster, simply that an electron and proton pair has been provided to the system. The electrons are transferred by NifH through the Fe protein cycle, <sup>77,261,262</sup> so by analogy the LT model is also referred to as the MoFe protein cycle. <sup>188</sup> In the literature, N<sub>2</sub> reduction is sometimes referred to as the first reduction of N<sub>2</sub> to a N<sub>2</sub>H<sub>2</sub>-level intermediate (can also be called N<sub>2</sub> activation), whereas elsewhere it can be used as an umbrella term covering the complete triple bond scission into two equivalents of NH<sub>3</sub>. In this review, we ascribe N<sub>2</sub> reduction to mean the entire process of N<sub>2</sub> bond cleavage to produce ammonia.

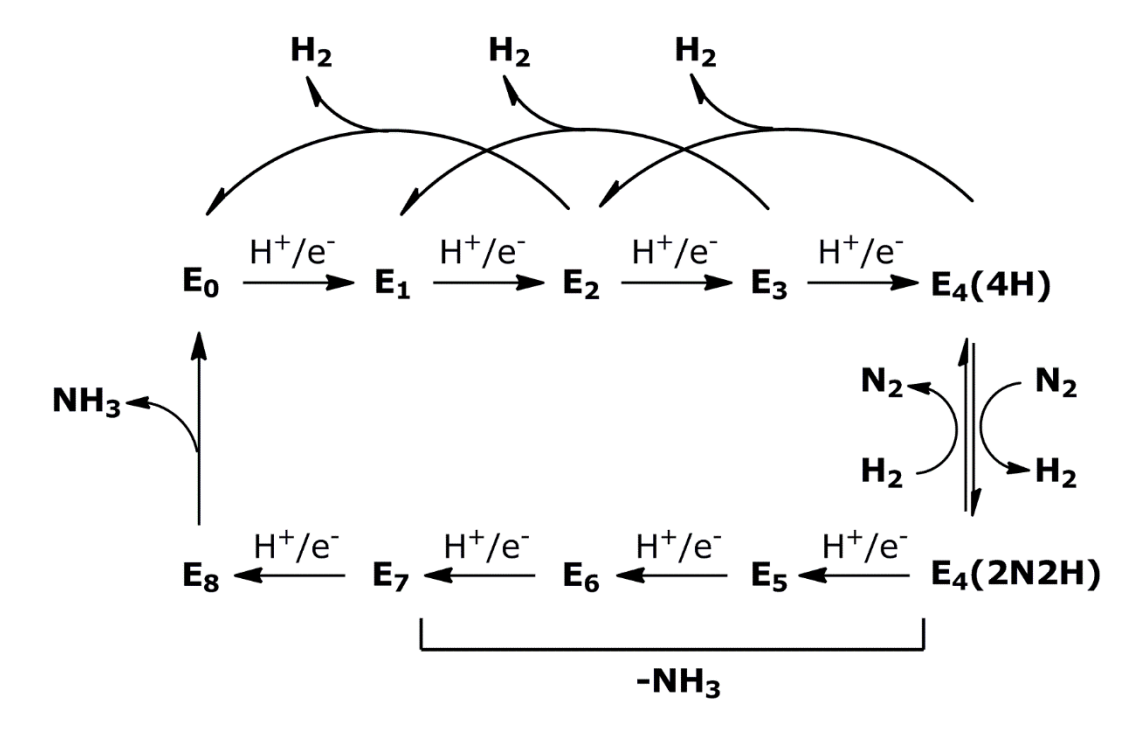


**Figure 21**. A modified Lowe-Thorneley scheme for  $N_2$  reduction in Mo-nitrogenase based on work from refs 188 and 197. The  $E_n$  notation refers to the n number of proton and electron equivalents loaded on to one αβ-dimer of NifDK. The resting state of the cycle is  $E_0$  and the release of  $H_2$  and  $NH_3$  during the cycle is indicated.

The first state,  $E_0$ , represents the resting state of NifDK and is consistent with an M-cluster in an S=3/2 state under dithionite reducing conditions. Much of the work on Monitrogenase reported in the 1970's and 80's has involved the characterization of this state of the enzyme. The  $E_0$  state has an odd number of unpaired electrons, so the even numbered states of the LT model (n = 2, 4, 6, 8) will also have an odd number of unpaired electrons loaded on NifDK. This property allows for a convenient spectroscopic handle to study these species using EPR techniques, including pulsed methods like electron nuclear double resonance (ENDOR) and

electron spin echo envelope modulation (ESEEM), if the intermediate species can be appreciably accumulated. The odd numbered  $E_n$  states (n = 1, 3, 5, 7) will have an even number of unpaired electrons, which should either lead to a diamagnetic species that is EPR silent or to an integer spin (S = 1, 2, 3, etc) that would show EPR transitions. The  $E_1$  through  $E_3$  states occur before  $N_2$  reduction, while  $E_4$  is the active state where  $N_2$  is proposed to bind and where reduction begins. Further addition of protons and electrons to nitrogenase through the  $E_5 - E_8$  states promotes the cleavage of the  $N_2$  bond, producing  $H_2$  and two equivalents of  $NH_3$ , returning the cycle to the  $E_0$  state. An additional feature of the cycle is that the  $E_2$ ,  $E_3$ , and  $E_4$  states can 'relax' by generation of  $H_2$ , converting back to the  $E_0$  and  $E_1$  and  $E_2$  states, respectively (Figure 21), which represents non-productive hydrogen release that competes with  $N_2$  reduction.  $E_3$ 

The initial LT model posited that N<sub>2</sub> could bind to either the E<sub>3</sub> or E<sub>4</sub> states, but the E<sub>4</sub> state was the point at which N<sub>2</sub> reduction could occur. <sup>188</sup> This proposal was based on kinetic measurements, as well as observations that with the A. vinelandii nitrogenase system (later for K. pneumoniae and C. pasteurianum as well<sup>263</sup>) HD gas could be produced from an atmosphere of  $D_2$  ( ${}^2H_2$ ) and  $N_2$ , and that TOH (T =  ${}^3H$ ) is not appreciably formed in an atmosphere of  $T_2$  ( ${}^3H_2$ ) and N<sub>2</sub>. <sup>188,210,263,264</sup> These results suggested that H<sub>2</sub> (or D<sub>2</sub>) can inhibit N<sub>2</sub> reduction by reversing N<sub>2</sub> binding (Figure 21), and this process is not a simple exchange with solvent but allows for the scrambling of the isotope label. The experiments also reinforced that one equivalent of H<sub>2</sub> is produced by NifDK during N<sub>2</sub> reduction. <sup>188,198</sup> Subsequently, active site point mutants of residues that are nearby the M-cluster were generated for NifDK of A. vinelandii at α-His195 and α-Gln191 by Newton and co-workers, <sup>152</sup> and these variant proteins were used to address the E<sub>3</sub> versus E<sub>4</sub> state for N<sub>2</sub> binding. The relevant nitrogenase variants were inactive for N<sub>2</sub> reduction, but in the presence of N<sub>2</sub>, the acetylene (C<sub>2</sub>H<sub>2</sub>) reduction activity was decreased. Activity could be restored through the addition of H<sub>2</sub>, implying that N<sub>2</sub> binds to the M-cluster and can be knocked off by H<sub>2</sub> (consistent with inhibition), but as the nitrogenase proteins in a N<sub>2</sub>/D<sub>2</sub> atmosphere are not active for N<sub>2</sub> reduction nor is HD produced, the E<sub>4</sub> state was not likely being accessed. 152 Based on these findings, Hoffman and co-workers argue that N2 must productively bind in the E<sub>4</sub> state, and propose a reductive elimination mechanism for H<sub>2</sub> production during N<sub>2</sub> reduction to rationalize the generation of HD in a N<sub>2</sub>/D<sub>2</sub> atmosphere. <sup>197</sup> This mechanism was tested by carrying out C<sub>2</sub>H<sub>2</sub> reduction assays in the presence of N<sub>2</sub> and D<sub>2</sub>, and it was observed

that deuterium was incorporated into the ethene  $(C_2H_4)$  product as either  $C_2H_2D_2$  or the more abundant  $C_2H_3D$ , supporting the proposed reductive elimination process.<sup>265</sup>

Consequently, the E<sub>4</sub> state is inherently of interest within the LT scheme because it is a central point in the cycle that either produces H<sub>2</sub>, reverting to the E<sub>2</sub> state, or can bind N<sub>2</sub> on the M-cluster pushing the reaction cycle forward. 188,197 As mentioned previously, when N<sub>2</sub> binds to the E<sub>4</sub> state (or E<sub>4</sub>(4H)), there is a concomitant loss of one equivalent of H<sub>2</sub> from NifDK, leaving an E<sub>4</sub>(2N2H) species (Figure 21). However, it is not clear the reason why nitrogenase produces H<sub>2</sub> as part of ammonia production, as 25% of the ATP (and therefore electrons) required for the reaction is funneled into this apparent byproduct. Recent DFT studies have suggested that the thermodynamically favorable formation of H<sub>2</sub> is coupled to the less favorable binding and reduction of N<sub>2</sub>, such that the overall process is slightly favored or thermoneutral, <sup>266,267</sup> though additional work is necessary to further explore this idea. To better understand the nature of the E<sub>4</sub> state, Hoffman and co-workers have used freeze-quench spectroscopic experiments to trap E<sub>4</sub> as well as other intermediate states. <sup>197</sup> A single-point mutant ( $\alpha$ -Val70 $\rightarrow \alpha$ -Ile70) of NifDK was identified that accumulated an intermediate, that was later assigned to be in the E<sub>4</sub>(4H) state. <sup>268,269</sup> <sup>1,2</sup>H, <sup>95</sup>Mo, and <sup>57</sup>Fe ENDOR experiments demonstrated that the intermediate was consistent with the presence of bound hydride (H<sup>-</sup>) ligands that were interacting with the core Fe atoms of the M-cluster, but were not involved with the Mo center. <sup>270-273</sup> This species, termed the "Janus intermediate," was then proposed to have an M-cluster model with two  $\mu_2$ -hydride ligands bridged between two different sets of Fe atoms and two protons bound elsewhere on the cluster. 197,273 It was later reported that spectroscopic features associated with the so-called Janus intermediate were observed in wild-type NifDK, suggesting that hydrides are not an artifact of the point-mutation, but are involved in the on-pathway mechanism of N<sub>2</sub> reduction.<sup>260</sup>

The proposal of hydride intermediates as part of nitrogen fixation provides a framework for storing the proton and electron equivalents without accumulating charge on the metallocofactor directly. There is also established chemistry that involves hydride species both in biology, such as in the hydrogenase systems,  $^{274,275}$  as well as extensive examples in synthetic transition metal systems.  $^{276,277}$  However, it is still unclear how protons/electrons or hydride species are involved in the  $N_2$  bond scission, specifically. There are two general pathways that have been proposed for the hydrogenation of  $N_2$  – the distal and alternating pathways (Figure

22). $^{66,197,278}$  In both cases,  $N_2$  is proposed to bind in an end-on mode to a metal center (M– $N_2$ ) of the M-cluster and eventually merge at the formation of a terminal amido species (M– $NH_2$ ). The final step of the mechanism is the delivery of one proton/electron equivalent to a terminal amido intermediate, releasing  $NH_3$  and regenerating the  $E_0$  state of NifDK. The two mechanisms differ in the specific sites of protonation of  $N_2$ , the intermediates formed during the reaction, and which of the  $E_n$  states allow for  $NH_3$  to be released.

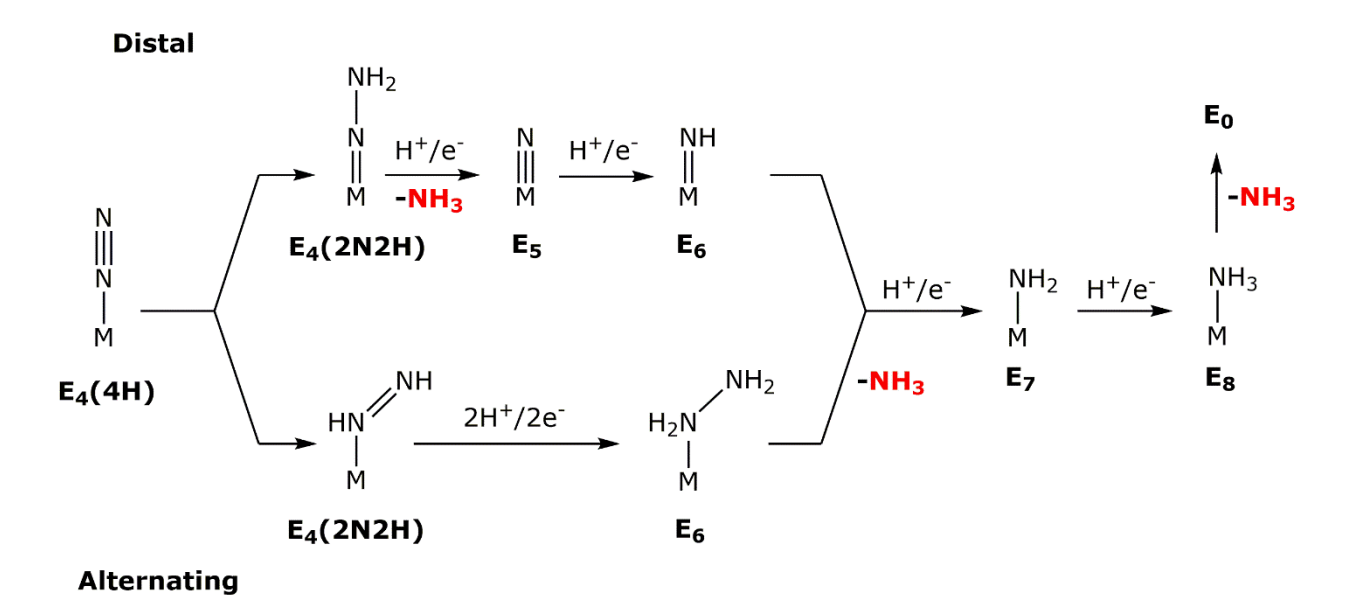


**Figure 22.** A mechanistic outline demonstrating a distal (top) and an alternating (bottom) pathway for the reduction of  $N_2$  by nitrogenase. The corresponding  $E_n$  state from the LT-model is indicated under each intermediate, along with the proposed release of NH<sub>3</sub>.

The distal pathway proposal is based on the chemistry of inorganic Mo complexes by Chatt<sup>279-282</sup> and Schrock.<sup>283,284</sup> In the first step,  $N_2$  binds to a metal center of the M-cluster in the  $E_4(4H)$  state, and this promotes two of the proton/electron equivalents loaded on NifDK to add to the distal site of  $N_2$ , forming a hydrazido (M=N-NH<sub>2</sub>) species, as well as  $H_2$ . The next proton/electron addition ( $E_5$ ) also occurs at the distal nitrogen atom, releasing one equivalent of NH<sub>3</sub> and generating a terminal metal nitrido (M=N) species. The following two protonation and reduction steps ( $E_6$ ,  $E_7$ ) promote the formation of metal imido (M=NH) and amido (M-NH<sub>2</sub>) species, respectively, with the final addition ( $E_8$ ) generating and releasing the second equivalent of NH<sub>3</sub>. In contrast to the distal pathway, the alternating pathway of  $N_2$  cleavage is derived from studies with Fe complexes.<sup>285,286</sup> The mechanism begins with  $N_2$  binding to the  $E_4$ (4H) state, but one proton/electron equivalent is added to each nitrogen atom, forming a diazene-bound species

(M–(H)N=NH) with the requisite loss of H<sub>2</sub>. The following two reduction/protonation steps (E<sub>5</sub> and E<sub>6</sub>) form a hydrazine-type species (M–(H<sub>2</sub>)N–NH<sub>2</sub>), alternating the site of addition to the nitrogen atom. Protonation and reduction in the following step (E<sub>7</sub>) releases NH<sub>3</sub>, generating an amido-bound species that is subsequently liberated as the second equivalent of NH<sub>3</sub> in the final step (E<sub>8</sub>).

There is currently no definitive consensus of the N<sub>2</sub> reduction mechanism that is operative in nitrogenase, or if this reduction takes place at the Mo or Fe centers. <sup>197</sup> Ammonia generation from N<sub>2</sub> has been reported using synthetic Mo-based complexes, and this extensive and thorough body of work supported a Mo-centered distal pathway for the mechanism in nitrogenase. 197,287 There is also a growing support for Fe-centered N2 reduction based on synthetic work with iron complexes, <sup>288-290</sup> as well as from calculations and active site point mutants that modify the area adjacent to the Fe face of the M-cluster. 200,278,291 However, there are several experimental observations that have been used to favor the alternating over the distal pathway. The first evidence of a reduced N<sub>2</sub> intermediate was shown by Thorneley, Eady and Lowe by use of acid/base quenching techniques during turnover of the *K. pneumoniae* enzyme.<sup>211</sup> Hydrazine (N<sub>2</sub>H<sub>4</sub>) was observed after quenching the reaction with acid or base, but the identity of the enzyme-bound intermediate was unclear. Subsequent studies with A. vinelandii and other variants demonstrated that nitrogenase could use hydrazine as a substrate to produce ammonia, showed that H<sub>2</sub> did not inhibit hydrazine consumption, and that HD formation was not enhanced in the presence of hydrazine. 198,210,292 Methyldiazene (CH<sub>3</sub>–N=NH) and diazene (HN=NH) were both found to be substrates for the Mo-nitrogenase from A. vinelandii, and additionally, diazene reduction was inhibited in the presence of H<sub>2</sub>. <sup>199,293,294</sup> These results, together with spectroscopic measurements, are suggestive of the alternating mechanism, as both diazene and hydrazine are substrates for nitrogenase that are competent to produce ammonia, and the mechanistic observations of inhibition and HD formation are in line with other N<sub>2</sub> reduction studies. 197,198

### 5.2. N<sub>2</sub> Reduction Mechanism by the Alternative Nitrogenases.

Compared to the Mo-dependent enzyme, the alternative nitrogenase systems have had far less characterization over the same time period, particularly with respect to the mechanism of  $N_2$ 

reduction.<sup>66,143</sup> The two best characterized V-nitrogenase proteins come from *A. chroococcum*<sup>141</sup> and *A. vinelandii*.<sup>142</sup> As mentioned, the stoichiometry for the Mo-dependent N<sub>2</sub> reduction has been established as:

$$\bar{A}_2 + 8\bar{A}^+ + 16\bar{A}\bar{A}\bar{A}\bar{A}\bar{A} + 8\bar{A}^- \rightarrow 2\bar{A}\bar{A}_3 + \bar{A}_2 + 16\bar{A}\bar{A}\bar{A}\bar{A}\bar{A} + 16\bar{A}_{\bar{A}}$$
 (16)

where for each molecule of  $N_2$  that is reduced, only one equivalent of  $H_2$  is produced, and it is unclear why this 1:1  $N_2$ : $H_2$  ratio occurs. However, analogous studies with the V-nitrogenase system from A. chroococcum<sup>295,296</sup> establish a 1:3 stoichiometry for  $N_2$  reduction:

$$\bar{A}_2 + 12\bar{A}^+ + 24\bar{A}\bar{A}\bar{A}\bar{A}\bar{A} + 12\bar{A}^- \rightarrow 2\bar{A}\bar{A}_3 + 3\bar{A}_2 + 24\bar{A}\bar{A}\bar{A}\bar{A}\bar{A} + 24\bar{A}_{\bar{A}}$$
 (17)

The source of this difference was also not clear, but was largely understood to be an inherent inefficiency of the V-nitrogenase to reduce N<sub>2</sub> compared to the Mo-dependent system, as the affinities of the Mo- and V-nitrogenases from A. chroococcum for the substrate  $N_2^{295}$  and the electron transfer behavior from the respective reductase are similar. 101,141 Additionally, the difference in reactivity was not believed to be the result of reaction conditions, as the differences were also observed during in vivo experiments with modified chemostat cultures of A. chroococcum<sup>297</sup> and A. vinelandii. 143,298 It was also observed that the V-nitrogenase from A. chroococcum produces a small amount hydrazine (~0.5% of the electron flux resulting in ammonia formation)<sup>207</sup> as a product that increases with increasing temperature, and for Monitrogenase, hydrazine is only observed when acid or base is used to quench the N<sub>2</sub> reduction reaction. 143,179,295 Intriguingly, hydrazine does not serve as a substrate for V-nitrogenase at low concentrations, but does so for Mo-nitrogenase. 207,209,292 It was also reported that for the Histagged A. vinelandii proteins, the well-known inhibitor of N2 reduction, CO, behaves differently for the Mo- and V-nitrogenases. 149 In the presence of CO (atmosphere, 90% CO, 10% N<sub>2</sub>) NH<sub>3</sub> formation was abolished in both systems, however, electron flux was diverted to H<sub>2</sub> formation in the Mo-dependent system whereas H<sub>2</sub> production and total electron flux was decreased by >50% in the V-dependent protein. This apparent loss of flux indicated that there may have been unidentified formation of products. Indeed, follow up studies (see Section 4.4) demonstrated that CO behaved as a substrate for V-nitrogenase, which facilitates C-C bond formation, further distinguishing the reactivity behaviors of the two nitrogenases. <sup>237,238</sup>

The Fe-only nitrogenase has been shown to follow similar reactivity trends as the V-nitrogenase system, demonstrating diminished reactivity compared to the Mo-dependent system, and also has little by way of mechanistic characterization. There are several Fe-only nitrogenase proteins that have been studied, from *R. capsulatus*, R. palustris R. palustris, R. rubrum, and A. vinelandii, with more variants continuing to be identified in biological nitrogen fixing systems. The N<sub>2</sub>:H<sub>2</sub> ratio for Fe-only nitrogenase was established in the R. capsulatus system by Müller and co-workers as 1:9 (reaction 18), demonstrating that even more of the electron flux is dedicated to generate H<sub>2</sub> during turnover than in V-nitrogenase. Thus, with respect to N<sub>2</sub> reduction, the efficiency of the reaction was established as Mo > V > Fe-only.

$$\bar{A}_2 + 24\bar{A}^+ + 48\bar{A}\bar{A}\bar{A}\bar{A}\bar{A} + 24\bar{A}^- \rightarrow 2\bar{A}\bar{A}_3 + 9\bar{A}_2 + 48\bar{A}\bar{A}\bar{A}\bar{A} + 48\bar{A}_{\bar{A}} \ (18)$$

However, the differences in the stoichiometry of the reaction between the nitrogenase variants raised several concerns about a unified mechanism for nitrogen fixation. Each variant had key mechanistic experiments carried out using nitrogenases from different species, and the analysis often was carried over between proteins without confirming that each behaved similarly. Why do the alternative nitrogenases produce more H<sub>2</sub> during N<sub>2</sub> reduction? If H<sub>2</sub> production and alternative substrate interactions varied by nitrogenase, how could this be reconciled in a unified mechanism?

Advancements by Seefeldt and Hoffman in recent years suggest that the mechanisms of  $N_2$  reduction for Mo-, V- and Fe-only nitrogenases are similar.  $^{180,220,259}$  Protocols were used to acquire V- and Fe-only nitrogenase from *A. vinelandii* without the use of an affinity tag,  $^{180,208}$  similar to what had been described during the initial discoveries.  $^{142}$  However, the V-nitrogenase protein expressed by Hales was in a *nifHDK* deletion strain that later was found to produce two different conformers during purification – the standard  $\alpha_2\beta_2(\delta)$  V-nitrogenase as well as a less active  $\alpha\beta_2(\delta)$  form,  $^{142,148}$  whereas the protein used by Seefeldt came from a wild-type bacterial strain that did not have any genetic modifications and without reported irregularities in the protein.  $^{208,220}$  On the other hand, the Fe-only nitrogenase Seefeldt reported was derived from a strain with deletions of the *nifHDK* and *vnfHDGK* genes encoding the Mo- and V-nitrogenases, consistent with previous expression strategies.

These recent mechanistic studies focused primarily on the  $E_4(4H)$  state and the ability of the enzymes to bind  $N_2$ . Both A. vinelandii V- and Fe-only nitrogenases showed inhibition of  $N_2$ 

reduction in the presence of H<sub>2</sub>, a phenomenon that was observed for the V-nitrogenase of A. chroococcum and is well established for Mo-nitrogenase. 66,180,217,220 Additionally, HD formation was measured in the presence of an N<sub>2</sub>/D<sub>2</sub> atmosphere, in line with Mo-dependent experiments described in Section 5.1. These results were together interpreted to mean that N<sub>2</sub> binds similarly to the respective nitrogenase cofactor, suggesting that the same E<sub>4</sub>(4H) 'Janus intermediate' was operative in all three systems. <sup>220</sup> However, spectroscopic evidence of the E<sub>4</sub>(4H) species analogous to the Mo-dependent system has not yet been reported for either the V- or Fenitrogenases. Kinetic analysis was also carried out with V- and Fe-only nitrogenases to determine the ratio of N<sub>2</sub>:H<sub>2</sub> to compare to the Mo system, such that all three enzymes come from the same organism. 180,220 Extrapolation of kinetic fits relating to the N<sub>2</sub>:H<sub>2</sub> ratio with respect to the pressure of N<sub>2</sub> indicated that at high pressures all three systems would have a ratio of  $\sim 1$ , and would therefore reduce  $N_2$  following the stoichiometry of reaction 16. This was compared to an experiment with Mo-nitrogenase by Simpson and Burris that measured N<sub>2</sub> reduction and H<sub>2</sub> production at high (50 atm) pressures of N<sub>2</sub>, and this study showed that H<sub>2</sub> production could not be abolished, and approached a N<sub>2</sub>:H<sub>2</sub> ratio of 1.<sup>216</sup> Analogous high pressure experiments were not conducted for the alternative nitrogenases due to the requirement of much higher pressures (>>50 atm) to carry out the same analysis, though there are no reported experimental values above 1 atm N<sub>2</sub>. <sup>180,220</sup> The difference in apparent N<sub>2</sub>:H<sub>2</sub> ratios was then contextualized with respect to the relative rates of N<sub>2</sub> binding to E<sub>4</sub>(4H), relaxation of E<sub>4</sub>(4H) to yield H<sub>2</sub>, and formation of E<sub>4</sub>(2N2H) with concomitant decrease of the N<sub>2</sub> bond order. The reported interpretation was that Mo-nitrogenase is able to produce E<sub>4</sub>(2N2H) faster than either of the alternative enzymes, so  $E_4(4H)$  is less likely to unproductively relax to a lower  $E_n$  state to generate H<sub>2</sub>, thus, less H<sub>2</sub> is observed.<sup>220</sup> Extensive substrate analog studies have not been reported for all of these systems, so it is unclear based on this work how the alternative nitrogenases move through the higher E<sub>n</sub> states as compared to Mo-nitrogenase.

Around the same time, Einsle and co-workers reported a crystal structure of V-nitrogenase from *A. vinelandii* with a putative reaction intermediate bound. <sup>150</sup> In the structure there was electron density for a light atom (X) smaller than sulfur that apparently displaced the S2B bridging sulfide ligand from the V-cluster. There was also density for an HS<sup>-</sup> ion present ~7 Å away from the S2B site in a 'holding pocket' as well as a bridging carbonate ( $CO_3^2$ -) ligand in the S3A position (see Figure 23 for labeling). Interactions from nearby residue  $\alpha$ -Gln176 to the

light X atom seemed to be indicative of a protonated species, however, protons cannot be directly observed from the diffraction experiments. These results together were used to assign the X atom as a nitrogen, and more specifically a  $\mu$ -HN<sup>-</sup> nitrene group, <sup>150</sup> although, this assignment is not strongly supported. As described in Section 3.3.1, the putative intermediate did not have metrics that compared well to the available model complex, 155 there was no reported independent verification of the light atom identity, and subsequent calculations were highly suggestive of a  $\mu$ -OH group. 156 Regardless, based on the assignment of the X atom as N, a mechanistic proposal was described for N<sub>2</sub> binding and reduction. The observation of the S<sup>2-</sup> loss was reported to be mechanistically important, as incipient hydride accumulation would force the sulfur ligand into the 'holding pocket' until returning later to kick out the final amido species in the E<sub>8</sub> state, regenerating the E<sub>0</sub> resting state. There is precedent in Mo-nitrogenase for the lability of the S2B ligand, as demonstrated in its replacement by both CO and Se<sup>2-</sup> in crystal structures from Rees, <sup>299,300</sup> however, theoretical calculations of Mo-nitrogenase disfavor complete sulfide loss during catalysis. 266,273,301-303 In addition, the release of S2B occurs after S3A has already been replaced by a carbonate, and the loss of two  $\mu$ -sulfido ligands from the cluster had not been otherwise explored as a mechanistic possibility. Einsle further suggested that the two  $\mu$ -hydride ligands bridge between Fe2 and Fe6 (equivalent to E<sub>4</sub>(4H) state) and the hydrides undergo reductive elimination to produce H<sub>2</sub>, leaving the V-cluster primed with 2 electrons and open coordination sites (termed E<sub>4</sub>\*), allowing for N<sub>2</sub> to bind to the cofactor and generate the E<sub>4</sub>(2N2H) state (Scheme 1B). This would allow for N<sub>2</sub> to bind symmetrically between Fe2 and Fe6 in a  $\mu_{1,1}$ -N-NH<sub>2</sub> bridging mode (Figure 23). The conversion between the E<sub>4</sub>(4H), E<sub>4</sub>\* and E<sub>4</sub>(2N2H) states would also all be reversible. <sup>150</sup> In this proposal, the crystallographically assigned HN species would then be consistent with the E<sub>6</sub> state following a distal-type reduction pathway (Figure 22). The authors also noted that N<sub>2</sub> could alternatively bind to the E<sub>4</sub>\* state between Fe2 and Fe6 in a  $\mu$ - $\eta^2$ : $\eta^2$  mode more similar to the  $\mu$ - $\eta^2$ : $\eta^1$  mode shown in Figure 23C to form diazene and subsequently hydrazine, as N<sub>2</sub>H<sub>4</sub> is a minor product of V-nitrogenase as described earlier (Scheme 1B). Interestingly, there was no discussion of the purpose the carbonate ligand serves in catalysis or why it appears in V-nitrogenase when carbonate is nonessential for turnover by Mo-nitrogenase.

If one assumes that the assignment of the X atom as N is confirmed, the result would seem to indicate that V-nitrogenase follows a different mechanism for N<sub>2</sub> reduction than Mo-

nitrogenase, or at minimum, there is more than one active N<sub>2</sub> reduction pathway. One pathway would be analogous to the Mo-dependent system that produces ammonia, and V-nitrogenase would follow a distal-type reduction mechanism opposed to an alternating mechanism (Figure 22). The second pathway in the V-dependent system would bind  $N_2$  in a  $\mu$ - $\eta^2$ : $\eta^2$  mode to terminally produce hydrazine in agreement with experimental observations.<sup>207</sup> The requirement of sulfur loss during catalysis is also an interesting idea, though validating biochemical investigations will be required to further understand this behavior. However, there are several issues with Einsle's proposal for N<sub>2</sub> binding and reduction by V-nitrogenase. The dubious identity of the X atom is problematic, but if to assess the proposal we assume this assignment is correct, the next issue stems from the existence of the E<sub>4</sub>\* state. As discussed in the previous sections, H<sub>2</sub> is an inhibitor of N<sub>2</sub> reduction, and the conversion of the E<sub>4</sub>(4H) state to the  $E_4(2N2H)$  state as shown in Scheme 1A requires  $N_2$  binding concomitant with  $H_2$  loss. Conversely, the presence of H<sub>2</sub> reverses N<sub>2</sub> binding and regenerates E<sub>4</sub>(4H) consistent with experimental observations of inhibition. Further, if nitrogenase is turned over in the presence of N<sub>2</sub> and D<sub>2</sub>, 2 equivalents of HD are observed per N<sub>2</sub>, but no isotopically scrambled dihydrogen is observed in the absence of N<sub>2</sub>. <sup>188,210,263,264</sup> In Einsle's proposal, the E<sub>4</sub>\* state is added, and that splits H<sub>2</sub> release from the N<sub>2</sub> binding step (Scheme 1, compare A to B). In the mechanism as described, it is less clear how H<sub>2</sub> could serve as an inhibitor to N<sub>2</sub> reduction, and more importantly, it would allow for the generation of HD if the E<sub>4</sub>(4H) species was exposed to D<sub>2</sub> in the absence of N<sub>2</sub>. This is in opposition to the experimental observations that HD is only formed in the presence of D<sub>2</sub> and N<sub>2</sub>. There is also no experimental evidence provided to support an alternate binding of N<sub>2</sub> to the V-cluster that could result in a reaction pathway that generates N<sub>2</sub>H<sub>4</sub>, though its inclusion was described as 'hypothetical.' This proposal also differs from the studies described by Seefeldt and Hoffman that indicate all nitrogenases follow a similar mechanism, and favor retention of the S2B sulfide ligand. 220,259,266,273 In addition, intermediate trapping studies with Mo-nitrogenase are supportive of an alternating type mechanism, <sup>197</sup> though it is also important to note that the proposal by Seefeldt and Hoffman does not currently explain the observation that V-nitrogenase can produce hydrazine without turning it over as a substrate. It is clear that more work is needed to assess these differing proposals.

A 
$$E_4(4H)$$
 $N_2$ 
 $N_2$ 

**Scheme 1**. Simplified scheme of N<sub>2</sub> binding for the proposed E<sub>4</sub> state of the nitrogen reduction mechanism. A: The concerted N<sub>2</sub> binding and H<sub>2</sub> release from the LT model for Mo-nitrogenase, with multiple arrows representing the remaining steps required to produce NH<sub>3</sub>. B: The mechanism for N<sub>2</sub> binding proposed for V-nitrogenase by Einsle and co-workers in ref 150. The multiple solid arrows represent the 'on pathway' reduction of N<sub>2</sub> to NH<sub>3</sub>, and the dashed arrow reflects a proposed 'off pathway' method to produce N<sub>2</sub>H<sub>4</sub>. C: Depiction of D<sub>2</sub> reacting with the E<sub>4</sub>(2N2H) state to produce a deuterium charged E<sub>4</sub>(4H) state (termed E<sub>4</sub>(2H2D)) and the subsequent relaxation as one means to produce HD.

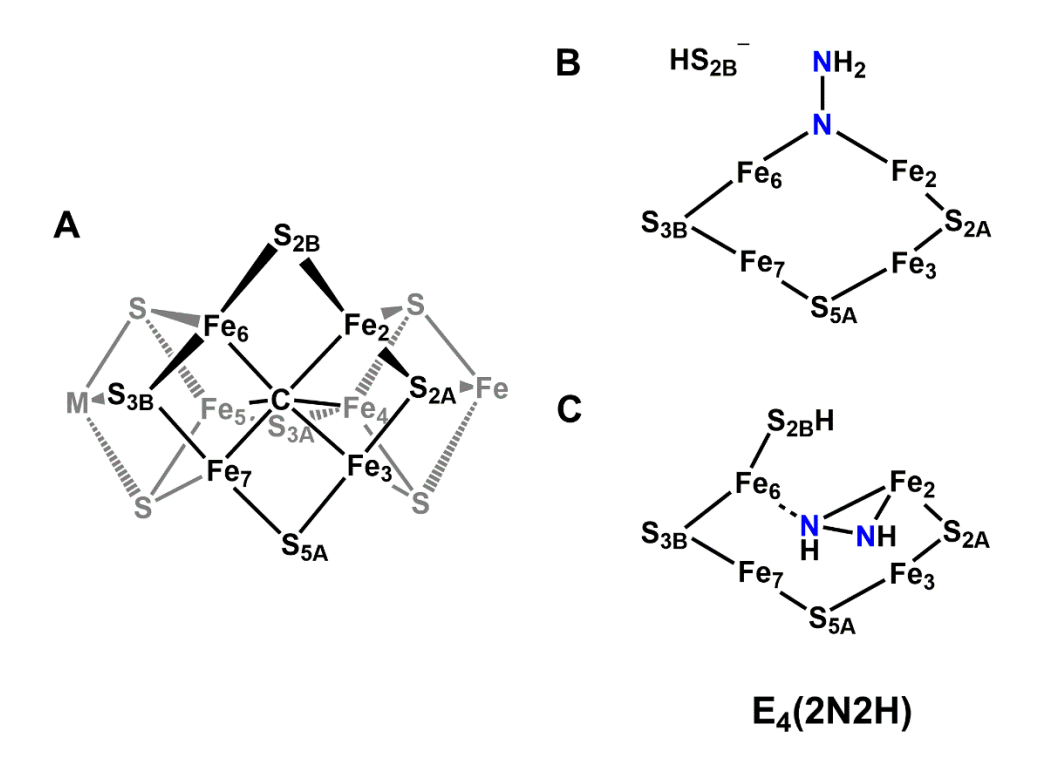


**Figure 23**. Proposed intermediates for the E<sub>4</sub>(2N2H) state of Mo/V-nitrogenase during N<sub>2</sub> reduction. A: Depiction of the catalytic cofactor (M = Mo for M-cluster, V for V-cluster), where S3A is replaced by carbonate (CO<sub>3</sub><sup>2-</sup>) in the crystal structure of VFe. The catalytic surface of the M-cluster as identified by Hoffman and co-workers is colored black. B: Proposed E<sub>4</sub> state by Einsle in ref 150 with a  $\mu_{1,1}$ -N-NH<sub>2</sub> species. C: Lowest energy configuration of E<sub>4</sub> state proposed by Raugei, Seefeldt and Hoffman in ref 266 with a  $\mu_{-\eta}^2$ : $\eta^1$ -diazene-type species.

## 5.3 Mechanism of Nitrogenases for the Reduction of Carbon Monoxide

In addition to N<sub>2</sub>, nitrogenase has been known to reduce a variety of small molecules, as described in Section 4. Historically, Mo-nitrogenase was known to reduce substrates such as alkynes, nitriles, hydrogen cyanide, azide, cyclopropene and isonitriles, and these reactions have been summarized and discussed in detail in previous reviews. <sup>66,197,198,200</sup> In the past two decades, exciting findings have established that V-nitrogenase can additionally moonlight as a CO reductase, with the ability to reduce and couple CO into hydrocarbons ranging from C<sub>1</sub> to C<sub>4</sub>. <sup>237,238</sup> In this context, there has been a renewed interest to study the reactions of CO, not only in the V-dependent system, but in Mo-nitrogenase as well. The objective of the following section is to present this development in light of the mechanistic insights that have been gained regarding these interesting reactions since their discovery.

# 5.3.1 The Binding and Reactivity of CO in Mo-Nitrogenase

It has long been established that CO behaves as an inhibitor of the Mo-nitrogenase, attenuating the reduction of all substrates except protons under conventional turnover conditions. 66,215 The binding of CO had been observed by EPR in early studies, in which Monitrogenase was subjected to turnover conditions with low electron flux.<sup>66</sup> Two distinct signals were observed in the spectra; one at a low concentration of CO (at 8% CO, 92% Ar atmosphere, designated as the 'lo-CO' state), with g-values of 2.10, 1.98, 1.92, and the other at a high concentration of CO (at 50% CO, 50% Ar) atmosphere, designated as the 'hi-CO' state), with gvalues of 2.17, 2.10, 2.05.<sup>213</sup> <sup>13</sup>C and <sup>57</sup>Fe ENDOR analysis of these signals confirmed that CO was bound to the Fe atom(s) of the M-cluster, and it was proposed that the lo-CO signal corresponded to a single molecule of CO bridging between two Fe atoms (Figure 24A), while the hi-CO signal corresponded to two CO molecules, each binding end-on to different Fe atoms (Figure 24B). 304-306 These assignments were further supported and explored using Fourier Transform-IR (FT-IR) spectroscopy. 307-309 In the Mo-nitrogenase from K. pneumoniae, the FT-IR spectrum of the lo-CO form had a single band at 1904 cm<sup>-1</sup>, while three additional bands corresponding to the hi-CO species were observed at 1906 cm<sup>-1</sup>, 1935.6 cm<sup>-1</sup>, and 1958 cm<sup>-1</sup>. 307 The multiple signals observed in the hi-CO form of the enzyme indicated that CO was binding to more than one Fe atom, and the time-dependent analysis of these IR bands also suggested that the lo-CO form was primarily responsible for the inhibitory effect of CO on nitrogenase activity. 307,308 The cryo-annealing (warming a sample to a higher temperature while remaining frozen) of EPR samples demonstrated that the lo-CO and hi-CO forms are inter-convertible, and real-time monitoring of this process using FT-IR revealed new spectroscopic features consistent with alternative CO binding modes that do not have an EPR signal. 308,310,311 Additionally, both EPR and FT-IR studies indicated that the bound CO ligands could be photolyzed from the protein. 308-311

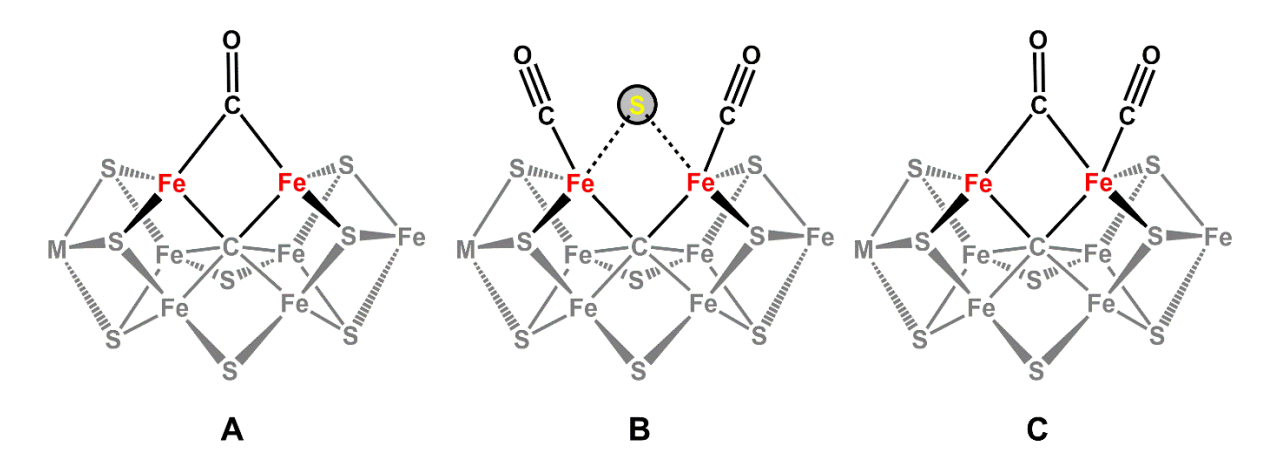


**Figure 24**. Possible CO binding configurations on the M- or V-clusters. A reflects a  $\mu_2$ -CO species bridged between two Fe centers of the catalytic cofactor, designated 'lo-CO.' This state was observed in both Mo- and V nitrogenase. B and C reflect potential 'hi-CO' species that were observed in Mo- and V-nitrogenase, respectively. B reflects two end-on-bound CO molecules (with uncertainty in the status of the bridging sulfide, as depicted with dashed lines), while C was proposed to be a combination of the  $\mu_2$ -CO moiety (i.e. 'lo-CO') in addition to an end-on bound CO (designated 'extra CO').

Perhaps the most exciting advance comes from the seminal work of the Rees group, in which the crystal structure of the CO bound MoFe protein from A. vinelandii was solved (Figure 25).<sup>299</sup> To capture intermediates in the MoFe protein during turnover, Rees and co-workers developed an innovative procedure where substrate turnover was initiated under an atmosphere of CO, potentially producing CO-inhibited species. The MoFe protein was then re-isolated from the reaction mixture and crystallized within several hours. In the crystal structure, CO was found to bind in a  $\mu_2$ -bridging mode between Fe2 and Fe6 at both of the M-cluster sites in the heterotetramer, within close proximity to the catalytically important residues  $\alpha$ -Val70 and  $\alpha$ -His195. 154,312,313 The former residue was previously indicated to be involved in CO binding, and single-point mutation of  $\alpha$ -Val70 led to minor reducing activities towards CO. <sup>309,314</sup> Surprisingly, the binding of CO in the structure was achieved by displacing the bridging sulfur atom (S2B) that was originally at that position; an unprecedented finding at the time. The replacement of S2B with a CO molecule causes the core geometry of the M-cluster to slightly distort from the known resting state structure, such that the molybdenum, the interstitial carbide, and Fe1 atoms no longer align along the 3-fold symmetry axis.<sup>299</sup> Importantly, S2B was shown to reappear in the original position after the CO inhibited MoFe protein was once again subjected to turnover conditions, but in the absence of CO. This experiment demonstrated the interconversion of the resting and CO-inhibited states of the MoFe protein and thereby, the physiological relevance of

the captured structural snapshot. A putative sulfur binding site was found ~22 Å away from the S2B position at the interface between the NifD and NifK subunits of NifDK, but it is unclear how the S2B sulfur would be able to reversibly migrate across such a long distance during activation and/or substrate turnover. This is in contrast to the 'holding pocket' observed in the crystal structure of VnfDGK, only ~7 Å away from the S2B position. <sup>150</sup>

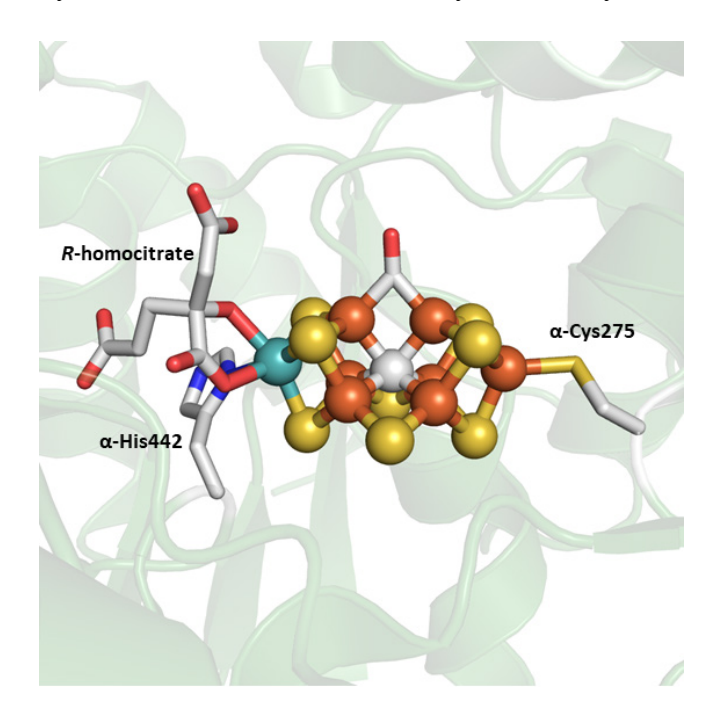


**Figure 25**. The crystal structure of *Av* NifDK with CO-bound to the M-cluster (PDB ID 4TKV). Coloration is the same as described in Figure 2.

While the CO-bound M-cluster observed in the crystal structure bore the same ligand-binding geometry as the lo-CO species proposed from EPR and ENDOR studies, it was unclear if the crystallographic and spectroscopic species were equivalent, due to notable differences in sample preparation. For example, the CO-bound MoFe protein from the crystal structure was generated under a saturating amount of CO (1 atm CO) with a high electron flux (excess Fe protein, high molar ratio), and the sample was allowed to sit idle for several hours under non-turnover conditions. In contrast, the lo-CO MoFe protein as described by EPR/ENDOR analysis was prepared using low concentrations of CO (0.08atm CO) with a low electron flux (excess MoFe protein, low molar ratio) and the samples were rapidly frozen. To resolve this ambiguity, an experiment was conducted to reproduce the sample using conditions reported by Rees and then analyzing it using EPR spectroscopy. A 'lo-CO' signal appeared in the spectra generated from this sample, and this demonstrated that the bound-CO species observed in the structure was

indeed the same as the species proposed from EPR and ENDOR experiments. This finding suggested that the displacement of the belt sulfur atom was now a mechanistic possibility, a notion that had not previously been considered. One potential complication with this finding is in understanding how the loss of a  $\mu_2$ -sulfide ligand would affect the spectroscopic properties of the metallocofactor, if at all. In a recent study, the biochemical characterization of the L-cluster, the [Fe<sub>8</sub>S<sub>9</sub>C] biosynthetic precursor of the M-cluster, showed that the presence or absence of a bridging sulfur atom only minimally affects the EPR spectrum. Thus, it is conceivable that the spectroscopically derived lo-CO state might also lack a 'belt' sulfur ligand, a feature that is difficult to detect using EPR spectroscopy alone, and warrants further evaluation.

Based on the unprecedented CO-bound structure, Rees and co-workers argued for the catalytic relevance of the displacement of S<sup>2</sup>- from the S2B position during N<sub>2</sub> and CO reduction.<sup>299</sup> They further suggested that S2B might be protonated by the nearby α-His195, generating HS<sup>-</sup> as the leaving group compared to a dianionic sulfide. The release of the sulfur species would then open up a reactive diiron face of the cluster that can more easily bind substrate. This idea was later supported in the context of N<sub>2</sub> reduction by calculations performed by Nørskov and co-workers, as well as experimental observations made by Einsle and coworkers, where a light atom assigned as HN-/HO- was observed in place of the bridging S2B sulfur atom in the crystal structure of the Av VFe protein. 150,316 It is unclear whether the release of the bridging sulfur and subsequent binding of CO involves the "Janus" intermediate (See Section 5.1), though previous work seems to indicate that inhibition of CO might occur at less reduced states than E<sub>4</sub>.<sup>317</sup> It is also uncertain if the binding of CO requires the reductive elimination of H<sub>2</sub>, analogous to N<sub>2</sub> reduction. One interesting fact to consider is that CO does not inhibit proton reduction in Mo-nitrogenase. 66 Since the binding of CO to the S2B position seems stable, the structural picture points to the possibility that hydrogen evolution, and perhaps hydride formation, might occur at a site different than the proposed Fe2 and Fe6 for the Janus intermediate, which would be consistent with the lack of inhibition of H<sub>2</sub> formation by CO. Further investigation is required to elucidate these structure-function relationships.

### 5.3.2 The Binding and Reactivity of CO in V-Nitrogenase

Initially, little was known about CO-binding to V-nitrogenase, but early observations were made that CO inhibits C<sub>2</sub>H<sub>2</sub> reduction less strongly when compared to Monitrogenase. 217,236 Later, it was discovered that unlike for Mo-nitrogenase, proton reduction by the V-nitrogenase from A. vinelandii could be inhibited by CO. 149 In addition, the lo-CO and hi-CO signals from EPR studies were not initially reported for the V-dependent protein when it was subjected to turnover conditions in a CO atmosphere, analogous to those for Mo-nitrogenase. 163 These findings could all be rationalized by the fact that CO is actually a substrate for Vnitrogenase, as demonstrated by Ribbe and co-workers in 2010. 237,238 Since this discovery, efforts have been made to use DFT calculations to gain insight into the mechanism of CO reduction. 318,319 While this early work did not have much by way of experimental calibration, it was recognized that reduction of CO likely occurs through sequential reduction and protonation of a bound CO moiety. In both the studies of Dance, and Nørskov and co-workers, the most energetically demanding step is the first reduction, where a cofactor bound CO (M–CO) species was converted to a metal-formyl (M–CHO) species. These theoretical calculations also suggested that a methylene moiety (H<sub>2</sub>C<sup>2</sup>-) was likely to be involved in the C–C coupling reaction for the formation of C<sub>2</sub> and C<sub>3</sub> products. Lastly, it was also noted that the mechanism of CO reduction to longer chain hydrocarbons may involve more steps than are proposed for N<sub>2</sub> reduction. The challenges in the experimental characterization of CO reactions with the VFe protein are equally daunting, and in many ways mirror those that have been encountered in the mechanistic investigation of Mo-nitrogenase. The chief hurdle is the complex and uninterrupted electron transfer process during substrate turnover, such that the isolation and characterization of bound substrate or reaction intermediates were unattainable by conventional means. In the case of Monitrogenase, this problem was overcome through site-directed mutagenesis near the active site, in combination with rapid freeze-quench spectroscopic techniques, as well as structural analysis of inhibitor- and analog-bound MoFe protein samples (See Section 5.3.1). Similar approaches have more recently been undertaken by the Ribbe and Hu groups to understand the mechanism of CO reduction by V-nitrogenase.

It was recognized by Ribbe and co-workers that when the V-nitrogenase of *A. vinelandii* was subjected to turnover conditions in a CO atmosphere, the protein displayed an EPR signal that is almost identical to the lo-CO signal that was observed in Mo-nitrogenase, albeit at much lower intensity.<sup>315</sup> This finding was reasonable, considering that the reaction of V-nitrogenase

with CO was slow (Table 6), so a small but still detectable spectroscopic feature can be observed. The result also agrees with predictions from DFT calculations that the initial reduction of a bound CO species would be rate determining, and therefore, has the highest likelihood to be trapped and studied. 318,319 Importantly, this result sheds light on the reduction of CO by Vnitrogenase by comparison to the well-established framework of CO binding in Mo-nitrogenase, as described in the previous section. Consequently, it was proposed that CO may also bind to the V-cluster in a  $\mu_2$ -bridging conformation, analogous to that observed for the Mo-dependent system, as evidenced by an identical 'lo-CO' signal.<sup>299</sup> To better characterize this species, strategies were devised to accumulate a CO-bound species by uncoupling the binding of CO to the VFe protein from further reaction. One strategy implemented was to subject the VFe protein to low redox potentials using the strong reductant Eu<sup>II</sup>-DTPA (-1.14 V versus SHE) under a CO atmosphere, with non-turnover conditions.315 At 1 atm CO, a dramatic increase of the lo-CO signal with g-values at 2.09, 1.99 and 1.91, was observed (Figure 26A). CO release experiments revealed that one CO per VFe protein was trapped under these conditions. This result was consistent with one bridging CO molecule binding the V-cluster in only one of the V-cluster sites. Starting from similar conditions but increasing the pressure of CO to 2.6 atm, a new composite signal emerged in the EPR spectrum, that was assigned to the hi-CO form of Vnitrogenase (Figure 26B).<sup>320</sup> The hi-CO state from the VFe protein is comprised of a lo-CO component similar to that observed for the MoFe protein, but when this species is subtracted from the spectrum, a residual component remains, which appears to have a more axial signal with g-values at 2.13 and 2.01 (Figure 26C). This residual signal was called the 'extra-CO' species, and CO release experiments identified that ~3-4 CO molecules per VFe protein were observed, a marked increase from the study of the lo-CO species from VnfDGK.<sup>315</sup> A model for the hi-CO species was then proposed to have 2 CO molecules bound on each of the V-clusters in the protein.  $^{320}$  One of the CO ligands was consistent with the previously described  $\mu_2$ -bridging mode, while the 'extra CO' signal was tentatively assigned as a terminally bound CO molecule, adjacent to the bridging CO (Figure 24C). This assignment was speculative and required verification through in-depth spectroscopic analysis.<sup>321</sup>

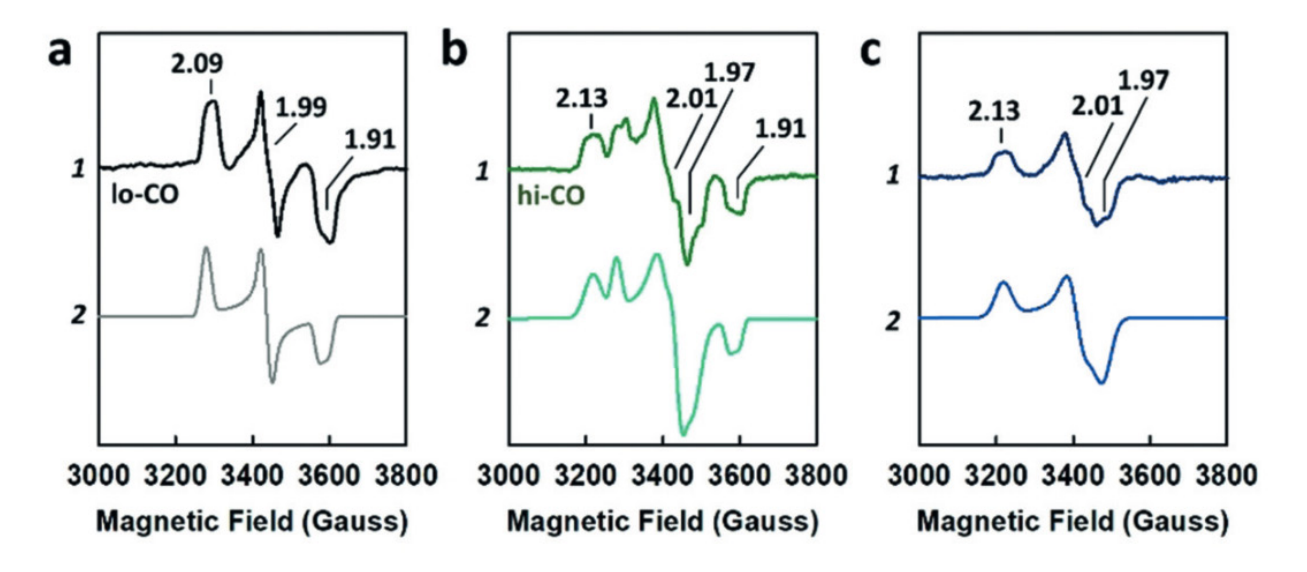


**Figure 26**. The EPR spectra (1) and respective simulation (2) for the *Av* VFe protein in the lo-CO (a) and hi-CO (b) states. The difference spectrum (c) of (hi-CO)–(lo-CO) uncovers a signal associated with the 'extra-CO' species. Adapted with permission from ref 320. Copyright 2018 John Wiley and Sons.

With the emergence of two distinct CO-bound species in the Av VFe protein, a question was raised regarding which of the species was competent for the reduction and coupling of CO into longer chain hydrocarbons. This notion had been previously considered for Mo-nitrogenase, as some kinetic and spectroscopic evidence suggested that the lo-CO species was responsible for the inhibitory effect on nitrogenase activity. On the other hand, the possibility of the hi-CO species with two CO molecules bound at the cofactor site seemed like a convenient starting point for C-C coupling. To address this question, Ribbe, Hu and co-workers tested the reactivity of the chemically generated lo-CO and hi-CO species of V-nitrogenase. 320 When the purified lo-CO species was subjected to turnover conditions in an argon atmosphere, CH<sub>4</sub> was detected. The origin of the generated CH<sub>4</sub> was traced to the CO bound to the V-cluster using isotopically labeled <sup>13</sup>CO. When the isolated <sup>13</sup>C-labeled lo-CO VFe protein was reacted with additional equivalents of <sup>12</sup>CO, ethylene and ethane with mixed carbon labels (<sup>12</sup>CH<sub>2</sub>=<sup>13</sup>CH<sub>2</sub> and <sup>12</sup>CH<sub>3</sub>-<sup>13</sup>CH<sub>3</sub>, respectively) were produced. <sup>315,320,321</sup> This strongly implied that the putatively bridging lo-CO species had catalytic relevance in V-nitrogenase. In contrast, when the hi-CO VFe protein was subjected to turnover conditions in an Ar atmosphere, C<sub>2</sub> products were not detected above the background. Treating the <sup>13</sup>C labeled hi-CO species with additional <sup>12</sup>CO only yielded mixed labeled ethylene and ethane (<sup>12</sup>CH<sub>2</sub>=<sup>13</sup>CH<sub>2</sub> and <sup>12</sup>CH<sub>3</sub>–<sup>13</sup>CH<sub>3</sub>), but not fully labeled products

(<sup>13</sup>CH<sub>2</sub>=<sup>13</sup>CH<sub>2</sub> and <sup>13</sup>CH<sub>3</sub>–<sup>13</sup>CH<sub>3</sub>). These results suggest that the lo-CO, but not the hi-CO species, was the catalytically relevant form for hydrocarbon formation and C–C coupling.

Another line of evidence that further supports this conclusion came from an alternative approach in trapping the bound CO species using a "mismatched" V-nitrogenase system. <sup>321</sup> In these studies, the A. vinelandii VFe protein (Av VnfDGK) was subjected to substrate turnover conditions in a CO atmosphere, but used a reductase protein from a different organism, M. acetivorans (Ma VnfH). This mismatched nitrogenase pair was previously shown to have much lower specific activity due to inefficient electron transfer. 104 The reduced electron flux served to stall CO reduction and allow for the accumulation of CO-bound species. The hi-CO signal on the VFe protein was reproduced at 1 atm of CO pressure, whereas previously it required 2.6 atm of CO. This enabled the study of the competition of N<sub>2</sub> and CO binding through the correlation between the N<sub>2</sub> reduction activities and the intensities of lo-CO and hi-CO EPR signals. <sup>320,321</sup> At 0.1 atm of N<sub>2</sub> and increasing concentrations of CO (0.1, 0.5, 0.9 atm), ammonium production dropped drastically – losing most of the activity at 0.1 atm of CO. Coincidentally, the intensity of the lo-CO EPR signal increased concomitantly with the decrease in activity, gaining more than half of its maximum intensity at 0.1 atm CO. In contrast, the hi-CO EPR signal on the VnfDGK increases more slowly, remaining at < 20% of the maximum signal intensity even at 0.5 atm CO. This implied that N<sub>2</sub> could be competing with the lo-CO species for reactive Fe sites on the Vcluster (but not the hi-CO species), likely at the S2B belt sulfide position.

Additional insights into the CO reduction pathway were gained from the novel aldehyde condensation reaction catalyzed by isolated M-cluster.<sup>252</sup> Driven by Eu<sup>II</sup>-DTPA, formaldehyde and acetaldehyde were found to be reduced to methane and ethene/ethane respectively (See Section 4.5).<sup>252</sup> Interestingly, these aldehydes can be coupled to form C<sub>2</sub> products from formaldehyde and C<sub>4</sub> products from acetaldehyde. This suggests that an aldehyde-like species could be a potential intermediate for CO reduction. The connection between the CO- and aldehyde-reduction pathways were shown through cross coupling experiments, where <sup>13</sup>C labeled formaldehyde and acetaldehyde were provided <sup>12</sup>CO and/or <sup>12</sup>CN<sup>-</sup>. The presence of mixed labeled products definitively showed that aldehydes can be coupled with CO and CN<sup>-</sup> and this is strongly indicative of reaction pathways that share a common coupling intermediate. This finding suggests that a direct coupling of two bound CO molecules, similar to the proposed hi-

CO structure, is not likely to occur. The natural question that follows is, at which point of the reduction pathway does C–C coupling occur? To that end, isotope analysis using <sup>2</sup>H labeling reveals that activation of formaldehyde leads to a metal bound hydroxymethyl moiety, which is supported by the finding that both substrate-derived hydrogen atoms (i.e. C<sub>2</sub>H<sub>2</sub>O) were retained in the product.<sup>252</sup> This observation agreed with the proposed reactivity of the lo-CO species, as described above, and further indicates that the plausible candidates of coupling intermediates may either be metal-bound alcohol (M–ROH), allyl (M–RCH<sub>2</sub>) and (M–RCH<sub>3</sub>) alkyl species.

## 6. Summary and Perspectives

Nitrogenase is a complex two-component metalloprotein capable of facilitating the difficult chemical transformation of  $N_2$  into  $NH_3$  under standard temperature and pressure. This multi-electron and multi-proton reaction involves the concerted effort of three different FeS clusters, with the activity taking place at the Mo-, V-, or Fe-clusters for the Mo-, V-, and Fe-only nitrogenases, respectively. On the surface, it may seem that all the nitrogenase variants should behave in the same way, as they carry out identical reactions, but closer investigation reveals that this may not be the case.

In general, the alternative nitrogenases are less effective at nitrogen fixation as well as the catalytic turnover of other small molecule substrates (C<sub>2</sub>H<sub>2</sub>, HN<sub>3</sub>, HCN) in comparison to Monitrogenase. There is a tendency to divert more reducing equivalents to the production of H<sub>2</sub> during substrate reductions, as observed in the increased specific activities (Table 4) during turnover of N<sub>2</sub> or C<sub>2</sub>H<sub>2</sub>. For N<sub>2</sub>, studies have demonstrated different stoichiometries for the concomitant generation of H<sub>2</sub> during N<sub>2</sub> fixation by each version of nitrogenase, pointing to different mechanisms for each nitrogenase variant. Additionally, V-nitrogenase was shown to produce hydrazine as a product, in contrast to the Mo system that can consume N<sub>2</sub>H<sub>4</sub> as a substrate. The source of these differences has not been clearly identified, but kinetic analysis hints at a unified mechanism for all three systems that show different relative rates for the reactions. However, new structural evidence suggests there could be different mechanisms for N<sub>2</sub> reduction by Mo and V-nitrogenases, so further work will help clarify these observations. On the other hand, V- and Fe-only nitrogenase have a weaker affinity for acetylene than does Monitrogenase, and so are less capable of turnover. Uniquely, acetylene can be reduced to ethane by

the alternative systems while this cannot be achieved with the Mo-dependent enzyme. This (along with other experiments) indicates that different binding sites for  $C_2H_2$  may exist in the alternative proteins, and further supports an alternate mechanism for the turnover of  $C_2H_2$  by these enzymes.

The alternative nitrogenases were also found capable of converting CO and CO<sub>2</sub> into hydrocarbons, an activity that was not observed in the Mo-dependent enzyme. CO normally inhibits the reduction of N<sub>2</sub> but not H<sub>2</sub> in Mo-nitrogenase, but both N<sub>2</sub> and H<sub>2</sub> activities were attenuated for V-nitrogenase. This coincided with an increase in the formation of C<sub>1</sub> to C<sub>4</sub> hydrocarbon products, with C<sub>2</sub> products (C<sub>2</sub>H<sub>4</sub>, C<sub>2</sub>H<sub>6</sub>) being favored. The reduction of CO was found to be a property of the VFe protein, as swapping the V-cluster for the M-cluster to make a hybrid enzyme (M-VFe protein) still allowed for hydrocarbon formation, albeit with lower rates than wild-type V-nitrogenase. Reconstituting the *apo*-MoFe protein with V-cluster (V-MoFe protein) did not confer increased CO-reducing capabilities, but it did allow for the reduction of acetylene to ethane, indicating that V-cluster itself carries some of the activity properties when in a protein scaffold. This contrasts with the activities of the isolated M- and V-clusters, which both react similarly towards small molecule substrates CO, CO<sub>2</sub> and CN<sup>-</sup>. The Fe-only nitrogenase was also discovered to convert CO<sub>2</sub> into methane, which was only observed for the V-nitrogenase in the presence of D<sub>2</sub>O. The unique properties of the alternative nitrogenases indicate that there may still be much to learn about the reactivity of nitrogenase.

While great effort has gone into the study of nitrogenase over the last two decades, the number of questions that still require answers seem to grow – partly due to the technical challenges of working with delicate nitrogenase proteins and partly due to the ever-increasing avenues of research. For instance, the proposed biosynthetic pathway for the metal cofactors of the VFe and FeFe proteins require experimental validation. In particular, the elucidation of the exact role of VnfEN will be crucial, as this protein is supposedly the central hub for the assembly for both the V- and Fe-clusters. Effort in this line is chiefly hindered by the isolation of intact VnfEN and other relevant protein components, but even with isolated protein, the analysis would be plagued by the lack of structural knowledge of the alternative nitrogenases. Most important would be the structure of the P- and Fe-clusters of the FeFe protein, as there is relatively little spectroscopic and structural characterization. Even for the more established V-nitrogenase,

several of the structural features remain controversial, including the exact configuration of the P-cluster of the VFe protein, as well as the relevance of the carbonate ligand that sits in place of a sulfur in the V-cluster.

Furthermore, the intriguing discoveries of the CO and CO<sub>2</sub> reducing abilities of V- and Fe-only nitrogenases seem to suggest that the alternative nitrogenases are more versatile small molecule reductases. This raises questions regarding the physiological relevance of these activities in the native environment, as well as in the evolution history of the enzyme. From a biochemical standpoint, there are ongoing efforts to try to address how much overlap, if any at all, there is between the mechanisms of CO/CO<sub>2</sub> reduction and that of N<sub>2</sub> reduction. One caveat here, as discussed earlier, is that there is no strong consensus whether the N<sub>2</sub> reduction mechanisms are identical for the three nitrogenase systems. Additional verification of the experimental parameters must be carefully carried out in each individual system for the best basis of comparison. However, one thing that is certain is that the trapping of any *bona fide* substrate- or intermediate-bound nitrogenase species will be crucial in gaining further insights. To this end, the investigation of V-nitrogenase has already proven to be greatly useful. Hopefully, future research will yield even more exciting details as the century-old enigma known as the N<sub>2</sub> reduction mechanism continues to be unraveled.

## **AUTHOR INFORMATION**

## **Corresponding Author**

E-mail: mribbe@uci.edu and yilinh@uci.edu

#### **Biographies**

Andrew J. Jasniewski is from West Allis, WI and received his B.S. degree (2011) from the University of Wisconsin—Madison working for Thomas Brunold on functional models of the Mn-dependent superoxide dismutase. He then moved to the University of Minnesota to study the structures and spectroscopy of nonheme diiron enzymes and related model complexes with Lawrence Que Jr., receiving his Ph.D. degree in 2017. He currently works at the University of California, Irvine with Markus Ribbe and Yilin Hu on the biochemistry and spectroscopy of nitrogenase.

Chi Chung Lee received a B.S. degree in Molecular Biology from the University of California, San Diego, and a Ph.D. degree in Molecular Biology and Biochemistry from the University of California, Irvine (UCI). He was a postdoctoral fellow at UCI for several years and is currently a Project Scientist at the same institute. During the last 13 years, his research interests have been centered on the assembly of nitrogenase cofactors as well as the mechanisms of substrate reduction.

Yilin Hu received a B.S. degree in Genetics from Fudan University, China, and a Ph.D. degree in Biochemistry from Loma Linda University. She was a postdoctoral fellow at the University of California, Irvine, and is currently Associate Professor at the same institute. During the last 17 years, she has been focused on studies related to nitrogenase mechanism and assembly, with an emphasis on the genetic manipulation of nitrogenase systems.

Markus W. Ribbe received a B.S. degree in Biology, a M.S. degree in Microbiology, and a Ph.D. degree in Microbiology from the University of Bayreuth, Germany. He was a postdoctoral fellow at the University of California, Irvine, and is now Chancellor's Professor at the same institute. During the past 25 years, he has focused on the mechanistic investigation of nitrogenase catalysis and assembly by combined biochemical, spectroscopic, and structural approaches.

# Acknowledgements

The authors were supported by NIH-NIGMS grant GM67626 (to M.W.R. and Y.H.), which funded research related to the assembly of nitrogenase. The authors were also supported by the Department of Energy grants DOE (BES) DE-SC0016510 (to Y.H. and M.W.R.) and DE-SC0014470 (to M.W.R. and Y.H.), which funded work related to the mechanistic investigation of ammonia formation by nitrogenase and hydrocarbon formation by nitrogenase hybrid systems, respectively. In addition, the authors were supported by NSF grants CHE-1904131 (to M.W.R. and Y.H.) and CHE-1651398 (to Y.H.) that supported work related to CO activation by nitrogenase and CO<sub>2</sub> reduction by nitrogenase Fe proteins, respectively.

#### References

- (1) Dos Santos, P. C.; Fang, Z.; Mason, S. W.; Setubal, J. C.; Dixon, R. Distribution of Nitrogen Fixation and Nitrogenase-Like Sequences Amongst Microbial Genomes. *BMC Genomics* **2012**, *13*, 162.
- (2) Mus, F.; Colman, D. R.; Peters, J. W.; Boyd, E. S. Geobiological Feedbacks, Oxygen, and the Evolution of Nitrogenase. *Free Radical Biol. Med.* **2019**, *140*, 250-259.
- (3) McRose, D. L.; Zhang, X.; Kraepiel, A. M. L.; Morel, F. M. M. Diversity and Activity of Alternative Nitrogenases in Sequenced Genomes and Coastal Environments. *Front. Microbiol.* **2017**, *8*, 267.
- (4) Affourtit, J.; Zehr, J. P.; Paerl, H. W. Distribution of Nitrogen-Fixing Microorganisms Along the Neuse River Estuary, North Carolina. *Microb. Ecol.* **2001**, *41*, 114-123.
- (5) Cleveland, C. C.; Townsend, A. R.; Schimel, D. S.; Fisher, H.; Howarth, R. W.; Hedin, L. O.; Perakis, S. S.; Latty, E. F.; Von Fischer, J. C.; Elseroad, A.et al. Global Patterns of Terrestrial Biological Nitrogen (N₂) Fixation in Natural Ecosystems. *Global Biogeochem. Cycles* **1999**, *13*, 623-645.
- (6) Noda, S.; Ohkuma, M.; Usami, R.; Horikoshi, K.; Kudo, T. Culture-Independent Characterization of a Gene Responsible for Nitrogen Fixation in the Symbiotic Microbial Community in the Gut of the Termite *Neotermes koshunensis*. *Appl. Environ. Microbiol.* **1999**, *65*, 4935-4942.
- (7) Betancourt, D. A.; Loveless, T. M.; Brown, J. W.; Bishop, P. E. Characterization of Diazotrophs Containing Mo-Independent Nitrogenases, Isolated from Diverse Natural Environments. *Appl. Environ. Microbiol.* **2008**, *74*, 3471-3480.
- (8) Bellenger, J. P.; Xu, Y.; Zhang, X.; Morel, F. M. M.; Kraepiel, A. M. L. Possible Contribution of Alternative Nitrogenases to Nitrogen Fixation by Asymbiotic N₂-Fixing Bacteria in Soils. *Soil Biol. Biochem.* **2014**, *69*, 413-420.
- (9) Joerger, R. D.; Bishop, P. E.; Evans, H. J. Bacterial Alternative Nitrogen Fixation Systems. *Crit. Rev. Microbiol.* **1988**, *16*, 1-14.
- (10) Raymond, J.; Siefert, J. L.; Staples, C. R.; Blankenship, R. E. The Natural History of Nitrogen Fixation. *Mol. Biol. Evol.* **2004**, *21*, 541-554.
- (11) Boyd, E.; Peters, J. New Insights into the Evolutionary History of Biological Nitrogen Fixation. *Front. Microbiol.* **2013**, *4*, 201.
- (12) Soboh, B.; Boyd, E. S.; Zhao, D.; Peters, J. W.; Rubio, L. M. Substrate Specificity and Evolutionary Implications of a NifDK Enzyme Carrying NifB-co at Its Active Site. *FEBS Lett.* **2010**, *584*, 1487-1492.
- (13) Oda, Y.; Samanta, S. K.; Rey, F. E.; Wu, L.; Liu, X.; Yan, T.; Zhou, J.; Harwood, C. S. Functional Genomic Analysis of Three Nitrogenase Isozymes in the Photosynthetic Bacterium *Rhodopseudomonas palustris. J. Bacteriol.* **2005**, *187*, 7784-7794.
- (14) Schneider, K.; Müller, A.; Schramm, U.; Klipp, W. Demonstration of a Molybdenum- and Vanadium-Independent Nitrogenase in a *nifHDK*-Deletion Mutant of *Rhodobacter capsulatus*. *Eur. J. Biochem.* **1991**, *195*, 653-661.
- (15) Boison, G.; Steingen, C.; Stal, L. J.; Bothe, H. The Rice Field Cyanobacteria *Anabaena azotica* and *Anabaena* sp. Ch1 Express Vanadium-Dependent Nitrogenase. *Arch. Microbiol.* **2006**, *186*, 367-376.
- (16) Joerger, R. D.; Jacobson, M. R.; Premakumar, R.; Wolfinger, E. D.; Bishop, P. E. Nucleotide Sequence and Mutational Analysis of the Structural Genes (*anfHDGK*) for the Second Alternative Nitrogenase from *Azotobacter vinelandii*. *J. Bacteriol.* **1989**, *171*, 1075-1086.
- (17) Mus, F.; Alleman, A. B.; Pence, N.; Seefeldt, L. C.; Peters, J. W. Exploring the Alternatives of Biological Nitrogen Fixation. *Metallomics* **2018**, *10*, 523-538.

- (18) Hamilton, T. L.; Ludwig, M.; Dixon, R.; Boyd, E. S.; Dos Santos, P. C.; Setubal, J. C.; Bryant, D. A.; Dean, D. R.; Peters, J. W. Transcriptional Profiling of Nitrogen Fixation in *Azotobacter vinelandii*. *J. Bacteriol.* **2011**, *193*, 4477-4486.
- (19) Demtröder, L.; Pfänder, Y.; Schäkermann, S.; Bandow, J. E.; Masepohl, B. NifA Is the Master Regulator of Both Nitrogenase Systems in *Rhodobacter capsulatus*. *MicrobiologyOpen* **2019**, *8*, e921.
- (20) Thiel, T.; Pratte, S. B. Regulation of Three Nitrogenase Gene Clusters in the Cyanobacterium *Anabaena variabilis* ATCC 29413. *Life* **2014**, *4*, 944-967.
- (21) Zhang, X.; McRose, D. L.; Darnajoux, R.; Bellenger, J. P.; Morel, F. M. M.; Kraepiel, A. M. L. Alternative Nitrogenase Activity in the Environment and Nitrogen Cycle Implications. *Biogeochemistry* **2016**, *127*, 189-198.
- (22) Darnajoux, R.; Zhang, X.; McRose, D. L.; Miadlikowska, J.; Lutzoni, F.; Kraepiel, A. M. L.; Bellenger, J.-P. Biological Nitrogen Fixation by Alternative Nitrogenases in Boreal Cyanolichens: Importance of Molybdenum Availability and Implications for Current Biological Nitrogen Fixation Estimates. *New Phytol.* **2017**, *213*, 680-689.
- (23) Rebelein, J. G.; Lee, C. C.; Newcomb, M.; Hu, Y.; Ribbe, M. W. Characterization of an M-Cluster-Substituted Nitrogenase VFe Protein. *mBio* **2018**, *9*, e00310-00318.
- (24) Anbar, A. D.; Knoll, A. H. Proterozoic Ocean Chemistry and Evolution: A Bioinorganic Bridge? *Science* **2002**, *297*, 1137-1142.
- (25) Boyd, E.; Hamilton, T.; Peters, J. An Alternative Path for the Evolution of Biological Nitrogen Fixation. *Front. Microbiol.* **2011**, *2*, 205.
- (26) Boyd, E. S.; Anbar, A. D.; Miller, S.; Hamilton, T. L.; Lavin, M.; Peters, J. W. A Late Methanogen Origin for Molybdenum-Dependent Nitrogenase. *Geobiology* **2011**, *9*, 221-232.
- (27) Zhang, X.; Sigman, D. M.; Morel, F. M. M.; Kraepiel, A. M. L. Nitrogen Isotope Fractionation by Alternative Nitrogenases and Past Ocean Anoxia. *Proc. Natl. Acad. Sci. U. S. A.* 2014, 111, 4782-4787
- (28) Stüeken, E. E.; Buick, R.; Guy, B. M.; Koehler, M. C. Isotopic Evidence for Biological Nitrogen Fixation by Molybdenum-Nitrogenase from 3.2 Gyr. *Nature* **2015**, *520*, 666-669.
- (29) Zerkle, A. L.; Junium, C. K.; Canfield, D. E.; House, C. H. Production of <sup>15</sup>N-Depleted Biomass During Cyanobacterial N<sub>2</sub>-Fixation at High Fe Concentrations. *J. Geophys. Res.: Biogeosci.* **2008**, *113*, G03014.
- (30) Sickerman, Nathaniel S.; Rettberg, Lee A.; Lee, Chi C.; Hu, Y.; Ribbe, Markus W. Cluster Assembly in Nitrogenase. *Essays Biochem.* **2017**, *61*, 271-279.
- (31) Hu, Y.; Ribbe, M. W. Biosynthesis of the Metalloclusters of Nitrogenases. *Annu. Rev. Biochem* **2016**, *85*, 455-483.
- (32) Ribbe, M. W.; Hu, Y.; Hodgson, K. O.; Hedman, B. Biosynthesis of Nitrogenase Metalloclusters. *Chem. Rev.* **2014**, *114*, 4063-4080.
- (33) Hu, Y.; Fay, A. W.; Lee, C. C.; Yoshizawa, J.; Ribbe, M. W. Assembly of Nitrogenase MoFe Protein. *Biochemistry* **2008**, *47*, 3973-3981.
- (34) Hu, Y.; Corbett, M. C.; Fay, A. W.; Webber, J. A.; Hedman, B.; Hodgson, K. O.; Ribbe, M. W. Nitrogenase Reactivity with P-Cluster Variants. *Proc. Natl. Acad. Sci. U. S. A.* **2005**, *102*, 13825-13830.
- (35) Blank, M. A.; Lee, C. C.; Hu, Y.; Hodgson, K. O.; Hedman, B.; Ribbe, M. W. Structural Models of the [Fe<sub>4</sub>S<sub>4</sub>] Clusters of Homologous Nitrogenase Fe Proteins. *Inorg. Chem.* **2011**, *50*, 7123-7128.
- (36) Hu, Y.; Ribbe, M. W. Biosynthesis of the Iron-Molybdenum Cofactor of Nitrogenase. *J. Biol. Chem.* **2013**, *288*, 13173-13177.
- (37) Hu, Y.; Ribbe, M. W. Maturation of Nitrogenase Cofactor—the Role of a Class E Radical SAM Methyltransferase Nifb. *Curr. Opin. Chem. Biol.* **2016**, *31*, 188-194.

- (38) Kennedy, C.; Dean, D. The *nifU*, *nifS* and *nifV* Gene Products Are Required for Activity of All Three Nitrogenases of *Azotobacter vinelandii*. *Mol. Gen. Genet.* **1992**, *231*, 494-498.
- (39) Zheng, L.; Dean, D. R. Catalytic Formation of a Nitrogenase Iron-Sulfur Cluster. *J. Biol. Chem.* **1994**, *269*, 18723-18726.
- (40) Shi, H.-w.; Wang, L.-y.; Li, X.-x.; Liu, X.-m.; Hao, T.-y.; He, X.-j.; Chen, S.-f. Genome-Wide Transcriptome Profiling of Nitrogen Fixation in *Paenibacillus sp.* WLY78. *BMC Microbiol.* **2016**, *16*, 25.
- (41) Fay, A. W.; Wiig, J. A.; Lee, C. C.; Hu, Y. Identification and Characterization of Functional Homologs of Nitrogenase Cofactor Biosynthesis Protein NifB from Methanogens. *Proc. Natl. Acad. Sci. U. S. A.* **2015**, *112*, 14829-14833.
- (42) Schwarz, G.; Mendel, R. R.; Ribbe, M. W. Molybdenum Cofactors, Enzymes and Pathways. *Nature* **2009**, *460*, 839-847.
- (43) Wiig, J. A.; Hu, Y.; Ribbe, M. W. Nifen-B Complex of *Azotobacter vinelandii* Is Fully Functional in Nitrogenase FeMo Cofactor Assembly. *Proc. Natl. Acad. Sci. U. S. A.* **2011**, *108*, 8623-8627.
- (44) Corbett, M. C.; Hu, Y.; Fay, A. W.; Ribbe, M. W.; Hedman, B.; Hodgson, K. O. Structural Insights into a Protein-Bound Iron-Molybdenum Cofactor Precursor. *Proc. Natl. Acad. Sci. U. S. A.* **2006**, *103*, 1238-1243.
- (45) Fay, A. W.; Blank, M. A.; Lee, C. C.; Hu, Y.; Hodgson, K. O.; Hedman, B.; Ribbe, M. W. Spectroscopic Characterization of the Isolated Iron–Molybdenum Cofactor (FeMoco) Precursor from the Protein NifEN. *Angew. Chem. Int. Ed.* **2011**, *50*, 7787-7790.
- (46) Wiig, J. A.; Hu, Y.; Lee, C. C.; Ribbe, M. W. Radical SAM-Dependent Carbon Insertion into the Nitrogenase M-Cluster. *Science* **2012**, *337*, 1672-1675.
- (47) Boal, A. K.; Rosenzweig, A. C. A Radical Route for Nitrogenase Carbide Insertion. *Science* **2012**, 337, 1617-1618.
- (48) Boal, A. K.; Grove, T. L.; McLaughlin, M. I.; Yennawar, N. H.; Booker, S. J.; Rosenzweig, A. C. Structural Basis for Methyl Transfer by a Radical SAM Enzyme. *Science* **2011**, *332*, 1089-1092.
- (49) Wiig, J. A.; Hu, Y.; Ribbe, M. W. Refining the Pathway of Carbide Insertion into the Nitrogenase M-Cluster. *Nat. Commun.* **2015**, *6*, 8034.
- (50) Rettberg, L. A.; Wilcoxen, J.; Lee, C. C.; Stiebritz, M. T.; Tanifuji, K.; Britt, R. D.; Hu, Y. Probing the Coordination and Function of Fe<sub>4</sub>S<sub>4</sub> Modules in Nitrogenase Assembly Protein NifB. *Nat. Commun.* **2018**, *9*, 2824.
- (51) Tanifuji, K.; Lee, C. C.; Sickerman, N. S.; Tatsumi, K.; Ohki, Y.; Hu, Y.; Ribbe, M. W. Tracing the 'Ninth Sulfur' of the Nitrogenase Cofactor Via a Semi-Synthetic Approach. *Nat. Chem.* **2018**, *10*, 568-572.
- (52) Jasniewski, A. J.; Wilcoxen, J.; Tanifuji, K.; Hedman, B.; Hodgson, K. O.; Britt, R. D.; Hu, Y.; Ribbe, M. W. Spectroscopic Characterization of an Eight-Iron Nitrogenase Cofactor Precursor That Lacks the "9th Sulfur". Angew. Chem. Int. Ed. 2019, 58, 14703-14707.
- (53) Fugate, C. J.; Jarrett, J. T. Biotin Synthase: Insights into Radical-Mediated Carbon–Sulfur Bond Formation. *Biochim. Biophys. Acta, Proteins Proteomics* **2012**, *1824*, 1213-1222.
- (54) Zheng, L.; White, R. H.; Cash, V. L.; Dean, D. R. Mechanism for the Desulfurization of L-Cysteine Catalyzed by the *nifS* Gene Product. *Biochemistry* **1994**, *33*, 4714-4720.
- (55) Kertesz, M. A. Riding the Sulfur Cycle Metabolism of Sulfonates and Sulfate Esters in Gram-Negative Bacteria. *FEMS Microbiol. Rev.* **2000**, *24*, 135-175.
- (56) Hu, Y.; Corbett, M. C.; Fay, A. W.; Webber, J. A.; Hodgson, K. O.; Hedman, B.; Ribbe, M. W. FeMo Cofactor Maturation on NifEN. *Proc. Natl. Acad. Sci. U. S. A.* **2006**, *103*, 17119-17124.
- (57) Yoshizawa, J. M.; Blank, M. A.; Fay, A. W.; Lee, C. C.; Wiig, J. A.; Hu, Y.; Hodgson, K. O.; Hedman, B.; Ribbe, M. W. Optimization of FeMoco Maturation on NifEN. *J. Am. Chem. Soc.* **2009**, *131*, 9321-9325.

- (58) Hu, Y.; Corbett, M. C.; Fay, A. W.; Webber, J. A.; Hodgson, K. O.; Hedman, B.; Ribbe, M. W. Nitrogenase Fe Protein: A Molybdate/Homocitrate Insertase. *Proc. Natl. Acad. Sci. U. S. A.* **2006,** *103*, 17125-17130.
- (59) Fay, A. W.; Blank, M. A.; Rebelein, J. G.; Lee, C. C.; Ribbe, M. W.; Hedman, B.; Hodgson, K. O.; Hu, Y. Assembly Scaffold NifEN: A Structural and Functional Homolog of the Nitrogenase Catalytic Component. *Proc. Natl. Acad. Sci. U. S. A.* **2016**, *113*, 9504-9508.
- (60) Fay, A. W.; Blank, M. A.; Yoshizawa, J. M.; Lee, C. C.; Wiig, J. A.; Hu, Y.; Hodgson, K. O.; Hedman, B.; Ribbe, M. W. Formation of a Homocitrate-Free Iron-Molybdenum Cluster on NifEN: Implications for the Role of Homocitrate in Nitrogenase Assembly. *Dalton Trans.* 2010, 39, 3124-3130.
- (61) Kaiser, J. T.; Hu, Y.; Wiig, J. A.; Rees, D. C.; Ribbe, M. W. Structure of Precursor-Bound NifEN: A Nitrogenase FeMo Cofactor Maturase/Insertase. *Science* **2011**, *331*, 91-94.
- (62) Schmid, B.; Ribbe, M. W.; Einsle, O.; Yoshida, M.; Thomas, L. M.; Dean, D. R.; Rees, D. C.; Burgess, B. K. Structure of a Cofactor-Deficient Nitrogenase MoFe Protein. *Science* **2002**, *296*, 352-356.
- (63) Yoshizawa, J. M.; Fay, A. W.; Lee, C. C.; Hu, Y.; Ribbe, M. W. Insertion of Heterometals into the NifEN-Associated Iron–Molybdenum Cofactor Precursor. *JBIC, J. Biol. Inorg. Chem.* **2010,** *15*, 421-428.
- (64) Wolfinger, E. D.; Bishop, P. E. Nucleotide Sequence and Mutational Analysis of the *vnfENX* Region of *Azotobacter vinelandii*. *J. Bacteriol*. **1991**, *173*, 7565-7572.
- (65) Howard, J. B.; Rees, D. C. Structural Basis of Biological Nitrogen Fixation. *Chem. Rev.* **1996,** *96*, 2965-2982.
- (66) Burgess, B. K.; Lowe, D. J. Mechanism of Molybdenum Nitrogenase. *Chem. Rev.* **1996**, *96*, 2983-3012.
- (67) Kim, J.; Rees, D. C. Crystallographic Structure and Functional Implications of the Nitrogenase Molybdenum–Iron Protein from *Azotobacter vinelandii*. *Nature* **1992**, *360*, 553-560.
- (68) Kim, J.; Rees, D. C. Structural Models for the Metal Centers in the Nitrogenase Molybdenum-Iron Protein. *Science* **1992**, *257*, 1677-1682.
- (69) Georgiadis, M. M.; Komiya, H.; Chakrabarti, P.; Woo, D.; Kornuc, J. J.; Rees, D. C. Crystallographic Structure of the Nitrogenase Iron Protein from *Azotobacter vinelandii*. *Science* **1992**, *257*, 1653-1659.
- (70) Schindelin, H.; Kisker, C.; Schlessman, J. L.; Howard, J. B.; Rees, D. C. Structure of ADP·AlF<sub>4</sub> Stabilized Nitrogenase Complex and Its Implications for Signal Transduction. *Nature* **1997**, *387*, 370-376.
- (71) Tezcan, F. A.; Kaiser, J. T.; Mustafi, D.; Walton, M. Y.; Howard, J. B.; Rees, D. C. Nitrogenase Complexes: Multiple Docking Sites for a Nucleotide Switch Protein. *Science* **2005**, *309*, 1377-1380.
- (72) George, G. N.; Coyle, C. L.; Hales, B. J.; Cramer, S. P. X-Ray Absorption of *Azotobacter vinelandii* Vanadium Nitrogenase. *J. Am. Chem. Soc.* **1988**, *110*, 4057-4059.
- (73) Arber, J. M.; Dobson, B. R.; Eady, R. R.; Stevens, P.; Hasnain, S. S.; Garner, C. D.; Smith, B. E. Vanadium K-Edge X-Ray Absorption Spectrum of the VFe Protein of the Vanadium Nitrogenase of *Azotobacter chroococcum*. *Nature* **1987**, *325*, 372-374.
- (74) Sippel, D.; Einsle, O. The Structure of Vanadium Nitrogenase Reveals an Unusual Bridging Ligand. *Nat. Chem. Biol.* **2017**, *13*, 956-960.
- (75) Rohde, M.; Trncik, C.; Sippel, D.; Gerhardt, S.; Einsle, O. Crystal Structure of VnfH, the Iron Protein Component of Vanadium Nitrogenase. *JBIC, J. Biol. Inorg. Chem.* **2018**, *23*, 1049-1056.
- (76) Krahn, E.; Weiss, B.; Kröckel, M.; Groppe, J.; Henkel, G.; Cramer, S.; Trautwein, A.; Schneider, K.; Müller, A. The Fe-Only Nitrogenase from *Rhodobacter capsulatus*: Identification of the Cofactor,

- an Unusual, High-Nuclearity Iron-Sulfur Cluster, by Fe K-Edge EXAFS and <sup>57</sup>Fe Mössbauer Spectroscopy. *JBIC, J. Biol. Inorg. Chem.* **2002,** *7*, 37-45.
- (77) Jasniewski, A.; Sickerman, N.; Hu, Y.; Ribbe, M. The Fe Protein: An Unsung Hero of Nitrogenase. *Inorganics* **2018**, *6*, 25.
- (78) Lee, C. C.; Stiebritz, M. T.; Hu, Y. Reactivity of [Fe<sub>4</sub>S<sub>4</sub>] Clusters toward C1 Substrates: Mechanism, Implications, and Potential Applications. *Acc. Chem. Res.* **2019**, *52*, 1168-1176.
- (79) Broach, R. B.; Rupnik, K.; Hu, Y.; Fay, A. W.; Cotton, M.; Ribbe, M. W.; Hales, B. J. Variable-Temperature, Variable-Field Magnetic Circular Dichroism Spectroscopic Study of the Metal Clusters in the Δ*nifB* and Δ*nifH* MoFe Proteins of Nitrogenase from *Azotobacter vinelandii*. *Biochemistry* **2006**, *45*, 15039-15048.
- (80) Cotton, M. S.; Rupnik, K.; Broach, R. B.; Hu, Y.; Fay, A. W.; Ribbe, M. W.; Hales, B. J. Vtvh-Mcd Study of the Δ*nifB*Δ*nifZ* MoFe Protein from *Azotobacter vinelandii*. *J. Am. Chem. Soc.* **2009,** *131*, 4558-4559.
- (81) Corbett, M. C.; Hu, Y.; Naderi, F.; Ribbe, M. W.; Hedman, B.; Hodgson, K. O. Comparison of Iron-Molybdenum Cofactor-Deficient Nitrogenase MoFe Proteins by X-Ray Absorption Spectroscopy: Implications for P-Cluster Biosynthesis. *J. Biol. Chem.* **2004**, *279*, 28276-28282.
- (82) Hu, Y.; Fay, A. W.; Dos Santos, P. C.; Naderi, F.; Ribbe, M. W. Characterization of *Azotobacter vinelandii nifZ* Deletion Strains: Indication of Stepwise MoFe Protein Assembly. *J. Biol. Chem.* **2004**, *279*, 54963-54971.
- (83) Seefeldt, L. C.; Hoffman, B. M.; Peters, J. W.; Raugei, S.; Beratan, D. N.; Antony, E.; Dean, D. R. Energy Transduction in Nitrogenase. *Acc. Chem. Res.* **2018**, *51*, 2179-2186.
- (84) Walker, J. E.; Saraste, M.; Runswick, M. J.; Gay, N. J. Distantly Related Sequences in the Alphaand Beta-Subunits of ATP Synthase, Myosin, Kinases and Other ATP-Requiring Enzymes and a Common Nucleotide Binding Fold. *EMBO J.* 1982, 1, 945-951.
- (85) Jang, S. B.; Seefeldt, L. C.; Peters, J. W. Insights into Nucleotide Signal Transduction in Nitrogenase: Structure of an Iron Protein with MgADP Bound. *Biochemistry* 2000, 39, 14745-14752.
- (86) Sen, S.; Krishnakumar, A.; McClead, J.; Johnson, M. K.; Seefeldt, L. C.; Szilagyi, R. K.; Peters, J. W. Insights into the Role of Nucleotide-Dependent Conformational Change in Nitrogenase Catalysis: Structural Characterization of the Nitrogenase Fe Protein Leu127 Deletion Variant with Bound MgATP. *J. Inorg. Biochem.* **2006**, *100*, 1041-1052.
- (87) Rebelein, J. G.; Stiebritz, M. T.; Lee, C. C.; Hu, Y. Activation and Reduction of Carbon Dioxide by Nitrogenase Iron Proteins. *Nat. Chem. Biol.* **2016**, *13*, 147-149.
- (88) Walker, G. A.; Mortenson, L. E. Effect of Magnesium Adenosine 5'-Triphosphate on the Accessibility of the Iron of *Clostridial* Azoferredoxin, a Component of Nitrogenase. *Biochemistry* **1974**, *13*, 2382-2388.
- (89) Ljones, T.; Burris, R. H. Nitrogenase: The Reaction between Iron Protein and Bathophenanthrolinedisulfonate as a Probe for Interactions with MgATP. *Biochemistry* **1978**, *17*, 1866-1872.
- (90) Deits, T. L.; Howard, J. B. Kinetics of Mgatp-Dependent Iron Chelation from the Fe-Protein of the *Azotobacter vinelandii* Nitrogenase Complex. Evidence for Two States. *J. Biol. Chem.* **1989,** *264*, 6619-6628.
- (91) Chen, L.; Gavini, N.; Tsuruta, H.; Eliezer, D.; Burgess, B. K.; Doniach, S.; Hodgson, K. O. MgATP-Induced Conformational Changes in the Iron Protein from *Azotobacter vinelandii*, as Studied by Small-Angle X-Ray Scattering. *J. Biol. Chem.* **1994**, *269*, 3290-3294.
- (92) Liu, J.; Chakraborty, S.; Hosseinzadeh, P.; Yu, Y.; Tian, S.; Petrik, I.; Bhagi, A.; Lu, Y. Metalloproteins Containing Cytochrome, Iron–Sulfur, or Copper Redox Centers. *Chem. Rev.* **2014**, *114*, 4366-4469.

- (93) Yates, M. G. Electron Transport to Nitrogenase in *Azotobacter chroococcum: Azotobacter* Flavodoxin Hydroquinone as an Electron Donor. *FEBS Lett.* **1972**, *27*, 63-67.
- (94) Duyvis, M. G.; Wassink, H.; Haaker, H. Nitrogenase of *Azotobacter vinelandii*: Kinetic Analysis of the Fe Protein Redox Cycle. *Biochemistry* **1998**, *37*, 17345-17354.
- (95) Bennett, L. T.; Jacobson, M. R.; Dean, D. R. Isolation, Sequencing, and Mutagenesis of the *nifF* Gene Encoding Flavodoxin from *Azotobacter vinelandii*. *J. Biol. Chem.* **1988**, *263*, 1364-1369.
- (96) Thorneley, R. N.; Deistung, J. Electron-Transfer Studies Involving Flavodoxin and a Natural Redox Partner, the Iron Protein of Nitrogenase. Conformational Constraints on Protein-Protein Interactions and the Kinetics of Electron Transfer within the Protein Complex. *Biochem. J* **1988**, 253, 587-595.
- (97) Martin, A. E.; Burgess, B. K.; Iismaa, S. E.; Smartt, C. T.; Jacobson, M. R.; Dean, D. R. Construction and Characterization of an *Azotobacter vinelandii* Strain with Mutations in the Genes Encoding Flavodoxin and Ferredoxin I. *J. Bacteriol.* **1989**, *171*, 3162-3167.
- (98) Watt, G. D.; Reddy, K. R. N. Formation of an All Ferrous Fe<sub>4</sub>S<sub>4</sub> Cluster in the Iron Protein Component of *Azotobacter vinelandii* Nitrogenase. *J. Inorg. Biochem.* **1994,** *53*, 281-294.
- (99) Watt, G. D.; Wang, Z. C.; Knotts, R. R. Redox Reactions of and Nucleotide Binding to the Iron Protein of *Azotobacter vinelandii*. *Biochemistry* **1986**, *25*, 8156-8162.
- (100) Lanzilotta, W. N.; Ryle, M. J.; Seefeldt, L. C. Nucleotide Hydrolysis and Protein Conformational Changes in *Azotobacter vinelandii* Nitrogenase Iron Protein: Defining the Function of Aspartate 129. *Biochemistry* **1995**, *34*, 10713-10723.
- (101) Bergström, J.; Eady, R. R.; Thorneley, R. N. F. The Vanadium- and Molybdenum-Containing Nitrogenases of *Azotobacter chroococcum*. Comparison of Mid-Point Potentials and Kinetics of Reduction by Sodium Dithionite of the Iron Proteins with Bound Magnesium Adenosine 5'- Diphosphate. *Biochem. J* 1988, 251, 165-169.
- (102) Lindahl, P. A.; Day, E. P.; Kent, T. A.; Orme-Johnson, W. H.; Münck, E. Mössbauer, EPR, and Magnetization Studies of the *Azotobacter vinelandii* Fe Protein. Evidence for a [4Fe-4S]<sup>1+</sup> Cluster with Spin S = 3/2. J. Biol. Chem. **1985**, 260, 11160-11173.
- (103) Orme-Johnson, W. H.; Hamilton, W. D.; Jones, T. L.; Tso, M. Y. W.; Burris, R. H.; Shah, V. K.; Brill, W. J. Electron Paramagnetic Resonance of Nitrogenase and Nitrogenase Components from *Clostridium pasteurianum* W5 and *Azotobacter vinelandii* Op. *Proc. Natl. Acad. Sci. U. S. A.* **1972**, 69, 3142-3145.
- (104) Hiller, C. J.; Stiebritz, M. T.; Lee, C. C.; Liedtke, J.; Hu, Y. Tuning Electron Flux through Nitrogenase with Methanogen Iron Protein Homologues. *Chem. Eur. J.* **2017**, *23*, 16152-16156.
- (105) Lindahl, P. A.; Gorelick, N. J.; Münck, E.; Orme-Johnson, W. H. EPR and Mössbauer Studies of Nucleotide-Bound Nitrogenase Iron Protein from *Azotobacter vinelandii*. *J. Biol. Chem.* **1987**, *262*, 14945-14953.
- (106) Lowery, T. J.; Wilson, P. E.; Zhang, B.; Bunker, J.; Harrison, R. G.; Nyborg, A. C.; Thiriot, D.; Watt, G. D. Flavodoxin Hydroquinone Reduces *Azotobacter vinelandii* Fe Protein to the All-Ferrous Redox State with a *S* = 0 Spin State. *Proc. Natl. Acad. Sci. U. S. A.* **2006**, *103*, 17131-17136.
- (107) Guo, M.; Sulc, F.; Ribbe, M. W.; Farmer, P. J.; Burgess, B. K. Direct Assessment of the Reduction Potential of the [4Fe–4S]<sup>1+/0</sup> Couple of the Fe Protein from *Azotobacter vinelandii*. *J. Am. Chem. Soc.* **2002**, *124*, 12100-12101.
- (108) Angove, H. C.; Yoo, S. J.; Burgess, B. K.; Münck, E. Mössbauer and Epr Evidence for an All-Ferrous Fe<sub>4</sub>S<sub>4</sub> Cluster with S = 4 in the Fe Protein of Nitrogenase. *J. Am. Chem. Soc.* **1997**, *119*, 8730-8731.
- (109) Vincent, K. A.; Tilley, G. J.; Quammie, N. C.; Streeter, I.; Burgess, B. K.; Cheesman, M. R.; Armstrong, F. A. Instantaneous, Stoichiometric Generation of Powerfully Reducing States of

- Protein Active Sites Using Eu(II) and Polyaminocarboxylate Ligands. *Chem. Commun.* **2003**, 2590-2591.
- (110) Chakrabarti, M.; Deng, L.; Holm, R. H.; Münck, E.; Bominaar, E. L. Mössbauer, Electron Paramagnetic Resonance, and Theoretical Studies of a Carbene-Based All-Ferrous Fe<sub>4</sub>S<sub>4</sub> Cluster: Electronic Origin and Structural Identification of the Unique Spectroscopic Site. *Inorg. Chem.* **2009**, *48*, 2735-2747.
- (111) Chakrabarti, M.; Münck, E.; Bominaar, E. L. Density Functional Theory Study of an All Ferrous 4Fe-4S Cluster. *Inorg. Chem.* **2011**, *50*, 4322-4326.
- (112) Yoo, S. J.; Angove, H. C.; Burgess, B. K.; Hendrich, M. P.; Münck, E. Mössbauer and Integer-Spin EPR Studies and Spin-Coupling Analysis of the [4Fe-4S]<sup>0</sup> Cluster of the Fe Protein from *Azotobacter vinelandii* Nitrogenase. *J. Am. Chem. Soc.* **1999**, *121*, 2534-2545.
- (113) Strop, P.; Takahara, P. M.; Chiu, H.-J.; Angove, H. C.; Burgess, B. K.; Rees, D. C. Crystal Structure of the All-Ferrous [4Fe-4S]<sup>o</sup> Form of the Nitrogenase Iron Protein from *Azotobacter vinelandii*. *Biochemistry* **2001**, *40*, 651-656.
- (114) Musgrave, K. B.; Angove, H. C.; Burgess, B. K.; Hedman, B.; Hodgson, K. O. All-Ferrous Titanium(III) Citrate Reduced Fe Protein of Nitrogenase: An XAS Study of Electronic and Metrical Structure. *J. Am. Chem. Soc.* **1998**, *120*, 5325-5326.
- (115) Schneider, K.; Gollan, U.; Dröttboom, M.; Selsemeier-Voigt, S.; Müller, A. Comparative Biochemical Characterization of the Iron-Only Nitrogenase and the Molybdenum Nitrogenase from *Rhodobacter capsulatus*. *Eur. J. Biochem.* **1997**, *244*, 789-800.
- (116) Spatzal, T.; Aksoyoglu, M.; Zhang, L.; Andrade, S. L. A.; Schleicher, E.; Weber, S.; Rees, D. C.; Einsle, O. Evidence for Interstitial Carbon in Nitrogenase FeMo Cofactor. *Science* **2011**, *334*, 940-940.
- (117) Einsle, O.; Tezcan, F. A.; Andrade, S. L. A.; Schmid, B.; Yoshida, M.; Howard, J. B.; Rees, D. C. Nitrogenase MoFe-Protein at 1.16 Å Resolution: A Central Ligand in the FeMo-Cofactor. *Science* **2002**, *297*, 1696-1700.
- (118) Chan, M. K.; Kim, J.; Rees, D. C. The Nitrogenase FeMo-Cofactor and P-Cluster Pair: 2.2 Å Resolution Structures. *Science* **1993**, *260*, 792-794.
- (119) Lancaster, K. M.; Roemelt, M.; Ettenhuber, P.; Hu, Y.; Ribbe, M. W.; Neese, F.; Bergmann, U.; DeBeer, S. X-Ray Emission Spectroscopy Evidences a Central Carbon in the Nitrogenase Iron-Molybdenum Cofactor. *Science* **2011**, *334*, 974-977.
- (120) Pierik, A. J.; Wassink, H.; Haaker, H.; Hagen, W. R. Redox Properties and EPR Spectroscopy of the P Clusters of Azotobacter *vinelandii* MoFe Protein. *Eur. J. Biochem.* **1993,** *212*, 51-61.
- (121) Huynh, B. H.; Henzl, M. T.; Christner, J. A.; Zimmermann, R.; Orme-Johnson, W. H.; Münck, E. Nitrogenase XII. Mössbauer Studies of the MoFe Protein from *Clostridium pasteurianum* W5. *Biochim. Biophys. Acta, Protein Struct.* **1980**, *623*, 124-138.
- (122) Rupnik, K.; Hu, Y.; Lee, C. C.; Wiig, J. A.; Ribbe, M. W.; Hales, B. J. P<sup>+</sup> State of Nitrogenase P-Cluster Exhibits Electronic Structure of a [Fe<sub>4</sub>S<sub>4</sub>]<sup>+</sup> Cluster. *J. Am. Chem. Soc.* **2012**, *134*, 13749-13754.
- (123) Mayer, S. M.; Lawson, D. M.; Gormal, C. A.; Roe, S. M.; Smith, B. E. New Insights into Structure-Function Relationships in Nitrogenase: A 1.6 Å Resolution X-Ray Crystallographic Study of Klebsiella pneumoniae MoFe-Protein. J. Mol. Biol. 1999, 292, 871-891.
- (124) Morgan, T. V.; Mortenson, L. E.; McDonald, J. W.; Watt, G. D. Comparison of Redox and EPR Properties of the Molybdenum Iron Proteins of *Clostridium pasteurianum* and *Azotobacter vinelandii* Nitrogenases. *J. Inorq. Biochem.* **1988**, *33*, 111-120.
- (125) Surerus, K. K.; Hendrich, M. P.; Christie, P. D.; Rottgardt, D.; Orme-Johnson, W. H.; Munck, E. Möessbauer and Integer-Spin EPR of the Oxidized P-Clusters of Nitrogenase: P<sup>ox</sup> Is a Non-

- Kramers System with a Nearly Degenerate Ground Doublet. J. Am. Chem. Soc. **1992**, 114, 8579-8590.
- (126) Peters, J. W.; Stowell, M. H. B.; Soltis, S. M.; Finnegan, M. G.; Johnson, M. K.; Rees, D. C. Redox-Dependent Structural Changes in the Nitrogenase P-Cluster. *Biochemistry* **1997**, *36*, 1181-1187.
- (127) Danyal, K.; Dean, D. R.; Hoffman, B. M.; Seefeldt, L. C. Electron Transfer within Nitrogenase: Evidence for a Deficit-Spending Mechanism. *Biochemistry* **2011**, *50*, 9255-9263.
- (128) Chan, J. M.; Christiansen, J.; Dean, D. R.; Seefeldt, L. C. Spectroscopic Evidence for Changes in the Redox State of the Nitrogenase P-Cluster During Turnover. *Biochemistry* **1999**, *38*, 5779-5785.
- (129) Danyal, K.; Mayweather, D.; Dean, D. R.; Seefeldt, L. C.; Hoffman, B. M. Conformational Gating of Electron Transfer from the Nitrogenase Fe Protein to MoFe Protein. *J. Am. Chem. Soc.* **2010**, *132*, 6894-6895.
- (130) Rawlings, J.; Shah, V. K.; Chisnell, J. R.; Brill, W. J.; Zimmermann, R.; Münck, E.; Orme-Johnson, W. H. Novel Metal Cluster in the Iron-Molybdenum Cofactor of Nitrogenase. Spectroscopic Evidence. *J. Biol. Chem.* **1978**, *253*, 1001-1004.
- (131) Burgess, B. K. The Iron-Molybdenum Cofactor of Nitrogenase. Chem. Rev. 1990, 90, 1377-1406.
- (132) Smith, B. E.; Lowe, D. J.; Bray, R. C. Studies by Electron Paramagnetic Resonance on the Catalytic Mechanism of Nitrogenase of *Klebsiella pneumoniae*. *Biochem. J* **1973**, *135*, 331-341.
- (133) Siemann, S.; Schneider, K.; Dröttboom, M.; Müller, A. The Fe-Only Nitrogenase and the Mo Nitrogenase from *Rhodobacter capsulatus*. *Eur. J. Biochem.* **2002**, *269*, 1650-1661.
- (134) Watt, G. D.; Burns, A.; Lough, S.; Tennent, D. L. Redox and Spectroscopic Properties of Oxidized MoFe Protein from *Azotobacter vinelandii*. *Biochemistry* **1980**, *19*, 4926-4932.
- (135) Watt, G. D.; Burns, A.; Tennent, D. L. Stoichiometry and Spectral Properties of the Molybdenum-Iron (MoFe) Cofactor and Noncofactor Redox Centers in the Molybdenum-Iron (MoFe) Protein of Nitrogenase from *Azotobacter vinelandii*. *Biochemistry* **1981**, *20*, 7272-7277.
- (136) Lough, S.; Burns, A.; Watt, G. D. Redox Reactions of the Nitrogenase Complex from *Azotobacter vinelandii*. *Biochemistry* **1983**, *22*, 4062-4066.
- (137) Schultz, F. A.; Gheller, S. F.; Burgess, B. K.; Lough, S.; Newton, W. E. Electrochemical Characterization of the Iron-Molybdenum Cofactor from *Azotobacter vinelandii* Nitrogenase. *J. Am. Chem. Soc.* **1985**, *107*, 5364-5368.
- (138) Pickett, C. J.; Vincent, K. A.; Ibrahim, S. K.; Gormal, C. A.; Smith, B. E.; Fairhurst, S. A.; Best, S. P. Synergic Binding of Carbon Monoxide and Cyanide to the FeMo Cofactor of Nitrogenase: Relic Chemistry of an Ancient Enzyme? *Chem. Eur. J.* **2004**, *10*, 4770-4776.
- (139) Lydon, B. R.; Lee, C. C.; Tanifuji, K.; Sickerman, N. S.; Newcomb, M. P.; Hu, Y.; Ribbe, M. W.; Yang, J. Y. Electrochemical Characterization of Isolated Nitrogenase Cofactors from *Azotobacter vinelandii*. *ChemBioChem* [Online Early Access]. DOI:10.1002/cbic.201900425. Published Online: Aug 7, 2019.
- (140) Hickey, D. P.; Cai, R.; Yang, Z.-Y.; Grunau, K.; Einsle, O.; Seefeldt, L. C.; Minteer, S. D. Establishing a Thermodynamic Landscape for the Active Site of Mo-Dependent Nitrogenase. *J. Am. Chem. Soc.* **2019**, *141*, 17150-17157.
- (141) Eady, R. R.; Robson, R. L.; Richardson, T. H.; Miller, R. W.; Hawkins, M. The Vanadium Nitrogenase of *Azotobacter chroococcum*. Purification and Properties of the VFe Protein. *Biochem. J* **1987**, *244*, 197-207.
- (142) Hales, B. J.; Case, E. E.; Morningstar, J. E.; Dzeda, M. F.; Mauterer, L. A. Isolation of a New Vanadium-Containing Nitrogenase from *Azotobacter vinelandii*. *Biochemistry* **1986**, *25*, 7251-7255.
- (143) Eady, R. R. Structure–Function Relationships of Alternative Nitrogenases. *Chem. Rev.* **1996,** *96,* 3013-3030.

- (144) Robson, R. L.; Woodley, P. R.; Pau, R. N.; Eady, R. R. Structural Genes for the Vanadium Nitrogenase from *Azotobacter chroococcum*. *EMBO J.* **1989**, *8*, 1217-1224.
- (145) Fallik, E.; Robson, R. L. Completed Sequence of the Region Encoding the Structural Genes for the Vanadium Nitrogenase of *Azotobacter chroococcum*. *Nucleic Acids Res.* **1990,** *18*, 4616-4616.
- (146) Dyer, D. H.; Rubio, L. M.; Thoden, J. B.; Holden, H. M.; Ludden, P. W.; Rayment, I. The Three-Dimensional Structure of the Core Domain of NafY from *Azotobacter vinelandii* Determined at 1.8-Å Resolution. *J. Biol. Chem.* **2003**, *278*, 32150-32156.
- (147) Homer, M. J.; Paustian, T. D.; Shah, V. K.; Roberts, G. P. The *nifY* Product of *Klebsiella pneumoniae* Is Associated with Apodinitrogenase and Dissociates Upon Activation with the Iron-Molybdenum Cofactor. *J. Bacteriol.* **1993**, *175*, 4907-4910.
- (148) Blanchard, C. Z.; Hales, B. J. Isolation of Two Forms of the Nitrogenase VFe Protein from *Azotobacter vinelandii*. *Biochemistry* **1996**, *35*, 472-478.
- (149) Lee, C. C.; Hu, Y.; Ribbe, M. W. Unique Features of the Nitrogenase VFe Protein from *Azotobacter vinelandii. Proc. Natl. Acad. Sci. U. S. A.* **2009**, *106*, 9209-9214.
- (150) Sippel, D.; Rohde, M.; Netzer, J.; Trncik, C.; Gies, J.; Grunau, K.; Djurdjevic, I.; Decamps, L.; Andrade, S. L. A.; Einsle, O. A Bound Reaction Intermediate Sheds Light on the Mechanism of Nitrogenase. *Science* **2018**, *359*, 1484-1489.
- (151) Fisher, K.; Dilworth, M. J.; Kim, C.-H.; Newton, W. E. *Azotobacter vinelandii* Nitrogenases with Substitutions in the FeMo-Cofactor Environment of the MoFe Protein: Effects of Acetylene or Ethylene on Interactions with H<sup>+</sup>, HCN, and CN<sup>-</sup>. *Biochemistry* **2000**, *39*, 10855-10865.
- (152) Fisher, K.; Dilworth, M. J.; Newton, W. E. Differential Effects on N<sub>2</sub> Binding and Reduction, HD Formation, and Azide Reduction with α-195<sup>His</sup>- and α-191<sup>Gln</sup>-Substituted MoFe Proteins of Azotobacter vinelandii Nitrogenase. Biochemistry 2000, 39, 15570-15577.
- (153) Scott, D. J.; May, H. D.; Newton, W. E.; Brigle, K. E.; Dean, D. R. Role for the Nitrogenase MoFe Protein α-Subunit in FeMo-Cofactor Binding and Catalysis. *Nature* **1990**, *343*, 188-190.
- (154) Kim, C.-H.; Newton, W. E.; Dean, D. R. Role of the MoFe Protein A-Subunit Histidine-195 Residue in FeMo-Cofactor Binding and Nitrogenase Catalysis. *Biochemistry* **1995**, *34*, 2798-2808.
- (155) Brown, S. D.; Mehn, M. P.; Peters, J. C. Heterolytic  $H_2$  Activation Mediated by Low-Coordinate  $L_3$ Fe- $(\mu$ -N)-Fe $L_3$  Complexes to Generate Fe $(\mu$ -NH) $(\mu$ -H)Fe Species. *J. Am. Chem. Soc.* **2005**, *127*, 13146-13147.
- (156) Benediktsson, B.; Thorhallsson, A. T.; Bjornsson, R. QM/MM Calculations Reveal a Bridging Hydroxo Group in a Vanadium Nitrogenase Crystal Structure. *Chem. Commun.* **2018**, *54*, 7310-7313.
- (157) Smith, B. E.; Eady, R. R.; Lowe, D. J.; Gormal, C. The Vanadium-Iron Protein of Vanadium Nitrogenase from *Azotobacter chroococcum* contains an Iron-Vanadium Cofactor. *Biochem. J* **1988**, *250*, 299-302.
- (158) Pierik, A. J. In *New Horizons in Nitrogen Fixation: Proceedings of the 9th International Congress on Nitrogen Fixation, Cancún, Mexico, December 6–12, 1992*; Lowe, D. J.;Eldridge, M. E.;Marritt, S.;Farrar, J. A.;Thomson, A. J.;Eady, R. R., Eds.; Springer Netherlands: Dordrecht, 1993, 147
- (159) Morningstar, J. E.; Johnson, M. K.; Case, E. E.; Hales, B. J. Characterization of the Metal Clusters in the Nitrogenase Molybdenum-Iron and Vanadium-Iron Proteins of *Azotobacter vinelandii* Using Magnetic Circular Dichroism Spectroscopy. *Biochemistry* **1987**, *26*, 1795-1800.
- (160) Morningstar, J. E.; Hales, B. J. Electron Paramagnetic Resonance Study of the Vanadium-Iron Protein of Nitrogenase from *Azotobacter vinelandii*. *J. Am. Chem. Soc.* **1987**, *109*, 6854-6855.
- (161) Ravi, N.; Moore, V.; Lloyd, S. G.; Hales, B. J.; Huynh, B. H. Mössbauer Characterization of the Metal Clusters in *Azotobacter vinelandii* Nitrogenase VFe Protein. *J. Biol. Chem.* **1994,** *269*, 20920-20924.

- (162) Tittsworth, R. C.; Hales, B. J. Oxidative Titration of the Nitrogenase VFe Protein from *Azotobacter vinelandii*: An Example of Redox-Gated Electron Flow. *Biochemistry* **1996**, *35*, 479-487.
- (163) Moore, V. G.; Tittsworth, R. C.; Hales, B. J. Construction and Characterization of Hybrid Component 1 from V-Nitrogenase Containing FeMo Cofactor. *J. Am. Chem. Soc.* **1994,** *116,* 12101-12102.
- (164) Tittsworth, R. C.; Hales, B. J. Detection of EPR Signals Assigned to the 1-Equiv-Oxidized P-Clusters of the Nitrogenase MoFe-Protein from *Azotobacter vinelandii*. *J. Am. Chem. Soc.* **1993**, *115*, 9763-9767.
- (165) Arber, J. M.; Dobson, B. R.; Eady, R. R.; Hasnain, S. S.; Garner, C. D.; Matsushita, T.; Nomura, M.; Smith, B. E. Vanadium K-Edge X-Ray-Absorption Spectroscopy of the Functioning and Thionine-Oxidized Forms of the VFe-Protein of the Vanadium Nitrogenase from *Azotobacter chroococcum*. *Biochem. J* **1989**, *258*, 733-737.
- (166) Harvey, I.; Arber, J. M.; Eady, R. R.; Smith, B. E.; Garner, C. D.; Hasnain, S. S. Iron K-Edge X-Ray-Absorption Spectroscopy of the Iron-Vanadium Cofactor of the Vanadium Nitrogenase from *Azotobacter chroococcum. Biochem. J* **1990**, *266*, 929-931.
- (167) Chen, J.; Christiansen, J.; Tittsworth, R. C.; Hales, B. J.; George, S. J.; Coucouvanis, D.; Cramer, S. P. Iron EXAFS of *Azotobacter vinelandii* Nitrogenase Molybdenum-Iron and Vanadium-Iron Proteins. *J. Am. Chem. Soc.* **1993**, *115*, 5509-5515.
- (168) Fay, A. W.; Blank, M. A.; Lee, C. C.; Hu, Y.; Hodgson, K. O.; Hedman, B.; Ribbe, M. W. Characterization of Isolated Nitrogenase FeVco. *J. Am. Chem. Soc.* **2010**, *132*, 12612-12618.
- (169) Rees, J. A.; Bjornsson, R.; Schlesier, J.; Sippel, D.; Einsle, O.; DeBeer, S. The Fe–V Cofactor of Vanadium Nitrogenase Contains an Interstitial Carbon Atom. *Angew. Chem. Int. Ed.* **2015**, *54*, 13249-13252.
- (170) Rees, J. A.; Bjornsson, R.; Kowalska, J. K.; Lima, F. A.; Schlesier, J.; Sippel, D.; Weyhermüller, T.; Einsle, O.; Kovacs, J. A.; DeBeer, S. Comparative Electronic Structures of Nitrogenase FeMoco and FeVco. *Dalton Trans.* **2017**, *46*, 2445-2455.
- (171) Bjornsson, R.; Lima, F. A.; Spatzal, T.; Weyhermuller, T.; Glatzel, P.; Bill, E.; Einsle, O.; Neese, F.; DeBeer, S. Identification of a Spin-Coupled Mo(III) in the Nitrogenase Iron-Molybdenum Cofactor. *Chem. Sci.* **2014**, *5*, 3096-3103.
- (172) Bjornsson, R.; Neese, F.; Schrock, R. R.; Einsle, O.; DeBeer, S. The Discovery of Mo(III) in FeMoco: Reuniting Enzyme and Model Chemistry. *JBIC, J. Biol. Inorg. Chem.* **2015**, *20*, 447-460.
- (173) Davis, R.; Lehman, L.; Petrovich, R.; Shah, V. K.; Roberts, G. P.; Ludden, P. W. Purification and Characterization of the Alternative Nitrogenase from the Photosynthetic Bacterium *Rhodospirillum rubrum. J. Bacteriol.* **1996**, *178*, 1445-1450.
- (174) Müller, A.; Schneider, K.; Gollan, U.; Krahn, E.; Dröttboom, M. Characterization of the "Iron Only" Nitrogenase from *Rhodobacter capsulatus*. *J. Inorg. Biochem.* **1995**, *59*, 551.
- (175) Chisnell, J. R.; Premakumar, R.; Bishop, P. E. Purification of a Second Alternative Nitrogenase from a *nifHDK* Deletion Strain of *Azotobacter vinelandii*. *J. Bacteriol.* **1988**, *170*, 27-33.
- (176) Pau, R. N.; Eldridge, M. E.; Lowe, D. J.; Mitchenall, L. A.; Eady, R. R. Molybdenum-Independent Nitrogenases of *Azotobacter vinelandii*: A Functional Species of Alternative Nitrogenase-3 Isolated from a Molybdenum-Tolerant Strain Contains an Iron-Molybdenum Cofactor. *Biochem. J* 1993, 293, 101-107.
- (177) Zheng, Y.; Harris, D. F.; Yu, Z.; Fu, Y.; Poudel, S.; Ledbetter, R. N.; Fixen, K. R.; Yang, Z.-Y.; Boyd, E. S.; Lidstrom, M. E.et al. A Pathway for Biological Methane Production Using Bacterial Iron-Only Nitrogenase. *Nat. Microbiol.* **2018**, *3*, 281-286.
- (178) Schneider, K.; Müller, A. In *Catalysts for Nitrogen Fixation: Nitrogenases, Relevant Chemical Models and Commercial Processes*; Smith, B. E.;Richards, R. L.;Newton, W. E., Eds.; Springer Netherlands: Dordrecht, 2004, 281-307

- (179) Hales, B. J. In *Catalysts for Nitrogen Fixation: Nitrogenases, Relevant Chemical Models and Commercial Processes*; Smith, B. E.;Richards, R. L.;Newton, W. E., Eds.; Springer Netherlands: Dordrecht, 2004, 255-279
- (180) Harris, D. F.; Lukoyanov, D. A.; Shaw, S.; Compton, P.; Tokmina-Lukaszewska, M.; Bothner, B.; Kelleher, N.; Dean, D. R.; Hoffman, B. M.; Seefeldt, L. C. Mechanism of N<sub>2</sub> Reduction Catalyzed by Fe-Nitrogenase Involves Reductive Elimination of H<sub>2</sub>. *Biochemistry* **2018**, *57*, 701-710.
- (181) McLean, P. A.; Papaefthymiou, V.; Orme-Johnson, W. H.; Münck, E. Isotopic Hybrids of Nitrogenase. Mössbauer Study of MoFe Protein with Selective <sup>57</sup>Fe Enrichment of the P-Cluster. *J. Biol. Chem.* **1987**, *262*, 12900-12903.
- (182) Yoo, S. J.; Angove, H. C.; Papaefthymiou, V.; Burgess, B. K.; Münck, E. Mössbauer Study of the MoFe Protein of Nitrogenase from *Azotobacter vinelandii* Using Selective <sup>57</sup>Fe Enrichment of the M-Centers. *J. Am. Chem. Soc.* **2000**, *122*, 4926-4936.
- (183) Harris, T. V.; Szilagyi, R. K. Comparative Assessment of the Composition and Charge State of Nitrogenase FeMo-Cofactor. *Inorg. Chem.* **2011**, *50*, 4811-4824.
- (184) Bjornsson, R.; Neese, F.; DeBeer, S. Revisiting the Mössbauer Isomer Shifts of the FeMoco Cluster of Nitrogenase and the Cofactor Charge. *Inorg. Chem.* **2017**, *56*, 1470-1477.
- (185) Kowalska, J. K.; Henthorn, J. T.; Van Stappen, C.; Trncik, C.; Einsle, O.; Keavney, D.; DeBeer, S. X-Ray Magnetic Circular Dichroism Spectroscopy Applied to Nitrogenase and Related Models: Experimental Evidence for a Spin-Coupled Molybdenum(III) Center. *Angew. Chem. Int. Ed.* 2019, 58, 9373-9377.
- (186) Einsle, O.; Andrade, S. L. A.; Dobbek, H.; Meyer, J.; Rees, D. C. Assignment of Individual Metal Redox States in a Metalloprotein by Crystallographic Refinement at Multiple X-Ray Wavelengths. *J. Am. Chem. Soc.* **2007**, *129*, 2210-2211.
- (187) Spatzal, T.; Schlesier, J.; Burger, E.-M.; Sippel, D.; Zhang, L.; Andrade, S. L. A.; Rees, D. C.; Einsle, O. Nitrogenase FeMoco Investigated by Spatially Resolved Anomalous Dispersion Refinement. Nat. Commun. 2016, 7, 10902.
- (188) Thorneley, R. N. F.; Lowe, D. J. In *Molybdenum Enzymes*; Spiro, T. G., Ed.; Wiley: New York, 1985, 221-284
- (189) Thorneley, R. N. F.; Ashby, G. A. Oxidation of Nitrogenase Iron Protein by Dioxygen without Inactivation Could Contribute to High Respiration Rates of *Azotobacter* Species and Facilitate Nitrogen Fixation in Other Aerobic Environments. *Biochem. J* **1989**, *261*, 181-187.
- (190) Barney, B. M.; Yurth, M. G.; Dos Santos, P. C.; Dean, D. R.; Seefeldt, L. C. A Substrate Channel in the Nitrogenase MoFe Protein. *JBIC, J. Biol. Inorg. Chem.* **2009**, *14*, 1015-1022.
- (191) Pham, D. N.; Burgess, B. K. Nitrogenase Reactivity: Effects of pH on Substrate Reduction and Carbon Monoxide Inhibition. *Biochemistry* **1993**, *32*, 13725-13731.
- (192) Imperial, J.; Hoover, T. R.; Madden, M. S.; Ludden, P. W.; Shah, V. K. Substrate Reduction Properties of Dinitrogenase Activated *in vitro* Are Dependent Upon the Presence of Homocitrate or Its Analogs During Iron-Molybdenum Cofactor Synthesis. *Biochemistry* **1989**, *28*, 7796-7799.
- (193) Morrison, C. N.; Hoy, J. A.; Zhang, L.; Einsle, O.; Rees, D. C. Substrate Pathways in the Nitrogenase MoFe Protein by Experimental Identification of Small Molecule Binding Sites. *Biochemistry* **2015**, *54*, 2052-2060.
- (194) Dance, I. The Pathway for Serial Proton Supply to the Active Site of Nitrogenase: Enhanced Density Functional Modeling of the Grotthuss Mechanism. *Dalton Trans.* **2015**, *44*, 18167-18186.
- (195) Siegbahn, P. E. M. A Major Structural Change of the Homocitrate Ligand of Probable Importance for the Nitrogenase Mechanism. *Inorg. Chem.* **2018**, *57*, 1090-1095.
- (196) Durrant, M. C. Controlled Protonation of Iron–Molybdenum Cofactor by Nitrogenase: A Structural and Theoretical Analysis. *Biochem. J* **2001**, *355*, 569-576.

- (197) Hoffman, B. M.; Lukoyanov, D.; Yang, Z.-Y.; Dean, D. R.; Seefeldt, L. C. Mechanism of Nitrogen Fixation by Nitrogenase: The Next Stage. *Chem. Rev.* **2014**, *114*, 4041-4062.
- (198) Burgess, B. K. In Molybdenum Enzymes, 1985, 161-219
- (199) Barney, B. M.; Yang, T.-C.; Igarashi, R. Y.; Dos Santos, P. C.; Laryukhin, M.; Lee, H.-I.; Hoffman, B. M.; Dean, D. R.; Seefeldt, L. C. Intermediates Trapped During Nitrogenase Reduction of N:N, CH<sub>3</sub>-NNH, and H<sub>2</sub>N-NH<sub>2</sub>. *J. Am. Chem. Soc.* **2005**, *127*, 14960-14961.
- (200) Seefeldt, L. C.; Hoffman, B. M.; Dean, D. R. Mechanism of Mo-Dependent Nitrogenase. *Annu. Rev. Biochem* **2009**, *78*, 701-722.
- (201) Watt, G. D.; Burns, A. Kinetics of Dithionite Ion Utilization and ATP Hydrolysis for Reactions Catalyzed by the Nitrogenase Complex from *Azotobacter vinelandii*. *Biochemistry* **1977**, *16*, 264-270.
- (202) Burgess, B. K.; Jacobs, D. B.; Stiefel, E. I. Large-Scale Purification of High Activity *Azotobacter vinelandii* Nitrogenase. *Biochim. Biophys. Acta, Enzymol.* **1980,** *614*, 196-209.
- (203) Hardy, R. W. F.; Holsten, R. D.; Jackson, E. K.; Burns, R. C. The Acetylene-Ethylene Assay for N<sub>2</sub> fixation: Laboratory and Field Evaluation. *Plant Physiol.* **1968**, *43*, 1185-1207.
- (204) Dalton, H.; Whittenbury, R. The Acetylene Reduction Technique as an Assay for Nitrogenase Activity in the Methane Oxidizing Bacterium *Methylococcus capsulatus* Strain Bath. *Arch. Microbiol.* **1976**, *109*, 147-151.
- (205) Miller, R. W.; Eady, R. R. Molybdenum and Vanadium Nitrogenases of *Azotobacter chroococcum*. Low Temperature Favours N₂ Reduction by Vanadium Nitrogenase. *Biochem. J* **1988**, *256*, 429-432.
- (206) Yates, M. G.; Planqué, K. Nitrogenase from *Azotobacter chroococcum*. *Eur. J. Biochem.* **1975,** *60*, 467-476.
- (207) Dilworth, M. J.; Eady, R. R. Hydrazine Is a Product of Dinitrogen Reduction by the Vanadium-Nitrogenase from *Azotobacter chroococcum*. *Biochem. J* **1991**, *277*, 465-468.
- (208) Sippel, D.; Schlesier, J.; Rohde, M.; Trncik, C.; Decamps, L.; Djurdjevic, I.; Spatzal, T.; Andrade, S. L. A.; Einsle, O. Production and Isolation of Vanadium Nitrogenase from *Azotobacter vinelandii* by Molybdenum Depletion. *JBIC, J. Biol. Inorg. Chem.* **2017**, *22*, 161-168.
- (209) Bulen, W. A. Proceedings of the First International Symposium on Nitrogen Fixation, Pullman, Washington, 1976; p 177-186.
- (210) Burgess, B. K.; Wherland, S.; Newton, W. E.; Stiefel, E. I. Nitrogenase Reactivity: Insight into the Nitrogen-Fixing Process through Hydrogen-Inhibition and HD-Forming Reactions. *Biochemistry* **1981**, *20*, 5140-5146.
- (211) Thorneley, R. N. F.; Eady, R. R.; Lowe, D. J. Biological Nitrogen Fixation by Way of an Enzyme-Bound Dinitrogen-Hydride Intermediate. *Nature* **1978**, *272*, 557-558.
- (212) Hardy, R. W. F. In *A Treatise on Dinitrogen Fixation*; Bottomley, F.;Burns, R. C., Eds.; Wiley: New York, NY, 1979; Vol. Section 1-2, 515-568
- (213) Davis, L. C.; Henzl, M. T.; Burris, R. H.; Orme-Johnson, W. H. Iron-Sulfur Clusters in the Molybdenum-Iron Protein Component of Nitrogenase. Electron Paramagnetic Resonance of the Carbon Monoxide Inhibited State. *Biochemistry* **1979**, *18*, 4860-4869.
- (214) Lowe, D. J.; Fisher, K.; Thorneley, R. N. *Klebsiella pneumoniae* Nitrogenase. Mechanism of Acetylene Reduction and Its Inhibition by Carbon Monoxide. *Biochem. J* **1990**, *272*, 621-625.
- (215) Rivera-Ortiz, J. M.; Burris, R. H. Interactions among Substrates and Inhibitors of Nitrogenase. *J. Bacteriol.* **1975**, *123*, 537-545.
- (216) Simpson, F.; Burris, R. A Nitrogen Pressure of 50 Atmospheres Does Not Prevent Evolution of Hydrogen by Nitrogenase. *Science* **1984**, *224*, 1095-1097.
- (217) Dilworth, M. J.; Eady, R. R.; Eldridge, M. E. The Vanadium Nitrogenase of *Azotobacter chroococcum*. Reduction of Acetylene and Ethylene to Ethane. *Biochem. J* **1988**, *249*, 745-751.

- (218) Lehman, L. J.; Roberts, G. P. Identification of an Alternative Nitrogenase System in *Rhodospirillum rubrum. J. Bacteriol.* **1991,** *173*, 5705-5711.
- (219) Dilworth, M. J.; Eady, R. R.; Robson, R. L.; Miller, R. W. Ethane Formation from Acetylene as a Potential Test for Vanadium Nitrogenase *in vivo*. *Nature* **1987**, *327*, 167-168.
- (220) Harris, D. F.; Lukoyanov, D. A.; Kallas, H.; Trncik, C.; Yang, Z.-Y.; Compton, P.; Kelleher, N.; Einsle, O.; Dean, D. R.; Hoffman, B. M.et al. Mo-, V-, and Fe-Nitrogenases Use a Universal Eight-Electron Reductive-Elimination Mechanism to Achieve N<sub>2</sub> Reduction. *Biochemistry* **2019**, *58*, 3293-3301.
- (221) Cai, R.; Milton, R. D.; Abdellaoui, S.; Park, T.; Patel, J.; Alkotaini, B.; Minteer, S. D. Electroenzymatic C–C Bond Formation from CO<sub>2</sub>. J. Am. Chem. Soc. **2018**, *140*, 5041-5044.
- (222) Lee, C. C.; Tanifuji, K.; Newcomb, M.; Liedtke, J.; Hu, Y.; Ribbe, M. W. A Comparative Analysis of the CO-Reducing Activities of MoFe Proteins Containing Mo- and V-Nitrogenase Cofactors. *ChemBioChem* **2018**, *19*, 649-653.
- (223) Siemann, S.; Schneider, K.; Oley, M.; Müller, A. Characterization of a Tungsten-Substituted Nitrogenase Isolated from *Rhodobacter capsulatus*. *Biochemistry* **2003**, *42*, 3846-3857.
- (224) Hales, B. J.; Case, E. E. Nitrogen Fixation by *Azotobacter vinelandii* in Tungsten-Containing Medium. *J. Biol. Chem.* **1987**, *262*, 16205-16211.
- (225) Schöllhorn, R.; Burris, R. H. Reduction of Azide by the N<sub>2</sub>-Fixing Enzyme System. *Proc. Natl. Acad. Sci. U. S. A.* **1967**, *57*, 1317-1323.
- (226) Dilworth, M. J.; Thorneley, R. N. F. Nitrogenase of *Klebsiella pneumoniae*. Hydrazine Is a Product of Azide Reduction. *Biochem. J* **1981**, *193*, 971-983.
- (227) Rubinson, J. F.; Burgess, B. K.; Corbin, J. L.; Dilworth, M. J. Nitrogenase Reactivity: Azide Reduction. *Biochemistry* **1985**, *24*, 273-283.
- (228) Guth, J. H.; Burris, R. H. Inhibition of Nitrogenase-Catalyzed Ammonia Formation by Hydrogen. *Biochemistry* **1983**, *22*, 5111-5122.
- (229) Boughton, J. H.; Keller, R. N. Dissociation Constants of Hydropseudohalic Acids. *J. Inorg. Nucl. Chem.* **1966**, *28*, 2851-2859.
- (230) Fisher, K.; Dilworth, M. J.; Newton, W. E. *Azotobacter vinelandii* Vanadium Nitrogenase: Formaldehyde Is a Product of Catalyzed HCN Reduction, and Excess Ammonia Arises Directly from Catalyzed Azide Reduction. *Biochemistry* **2006**, *45*, 4190-4198.
- (231) Hardy, R. W. F.; Knight, E. ATP-Dependent Reduction of Azide and HCN by N<sub>2</sub>-Fixing Enzymes of Azotobacter vinelandii and Clostridium pasteurianum. Biochim. Biophys. Acta, Enzymol. **1967**, 139, 69-90.
- (232) Kelly, M.; Postgate, J. R.; Richards, R. L. Reduction of Cyanide and Isocyanide by Nitrogenase of *Azotobacter chroococcum. Biochem. J* **1967**, *102*, 1C-3C.
- (233) Li, J.; Burgess, B. K.; Corbin, J. L. Nitrogenase Reactivity: Cyanide as Substrate and Inhibitor. *Biochemistry* **1982**, *21*, 4393-4402.
- (234) Izatt, R. M.; Christensen, J. J.; Pack, R. T.; Bench, R. Thermodynamics of Metal-Cyanide Coordination. I. pK,  $\Delta H^0$ , and  $\Delta S^0$  Values as a Function of Temperature for Hydrocyanic Acid Dissociation in Aqueous Solution. *Inorg. Chem.* **1962**, *1*, 828-831.
- (235) Rofer-DePoorter, C. K. A Comprehensive Mechanism for the Fischer-Tropsch Synthesis. *Chem. Rev.* **1981**, *81*, 447-474.
- (236) Cameron, L. M.; Hales, B. J. Unusual Effect of CO on C<sub>2</sub>H<sub>2</sub> Reduction by V Nitrogenase from *Azotobacter vinelandii. J. Am. Chem. Soc.* **1996**, *118*, 279-280.
- (237) Hu, Y.; Lee, C. C.; Ribbe, M. W. Extending the Carbon Chain: Hydrocarbon Formation Catalyzed by Vanadium/Molybdenum Nitrogenases. *Science* **2011**, *333*, 753-755.
- (238) Lee, C. C.; Hu, Y.; Ribbe, M. W. Vanadium Nitrogenase Reduces CO. Science 2010, 329, 642-642.
- (239) Rebelein, J. G.; Lee, C. C.; Hu, Y.; Ribbe, M. W. The *in Vivo* Hydrocarbon Formation by Vanadium Nitrogenase Follows a Secondary Metabolic Pathway. *Nat. Commun.* **2016**, *7*, 13641.

- (240) Seefeldt, L. C.; Rasche, M. E.; Ensign, S. A. Carbonyl Sulfide and Carbon Dioxide as New Substrates, and Carbon Disulfide as a New Inhibitor, of Nitrogenase. *Biochemistry* **1995**, *34*, 5382-5389.
- (241) Yang, Z.-Y.; Moure, V. R.; Dean, D. R.; Seefeldt, L. C. Carbon Dioxide Reduction to Methane and Coupling with Acetylene to Form Propylene Catalyzed by Remodeled Nitrogenase. *Proc. Natl. Acad. Sci. U. S. A.* **2012**, *109*, 19644-19648.
- (242) Rebelein, J. G.; Hu, Y.; Ribbe, M. W. Differential Reduction of CO<sub>2</sub> by Molybdenum and Vanadium Nitrogenases. *Angew. Chem. Int. Ed.* **2014**, *53*, 11543-11546.
- (243) Rebelein, J. G.; Hu, Y.; Ribbe, M. W. Widening the Product Profile of Carbon Dioxide Reduction by Vanadium Nitrogenase. *ChemBioChem* **2015**, *16*, 1993-1996.
- (244) Hu, B.; Harris, D. F.; Dean, D. R.; Liu, T. L.; Yang, Z.-Y.; Seefeldt, L. C. Electrocatalytic CO<sub>2</sub> Reduction Catalyzed by Nitrogenase MoFe and FeFe Proteins. *Bioelectrochemistry* **2018**, *120*, 104-109.
- (245) Shah, V. K.; Brill, W. J. Isolation of an Iron-Molybdenum Cofactor from Nitrogenase. *Proc. Natl. Acad. Sci. U. S. A.* **1977,** *74*, 3249-3253.
- (246) Fay, A. W.; Lee, C.-C.; Wiig, J. A.; Hu, Y.; Ribbe, M. W. In *Nitrogen Fixation: Methods and Protocols*; Ribbe, M. W., Ed.; Humana Press: Totowa, NJ, 2011, 239-248
- (247) Lee, C. C.; Hu, Y.; Ribbe, M. W. ATP-Independent Formation of Hydrocarbons Catalyzed by Isolated Nitrogenase Cofactors. *Angew. Chem. Int. Ed.* **2012,** *51*, 1947-1949.
- (248) Lee, C. C.; Hu, Y.; Ribbe, M. W. Catalytic Reduction of CN<sup>-</sup>, CO, and CO<sub>2</sub> by Nitrogenase Cofactors in Lanthanide-Driven Reactions. *Angew. Chem. Int. Ed.* **2015**, *54*, 1219-1222.
- (249) Lee, C. C.; Hu, Y.; Ribbe, M. W. Insights into Hydrocarbon Formation by Nitrogenase Cofactor Homologs. *mBio* **2015**, *6*, e00307-00315.
- (250) Sickerman, N. S.; Tanifuji, K.; Lee, C. C.; Ohki, Y.; Tatsumi, K.; Ribbe, M. W.; Hu, Y. Reduction of C<sub>1</sub> Substrates to Hydrocarbons by the Homometallic Precursor and Synthetic Mimic of the Nitrogenase Cofactor. *J. Am. Chem. Soc.* **2017**, *139*, 603-606.
- (251) Tanifuji, K.; Sickerman, N.; Lee, C. C.; Nagasawa, T.; Miyazaki, K.; Ohki, Y.; Tatsumi, K.; Hu, Y.; Ribbe, M. W. Structure and Reactivity of an Asymmetric Synthetic Mimic of Nitrogenase Cofactor. *Angew. Chem.* **2016**, *128*, 15862-15865.
- (252) Lee, C. C.; Hu, Y.; Ribbe, M. W. Reduction and Condensation of Aldehydes by the Isolated Cofactor of Nitrogenase. *ACS Cent. Sci.* **2018**, *4*, 1430-1435.
- (253) Fisher, K.; Lowe, D. J.; Petersen, J. Vanadium(V) Is Reduced by the 'as Isolated' Nitrogenase Fe-Protein at Neutral pH. *Chem. Commun.* **2006**, 2807-2809.
- (254) Stiebritz, M. T.; Hiller, C. J.; Sickerman, N. S.; Lee, C. C.; Tanifuji, K.; Ohki, Y.; Hu, Y. Ambient Conversion of CO<sub>2</sub> to Hydrocarbons by Biogenic and Synthetic [Fe<sub>4</sub>S<sub>4</sub>] Clusters. *Nat. Catal.* **2018**, 1, 444-451.
- (255) Lowe, D. J.; Thorneley, R. N. The Mechanism of *Klebsiella pneumoniae* Nitrogenase Action. Pre-Steady-State Kinetics of H<sub>2</sub> Formation. *Biochem. J* **1984**, *224*, 877-886.
- (256) Lowe, D. J.; Thorneley, R. N. F. The Mechanism of *Klebsiella pneumoniae* Nitrogenase Action. The Determination of Rate Constants Required for the Simulation of the Kinetics of N<sub>2</sub> Reduction and H<sub>2</sub> Evolution. *Biochem. J* **1984**, *224*, 895-901.
- (257) Thorneley, R. N. F.; Lowe, D. J. The Mechanism of *Klebsiella pneumoniae* Nitrogenase Action. Pre-Steady-State Kinetics of an Enzyme-Bound Intermediate in N₂ Reduction and of NH₃ Formation. *Biochem. J* **1984**, *224*, 887-894.
- (258) Thorneley, R. N. F.; Lowe, D. J. The Mechanism of *Klebsiella pneumoniae* Nitrogenase Action. Simulation of the Dependences of H<sub>2</sub>-Evolution Rate on Component-Protein Concentration and Ratio and Sodium Dithionite Concentration. *Biochem. J* **1984**, *224*, 903-909.

- (259) Harris, D. F.; Yang, Z.-Y.; Dean, D. R.; Seefeldt, L. C.; Hoffman, B. M. Kinetic Understanding of  $N_2$  Reduction Versus  $H_2$  Evolution at the  $E_4$ (4H) Janus State in the Three Nitrogenases. *Biochemistry* **2018**, *57*, 5706-5714.
- (260) Lukoyanov, D.; Khadka, N.; Yang, Z.-Y.; Dean, D. R.; Seefeldt, L. C.; Hoffman, B. M. Reductive Elimination of H₂ Activates Nitrogenase to Reduce the N≡N Triple Bond: Characterization of the E₄(4H) Janus Intermediate in Wild-Type Enzyme. *J. Am. Chem. Soc.* **2016**, *138*, 10674-10683.
- (261) Yang, Z.-Y.; Ledbetter, R.; Shaw, S.; Pence, N.; Tokmina-Lukaszewska, M.; Eilers, B.; Guo, Q.; Pokhrel, N.; Cash, V. L.; Dean, D. R.et al. Evidence That the P<sub>i</sub> Release Event Is the Rate-Limiting Step in the Nitrogenase Catalytic Cycle. *Biochemistry* **2016**, *55*, 3625-3635.
- (262) Duval, S.; Danyal, K.; Shaw, S.; Lytle, A. K.; Dean, D. R.; Hoffman, B. M.; Antony, E.; Seefeldt, L. C. Electron Transfer Precedes ATP Hydrolysis During Nitrogenase Catalysis. *Proc. Natl. Acad. Sci. U. S. A.* **2013**, *110*, 16414-16419.
- (263) Jensen, B. B.; Burris, R. H. Effect of High pN₂ and High pD₂ on Ammonia Production, Hydrogen Evolution, and Hydrogen Deuteride Formation by Nitrogenases. *Biochemistry* **1985**, *24*, 1141-1147.
- (264) Burgess, B. K.; Corbin, J. L.; Rubinson, J. F.; Li, J. g.; Dilworth, M. J.; Newton, W. E. In *Advances in Nitrogen Fixation Research: Proceedings of the 5th International Symposium on Nitrogen Fixation, Noordwijkerhout, the Netherlands, August 28 September 3, 1983*; Veeger, C.; Newton, W. E., Eds.; Springer Netherlands: Dordrecht, 1984, 146-146
- (265) Yang, Z.-Y.; Khadka, N.; Lukoyanov, D.; Hoffman, B. M.; Dean, D. R.; Seefeldt, L. C. On Reversible H<sub>2</sub> Loss Upon N<sub>2</sub> Binding to FeMo-Cofactor of Nitrogenase. *Proc. Natl. Acad. Sci. U. S. A.* **2013**, *110*, 16327-16332.
- (266) Raugei, S.; Seefeldt, L. C.; Hoffman, B. M. Critical Computational Analysis Illuminates the Reductive-Elimination Mechanism That Activates Nitrogenase for N₂ reduction. *Proc. Natl. Acad. Sci. U. S. A.* **2018**, *115*, 10521-10530.
- (267) Thorhallsson, A. T.; Benediktsson, B.; Bjornsson, R. A Model for Dinitrogen Binding in the E<sub>4</sub> State of Nitrogenase. *Chem. Sci.* **2019**, *10*, 11110-11124.
- (268) Igarashi, R. Y.; Laryukhin, M.; Dos Santos, P. C.; Lee, H.-I.; Dean, D. R.; Seefeldt, L. C.; Hoffman, B. M. Trapping H⁻ Bound to the Nitrogenase FeMo-Cofactor Active Site During H₂ Evolution: Characterization by ENDOR Spectroscopy. J. Am. Chem. Soc. 2005, 127, 6231-6241.
- (269) Lukoyanov, D.; Barney, B. M.; Dean, D. R.; Seefeldt, L. C.; Hoffman, B. M. Connecting Nitrogenase Intermediates with the Kinetic Scheme for N<sub>2</sub> Reduction by a Relaxation Protocol and Identification of the N<sub>2</sub> Binding State. *Proc. Natl. Acad. Sci. U. S. A.* **2007**, *104*, 1451-1455.
- (270) Kinney, R. A.; Saouma, C. T.; Peters, J. C.; Hoffman, B. M. Modeling the Signatures of Hydrides in Metalloenzymes: ENDOR Analysis of a Di-Iron Fe(μ-NH)(μ-H)Fe Core. *J. Am. Chem. Soc.* **2012**, 134, 12637-12647.
- (271) Lukoyanov, D.; Yang, Z.-Y.; Dean, D. R.; Seefeldt, L. C.; Hoffman, B. M. Is Mo Involved in Hydride Binding by the Four-Electron Reduced (E<sub>4</sub>) Intermediate of the Nitrogenase MoFe Protein? *J. Am. Chem. Soc.* **2010**, *132*, 2526-2527.
- (272) Doan, P. E.; Telser, J.; Barney, B. M.; Igarashi, R. Y.; Dean, D. R.; Seefeldt, L. C.; Hoffman, B. M. <sup>57</sup>Fe ENDOR Spectroscopy and 'Electron Inventory' Analysis of the Nitrogenase E<sub>4</sub> Intermediate Suggest the Metal-Ion Core of FeMo-Cofactor Cycles through Only One Redox Couple. *J. Am. Chem. Soc.* **2011**, *133*, 17329-17340.
- (273) Hoeke, V.; Tociu, L.; Case, D. A.; Seefeldt, L. C.; Raugei, S.; Hoffman, B. M. High-Resolution ENDOR Spectroscopy Combined with Quantum Chemical Calculations Reveals the Structure of Nitrogenase Janus Intermediate E<sub>4</sub>(4H). *J. Am. Chem. Soc.* **2019**, *141*, 11984-11996.
- (274) Lubitz, W.; Ogata, H.; Rüdiger, O.; Reijerse, E. Hydrogenases. Chem. Rev. 2014, 114, 4081-4148.

- (275) Wiedner, E. S. Thermodynamic Hydricity of [FeFe]-Hydrogenases. *J. Am. Chem. Soc.* **2019,** *141,* 7212-7222.
- (276) Belkova, N. V.; Epstein, L. M.; Filippov, O. A.; Shubina, E. S. Hydrogen and Dihydrogen Bonds in the Reactions of Metal Hydrides. *Chem. Rev.* **2016**, *116*, 8545-8587.
- (277) Wiedner, E. S.; Chambers, M. B.; Pitman, C. L.; Bullock, R. M.; Miller, A. J. M.; Appel, A. M. Thermodynamic Hydricity of Transition Metal Hydrides. *Chem. Rev.* **2016**, *116*, 8655-8692.
- (278) Neese, F. The Yandulov/Schrock Cycle and the Nitrogenase Reaction: Pathways of Nitrogen Fixation Studied by Density Functional Theory. *Angew. Chem. Int. Ed.* **2006**, *45*, 196-199.
- (279) Chatt, J.; Pearman, A. J.; Richards, R. L. Diazenido (Iminonitrosyl) (N<sub>2</sub>H), Hydrazido(2-) (N<sub>2</sub>H<sub>2</sub>, and Hydrazido(1-) (N<sub>2</sub>H<sub>3</sub>) Ligands as Intermediates in the Reduction of Ligating Dinitrogen to Ammonia. *J. Organomet. Chem.* **1975**, *101*, C45-C47.
- (280) Chatt, J.; Pearman, A. J.; Richards, R. L. The Reduction of Mono-Coordinated Molecular Nitrogen to Ammonia in a Protic Environment. *Nature* **1975**, *253*, 39-40.
- (281) Chatt, J.; Pearman, A. J.; Richards, R. L. Relevance of Oxygen Ligands to Reduction of Ligating Dinitrogen. *Nature* **1976**, *259*, 204.
- (282) Chatt, J.; Pearman, A. J.; Richards, R. L. Conversion of Dinitrogen in Its Molybdenum and Tungsten Complexes into Ammonia and Possible Relevance to the Nitrogenase Reaction. *J. Chem. Soc., Dalton Trans.* **1977**, 1852-1860.
- (283) Yandulov, D. V.; Schrock, R. R. Reduction of Dinitrogen to Ammonia at a Well-Protected Reaction Site in a Molybdenum Triamidoamine Complex. *J. Am. Chem. Soc.* **2002**, *124*, 6252-6253.
- (284) Yandulov, D. V.; Schrock, R. R. Catalytic Reduction of Dinitrogen to Ammonia at a Single Molybdenum Center. *Science* **2003**, *301*, 76-78.
- (285) Hinnemann, B.; Nørskov, J. K. Catalysis by Enzymes: The Biological Ammonia Synthesis. *Top. Catal.* **2006**, *37*, 55-70.
- (286) Tanabe, Y.; Nishibayashi, Y. Developing More Sustainable Processes for Ammonia Synthesis. *Coord. Chem. Rev.* **2013**, *257*, 2551-2564.
- (287) Schrock, R. R. Catalytic Reduction of Dinitrogen to Ammonia at a Single Molybdenum Center. *Acc. Chem. Res.* **2005**, *38*, 955-962.
- (288) MacLeod, K. C.; Holland, P. L. Recent Developments in the Homogeneous Reduction of Dinitrogen by Molybdenum and Iron. *Nat. Chem.* **2013**, *5*, 559-565.
- (289) Rodriguez, M. M.; Bill, E.; Brennessel, W. W.; Holland, P. L. N<sub>2</sub> Reduction and Hydrogenation to Ammonia by a Molecular Iron-Potassium Complex. *Science* **2011**, *334*, 780-783.
- (290) Rittle, J.; Peters, J. C. An Fe-N<sub>2</sub> Complex That Generates Hydrazine and Ammonia Via Fe=NNH<sub>2</sub>: Demonstrating a Hybrid Distal-to-Alternating Pathway for N<sub>2</sub> Reduction. *J. Am. Chem. Soc.* **2016**, 138, 4243-4248.
- (291) Seefeldt, L. C.; Dance, I. G.; Dean, D. R. Substrate Interactions with Nitrogenase: Fe Versus Mo. *Biochemistry* **2004**, *43*, 1401-1409.
- (292) Davis, L. C. Hydrazine as a Substrate and Inhibitor of *Azotobacter vinelandii* Nitrogenase. *Arch. Biochem. Biophys.* **1980**, *204*, 270-276.
- (293) Barney, B. M.; McClead, J.; Lukoyanov, D.; Laryukhin, M.; Yang, T.-C.; Dean, D. R.; Hoffman, B. M.; Seefeldt, L. C. Diazene (HNNH) Is a Substrate for Nitrogenase: Insights into the Pathway of N<sub>2</sub> Reduction. *Biochemistry* **2007**, *46*, 6784-6794.
- (294) Barney, B. M.; Lukoyanov, D.; Yang, T.-C.; Dean, D. R.; Hoffman, B. M.; Seefeldt, L. C. A Methyldiazene (HN=N-CH<sub>3</sub>)-Derived Species Bound to the Nitrogenase Active-Site FeMo Cofactor: Implications for Mechanism. *Proc. Natl. Acad. Sci. U. S. A.* **2006**, *103*, 17113-17118.
- (295) Dilworth, M. J.; Eldridge, M. E.; Eady, R. R. The Molybdenum and Vanadium Nitrogenases of *Azotobacter chroococcum*: Effect of Elevated Temperature on N₂ reduction. *Biochem. J* **1993**, 289, 395-400.

- (296) Dilworth, M. J.; Eldridge, M. E.; Eady, R. R. Correction for Creatine Interference with the Direct Indophenol Measurement of NH<sub>3</sub> in Steady-State Nitrogenase Assays. *Anal. Biochem.* **1992,** *207,* 6-10.
- (297) Robson, R. L. Nitrogen Fixation in Strains of *Azotobacter chroococcum* Bearing Deletions of a Cluster of Genes Coding for Nitrogenase. *Arch. Microbiol.* **1986**, *146*, 74-79.
- (298) Bishop, P. E.; Hawkins, M. E.; Eady, R. R. Nitrogen Fixation in Molybdenum-Deficient Continuous Culture by a Strain of *Azotobacter vinelandii* carrying a Deletion of the Structural Genes for Nitrogenase (*nifHDK*). *Biochem. J* **1986**, *238*, 437-442.
- (299) Spatzal, T.; Perez, K. A.; Einsle, O.; Howard, J. B.; Rees, D. C. Ligand Binding to the FeMo-Cofactor: Structures of CO-Bound and Reactivated Nitrogenase. *Science* **2014**, *345*, 1620-1623.
- (300) Spatzal, T.; Perez, K. A.; Howard, J. B.; Rees, D. C. Catalysis-Dependent Selenium Incorporation and Migration in the Nitrogenase Active Site Iron-Molybdenum Cofactor. *eLife* **2015**, *4*, e11620.
- (301) Dance, I. Mechanisms of the S/Co/Se Interchange Reactions at FeMo-Co, the Active Site Cluster of Nitrogenase. *Dalton Trans.* **2016**, *45*, 14285-14300.
- (302) Dance, I. How Feasible Is the Reversible S-Dissociation Mechanism for the Activation of FeMo-CO, the Catalytic Site of Nitrogenase? *Dalton Trans.* **2019**, *48*, 1251-1262.
- (303) Siegbahn, P. E. M. The Mechanism for Nitrogenase Including All Steps. *Phys. Chem. Chem. Phys.* **2019**, *21*, 15747-15759.
- (304) Pollock, R. C.; Lee, H.-I.; Cameron, L. M.; DeRose, V. J.; Hales, B. J.; Orme-Johnson, W. H.; Hoffman, B. M. Investigation of CO Bound to Inhibited Forms of Nitrogenase MoFe Protein by <sup>13</sup>C ENDOR. *J. Am. Chem. Soc.* **1995**, *117*, 8686-8687.
- (305) Christie, P. D.; Lee, H.-I.; Cameron, L. M.; Hales, B. J.; Orme-Johnson, W. H.; Hoffman, B. M. Identification of the CO-Binding Cluster in Nitrogenase MoFe Protein by ENDOR of <sup>57</sup>Fe Isotopomers. *J. Am. Chem. Soc.* **1996**, *118*, 8707-8709.
- (306) Lee, H.-I.; Cameron, L. M.; Hales, B. J.; Hoffman, B. M. Co Binding to the FeMo Cofactor of CO-Inhibited Nitrogenase: <sup>13</sup>CO and <sup>1</sup>H Q-Band ENDOR Investigation. *J. Am. Chem. Soc.* **1997,** *119*, 10121-10126.
- (307) George, S. J.; Ashby, G. A.; Wharton, C. W.; Thorneley, R. N. F. Time-Resolved Binding of Carbon Monoxide to Nitrogenase Monitored by Stopped-Flow Infrared Spectroscopy. *J. Am. Chem. Soc.* **1997**, *119*, 6450-6451.
- (308) Yan, L.; Pelmenschikov, V.; Dapper, C. H.; Scott, A. D.; Newton, W. E.; Cramer, S. P. IR-Monitored Photolysis of CO-Inhibited Nitrogenase: A Major EPR-Silent Species with Coupled Terminal CO Ligands. *Chem. Eur. J.* **2012**, *18*, 16349-16357.
- (309) Yang, Z.-Y.; Seefeldt, L. C.; Dean, D. R.; Cramer, S. P.; George, S. J. Steric Control of the Hi-CO MoFe Nitrogenase Complex Revealed by Stopped-Flow Infrared Spectroscopy. *Angew. Chem. Int. Ed.* **2011**, *50*, 272-275.
- (310) Maskos, Z.; Hales, B. J. Photo-Lability of CO Bound to Mo-Nitrogenase from *Azotobacter vinelandii*. *J. Inorg. Biochem.* **2003**, *93*, 11-17.
- (311) Yan, L.; Dapper, C. H.; George, S. J.; Wang, H.; Mitra, D.; Dong, W.; Newton, W. E.; Cramer, S. P. Photolysis of Hi-CO Nitrogenase Observation of a Plethora of Distinct CO Species Using Infrared Spectroscopy. *Eur. J. Inorg. Chem.* **2011**, 2011, 2064-2074.
- (312) Barney, B. M.; Igarashi, R. Y.; Dos Santos, P. C.; Dean, D. R.; Seefeldt, L. C. Substrate Interaction at an Iron-Sulfur Face of the FeMo-Cofactor During Nitrogenase Catalysis. *J. Biol. Chem.* **2004**, *279*, 53621-53624.
- (313) Benton, P. M. C.; Laryukhin, M.; Mayer, S. M.; Hoffman, B. M.; Dean, D. R.; Seefeldt, L. C. Localization of a Substrate Binding Site on the FeMo-Cofactor in Nitrogenase: Trapping Propargyl Alcohol with an  $\alpha$ -70-Substituted MoFe Protein. *Biochemistry* **2003**, *42*, 9102-9109.

- (314) Yang, Z.-Y.; Dean, D. R.; Seefeldt, L. C. Molybdenum Nitrogenase Catalyzes the Reduction and Coupling of CO to Form Hydrocarbons. *J. Biol. Chem.* **2011**, *286*, 19417-19421.
- (315) Lee, C. C.; Fay, A. W.; Weng, T.-C.; Krest, C. M.; Hedman, B.; Hodgson, K. O.; Hu, Y.; Ribbe, M. W. Uncoupling Binding of Substrate CO from Turnover by Vanadium Nitrogenase. *Proc. Natl. Acad. Sci. U. S. A.* **2015**, *112*, 13845-13849.
- (316) Varley, J. B.; Wang, Y.; Chan, K.; Studt, F.; Nørskov, J. K. Mechanistic Insights into Nitrogen Fixation by Nitrogenase Enzymes. *Phys. Chem. Chem. Phys.* **2015**, *17*, 29541-29547.
- (317) Lee, H.-I.; Sørlie, M.; Christiansen, J.; Yang, T.-C.; Shao, J.; Dean, D. R.; Hales, B. J.; Hoffman, B. M. Electron Inventory, Kinetic Assignment (E<sub>n</sub>), Structure, and Bonding of Nitrogenase Turnover Intermediates with C<sub>2</sub>H<sub>2</sub> and CO. *J. Am. Chem. Soc.* **2005**, *127*, 15880-15890.
- (318) Dance, I. How Does Vanadium Nitrogenase Reduce CO to Hydrocarbons? *Dalton Trans.* **2011**, *40*, 5516-5527.
- (319) Varley, J. B.; Nørskov, J. K. First-Principles Calculations of Fischer–Tropsch Processes Catalyzed by Nitrogenase Enzymes. *ChemCatChem* **2013**, *5*, 732-736.
- (320) Lee, C. C.; Wilcoxen, J.; Hiller, C. J.; Britt, R. D.; Hu, Y. Evaluation of the Catalytic Relevance of the CO-Bound States of V-Nitrogenase. *Angew. Chem. Int. Ed.* **2018**, *57*, 3411-3414.
- (321) Hiller, C. J.; Lee, C. C.; Stiebritz, M. T.; Rettberg, L. A.; Hu, Y. Strategies Towards Capturing Nitrogenase Substrates and Intermediates Via Controlled Alteration of Electron Fluxes. *Chem. Eur. J.* **2019**, *25*, 2389-2395.

#### **Table of Contents (TOC) Graphic**

